

Department of Experimental Pharmacology and Toxicology

University Medical Centre Hamburg-Eppendorf

Director: Prof. Dr. med. Thomas Eschenhagen

Disease modelling of a phospholamban p.Arg14del mutation in hiPSC-derived cardiomyocytes

Dissertation

Submitted to the Department of Chemistry

Faculty of Mathematics, Informatics, and Natural Sciences

University of Hamburg

for the degree of

Doctor of Natural Sciences

(Dr. rer. nat.)

by

Anika Eike Knaust

Hamburg, 2017

February 2014 - December 2017

Date of the oral defence: 23.02.2018

1. Referee: Prof. Dr. med. Thomas Eschenhagen

2. Referee: Prof. Dr. med. Elke Oetjen

This dissertation was practically supervised and supported by Prof. Dr. med. Arne Hansen.

“No guilt is more urgent than to say, thanks.”

„Keine Schuld ist dringender, als die, Dank zu sagen.“

(Marcus T. Cicero, 106 B.C. - 43 B.C.)

Dedicated to my grandfather.

TABLE OF CONTENT

TABLE OF CONTENT	I
LIST OF FIGURES AND MOVIES	V
LIST OF TABLES	VIII
LIST OF ABBREVIATIONS	X
1 INTRODUCTION	1
1.1 Pathophysiology of human heart failure	1
1.1.1 <i>Heart failure and inherited cardiomyopathies</i>	1
1.1.2 <i>Physiological excitation-contraction coupling and calcium homeostasis</i>	3
1.1.3 <i>Impairment of calcium handling in heart failure</i>	4
1.1.4 <i>Phospholamban protein structure and function</i>	5
1.1.5 <i>Phospholamban in heart failure</i>	6
1.1.6 <i>The PLN p.Arg14del mutation</i>	8
1.2 Genome editing with the CRISPR/Cas9 system	10
1.2.1 <i>Principles of the CRISPR/Cas system</i>	10
1.2.2 <i>Optimization of the CRISPR system for genome editing of eukaryotic cells</i>	11
1.2.3 <i>DNA lesion repair via non homology end-joining or homology-directed repair</i>	12
1.2.4 <i>DNA-based and RNP-based CRISPR/Cas approaches</i>	14
1.2.5 <i>Off-target considerations</i>	15
1.2.6 <i>Applications of the CRISPR/Cas system</i>	16
1.3 Human induced pluripotent stem cells	17
1.3.1 <i>Generation and properties of human induced pluripotent stem cells</i>	17
1.3.2 <i>Applications and limitations of human induced pluripotent stem cells</i>	19
1.4 Cardiomyocyte differentiation	21
1.4.1 <i>Embryoid body-based cardiac differentiation</i>	21
1.4.2 <i>Maturity of hiPSC-derived cardiomyocytes</i>	22
1.4.3 <i>Disease modelling with hiPSC-derived cardiomyocytes</i>	22
1.5 Engineered heart tissues	24
2 AIM OF THE THESIS	26
3 MATERIALS AND METHODS	27
3.1 Media compositions	27
3.2 Cell culture of human induced pluripotent stem cells	30
3.2.1 <i>Fibroblast reprogramming to hiPSC</i>	30
3.2.2 <i>Immunofluorescence staining of pluripotency markers in hiPSC</i>	31
3.2.3 <i>Karyotyping</i>	31
3.2.4 <i>HiPSC culture and expansion</i>	31

3.2.5	<i>Freezing and thawing of hiPSC</i>	32
3.2.6	<i>Mycoplasma test and treatment</i>	32
3.3	CRISPR/Cas9-mediated gene editing of hiPSC	34
3.3.1	<i>Validation of the PLN target sequence</i>	34
3.3.2	<i>Design of the CRISPR/Cas9 experiment</i>	35
3.3.3	<i>Preparation of the DNA-based CRISPR approach</i>	36
3.3.4	<i>The ribonucleoprotein-based CRISPR approach</i>	39
3.3.5	<i>Nucleofection of hiPSC with the Amaxa 4D System</i>	42
3.3.6	<i>Clonal isolation by FACS, sub-cultivation and clonal expansion of nucleofected hiPSC</i>	44
3.3.7	<i>Validation of recombination efficiency and off-target activity</i>	45
3.4	Differentiation of hiPSC to cardiomyocytes	47
3.4.1	<i>Embryoid body formation in spinner flasks</i>	48
3.4.2	<i>Mesodermal progenitor cell induction</i>	49
3.4.3	<i>Cardiac specification</i>	49
3.4.4	<i>Dissociation of hiPSC-cardiomyocytes in cEB or adherent format</i>	50
3.4.5	<i>Freezing of hiPSC-derived cardiomyocytes</i>	51
3.4.6	<i>Flow cytometric analysis for cardiac marker positivity</i>	51
3.4.7	<i>Thawing of hiPSC-derived cardiomyocytes</i>	51
3.5	Engineered heart tissue model	52
3.5.1	<i>EHT generation and maintenance</i>	52
3.5.2	<i>Contractility measurement and electrical stimulation of EHTs</i>	53
3.5.3	<i>Monitoring of the EHT development over time</i>	54
3.5.4	<i>Disease modelling protocols</i>	54
3.5.5	<i>Immunohistochemical analysis of EHTs</i>	56
3.5.6	<i>Molecular analysis</i>	56
3.6	Cardiomyocyte monolayer-based analyses	59
3.6.1	<i>Cardiomyocyte plating and maintenance</i>	59
3.6.2	<i>Calcium transient measurements after caffeine application</i>	59
3.6.3	<i>Immunofluorescence analysis of 2D hiPSC-CM</i>	60
3.6.4	<i>Analysis of 2D hiPSC-CM cell area</i>	60
4	RESULTS	61
4.1	Characterization of hiPSC PLN p.Arg14del clones	61
4.1.1	<i>Patient background</i>	61
4.1.2	<i>Reprogramming of hiPSCs</i>	61
4.2	CRISPR/Cas9-mediated genomic correction of PLN c.40-42AGAdel gene locus ...	65
4.2.1	<i>PLN sequence validation prior to the in silico CRISPR experiment design</i>	65

4.2.2	<i>In silico design of the gRNA and repair template</i>	66
4.2.3	<i>Preparation of the DNA-based approach</i>	68
4.2.4	<i>Preparation of the RNP-based approach</i>	69
4.2.5	<i>Evaluation of DNA- and RNP-based generation of PLNic</i>	72
4.2.6	<i>Off-target validation</i>	80
4.2.7	<i>Karyotype analysis of the isogenic control hiPSC clones</i>	84
4.3	Cardiac differentiation of PLNic and PLN p.Arg14del hiPSC	85
4.3.1	<i>Successful differentiation of hiPSC into beating cardiomyocytes</i>	85
4.3.2	<i>Cardiac differentiation with high hiPSC-cardiomyocyte yields and purities</i>	86
4.4	Physiological and pharmacological analysis of PLNic and PLN p.Arg14del EHTs	88
4.4.1	<i>Differences in force development of spontaneously beating EHTs</i>	88
4.4.2	<i>Baseline characterization of paced EHTs</i>	91
4.4.3	<i>Calcium concentration-response curve</i>	93
4.4.4	<i>Isoprenaline and carbachol response</i>	94
4.4.5	<i>Long-term exposure to calcium</i>	97
4.5	Molecular characterization of PLNic and PLN p.Arg14del EHTs	98
4.5.1	<i>PLN gene expression analysis</i>	98
4.5.2	<i>Western blot analysis of PLN protein levels and autophagy marker in PLNic and PLN p.Arg14del EHTs</i>	101
4.5.3	<i>Histological analysis</i>	104
4.6	HiPSC-CM characterization in 2D	108
4.6.1	<i>Calcium transients and caffeine responses of PLNic and PLN p.Arg14del cardiomyocytes in 2D format</i>	108
4.6.2	<i>Confocal microscopy</i>	109
4.6.3	<i>Cardiomyocyte cell area analysis</i>	112
5	DISCUSSION	113
5.1	Establishment of isogenic control hiPSC lines from patient-specific hiPSCs by CRISPR/Cas9 genome editing technology	113
5.1.1	<i>CRISPR/Cas9-mediated genomic correction of PLN c.40-42AGAdel</i>	113
5.1.2	<i>Application of the Cas9n approach</i>	113
5.1.3	<i>Comparison and evaluation of the established DNA- and RNP-based Cas9 nuclease approaches</i>	114
5.1.4	<i>Evaluation of the CRISPR/Cas9 technology in this study</i>	118
5.2	Efficient differentiation of cardiomyocytes from disease-specific and isogenic control hiPSCs	119

5.3	The establishment of a human cardiac <i>in vitro</i> tissue model for disease modelling with patient-specific and isogenic control hiPSC-derived cardiomyocytes.....	120
5.4	Phenotypic analysis of hiPSC-CM in 2D and 3D format	121
5.4.1	<i>Investigation of contractile parameters and pharmacological responses of hiPSC-derived PLN^{ic} and PLN p.Arg14del cardiomyocytes.....</i>	<i>121</i>
5.4.2	<i>Investigation of possible pathological pathways based on the analysis of histological and molecular markers in PLN^{ic} and PLN p.Arg14del hiPSC-CMs</i>	<i>124</i>
6	FUTURE PERSPECTIVES.....	128
7	SUMMARY.....	130
8	ZUSAMMENFASSUNG	132
9	BIBLIOGRAPHY	134
10	SUPPLEMENT	150
10.1	Devices, materials and substances	150
10.1.1	<i>Devices</i>	<i>150</i>
10.1.2	<i>Software.....</i>	<i>152</i>
10.1.3	<i>Materials and equipment.....</i>	<i>152</i>
10.1.4	<i>Media and serum</i>	<i>154</i>
10.1.5	<i>Reagents, proteins and small molecules</i>	<i>154</i>
10.1.6	<i>Small molecules and pharmacological agents.....</i>	<i>157</i>
10.1.7	<i>Kits.....</i>	<i>157</i>
10.1.8	<i>Reagent setup, buffer and solutions</i>	<i>158</i>
10.1.9	<i>Antibodies</i>	<i>163</i>
10.1.10	<i>Primer and oligomers.....</i>	<i>165</i>
10.2	Security information.....	167
10.2.1	<i>Security information for the used substances.....</i>	<i>167</i>
10.2.2	<i>EU-GHS Hazard (H) and Precaution (P) statements.....</i>	<i>170</i>
10.3	Figures and tables.....	177
10.4	Movies.....	181
10.5	Financial support	182
10.6	Publications and congress participations	182
10.6.1	<i>Publications</i>	<i>182</i>
10.6.2	<i>Congress and meeting participations.....</i>	<i>182</i>
11	ACKNOWLEDGEMENTS	184
12	DECLARATION OF ACADEMIC HONESTY - EIDESSTATTLICHE ERKLÄRUNG.....	185

LIST OF FIGURES AND MOVIES

Figure 1: Cardiomyopathy forms of the human heart.	1
Figure 2: HCM-, DCM- and ARVC-associated gene mutations and cellular pathological hallmarks of the respective cardiomyopathy type.	2
Figure 3: Schematic overview of calcium handling proteins important for the excitation-contraction coupling (ECC) process in cardiomyocytes.	3
Figure 4: Topology of the monomeric PLN protein.....	5
Figure 5: Signalling pathway interactions in the cardiomyocyte.	6
Figure 6: Schematic overview of the CRISPR/Cas system as part of the adaptive immune system of bacteria and archaea.	10
Figure 7: Schematic formation of the sgRNA and the sgRNA:DNA heteroduplex.	12
Figure 8: Cas9-mediated double strand cleavage of the genomic locus after sgRNA-mediated guidance to the PAM.	13
Figure 9: Overview of selected Cas9 delivery methods.	15
Figure 10: Embryonic (ESC) and induced pluripotent stem cells (iPSC) are pluripotent and can differentiate to ecto-, meso- and endodermal progenitor multipotent stem cells.....	17
Figure 11: Overview of patient-derived hiPSC applications.....	19
Figure 12: Overview of the cardiomyocyte differentiation cell stages with respective molecular markers and involved signalling pathways.	21
Figure 13: EHT generation..	24
Figure 14: Video-optical recording system.....	25
Figure 15: Cloning of the sgRNA-DNA oligo into the pSpCas9(BB)-2A-GFP vector.....	37
Figure 16: Design of the sgDNA.	39
Figure 17: Embryoid body, growth factor-based three-stage protocol.	47
Figure 18: EHT casting and development.....	53
Figure 19: Representative characterization of the PLN p.Arg14del hiPSC clone #1201.....	61
Figure 20: Morphological characterization of the selected hiPSC clones.	62
Figure 21: Karyotyping results of PLN p.Arg14del hiPSC clones.	63
Figure 22: Representative SnapGene alignment of the PLN wildtype sequence with the hiPSC clones #1198 and #1201..	64
Figure 23: 1% Agarose gel electrophoreses of the PLN 1258 bp PCR product.....	65
Figure 24: Job submission result of the <i>in silico</i> design using the online CRISPR design tool of the Zhang lab (MIT).....	66
Figure 25: SnapGene alignment of the gRNA #3 sequence with the PLN c.40-42AGAdel sequence.	66

Figure 26: SnapGene alignment of the PLN c.40-42AGAdel, gRNA #3 and ssODN sequences with the wildtype PLN gene.	67
Figure 27: Schematic summary of the <i>in silico</i> design of the CRISPR/Cas9 experiment.....	68
Figure 28: 1% Agarose gel electrophoresis as quality control of the linearized pSpCas9(BB)-2A-GFP vector after BbsI restriction digest.....	68
Figure 29: Representative SnapGene alignment of the sequencing result to the <i>in silico</i> designed sgRNA after the ligation of the gRNA #3 into the pSpCas9(BB)-2A-GFP vector upstream of the sgRNA scaffold.	69
Figure 30: 2% Agarose gel electrophoresis to verify quality and size of the generated sgDNA #3 construct.	69
Figure 31: SnapGene alignment of the sequencing result of the generated sgDNA to the <i>in silico</i> designed sgDNA #3 construct.	70
Figure 32: 2% Agarose gel analysis to check for IVT-derived sgRNA #3 and possible RNA degradation	71
Figure 33: 1.5 % Agarose gel analysis to verify the <i>in vitro</i> Cas9 functionality and sgRNA #3 guiding ability.	72
Figure 34: Clonal growth of nucleofected and low-density seeded PLN p.Arg14del hiPSC..	73
Figure 35: SnapGene alignment of the DNA sequencing result of the successfully generated isogenic control clone PLNic #28.....	74
Figure 36: SnapGene alignments of the DNA sequencing results of two representative clones (#21, #26) not successfully corrected.....	75
Figure 37: Microscopic analysis of pSpCas9-sgRNA#3-2A-GFP plasmid expression of confluent hiPSC monolayer to check for transfection efficiency 48 hours after nucleofection.....	76
Figure 38: FACS-sorting of GFP-positive hiPSC.....	77
Figure 39: Representative cell clone sizes and morphologies before picking and clonal expansion.....	78
Figure 40: SnapGene alignment of the DNA sequences of the successfully generated isogenic control clones PLNic #15, PLNic #24 and PLNic #45.	79
Figure 41: SnapGene alignment of the DNA sequences of three representative clones (#2, #6 and #14) not successfully corrected.	80
Figure 42: The 10 most likely off-target loci for the gRNA #3 according to the online CRISPR design tool of the Zhang lab (MIT).....	81
Figure 43: 1.8% Agarose gel analyses of the PCR-amplified off-target sequences (OT1-10) representative for PLNic #15.	81

Figure 44: Representative SnapGene alignment of the sequencing results of the PLNic #15, #24 and #45 clones (DNA-based approach) as well as PLNic #28 (RNP-based approach) for the validation of gRNA #3 off-targets.	82
Figure 45: Sequencing results of PLN p.Arg14del hiPSC and for further experiments chosen PLNic clones generated with DNA- or RNP-based approach, respectively.	83
Figure 46: Morphological characterization of the selected hiPSC PLNic clones.	83
Figure 47: Karyotyping results of PLNic hiPSC clones.	84
Figure 48: Spontaneously beating hiPSC-derived cardiomyocytes of the cardiac specification stage one day before dissociation.	85
Figure 49: Cardiomyocyte differentiation results.	86
Figure 50: Differentiation efficiencies of all differentiation runs.	87
Figure 51: Representative baseline recordings of unrelated control, PLN p.Arg14del #1198 and PLNic #15 EHTs.	88
Figure 52: EHT development over time.	89
Figure 53: Comparison of EHT force and spontaneous beating frequency.	90
Figure 54: Analysis of the EHTs' average peaks and contractile parameters.	91
Figure 55: Comparison of the normalized early contraction phases of PLNic #15 and PLN p.Arg14del #1198 EHTs.	92
Figure 56: Calcium concentration-response curves of PLNic #15 and PLN p.Arg14del #1198 EHTs.	93
Figure 57: Isoprenaline and carbachol response.	96
Figure 58: Long-term exposure to calcium.	97
Figure 59: Total PLN relative transcript levels in human tissue and EHTs analysed with NanoString technology.	98
Figure 60: Ratio of PLN wildtype to mutant relative transcript levels of PLNic and PLN p.Arg14del EHTs.	99
Figure 61: Ratio of PLN wildtype to mutant relative transcript levels of PLN p.Arg14del human tissue and EHTs.	100
Figure 62: Western blot analysis of PLN total protein levels.	101
Figure 63: Western blot analysis of PLN-PSer16 protein levels.	102
Figure 64: Western blot analysis of p62, LC3-II and LAMP2 protein levels.	103
Figure 65: 20x Magnification of the immunohistological staining for hPLN in EHT longitudinal sections.	104
Figure 66: 40x Magnification of the immunohistological staining for hPLN in EHT longitudinal sections.	105
Figure 67: 20x Magnification of the immunohistological staining for dystrophin in EHT cross sections.	106

Figure 68: 40x Magnification of the immunohistological staining for dystrophin in EHT cross sections.....	107
Figure 69: Calcium transient analysis in PLN p.Arg14del and PLNic CM in 2D format.....	108
Figure 70: Immunofluorescence of PLN (red), ACTN2 (green) and Hoechst (blue) staining in 30 days old hiPSCs-CM in 2D format..	110
Figure 71: Immunofluorescence of PLN (red), Serca2a (green) and Hoechst (blue) staining in 30 days old hiPSC-CM in 2D format.	111
Figure 72: PLNic and PLN p.Arg14del cardiomyocyte cell area evaluation by confocal microscopy and ImageJ analysis after 7 and 30 days of cultivation.....	112
Figure S1: Part of the sequencing result of the hPLN sequences of 10 picked clones aligned to NCBI-derived hPLN wildtype sequence with SnapGene to analyse both alleles individually..	178
Figure S2: Vector map of the pSpCas9-gRNA#3-2A-GFP plasmid.....	179
Figure S3: Representative flow cytometry plots of dissociated hiPSC-derived cardiomyocytes.	181
Movie S1: Representative original video recordings of beating hiPSC-derived cardiomyocytes in their cardiac specification stage one day before dissociation.	181
Movie S2: Representative original video recordings of spontaneously beating 20 day old EHTs in cultivation medium.	181

LIST OF TABLES

Table 1: Cell culture media compositions, production and storage details.....	27
Table 2: Overview of the used reprogrammed cell lines.....	31
Table 3: Mycoplasma detection PCR reaction with the Taq-DNA polymerase kit.	33
Table 4: PCR programme for mycoplasma DNA locus amplification.	33
Table 5: PrimeSTAR PCR reaction.	34
Table 6: Touchdown PCR program.....	34
Table 7: Ligation protocol.....	35
Table 8: Preparation of 10x annealing buffer.	37
Table 9: DNA oligomer annealing approach.....	37
Table 10: BbsI restriction digest approach for the linearization of pSpCas9(BB)-2A-GFP plasmid.....	38

Table 11: Ligation approach using the 'Rapid DNA Ligation Kit' (Thermo Fisher Scientific).	38
Table 12: Primer annealing solution.	40
Table 13: Extension PCR of the annealed sgDNA.	40
Table 14: PCR programme of the extension PCR.	40
Table 15: <i>In vitro</i> transcription of the sgDNA to the sgRNA.	41
Table 16: Preparation of the sgRNA and Cas9 nuclease reaction mixture for the <i>in vitro</i> test.	42
Table 17: AmpliTaqGold PCR-mediated amplification of suspected off-target loci.	46
Table 18: Touchdown PCR programme for AmpliTaqGold PCR.	46
Table 19: Overview of spinner flask types, minimal and maximal medium volumes and cell number ranges.	48
Table 20: Master mixture calculated per EHT containing 1.0×10^6 cardiomyocytes.	52
Table 21: RT-PCR master mixture set-up.	57
Table 22: RT-qPCR reaction set up.	57
Table 23: Western blot conditions of each target protein.	58
Table 24: Plating format, coating procedure, cell number per area and medium volumes for each respective cardiomyocyte monolayer experiment.	59
Table 25: Summarized overview of the RNP-based CRISPR experiment.	75
Table 26: Summarized overview of the DNA-based CRISPR experiments.	80
Table 27: Calculation of isoprenaline and carbachol effects.	94
Table S1: Reagent setup, buffer and solutions.	158
Table S2: Primary antibodies used for flow cytometry/FACS, western blot (WB), immunofluorescence (IF) and immunohistochemistry (IHC) analysis.	163
Table S3: Primary antibodies used for flow cytometry/FACS, western blot (WB), immunofluorescence (IF) analysis.	164
Table S4: Primer for PCR, sequencing (Seq) and sgDNA synthesis.	165
Table S5: Primer for RT-qPCR analysis.	166
Table S6: CRISPR/Cas9 - ssODN repair template and sgRNA sequences.	167
Table S7: Security information (H- and P-statements) of all used substances.	167
Table S8: Hazard (H) statements according to the 8th ATP of the CLP regulation of May 19, 2016.	170
Table S9: Precaution (P) statements according to the 8th ATP of the CLP regulation of May 19, 2016.	173
Table S10: Acronyms and names of human genes evaluated with the NanoString nCounter® Elements system.	177

LIST OF ABBREVIATIONS

Abbreviation	Meaning
°C	Degree Celsius
µg	Micrograms
µL	Microliter
µm	Micrometre
µM	Micromolar
2D	Two-dimensional
3D	Three-dimensional
aa	Amino acid
ABCF1	ATP binding cassette subfamily F member 1
ACTB	Actin beta
ACTN2	Alpha-actinin 2
ANOVA	Analysis of variances
AP	Action potential
APD	Action-potential duration
Aqua dest.	Aqua destillata (distilled water)
ARVC	Arrhythmogenic restrictive cardiomyopathy
ATP	Adenosine triphosphat
BB	Backbone
bFGF	Basic fibroblast growth factor
BL	Baseline
BMP4	Bone-morphogenetic protein 4
bp	Base pairs
bpm	Beats per minute
BSA	Bovine serum albumin
CaMKII	Ca ²⁺ /calmodulin-dependent protein kinase II
cAMP	3',5' Cyclic adenosine monophosphate
Cas	CRISPR-associated protein
Cas9n	CRISPR-associated protein 9 nickase
CASQ2	Calsequestrin 2
CCh	Carbachol
cDNA	Complementary DNA
cEB	Cardiac embryoid body
CLTC	Clathrin heavy chain
CM	Cardiomyocyte

cm	Centimetre
c-Myc	Cellular myelocytomatosis
CRISPR	Clustered Regularly Interspaced Short Palindromic Repeats
crRNA	CRISPR RNA
cTNT	Cardiac troponin T
d	Days
DAD	Delayed after-depolarization
DCM	Dilated cardiomyopathy
del	Deletion
DEPT	Department of Experimental Pharmacology
DMEM	Dulbecco's Modified Eagle Medium
DMSO	Dimethyl sulfoxide
DNA	Deoxyribonucleic acid
dNTP	Deoxy-nucleoside triphosphate
DSB	Double strand break
EB	Embryoid body
EC₅₀	Half maximal effective concentration
ECC	Excitation-contraction coupling
ECG	Electrocardiographs
ECL	Enhanced chemiluminescence
EDTA	Ethylenediaminetetraacetic acid
EHT	Engineered heart tissue
ESC	Embryonic stem cell
et al.	Et alii (and others)
FACS	Fluorescence-activated cell sorting
FBS	Fetal bovine serum
FCS	Fetal calf serum
FTDA	bFGF, TGF β 1, dorsomorphin and activin A-based hiPSC culture medium
Fw	Forward
g	Gram
GAPDH	Glyceraldehyde-3-phosphate dehydrogenase
GFP	Green fluorescent protein
gRNA	Guide RNA
GUSB	Glucuronidase-beta

HBSS	Hank's Balanced Salt Solution
HCl	Hydrogen chloride
HCM	Hypertrophic cardiomyopathy
HDR	Homology-directed repair
HEK	Human embryonic kidney
HEPES	4-(2-hydroxyethyl)-1-piperazineethanesulfonic acid
hESC	Human embryonic stem cell
hiPSC	Human induced pluripotent stem cells
HRE	Homologous recombination efficiency
Hz	Hertz
IBP	Irregular beating pattern
ICD	Implantable cardioverter-defibrillator
IHC	Immunohistochemistry
indels	Insertions or deletions
iPSC	Induced pluripotent stem cell
IR	Ischemia/reperfusion
Iso	Isoprenaline
IVT	<i>In vitro</i> transcription
IWR-1	4-(1,3,3a,4,7,7a-hexahydro-1,3-dioxo-4,7-methano-2H-isoindol-2-yl)-N-8-quinolinyl-benzamide
kb	Kilobase
kDa	Kilodalton
Klf4	Kruppel-like factor 4
KSOM	Klf4; Sox2; Oct4; c-Myc
L	Litre
LAMP2	Lysosome-associated membrane protein 2
LB	Lysogeny broth
LC3-II	Autophagic marker light chain 3-II
log	Logarithm
LTCC	Long lasting-type calcium channel
LV	Left ventricle
M	Molar
mA	Milliampere
MEF	Mouse embryonic fibroblasts
mg	Milligrams

min	Minutes
miRNA	Micro RNA
mL	Millilitre
MLC2v	Myosin regulatory light chain 2V (ventricular)
mm	Millimetre
mM	Millimolar
mN	Millinewton
mRNA	Messenger RNA
mt	Mutant
MYH7	Beta (β)-myosin heavy chain
NCBI	National Centre for Biotechnology Information
NCX	Sodium-calcium exchanger
NEB	NewEngland Biolabs
NFH	Non failing heart
NHEJ	Non-homologous end joining
NLS	Nuclear localization signal
nm	Nanometre
nmol	Nanomolar
ns	Not significant
nt	Nucleotide
Oct4	Octamerbinding transcription factor 4
PAM	Protospacer adjacent motif
PBS	Phosphate-buffered saline
PCR	Polymerase chain reaction
PDMS	Polydimethylsiloxane
pg	Picogram
PGK1	Phosphoglycerate kinase 1
pH	-Log ₁₀ hydrogen ion activity
PKA	Protein kinase A
PLN	Phospholamban
PLNic	Isogenic control derived from the PLN p.Arg14del hiPSC clone
pM	Picomolar
PMCA	Plasma membrane calcium ATPase
PPI	Protein phosphatase I
PVDF	Polyvinylidene fluoride

qPCR	Quantitative real-time PCR
R²	Correlation coefficient
Rev	Reverse
RNA	Ribonucleic acid
RNP	Ribonucleoprotein complex
ROS	Reactive oxygen species
rpm	Rounds per minute
RPMI	Roswell Park Memorial Institute
RR scatter	Interdecile range of average beat-to-beat variation
RT	Reverse transcription
RyR2	Ryanodin receptor 2
s	Seconds
SDS-PAGE	Sodium dodecyl sulfate polyacrylamide gel electrophoresis
sec	Seconds
SEM	Standard error of the mean
SERCA2a	Sarcoplasmic-endoplasmic reticulum calcium ATPase 2a
sgRNA	Single guide RNA
shRNA	Short hairpin RNA
siRNA	Small interfering RNA
SNP	Single nucleotide polymorphism
Sox2	Sex determining region Y-box 2
Sp	<i>Streptococcus pyogens</i>
SR	Sarcoplasmic reticulum
ssODN	Single-stranded donor oligonucleotides
T1	Contraction time
T2	Relaxation time
TALEN	Transcription activator-like effector nucleases
TBS	Tris-buffered saline
TBS-T	TBS with Tween 20
TEMED	Tetramethylethane-1,2-diamine
TGFβ	Transforming growth factor-β
TN-C	Troponin C
tracrRNA	Trans-activating crRNA

Tris	2-Amino-2-(hydroxymethyl)propane-1,3-diol
T-tubule	Transverse tubules
TUBB	Tubulin beta class 1
UKE	University Medical Centre Hamburg- Eppendorf
V	Volt
v/v	Volume/volume
Vol	Volume
vs.	Versus
w/v	Weight/volume
wt	Wildtype
x	Times
xg	X gravity
ZFN	Zinc-finger nucleases

Amino acid code

3-letter code	Single letter code	Amino Acid
Ala	A	Alanine
Arg	R	Arginine
Asn	N	Asparagine
Asp	D	Aspartic acid
Cys	C	Cysteine
Gln	Q	Glutamine
Glu	E	Glutamic acid
Gly	G	Glycine
His	H	Histidine
Ile	I	Isoleucine
Leu	L	Leucine
Lys	K	Lysine
Met	M	Methionine
Phe	F	Phenylalanine
Pro	P	Proline
Ser	S	Serine
Stop	Stop	Stop codons
Thr	T	Threonine
Trp	W	Tryptophan
Tyr	Y	Tyrosine
Val	V	Valine

Nucleotide code

Letter	Nucleotide
A	Adenine
G	Guanine
C	Cytosine
T	Thymine
U	Uracil
N	Any nucleotide

1 INTRODUCTION

1.1 Pathophysiology of human heart failure

1.1.1 Heart failure and inherited cardiomyopathies

“Heart failure is a major killer; roughly half of deaths are gradual, due to the inability of the heart to pump enough blood, while the remainder occur suddenly from arrhythmias” (Eisner 2014, page 1277). With this statement David Eisner summarized the severity of a major cause of death and health-care disbursements world-wide (von Lueder and Krum 2015). Heart failure is a clinical syndrome and the consequence of many disorders. The heart’s ejection fraction is not sufficient to supply peripheral organs and tissues with oxygen enriched blood (systolic heart failure), or the diastolic filling can be primarily impaired (diastolic heart failure). The most common acquired causes for heart failure are chronic overload (arterial hypertension, aortic stenosis), coronary heart disease with consecutive loss of functional cardiac muscle mass, volume-related stress (arteriovenous shunt, mitral insufficiency) and cardiomyopathies (Eschenhagen et al. 2013).

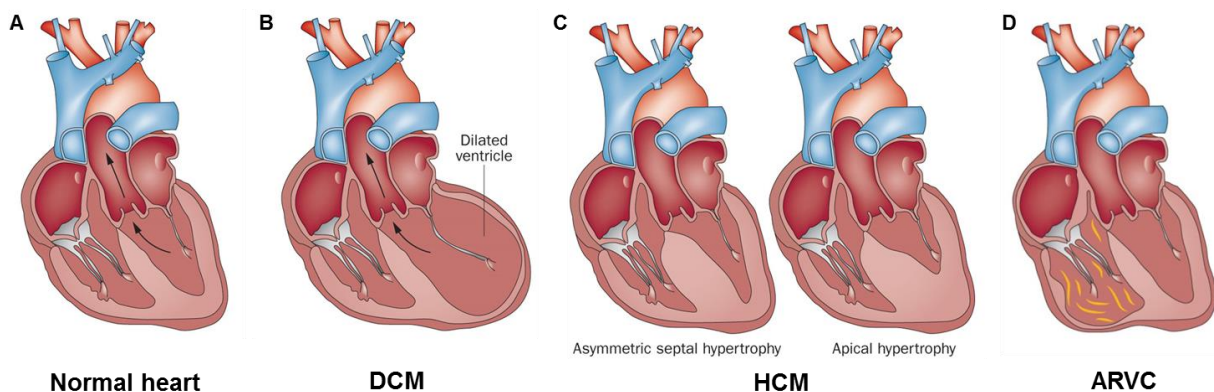


Figure 1: Cardiomyopathy forms of the human heart. Comparative representative anatomy of **A)** normal healthy heart, **B)** DCM-, **C)** HCM- and **D)** ARVC-diseased hearts (modified from Wilde & Behr 2013).

Cardiomyopathies are defined as heart muscle diseases associated with cardiac dysfunction and are subdivided into the following main forms: dilated cardiomyopathy (DCM), hypertrophic cardiomyopathy (HCM), restrictive cardiomyopathy (RCM), arrhythmogenic restrictive cardiomyopathy (ARVC) and not-classifiable CM (Richardson et al. 1996). They can be further classified into primary and secondary cardiomyopathies. Primary cardiomyopathies are caused by inherited or sporadic genetic mutations (DCM, HCM, channelopathies, arrhythmogenic right ventricular cardiomyopathy/dysplasia [ARVC/D]) or acquired predispositions (e. g. stress-provoked, tachycardia-induced or inflammatory; Maron

2008). Secondary cardiomyopathies are caused by bacterial or viral infections or can be toxic, endocrine or metabolic-related (Eschenhagen et al. 2013).

Disease	Mutated gene	Pathology
Hypertrophic cardiomyopathy	Myosin binding protein C	Increased heart mass
	β-Myosin heavy chain	Left ventricular wall thickening
	α-Myosin heavy chain	Increased cardiomyocyte size
	α-Tropomyosin	Myofibrillar disarray
	Troponin T	Decreased volume of left ventricular chamber
	α-Cardiac actin	Interstitial fibrosis
	Troponin I	Enlarged nuclei
	Titin	Ventricular wall stiffness
	Myosin light chains	Inflammation
	Troponin C	
	Vinculin	
	Muscle LIM protein	
	Telothonin	
	Dilated cardiomyopathy	β-Myosin heavy chain
Desmin		Ventricular chamber enlargement
N-cadherin		Cardiomyocyte apoptosis
α-Cardiac actin		Interstitial fibrosis
Skeletal muscle myopathies		Enlarged nuclei
α-Tropomyosin 1		Ventricular wall stiffness
Muscle LIM protein δ-sarcoglycan		Inflammation
Lamin A/C		
TAZ (G4.5)		
Titin		
Phospholamban		
Vinculin		
Troponin I		
Troponin T2		
SCN5A		
Presentin 1 & 2		
Troponin C		
α-Cardiac actinin		
Arrhythmogenic right ventricular cardiomyopathy	Plakoglobin	Right ventricular dilation
	Plakophilin-2	Right ventricular fibrosis
	Junctional plakoglobin	Fibrofatty infiltration
	Desmocollin-2	Apoptosis
	Desmoglein-2	
	Desmoplakin	

Bold: mutations that are common to multiple forms of cardiomyopathy.

Figure 2: HCM-, DCM- and ARVC-associated gene mutations and cellular pathological hallmarks of the respective cardiomyopathy type (modified from Harvey and Leinwand 2011).

Typical morphological alterations at early stages of disease development are a dilation and wall thinning for DCM and septal or apical hypertrophy for HCM (Figure 1). In 1990 the first cardiomyopathy-related gene was identified when in a large family a point mutation in the β cardiac myosin heavy chain (MHC) gene in exon 13 was associated with familial HCM (Geisterfer-Lowrance et al. 1990). This finding initiated the research field of genetics in cardiomyopathy, which resulted in the discovery of at least 50 genes associated with DCM (Cahill et al. 2013) and more than 400 mutations in over 27 gene loci were associated with HCM predominantly occurring in sarcomeric protein encoding genes (summarized in Figure 2; Herold 2012).

DCM is the second most frequent hereditary form of cardiomyopathy after HCM. Gene-related factors with familial aggregation in up to 50% of all cases can contribute to the development of DCM (Herold 2012). For inherited DCM the spectrum of associated genes is more diverse, and includes mutations in proteins involved in force regulation, generation and transduction or nuclear proteins (reviewed in Harvey and Leinwand 2011; Cahill et al. 2013). In addition to inherited forms of DCM also environmental (viral, alcohol-related), autoimmune, toxic and idiopathic forms are described.

1.1.2 Physiological excitation-contraction coupling and calcium homeostasis

Coordinated contraction and relaxation is the most prominent function of the heart. This is enabled by the cardiac excitation-contraction coupling (ECC) mechanism. Figure 3 shows the schematic molecular overview of the cardiomyocyte and important proteins involved in this process.

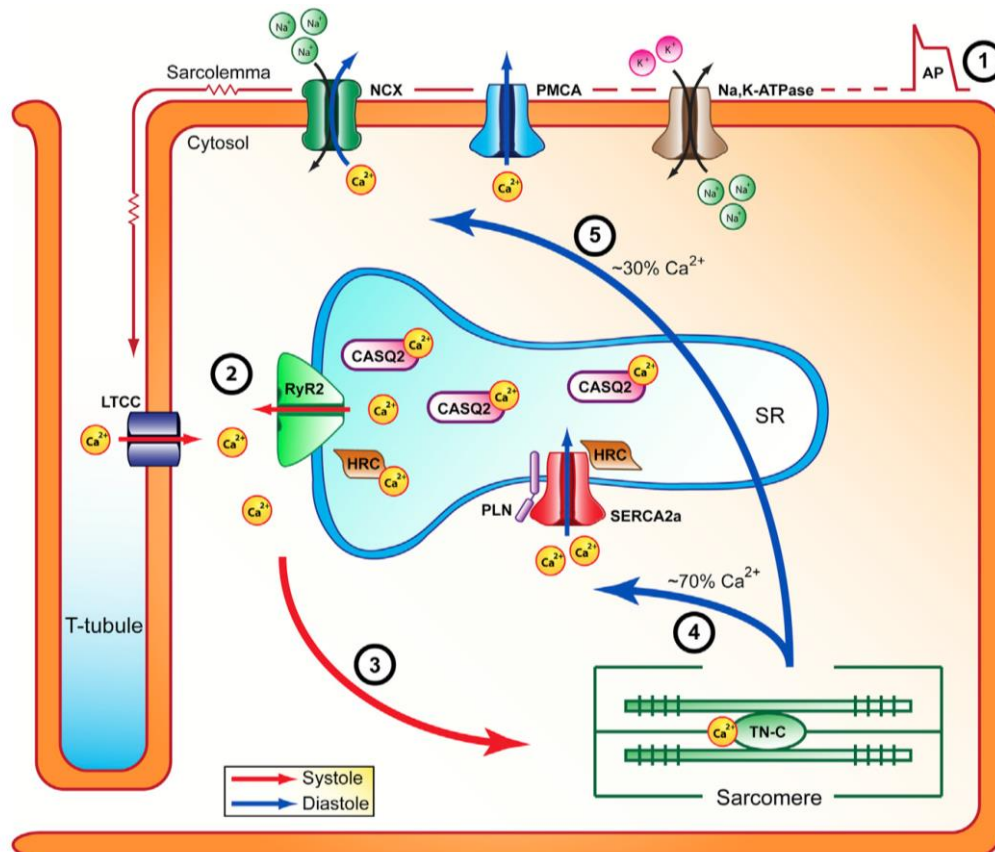


Figure 3: Schematic overview of calcium handling proteins important for the excitation-contraction coupling (ECC) process in cardiomyocytes. AP: action potential; LTCC: L-type calcium channel; RyR2: ryanodine receptor 2; SR: sarcoplasmic reticulum; PLN: phospholamban; SERCA2a: sarcoplasmic-endoplasmic reticulum calcium ATPase 2a; PMCA: plasma membrane calcium ATPase; NCX: sodium-calcium exchanger; TN-C: troponin C; HRC: histidine-rich calcium binding protein; CASQ2: calsequestrin 2 (Gorski et al. 2015).

The ECC process is initiated by the action potential-mediated excitation of the cell's membrane. The transverse tubules (T-tubule), which are membrane invaginations, conduct the excitation fast and deep into the cell. Conduction of this depolarisation is propagated by voltage-gated sodium channels. The depolarisation triggers the opening of the voltage-gated L-type calcium channels (LTCC; in ventricular cardiomyocytes mostly $Ca_{V1.2}$). The triggered calcium influx into the cell along the concentration gradient induces the calcium-induced calcium release. Therefore calcium sensitive ryanodine receptors (RyR2) open and calcium is released out of the sarcoplasmic reticulum (SR), the calcium main storage of the cardiomyocyte. The cytosolic calcium concentration increases about 10-fold ($\sim 1 \mu\text{M}$) and the calcium ions bind to troponin C (TN-C), which is one part of the troponin-tropomyosin complex on the sarcomere actin filaments. The actin-myosin cross bridging is promoted, leading to the contraction of the myocyte and thereby enabling myocardial contraction. The relaxation is induced by cellular repolarisation, which leads to voltage-dependent inactivation of the inward calcium current. The second important parameter for the reduction of cytoplasmic calcium concentration is SERCA2a-mediated reuptake of calcium into the sarcoplasmic reticulum and NCX-mediated transport via the cytoplasmic membrane. This leads to the dissociation of calcium from the troponin C binding domains and relaxation of the myofilaments. During myofilament relaxation cytoplasmic calcium concentration are 10-fold lower and in the range of 100 nM (Bers 2002; Eschenhagen et al. 2013; Marks 2013; Luo and Anderson 2013).

1.1.3 Impairment of calcium handling in heart failure

Disturbance of cardiomyocyte calcium handling contributes to the development of heart failure (Shan et al. 2010; Kho et al. 2012). This disturbance leads to (diastolic) cytosolic calcium overload, SR calcium re-uptake deficiency, reduction of SR calcium levels, reduced calcium transients or leakiness of the SR calcium (Gorski et al. 2015). Potential contributors to this are the increased instability of the RyR2 leading to decreased SR content and reduced calcium transient amplitudes (Brillantes et al. 1994; Marx et al. 2000; Lehnart et al. 2006; Lehnart et al. 2008; Andersson and Marks 2010; Shan et al. 2010) and reduced activity and expression levels of SERCA2a leading to decreased calcium re-uptake rates into the SR (Mercadier et al. 1990; Arai et al. 1993; Hasenfuss et al. 1994). Also, increased diastolic calcium levels with subsequent prolongation of relaxation time and decreased calcium transient amplitude contribute to the disturbances.

1.1.4 *Phospholamban protein structure and function*

In 1975 the phosphoprotein phospholamban (PLN) was identified by Katz and co-workers (Tada et al. 1975). It was named according to its function derived from the Greek words 'phosphorous' and 'lambano' (receive), meaning 'phosphate receptor' (reviewed in Katz 1998).

PLN is an important 52 amino acid (aa) transmembrane protein located in the SR. Structurally it is divided into two subdomains as shown in Figure 4. Domain I is composed of the aa 1-30 and is reaching into the cytosol of the cell containing PLN-inactivating phosphorylation sites. Domain II is the conserved membrane spanning part (aa 31-49), reaches into the SR lumen (aa 50-52) and is important for SERCA2a inhibition (MacLennan and Kranias 2003; Young et al. 2015). Functionally, PLN is involved in the regulation of calcium cycling and homeostasis of the cardiomyocyte by modulating the activity of SERCA2a. In its active state, PLN acts as a monomer (6 kilodalton [kDa]). By interaction with SERCA2a a conformational change of the calcium pump is induced reducing its apparent calcium affinity and inhibiting the calcium reuptake into the SR (Cantilina et al. 1993; Koss and Kranias 1996). Upon phosphorylation and increased cytosolic calcium levels during the ECC process PLN gets inactivated and dissociates from SERCA2a, which in turn actively pumps the calcium back into the SR. The dissociation is driven by calcium binding to SERCA2a breaking physical PLN-SERCA2a heterodimer interactions and by the disruption of the functional interaction upon PLN phosphorylation (Asahi et al. 2000).

Inactive PLN forms a homopentamer (22 kDa) in the SR membrane (Kimura et al. 1997). PLN phosphorylation is reversible and mediated by β -adrenergic stimulation (e.g. adrenaline, isoprenaline; see Figure 5). The β -adrenergic stimulation initiates the activation of the adenylate cyclase which catalyses the conversion of adenosine triphosphate (ATP) to the second messenger 3',5' cyclic adenosine monophosphate (cAMP) and pyrophosphate. The increase in cytosolic cAMP concentration activates the cAMP-dependent protein kinase A (PKA), which phosphorylates multiple effector proteins in the cardiomyocyte such as the RyR2, LTCC, cardiac troponin I and PLN at serine 16 (Ser16). Also the activation of the calmodulin-dependent kinase II (CaMKII) leads to PLN phosphorylation at threonine 17 (Thr17). The β -adrenergic stimulation-mediated inhibition of

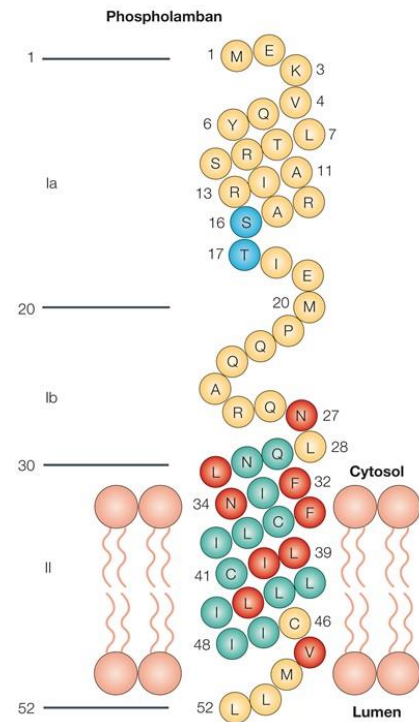


Figure 4: Topology of the monomeric PLN protein (adapted from MacLennan & Kranias 2003).

phospholamban causes a positive inotropic and positive lusitropic effect (Lindemann et al. 1983; Wegener et al. 1989; Talosi et al. 1993; Mundiña-Weilenmann et al. 1996) and is attenuated by the SR-associated protein phosphatase I (PPI) catalysing PLN dephosphorylation (MacDougall et al. 1991).

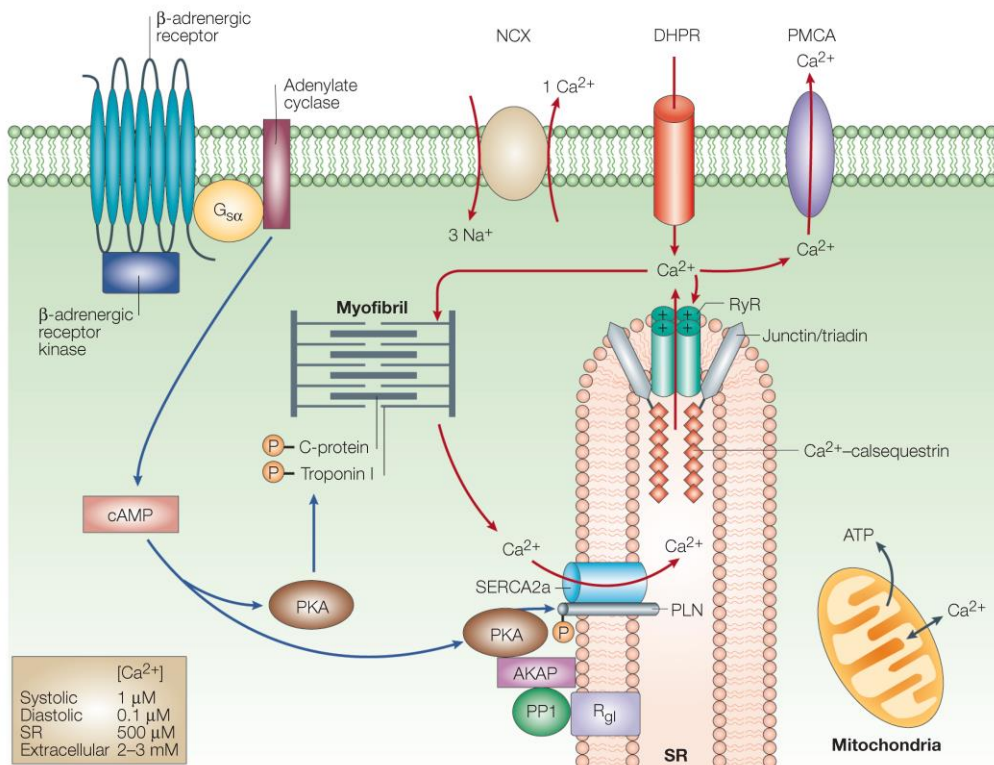


Figure 5: Signalling pathway interactions in the cardiomyocyte. The calcium cycling pathway (red arrows) important for the ECC process is regulated by PKA activated via the β -adrenergic receptor signalling pathway (blue arrows; adapted from MacLennan & Kranias 2003).

1.1.5 *Phospholamban in heart failure*

Animal studies especially in mice revealed important insights into PLN biology in health and disease. It is suggested that the over-expression of wildtype PLN or super-inhibitory PLN variants lead to smaller calcium transients, reduced force and could be associated with a DCM phenotype due to disturbed calcium cycling and homeostasis. Characteristics of super-inhibitory PLN variants (Asn27Ala, Leu37Ala, Ile40Ala and Val49Gly) showed decreased calcium transients and forces with incomplete reversibility in the presence of cAMP/PKA stimulation and cardiomyocyte remodelling (Zhai et al. 2000; Zvaritch et al. 2000; Haghighi et al. 2001; Schmidt et al. 2002; Zhao et al. 2006).

PLN protein expression was reported to be unchanged in heart failure, but due to a reduction of SERCA2a expression a reduced calcium pump activity was detected (Meyer et al. 1995). Additionally, reduced PLN phosphorylation increases SERCA2a inhibition and impairs

calcium cycling. Accordingly, reduced phosphorylation of Ser16, Thr17 or both was reported in heart failure animal models. This resulted in a reduced calcium sensitivity of SERCA2a (Huang et al. 1999; Schwinger et al. 1999; Sande et al. 2002).

To counteract the hyperactive less phosphorylated PLN it was postulated that ablation of the malfunctioning protein could be a therapeutic option against calcium cycling disturbance and heart failure progression. Only very recently, the first low potent PLN inhibitor was found. This pyridone derivate, named compound A, attenuated the PLN inhibitory effect on SERCA2a and has been suggested as a novel therapeutic option enhancing systolic and diastolic heart function *in vivo* and *in vitro* (Kaneko et al. 2017). Given the lack of potent PLN inhibitors, cardiomyopathy mouse models were investigated with promising results representing SR calcium cycling improvements under PLN ablation (Minamisawa et al. 1999; Freeman et al. 2001; Sato et al. 2001). Also, hemodynamic parameter were improved by RNA interference-mediated PLN silencing in a rat heart failure model (Suckau et al. 2009).

Based on these animal studies it was suggested that PLN ablation could slow down or prevent heart failure progression in patients. But the opposite was found after the discovery of the naturally-occurring homozygous PLN p.Leu39stop mutation identified in two patients with DCM and heart failure. The truncated PLN mutant resembles a loss-of-function mutation (PLN null) leading to an early-onset of a DCM phenotype and fast progression of heart failure. These patients needed heart transplantation at the age of 16 and 27 (Haghighi et al. 2003). This is interpreted as an indicator for the substantial differences in calcium cycling physiology between mice and humans. In human ventricular cardiomyocytes about 70% of the calcium is recycled through the SR. The remaining 30% is removed by NCX. The sarcolemmal and mitochondrial calcium uniporter system contributes only minimally. In contrast, in rat and mice 92% is recycled by the SR and only 7% by NCX (Bers 2002). This underlines the importance of humanized disease models to investigate PLN-associated cardiac diseases.

In addition, other PLN gene mutations were identified in patients with familial DCM. In 2003 the arginine 9 to cysteine (PLN p.Arg9Cys) dominant missense mutation was published. Mice expressing this mutation also developed terminal heart failure followed by premature death (Schmitt et al. 2003). It is suggested that this mutation leads to a more efficient formation of PLN-SERCA2a heterodimers, thereby decreasing the calcium re-uptake rate into the SR and impairing calcium cycling homeostasis. This is also assumed for the familial DCM-associated PLN p.Arg14del founder mutation described in detail in the following section (Schmitt et al. 2003; Haghighi et al. 2006).

1.1.6 The PLN p.Arg14del mutation

The heterozygous deletion of the 14th codon (PLN c.40-42delAGA) within the phospholamban coding sequence encoding for the alkaline amino acid arginine (PLN p.Arg14del) was first described in 2006 (Haghighi et al. 2006). This mutation was identified in a large Greek family by genetic screening. Heterozygous individuals developed DCM with diminished ejection fraction ($23\pm 10\%$) and immense interstitial fibrosis as well as myocardial disarray. Patients were suffering from heart failure with cardiac death by middle age. A transgenic mouse model over-expressing the human PLN p.Arg14del mutation replicated the DCM phenotype. The Ca^{2+} uptake rate in HEK293 (human embryonic kidney) cells and cardiac homogenates suggested a super-inhibition of SERCA2a when PLN p.Arg14del and wildtype PLN were co-expressed but not by PLN p.Arg14del alone. Also, PLN pentamer formation seemed to be destabilized (Haghighi et al. 2006). The dependence of the p.Arg14del mutation on the wildtype allele was supported in a follow-up study where PLN p.Arg14del did not show a super-inhibitory effect on Ca^{2+} uptake in a transgenic model expressing PLN p.Arg14del in a PLN null mouse model. Mechanistically, PLN p.Arg14del did not co-immuno-precipitate with SERCA2a but with Na^+/K^+ -ATPase, suggesting that the affinity of PLN p.Arg14del for SERCA2a was reduced and the mutated PLN protein misrouted to the plasma membrane when wildtype PLN is not simultaneously expressed (Haghighi et al. 2012).

It is further suggested that the PKA recognition motif is disrupted by the deletion of the highly conserved amino acid arginine 14, which should have an impact on the phosphorylation of serine 16 due to its positive charge. This would cause a super-inhibitory function of PLN lacking proper β -adrenergic control (Ceholski et al. 2012b).

Clinical data of mutation carriers from 20 families revealed the development of familial DCM with cardiac death between the ages of 26 and 50 years. Low and attenuated R amplitudes were found as an early phenotype in the standard ECGs (electrocardiographs) of adult subjects indicating a remodelling process towards ventricular dysfunction (Posch et al. 2009). The PLN p.Arg14del mutation was also identified in patients suffering from ARVC. In a study of van der Zwaag et al. (2012) the PLN mutation was found to be especially prevalent in the Netherlands. It was identified in 15% of all DCM (39/257) patients and in 12% of ARVC (12/97) subjects appearing to be inherited from a common founder (van der Zwaag et al. 2012; van der Heijden and Hassink 2013; van der Zwaag et al. 2013). In a follow up study it was further stated that PLN p.Arg14del carriers develop malignant ventricular arrhythmias and end-stage heart failure at high risk with poor prognosis and high mortality rates (van Rijsingen et al. 2014).

Histological analysis of heart tissue samples (autopsies and organ explants) from PLN p.Arg14del mutation carriers revealed large perinuclear PLN aggregates in cardiomyocytes, aggresome appearances and evidence for autophagy-mediated PLN aggregate degradation indicating a protein imbalance since autophagy is increasingly activated for clearance of stress-induced aggregates in the pathogenesis of cardiomyopathy (Willis and Patterson 2013; te Rijdt et al. 2016).

To model this mutation in patient-derived human induced pluripotent stem cell-cardiomyocytes (hiPSC-CM) a study was recently published demonstrating correction of PLN p.Arg14del by a TALEN (transcription activator-like effector nucleases) genome editing approach. The study revealed calcium handling abnormalities, electrical instability and abnormal cytoplasmic distribution of PLN in line with a DCM phenotype. However, a higher caffeine response in heterozygous PLN p.Arg14del hiPSC-CM versus isogenic controls was not compatible with PLN p.Arg14del-mediated SERCA2a super-inhibition (Karakikes et al. 2015). Given the key role of PLN at the interplay between calcium homeostasis and force this study was followed by a proof-of-principle study demonstrating weaker force development of heterozygous PLN p.Arg14del hiPSC-CM versus genetically corrected wildtype hiPSC-CM in a three-dimensional human engineered cardiac tissue model (Stillitano et al. 2016). In this publication the morphological characterization of hiPSC-CM revealed a punctuated α -actinin staining pattern suggesting a very immature organisation of myofilament proteins in sarcomeres. This is in contrast to many other human cardiac engineering models which demonstrate three-dimensional networks with aligned cardiomyocytes and advanced sarcomere organization of myofilament proteins (Schaaf et al. 2011; Hinson et al. 2015; Mannhardt et al. 2016). Other limitations include the low numbers of replicates ($n = 3-4$), the restriction to baseline recordings and the lack of paralleled calcium transient analysis.

1.2 Genome editing with the CRISPR/Cas9 system

1.2.1 Principles of the CRISPR/Cas system

The clustered regularly interspaced short palindromic repeats (CRISPR)/CRISPR-associated protein (Cas) system was identified as a RNA-guided adaptive immune response mechanism in many prokaryotes. It is subdivided into the Class 1 (type I, III, IV in which more than one protein is used) and the Class 2 system (Type II, V, VI in which one multi-domain protein is used; Song 2017). The underlying self-defence mechanism protects against invading foreign DNA of virus, bacteriophages or plasmid transfer by cleaving these genetic elements into small fragments.

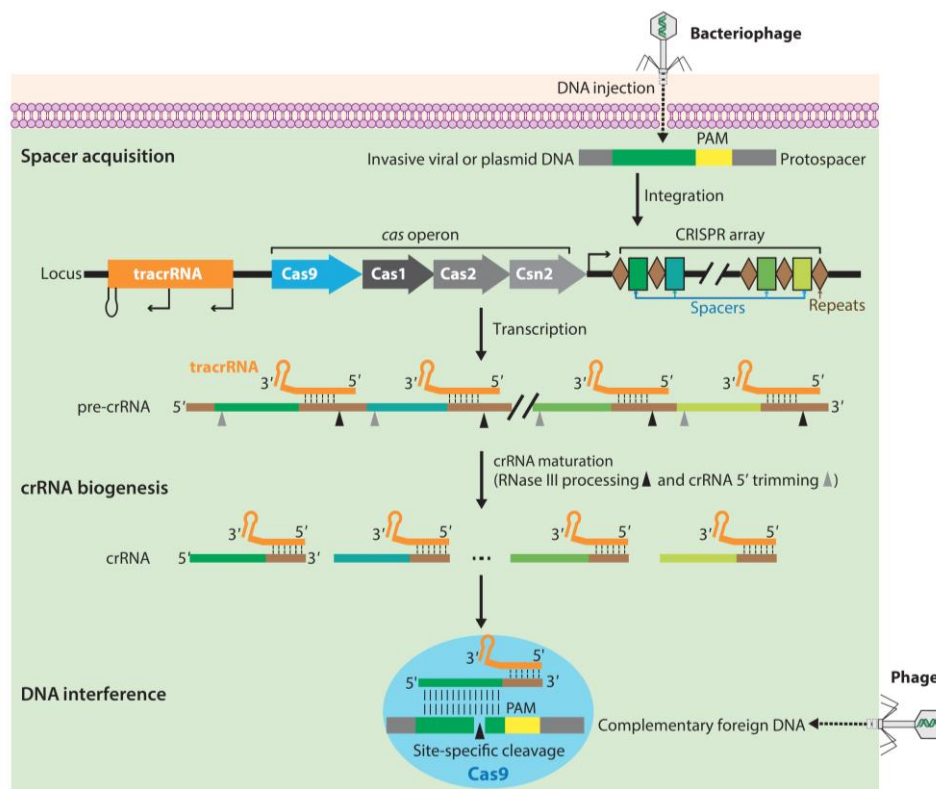


Figure 6: Schematic overview of the CRISPR/Cas system as part of the adaptive immune system of bacteria and archaea. Foreign invasive DNA sequences are integrated into the CRISPR array of the host. These new spacers are transcribed, bound by the *tracrRNA* and processed within the crRNA biogenesis process. The mature crRNA contains the unique sequence of the spacer and complexes with the Cas nuclease to guide the ribonucleoprotein (RNP) complex to the complementary invasive foreign DNA to silence it through cleavage (Jiang and Doudna 2017).

Upon the first infection the invasive foreign genetic element is cleaved and integrated into the bacterial CRISPR array as a new spacer (short non-repetitive sequences) flanked by arrays of repeats (repetitive sequences) as shown in Figure 6. This is supported by the acquisition machinery *Cas1*, *Cas2* and *Csn2*. The CRISPR array, containing all former and the newly

integrated spacers as well as repetitive sequences, is transcribed to the long precursor CRISPR RNA (pre-crRNA). The separately expressed fixed trans-activating crRNA (tracrRNA) binds to the pre-crRNA. This initiates the maturation of the crRNA mediated by RNase III processing and crRNA 5' trimming generating a crRNA guide sequence length of 20 nucleotides (nt). This mature crRNA:tracrRNA heteroduplex forms a ribonucleoprotein (RNP) complex with the Cas9 endonuclease. The RNP complex is guided to the DNA target sequence (protospacer), which is complementary to the 20-nt guide sequence of the crRNA and precedes the protospacer adjacent motif (PAM). The invading foreign DNA is then degraded by the Cas9. This form of prokaryotic adaptive immune system provides a long term immunity preventing a re-infection with the same pathogen (Mei et al. 2016; Jiang and Doudna 2017).

1.2.2 Optimization of the CRISPR system for genome editing of eukaryotic cells

In 2010-2012 first reports about the CRISPR/Cas system as a versatile programmable tool to cut DNA at defined locations in prokaryotes were published (Garneau et al. 2010; Deltcheva et al. 2011; Jinek et al. 2012; Gasiunas et al. 2012). The system was improved and adapted to create an efficient gene editing tool in eukaryotic cells (Cho et al. 2013; Cong et al. 2013; Mali et al. 2013b; Jinek et al. 2013). The CRISPR/Cas system became the third programmable designer nuclease generation after the zinc-finger nucleases (ZFN) and TALEN with the potential advantages of easier customization, increased targeting efficiency and the possibility of multiplex genome editing (Ran et al. 2013b).

To enable precise gene editing at the location of interest the Cas9 endonuclease protein forms a RNP complex with a single guide RNA (sgRNA). The sgRNA is composed of the crRNA for target specificity encoding the 20-nt guide sequence fused to the tracrRNA. By connecting the two RNAs with a linker loop the system was simplified and its utility improved for the laboratory usage (see Figure 7A; Jinek et al. 2012; Cong et al. 2013; Wu et al. 2014). The 20-nt guide sequence of the sgRNA is designed to be complementary to the DNA target sequence and has to precede the PAM. Depending on the chosen Cas9 enzyme derived from different bacterial strains, the PAM nucleotide sequence can vary (summarized in Ran et al. 2013b). The CRISPR/Cas system used in this thesis belongs to the Type II system and is derived from *Streptococcus pyogenes* (Sp). The respective PAM sequence is encoded by a 5'-NGG and recognized by the SpCas9 endonuclease (Jinek et al. 2012). This system is commonly used since on average every 8-12 base pairs (bp), a NGG-PAM can be found in the human genome (Cong et al. 2013; Hsu et al. 2013).

The Cas9 nuclease lobe (NUC) contains the two nuclease domains RuvC and HNH as well as the PAM-interacting (PI) domains (Nishimasu et al. 2014) as schematically shown in Figure 7B. The unique PI domain structure of the Cas9 protein recognizes the PAM

sequence on the non-complementary strand (Hsu et al. 2014). The 20-nt guide RNA unit of the sgRNA forms the gRNA:DNA target sequence hetero-duplex via Watson-Crick base pairing due to its complementarity to the target locus (Nishimasu et al. 2014). These interactions cause the formation of the Cas9-sgRNA-target DNA ternary complex. This initiates the strand-specific blunt cleavage of the complementary DNA strand by the HNH domain and the non-complementary strand by the RuvC domain of the Cas9 nuclease three base pairs upstream of the PAM sequence (Jinek et al. 2012).

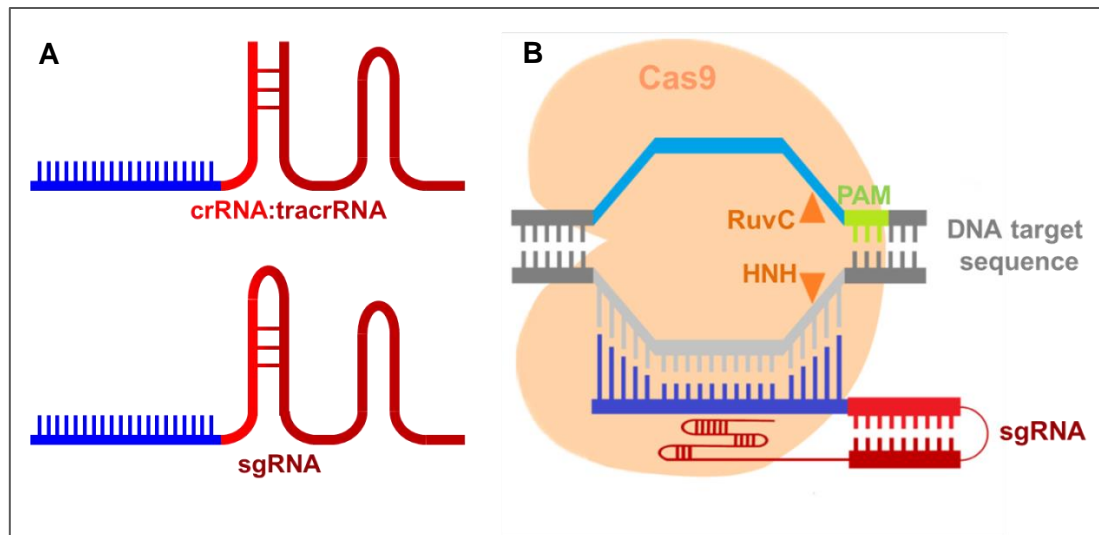


Figure 7: Schematic formation of the sgRNA and the sgRNA:DNA heteroduplex. **A** - The linkage of the crRNA and tracrRNA units generates the sgRNA. The crRNA domain encodes the 20-nt gRNA targeting the DNA locus of interest (blue), thereby determining the target specificity. **B** - sgRNA:DNA hetero-duplex formation after recognition of the PAM sequence (green) on the non-complementary strand initiating the Cas9 mediated double strand cleavage (orange arrows). The complementary strand is blunt cut by the HNH domain and the non-complementary strand by RuvC domain 3 bp 5' of the PAM (adapted from Mei et al. 2016; Kim et al. 2017).

1.2.3 DNA lesion repair via non homology end-joining or homology-directed repair

The induced double strand break (DSB) causes the recruitment of the cell's DNA repair machinery as shown in Figure 8. Two possible pathways can be activated: 1) non homologous end-joining (NHEJ) or 2) homology-directed repair (HDR).

If there is a lack of repair template (e. g. the sister chromatid), the dominant NHEJ pathway is promoted. This mechanism is active throughout the whole cell cycle and re-ligates free ends of broken DNA but with the possibility of creating insertions or deletions (indels) or substitutions at the lesion with efficiencies of 20-60% (Mei et al. 2016). Due to this error-prone machinery e. g. frameshift mutations in coding sequences can cause gene disruption leading to the translation of truncated or non-functional proteins as well as nonsense-

mediated decay of micro-RNAs (miRNA). The induction of the NHEJ pathway is favoured for loss-of-function approaches (reviewed in Kim et al. 2017).

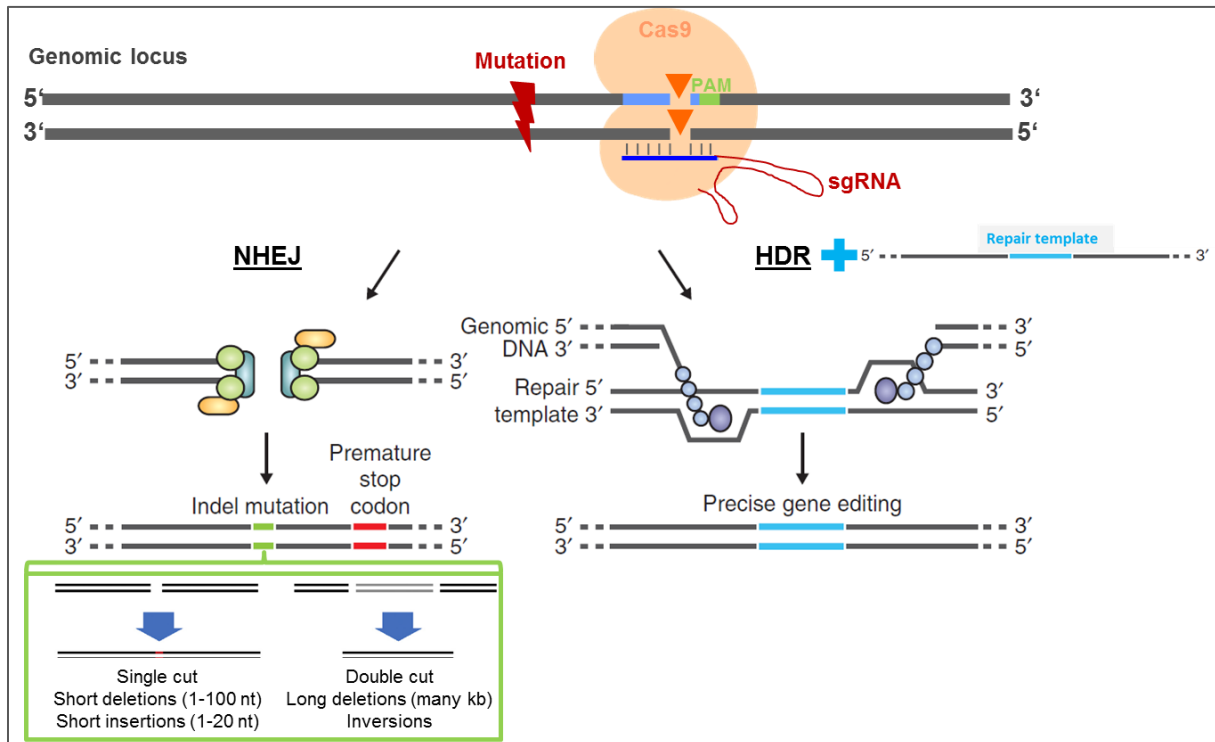


Figure 8: Cas9-mediated double strand cleavage of the genomic locus after sgRNA-mediated guidance to the PAM. Either the NHEJ pathway is activated possibly leading to indels or the HDR machinery is recruited if a repair template is available within the S and G2 phase of the cell cycle (adapted from Ran et al. 2013b; Bassett and Liu 2014).

The HDR machinery is only recruited during the S and G2 phases of the cell cycle. For homologous recombination it uses template DNA, such as single-stranded donor oligonucleotides (ssODN) or double stranded DNA e.g. plasmid targeting vector, for the recombination and repair of the DNA lesion. With this mechanism precise and efficient gene editing is possible or the insertion of an entire transgene.

The repair template can encode new sequences to induce or correct mutations and to insert or delete new DNA sequences into the gene of interest. Depending on the size of the modification ssODN with homology arms of 40-60 nt each can be used or plasmids for multi-kilobase gene replacements. For a plasmid-based repair template approach flanking homology arms of at least 500 bp but up to 2 kb (kilobases) each should be designed for hiPSC genome editing (Hasty et al. 1991; Ran et al. 2013b; Byrne et al. 2014). It is controversially discussed whether the target modification should be flanked 1:1 by homology arms (Ran et al. 2013b) or whether it should be asymmetrically inserted into the repair template for increased HDR frequencies (Richardson et al. 2016).

Pharmacological inhibitors of the NHEJ pathway have been reported to promote HDR over NHEJ such as the small molecule inhibitor SCR7 (Chu et al. 2015; Maruyama et al. 2015). This inhibitor was initially identified as an anti-cancer drug targeting the DNA binding domain of the DNA ligase IV, a NHEJ key enzyme. The effect is transient and reversible since SCR7 binds noncovalent to the ligase subunit (Srivastava et al. 2012). HDR is favoured for gene correction, insertions or replacements. It enables precise gene knockouts, point mutations and gain-of-function mutations. In addition, tags, reporter or selection cassettes can be introduced (Jiang and Doudna 2017).

1.2.4 DNA-based and RNP-based CRISPR/Cas approaches

The editing efficiency and off-target activity is dependent on the Cas9 and sgRNA delivery method which are depicted in Figure 9. Within the DNA-based approach the designed sgRNA can be cloned into a Cas9 expressing vector under a strong promoter (e. g. U6) and easily replaced via restriction digestion for targeting other genomic loci. Selection cassettes encoding fluorophores (green fluorescent protein [GFP]) or antibiotic resistances (puromycin) can also be introduced enabling screening for successfully transfected cells (Ran et al. 2013b). Additionally, multiplex genome editing is feasible with only a single vector encoding more than one sgRNA (Cong et al. 2013; Sakuma et al. 2014). On the other hand plasmids can integrate randomly into the host's genome (stable transfection; Gabriel et al. 2011). DNA transfection is stressful for cells (Sun et al. 2013) and plasmids persist in the cell for a few days after transfection resulting in a prolonged expression of sgRNA and Cas9 which increases the off-target probability (Liang et al. 2015). The delivery of the plasmid can also be difficult in 'hard-to-transfect' cell lines such as human embryonic stem cells (hESC) reducing genome editing frequencies (Kim et al. 2014).

In this context Liang et al. (2015) published that the transfection (via electroporation) and editing efficiency were increased in hiPSC (DNA-based: 20% vs. RNP-based: 87%) and hESC (DNA-based: 8% vs. RNP-based: 64%) by Cas9 RNP approach. Since the sgRNA is complexed with the Cas9 protein before transfection, the RNA is protected in the cell from degradation possibly leading to higher efficiencies. Additionally, Kim et al. (2014) found lower cytotoxic effects of transfected RNPs compared to plasmid-mediated DNA delivery in hESC. Since the transfection of the RNP complex circumvents the transcription and translation the Cas9 nuclease is directly active. After 72 hours the Cas9 is cleared out and not detectable any longer by western blot. This is a potential reason for the lower off/on-target ratio compared to the DNA-based approach (Kim et al. 2014; Liang et al. 2015).

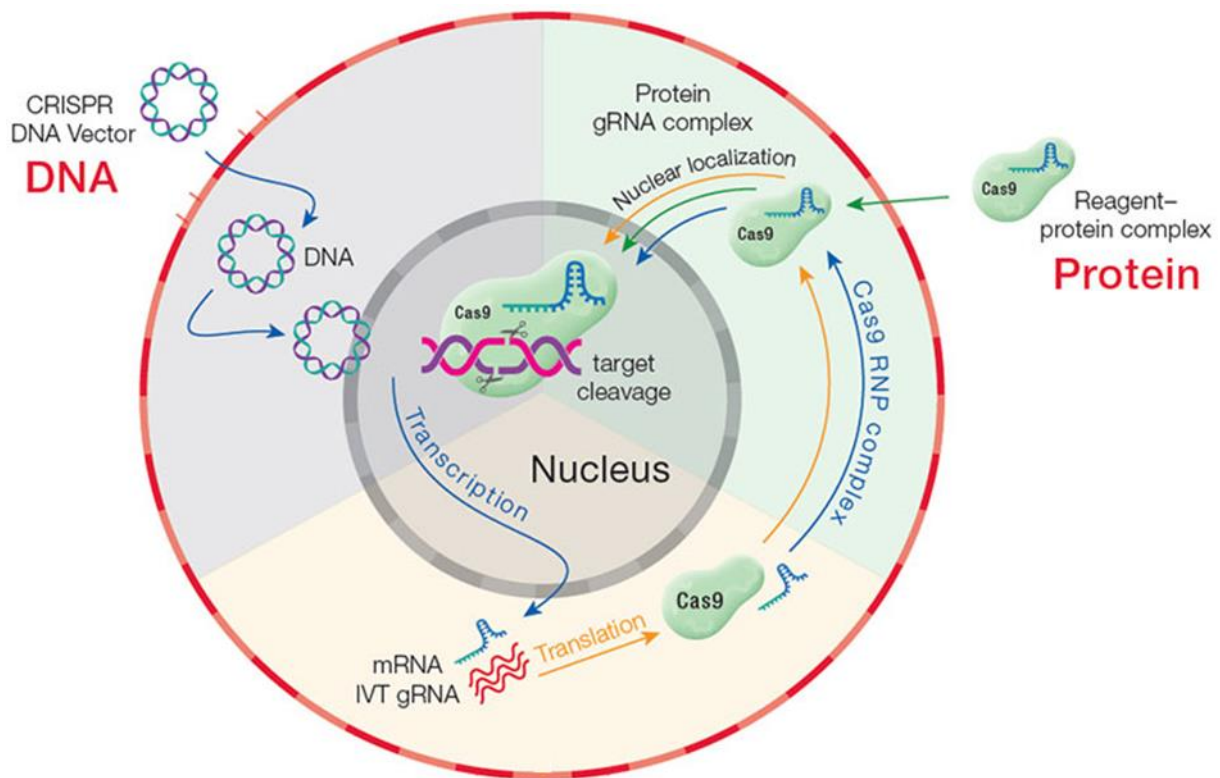


Figure 9: Overview of selected Cas9 delivery methods. The Cas9 gene can be encoded on a DNA vector and nucleofected into the cell. To circumvent the transcription and translation process a directly active Cas9 the ribonucleoprotein complex, in which the sgRNA is already associated to the recombinant Cas9 protein, can be also transfected into the target cell (modified from Thermo Fisher Scientific, 2017 [11:38 am, 11th August 2017]).

1.2.5 Off-target considerations

The 20-nt gRNA sequence of the sgRNA determines the target specificity, but off-target activity of the Cas9 at low frequencies can occur (Jiang et al. 2013; Fu et al. 2013; Hsu et al. 2013; Cradick et al. 2013). Crucial factors are 1) the transfected DNA amounts especially of the Cas9 and the sgRNA:Cas9 relative ratio as well as 2) the number and position of sgRNA-target DNA mismatches.

The Cas9 nuclease does not tolerate more than three base pair mismatches. Besides, PAM-distal mismatches are more tolerated than mismatches proximal to the PAM since specificity is defined by the 8-12 PAM-proximal base pairs (Hsu et al. 2013). PAM recognition is a limiting factor, too, and contributes to off-target effects. Not only 5'-NGG-PAM is recognized by the SpCas9. Also 5'-NAG can be targeted but with only one-fifth efficiency. This should be taken into consideration for the sgRNA and repair template design (Jiang et al. 2013; Hsu et al. 2013; Zhang et al. 2014). There are screening tools available to design and select suitable gRNA sequences and to screen for possible off-target locations in the target genome considering the described parameters for the *in silico* screen (Zhang et al. 2015).

The Cas9 nickase (Cas9n) is a mutated form of the Cas9 nuclease. The endonuclease activity was abolished by the D10A mutation in the RuvC domain or a H847A mutation in the HNH domain. The nickase can thereby only perform a single stranded nick in the DNA. In combination with two separate sgRNAs and a repair template HDR repair process can be initiated. This reduces indel formations and off-target effects by increasing target specificity but with reduced efficiencies (Ran et al. 2013a).

1.2.6 Applications of the CRISPR/Cas system

CRISPR/Cas9 technology became a versatile gene editing tool in many research areas ranging from agriculture and synthetic biology to cancer research, therapeutics and drug target validation as well as gene therapy and disease modelling (Kim et al. 2017).

The combination of the CRISPR/Cas9 system and the hiPSC technology provides a powerful and versatile platform for disease modelling. This combination allows for creating isogenic controls of patient-specific hiPSCs and genetic engineering of wildtype hiPSCs to analyse the effect of specific mutations on a defined genetic background.

1.3 Human induced pluripotent stem cells

1.3.1 Generation and properties of human induced pluripotent stem cells

Stem cells are able to self-renew and differentiate into progeny (Figure 10). They are clustered according to their differentiation potential. Totipotent cells are able to differentiate in all cell types of the organism and extraembryonic syncytiotrophoblast (placenta in mammalian development). Fertilized eggs are totipotent but the totipotency is lost after the first two cell divisions. Pluripotent stem cells can commit to all three germ lines and differentiate into all cell types of an organism: ectoderm, endoderm and mesoderm, but not into the extraembryonic syncytiotrophoblast. Pluripotent stem cells are present in early embryonic development in the inner cell mass at the blastocyst stage of mammalian development. Multipotent stem cells have a more restricted differentiation potential and can only give rise to some cell types of one germ layer e. g. CD34-positive hematopoietic stem cells can differentiate to thrombocytes, granulocytes or erythrocytes. Unipotent stem cells can only give rise to one single differentiated cell type. These include stem cells of the hair follicle, the crypt of the gastrointestinal epithelium or spermatogonial stem cells.

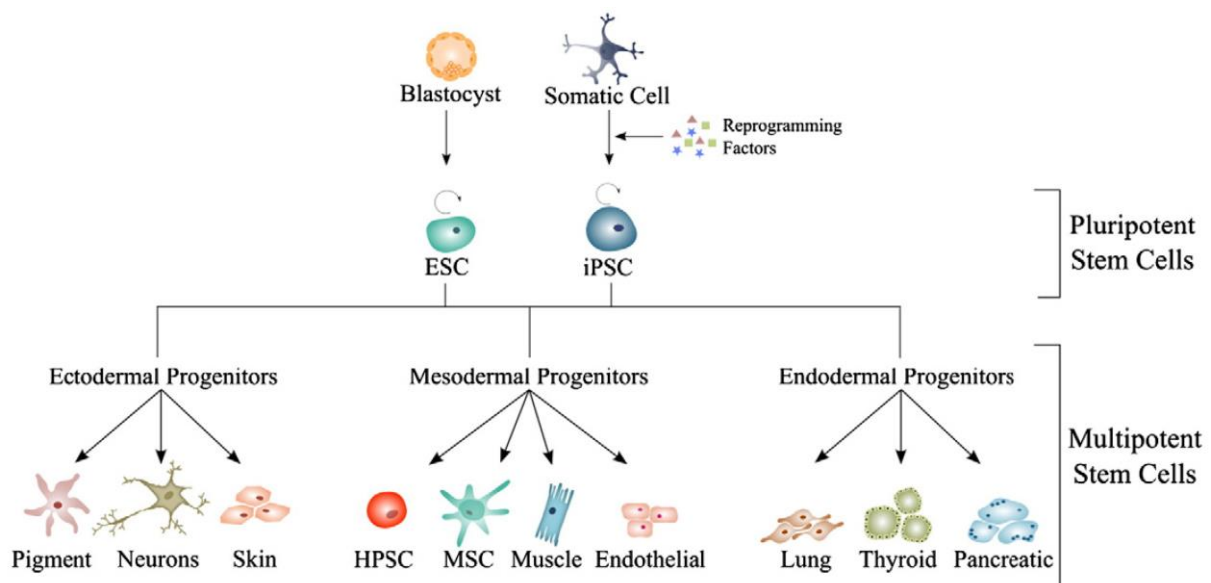


Figure 10: Embryonic (ESC) and induced pluripotent stem cells (iPSC) are pluripotent and can differentiate to ecto-, meso- and endodermal progenitor multipotent stem cells (adapted from Kaebisch et al. 2015).

Given the versatility of pluripotent stem cells for biomedical research protocols to establish and maintain pluripotent stem cells were an important research focus during the last 20 years and two possibilities have evolved.

Embryonic stem cells (ESCs) are derived from the inner cell mass of mammalian blastocysts. These pluripotent cells can differentiate into all cell types of the three germ layers and show

unlimited self-renewal (Martin 1981; Evans and Kaufman 1981). The first human ESC line was produced by outgrowth of the inner cell mass from isolated blastocysts (Thomson et al. 1998). However, the usage of hESC derived from human embryos still causes ethical debates because a human embryo needs to be dissociated. For this reason, in many countries research on hESCs is restricted or forbidden by law.

This issue was circumvented by the revolutionizing technology of the generation of hiPSC, established by Takahashi and Yamanaka in 2006/2007. By a transient ectopic expression of a minimal set of the key transcription factors Klf4 (Kruppel-like factor 4), Sox2 (sex determining region Y-box 2), Oct4 (octamerbinding transcription factor 4) and c-Myc (cellular myelocytomatosis), (KSOM), somatic cells can be reprogrammed to self-renewing cells showing a very early state of embryogenesis. This reprogramming was firstly achieved by retroviral-mediated delivery of the KSOM transcription factor cocktail in mice fibroblasts (Takahashi and Yamanaka 2006), followed by the successful generation of human iPSC from human fibroblasts (Takahashi et al. 2007b). The reprogramming into hiPSC was not only achieved with the KSOM cocktail but also with modified combinations (e.g. SOX2, Oct3/4, Nanog and Lin28, J. Yu et al. 2007). In addition, hiPSC cannot be only generated from skin fibroblasts but also from keratinocytes (Aasen et al. 2008), CD34-positive hematopoietic precursor cells (Loh et al. 2009) and from human peripheral blood-isolated differentiated T-cells (Loh et al. 2010) among other cell types.

The hiPSC are very similar to hESC. They can differentiate *in vitro* and *in vivo* to all cell types of the three germ layers. HiPSC show a similar morphology, proliferation, promotor and telomerase activity, gene expression profile and surface markers as well as teratoma formation and a pluripotent cell-specific gene epigenetic status (Takahashi et al. 2007b). To better standardize hiPSC reprogramming, protocols based on non-integrating viral vectors such as sendai virus were established (Fusaki et al. 2009). Also reprogramming factors could be removed by using the Cre recombinase (Soldner et al. 2009) or piggyback system (Kaji et al. 2009; Woltjen et al. 2009; Yusa et al. 2009). Transfection of episomal vectors (Yu et al. 2009), mRNA (Warren et al. 2010) or protein e. g. by fusion to cell penetrating peptides (Kim et al. 2009) also led to successful reprogramming.

1.3.2 Applications and limitations of human induced pluripotent stem cells

HiPSC technology has the potential to contribute to regenerative approaches by transplanting hiPSC-derived differentiated cells, disease modelling and the development of individualized new treatment approaches as summarized in Figure 11.

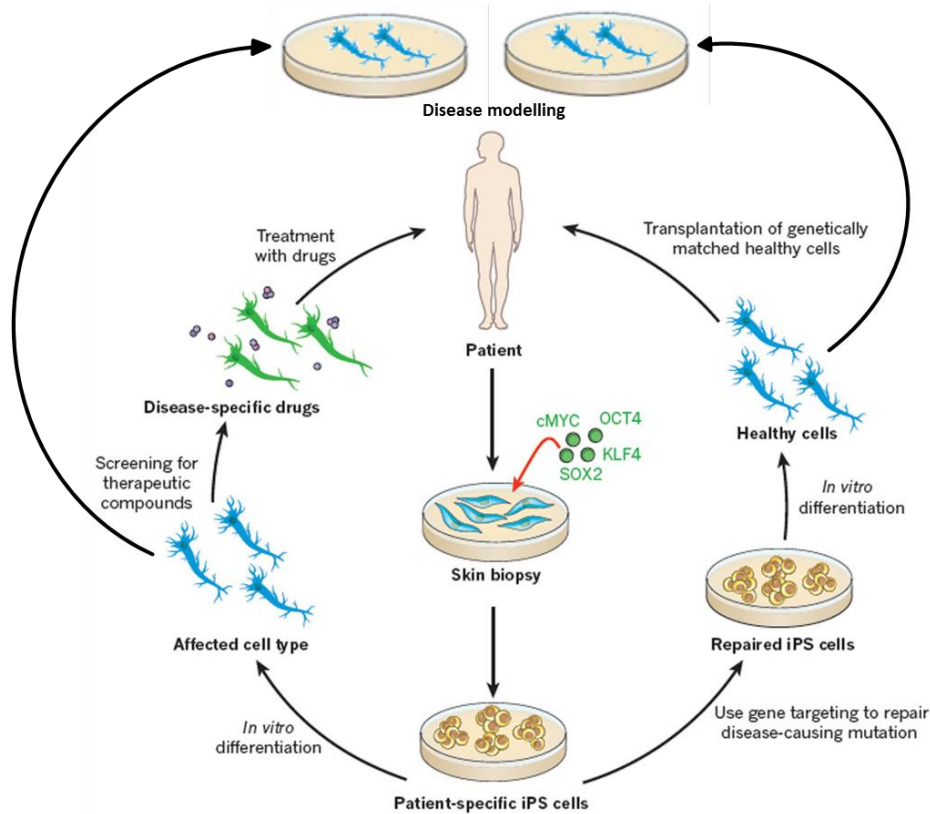


Figure 11: Overview of patient-derived hiPSC applications. Patient's skin fibroblasts can be reprogrammed to patient-specific iPSC with a reprogramming transcription factor cocktail. The hiPSC can be differentiated to a desired cell type, which can then be used for disease modelling and optimizing individual treatment options (left part of the scheme). With gene editing approaches (e.g. CRISPR/Cas9) disease-causing mutations can be repaired. Autologous iPSC could be differentiated into a desired cell type and transplanted back into the patient (right part of the scheme; modified from Robinton and Daley 2012).

The hiPSC technology has the potential to be a powerful addition to the toolset for the disease modelling of genetic diseases. The genome of patient-derived somatic cells carries a disease-associated mutation which is sustained after reprogramming and hiPSC differentiation into the affected cell type. Combined with genome editing approaches, this enables *in vitro* modelling of the 'disease in a dish' to evaluate genetic variations and to clarify the pathological significance as well as the contribution of a mutated gene to the human disease versus isogenic control hiPSCs (Soldner et al. 2011; Soldner and Jaenisch 2012; Li et al. 2015; Stillitano et al. 2016; Lee et al. 2017). Pathological molecular pathways can be discovered and clarified for risk stratification and prediction of disease development.

On the basis of this, treatment options can be tested patient- or mutation-specifically to evaluate suitable drug or gene therapy approaches (summarized by Robinton and Daley 2012; Eschenhagen et al. 2015).

But the field of hiPSC technology also has its limitations. HiPSCs are genetically instable and acquire karyotypic alterations after reprogramming and upon *in vitro* expansion (reviewed in Rebuzzini et al. 2016; Yoshihara et al. 2017). Differentiation of hiPSCs into a defined cell type is difficult and the differentiated cell population is composed of several different cell types and not only the desired one. It is not clear if and how the biology of differentiated cells differs from one lot to the other, between different laboratories and between differentiation protocols. The differentiated cells are immature and often resemble a fetal or neonatal state of human development. The question how to promote further maturation is unanswered for many cell types. The immaturity and thereby compromised functionality of the immature cell type can limit the significance of the results especially if the investigated disease shows an adult/late onset in patients (Forster et al. 2014; Hrvatin et al. 2014; Bedada et al. 2016). The *in vitro* cell cultivation in isolated investigation of single cell types does not reflect the defined composition of different cell types in an organ *in vivo*, which might also restrict the validity of diseases affecting an entire organ. To counteract these issues, co-culture approaches and 3-dimensional (3D) tissue systems are an important research field. This should support the cell's functionality, cell-to-cell interaction and morphology within a more organ-like environment (summarized from Hockemeyer and Jaenisch 2016; Watanabe et al. 2017).

1.4 Cardiomyocyte differentiation

1.4.1 Embryoid body-based cardiac differentiation

HiPSC are capable of *in vitro* differentiation into beating cardiomyocytes (Laflamme et al. 2007; Zhang et al. 2009). This process resembles *in vivo* embryonic heart development (Yang et al. 2008). Accordingly, the protocols for directed cardiac differentiation of hiPSCs replicate mechanisms of early human heart development. An overview is illustrated in Figure 12.

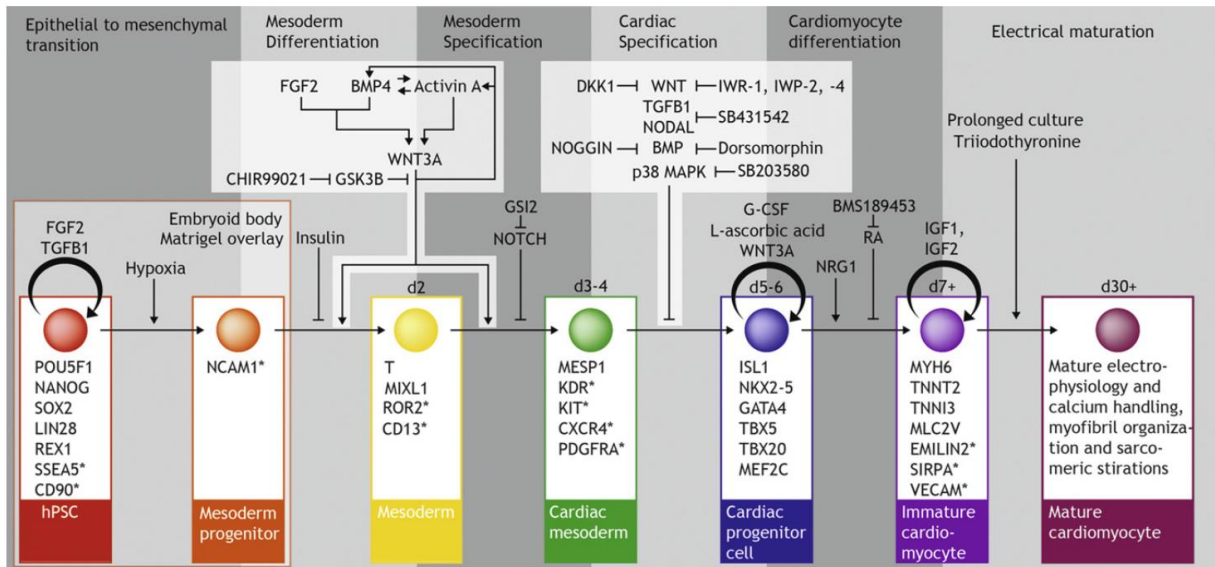


Figure 12: Overview of the cardiomyocyte differentiation cell stages with respective molecular markers and involved signalling pathways (Burrige et al. 2012).

From a biotechnological perspective, the differentiation protocols are subdivided into 2D monolayer- and 3D embryoid body (EB)-based protocols. EBs are 3D aggregates composed of pluripotent stem cells in which hiPSCs spontaneously differentiate into cell types of all three germ layer when factors which support pluripotency are removed. Based on this, directed differentiation protocols were established for the generation of specific cell lineage of the three germ layers (Desbaillets et al. 2000; Itskovitz-Eldor et al. 2000). This method was first applied to murine embryonic stem cells by Wobus et al. (1991) and was transferred to hiPSC differentiation protocols (Haase et al. 2009; Zhang et al. 2009). EB generation is achieved e. g. by suspension culture, hanging-drop formation, by cultivation in round bottom shaped 96-well plates or by incubation in constant-rotating spinner flasks, which especially enable a high scalability and high yields of cardiomyocytes (Kurosawa 2007). 2D protocols are less labour-intensive and difficult to scale-up. 3D protocols require an additional step to generate EBs and are more suitable for scale-up. Towards the end of the differentiation protocol when differentiated cardiomyocytes start to beat spontaneously cell loss due to detachment of beating cell layers represents a substantial problem for 2D approaches but

not for 3D. Also in 2D experiments more specific media compositions are needed and the cardiomyocyte yield is lower but the development of single cells can be closer monitored (Eschenhagen et al. 2015).

Both 2D and 3D approaches rely on the sequential addition of a cocktail of defined growth factors in defined media to induce mesodermal commitment, followed by cardiac specification as shown in Figure 12. Mesodermal differentiation-induction is usually driven by activation of TGF β nodal signalling (bone-morphogenetic protein 4 [BMP4]), activin A and/or WNT-signalling activators (CHIR99021, Gsk3 inhibitor). For cardiac lineage specification, the canonical WNT signalling pathway is inhibited by e.g. IWR-1 (4-(1,3,3a,4,7,7a-hexahydro-1,3-dioxo-4,7-methano-2H-isoindol-2-yl)-N-8-quinolinyl-benzamide; Willems et al. 2011). Successful cardiomyocyte differentiation can be usually detected after 7 days by the on-set of beating of the immature cardiomyocytes.

1.4.2 Maturity of hiPSC-derived cardiomyocytes

HPSC-derived cardiomyocytes show an immature and fetal-like phenotype which is assumed to be similar to human fetal CM at an age of 16-weeks (Chen et al. 1999). They display spontaneous beating, a fetal-like gene-expression profile (Cao et al. 2008), ion channel expression (Beqqali et al. 2006) and electrophysiology (Davis et al. 2011). It is a matter of debate how immature hiPSC-CM can be used as a model system for adult-onset cardiac diseases (Eschenhagen et al. 2015) and it is also a matter of intense research activities to identify procedures to further mature hiPSC-CM. Factors or procedures that have been shown to promote maturation, including long term *in vitro* differentiation and culture (more than 80 days; Lundy et al. 2013), co-cultivation (Tulloch et al. 2011) or electrical or mechanical stimulation (Nunes et al. 2013). Within 3D tissues (which combines cultivation under mechanical load and as a 3D cell network) the maturation state is also less fetal, but still not adult-like (Schaaf et al. 2011; Mannhardt et al. 2016; Uzun et al. 2016; Lemoine et al. 2017). All of these procedures induce only partial degree of maturation and none of them is sufficient to drive maturation to the state of an adult human cardiomyocyte.

1.4.3 Disease modelling with hiPSC-derived cardiomyocytes

HiPSC became a powerful basis for the investigation of cardiac research especially for analysing inherited cardiac diseases on a human-based platform despite their immaturity. Studies on the long-QT syndrome 1 and 2 revealed that ion channel mutation-related arrhythmic disorders (channelopathies) can be modelled since the hiPSC-derived cardiomyocyte's phenotype resembles the corresponding patients clinical data (action potential prolongation, increased arrhythmia risk; Moretti et al. 2010; Itzhaki et al. 2011; Sinnecker et al. 2013).

In 2010 Carvajal-Vergara et al. modelled the LEOPARD syndrome associated with inherited hypertrophic cardiomyopathy in patient-derived hiPSC-CM. This was one of the first studies investigating contractile protein mutation-associated sarcomeric cardiomyopathies showing that also hiPSC-CM depict an enhanced degree of sarcomere organization and increased median surface area (Carvajal-Vergara et al. 2010). A missense mutation in the MYH7 gene (MYH7 p.Arg663His) causing HCM also resembled HCM-related phenotypes (e. g. arrhythmias, delayed after depolarizations, hypercontractile cell function, cell hypertrophy) in hiPSC-CM (Lan et al. 2013).

Also, DCM-defining mutations were modelled with hiPSC-CM. The cardiac troponin T (cTNT p.Arg173Trp) mutation showed disorganized sarcomeres, impairment of SR mediated calcium re-uptake, cardiomyocyte contractility and calcium transients in hiPSC-CM (Sun et al. 2012). Treatment responses for different lamin A/C gene mutations were analysed in hiPSC-CM (Lee et al. 2017) as well as the impact of the PLN p.Arg14del mutation on the patient-specific hiPSC-CM phenotype in comparison to TALEN-generated isogenic controls and miRNA-mediated endogenous PLN knock-down in PLN p.Arg14del carrying cells. Calcium handling abnormalities, disturbed PLN protein distribution, and instability of the electrophysiology as well as induction of hypertrophic molecular markers were detected. This was reversed upon gene-correction and after the miRNA-mediated knock-down of endogenous PLN (Karakikes et al. 2015).

1.5 Engineered heart tissues

In 1994 the first 3D *in vitro* model of a heart muscle was generated. The engineered heart tissue (EHT) was composed of embryonic chicken cells from the heart embedded in collagen I (Eschenhagen et al. 1997). The system was optimized and made compatible with neonatal rat heart cells embedded in Matrigel™ and collagen I and casted to form a circular-shaped muscle. These spontaneously beating EHTs generated force, showed cell-cell interactions and cell orientation along the longitudinal axis of the construct (Zimmermann et al. 2002).

The next round of optimisation led to substantial changes in the EHT generation and analysis protocols (Hansen et al. 2010). The EHT format was miniaturized and thereby optimized for testing in 24-well formats. The format was changed to a strip shape between flexible silicone posts and the extracellular matrix was switched from collagen I to fibrin. The casting molds were generated with Teflon spacers in agarose (Figure 13). The application of fibrinogen together with thrombin leads to faster solidification of the hydrogel scaffold, more homogenous cellular distribution and higher cell survival within the fibrin matrix. The generation of strip-format muscles on silicone posts enables a directed mechanical, auxotonic load improving the EHT development when working against the elastic resistance. The analysis was no longer based on manual transfer to unsterile force transducers, but was based on a sterile and automated video-optical analysis as depicted in Figure 14.

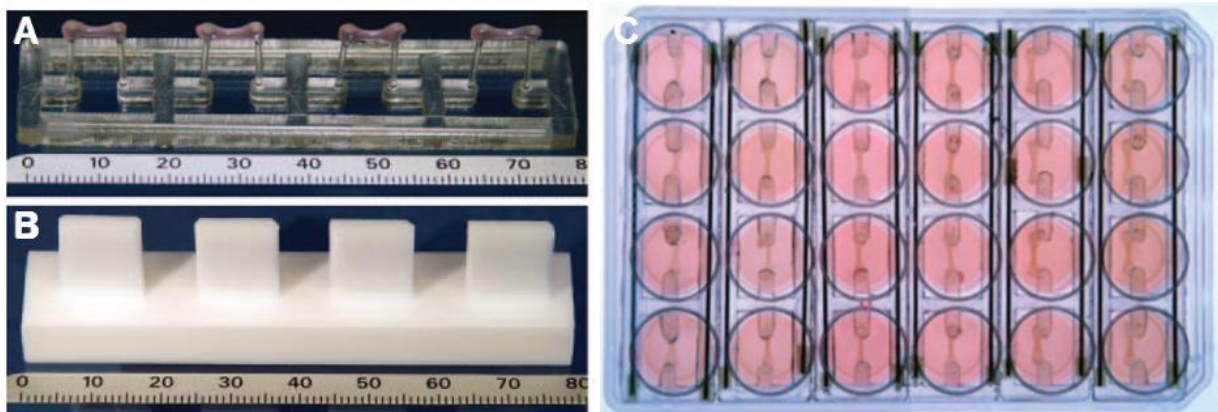


Figure 13: EHT generation. **A** - PDMS (polydimethylsiloxane) rack with four EHTs attached to the pairs of flexible silicone posts. **B** - Teflon spacer (upside down) used for the generation of the EHT casting molds in agarose. Scale in millimetre. **C** - View from above on the EHTs in the 24-well format culture condition (adapted from Hansen et al. 2010).

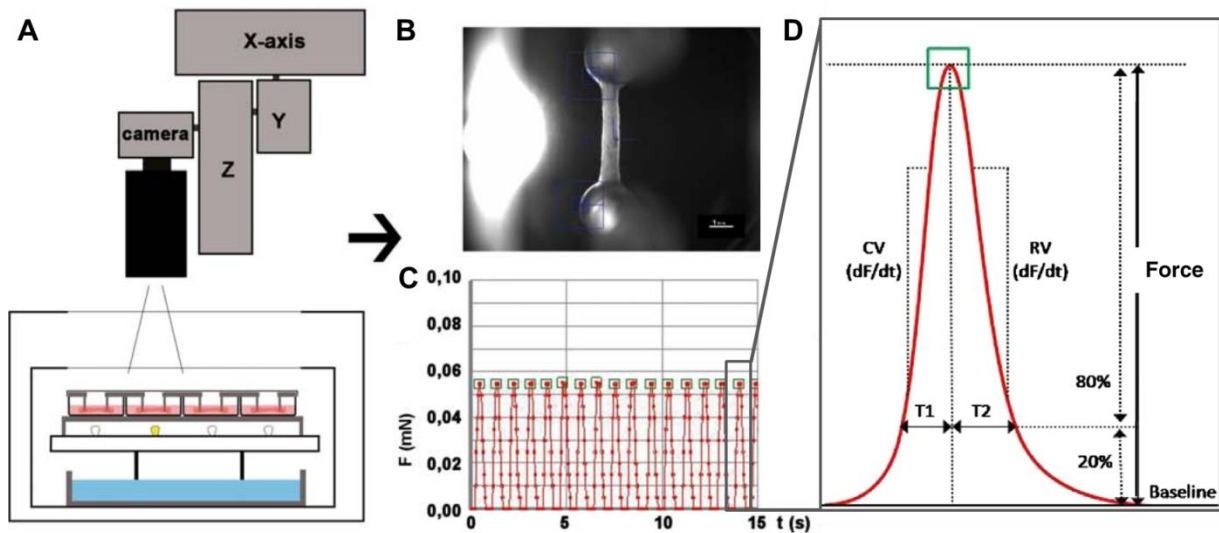


Figure 14: Video-optical recording system. **A** - The EHTs cultivated in a 24-well plate are placed in an incubator chamber with a glass roof. The camera moves along the X-Y-Z axis to each single EHT to measure contractile parameters by video-optical recording. **B** - The customized software recognizes the top and bottom end of the EHT (blue recognition squares) and **C** - calculates the generated force (in millinewton [mN]) over time (in seconds [s]) according to the deflection, geometry and elastic propensity of the PDMS posts. **D** - Contraction peak illustration with respective calculated contractile parameters: T1: contraction time; T2: relaxation time; CV: contraction velocity; RV: relaxation velocity (Modified from Schaaf et al. 2011; Mannhardt et al. 2016; Eder et al. 2016).

In this model the remodelling of the extracellular matrix leads to reduction of both diameter and the total length of the construct. This shortening of the longitudinal axis leads to bending of the flexible silicone posts. Cardiomyocytes align along the force line of the longitudinal axis, intercellular contacts can be detected, and the EHT length as well as diameter decrease (Hansen et al. 2010). The system was further expanded and optimized to generate EHTs also from mouse, hESC and hiPSC (Schaaf et al. 2011; Stoehr et al. 2014; Mannhardt et al 2016). EHTs can be used repeatedly for pharmacological testing to analyse physiological and pharmacological effects (Hansen et al. 2010; Schaaf et al. 2011; Mannhardt et al. 2016; Mannhardt et al. 2017). The use of this humanized 3D model is advantageous to investigate drug safety screenings and drug development because drug effects on force, frequency or influence on beating regularity can be evaluated without bias related to inter-species differences.

2 **AIM OF THE THESIS**

Phospholamban is an important regulator of cardiomyocyte's calcium homeostasis and mutations are associated with the development of cardiomyopathies. Specifically, it was suggested that the PLN p.Arg14del is a DCM-defining mutation based on analyses of familial genetics, biochemical *in vitro* investigations and transgenic mouse models. However, the precise disease defining mechanisms are still unclear, in part because a human *in vitro* disease model did not exist. Therefore the aim of this thesis was the establishment of a human *in vitro* PLN p.Arg14del disease model.

To this end, patient specific fibroblasts carrying PLN p.Arg14del were reprogrammed into hiPSCs. Isogenic controls were generated by establishing, optimizing and applying the DNA- and RNP-based CRISPR/Cas9 technology to enable a seamless gene correction of the PLN p.Arg14del mutation in disease-specific hiPSC. Cardiomyocytes were differentiated from PLN p.Arg14del-mutated and CRISPR-corrected hiPSC with an EB- and growth factor-based three-stage protocol. The human iPSC-CM-based EHT *in vitro* model served as a three-dimensional disease modelling platform. Protocols for the analysis of physiological and pharmacological effects on contractile parameters of isogenic controls compared to PLN p.Arg14del hiPSC-CM were established and optimized to define a disease-specific contractility pattern. Histological and molecular investigations were performed to analyse potential pathological changes. Additionally, monolayer hiPSC-CM were analysed for differences in morphology and calcium-cycling function.

3 MATERIALS AND METHODS

A detailed overview of used materials, reagents and devices can be found in the supplement.

3.1 Media compositions

Table 1: Cell culture media compositions, production and storage details.

Medium	Composition
Fibroblast medium	DMEM 10% (v/v) Fetal calf serum (FCS) 2 mM L-glutamine 0.5% (v/v) Penicillin/streptomycin
Conditioned medium	DMEM/F12 without glutamine 1% (v/v) Non-essential amino acids (NEAA) 1% (v/v) L-glutamine 0.5% (v/v) Penicillin/streptomycin 3.5 µL/500 mL 2-Mercaptoethanol 20% (v/v) Knockout serum replacement 10 ng/mL Basic fibroblast growth factor (bFGF) was added immediately before use on MEFs (mouse embryonic fibroblasts). The MEFs (strain CF-1) were mitotically inactivated with mitomycin C (10 µg/mL, 2.5 hours) and seeded after trypsin dissociation into a 0.1% (w/v) gelatine-coated culture flask with a density of 60,000/cm ² . After 24 hours of cultivation, the culture medium was collected and sterile filtered (0.1 µm filter). Directly before use bFGF (30 ng/mL) was added. This medium was kindly prepared and provided by the HEXT Core Stem Cell Facility (UKE, Hamburg, Germany).
FTDA (bFGF, TGFβ1, dorsomorphin and activin A-based hiPSC culture medium)	DMEM/F12 without glutamine 2 mM L-glutamine 5 mg/L Transferrin 5 µg/L Sodium selenite 0.1% (v/v) Human serum albumin 1/1000 (v/v) Lipid mix 5 mg/L Human recombinant insulin 50 nM Dorsomorphin

	<p>2.5 ng/mL Activin A 0.5 ng/mL Transforming growth factor-β 1 (TGFβ1) 30 ng/mL bFGF 0.5% (v/v) Penicillin/streptomycin (optional)</p> <p>The medium was sterile filtered and stored at 4 °C for up to one week. bFGF was supplemented immediately before usage.</p>
EB formation medium	<p>FTDA 4 mg/mL Polyvinyl alcohol in 1x PBS 10 μM Y-27632</p> <p>The medium was always prepared freshly and sterile filtered.</p>
Mesoderm induction medium	<p>RPMI 1640 4 mg/mL Polyvinyl alcohol 10 mM HEPES (pH 7.4) 0.05% (v/v) Human serum albumin 250 μM Phosphoascorbate 5 mg/L Transferrin 5 μg/L Sodium selenite 1/1000 (v/v) Lipid mix 10 μM Y-27632 3 ng/mL Activin-A 10 ng/mL BMP-4 5 ng/mL bFGF</p> <p>The medium was filter sterilized (0.2 μm filter) and stored at 4°C for up to 1 week without growth factors. 30 ng/mL bFGF was additionally supplemented immediately before usage.</p>
Mesoderm induction washing medium	<p>RPMI 1640 10 mM HEPES 4 mg/mL Polyvinyl alcohol 0.5-1% (v/v) Penicillin/streptomycin (optional)</p>
Cardiac specification washing medium	<p>RPMI 1640 10 mM HEPES (pH 7.4) 0.5% (v/v) Penicillin/streptomycin</p>

Cardiac specification medium I	<p>RPMI 1640</p> <p>5 mg/L Transferrin</p> <p>5 µg/L Sodium selenite</p> <p>0.5% (v/v) Penicillin/streptomycin</p> <p>250 µM Phosphoascorbate</p> <p>1/1000 (v/v) Lipid mix</p> <p>1 µM Y-27632</p> <p>1 µM XAV-939 or 100 nM DS-I-7</p> <p>10 mM HEPES</p> <p>Human serum albumin</p> <ul style="list-style-type: none"> → <u>For cEB-based protocol:</u> + 0.05% (v/v) Human serum albumin → <u>For monolayer-based protocol:</u> + 0.005% (v/v) Human serum albumin <p>The medium was filter sterilized (0.2 µm filter) and stored at 4°C for up to 1 week without XAV-939/DS-I-7, which was added freshly before usage.</p>
Cardiac specification medium II	<p>RPMI 1640</p> <p>500 µM 1-Thioglycerol</p> <p>10 mM HEPES (pH 7.4)</p> <p>0.5% (v/v) Penicillin/streptomycin</p> <p>1 µM Y-27632</p> <p>2% (v/v) B27 with insulin</p> <p>1 µM XAV-939 or 100 nM DS-I-7</p> <p>The medium was filter sterilized (0.2 µm filter) and stored at 4°C for up to 1 week without B27 and XAV-939 /DS-I-7, which was added freshly before usage.</p>
Cardiac specification medium III	<p>RPMI 1640</p> <p>500 µM 1-Thioglycerol</p> <p>10 mM HEPES</p> <p>0.5% (v/v) Penicillin/streptomycin</p> <p>1 µM Y-27632</p> <p>2% (v/v) B27 with insulin</p> <p>The medium was filter sterilized (0.2 µm filter) and stored at 4°C for up to 1 week without B27, which was added freshly.</p>

EHT casting medium	DMEM 1% (v/v) Penicillin/streptomycin 10% (v/v) Fetal calf serum (FCS), heat inactivated 2 mM L-glutamine The medium was filter sterilized (0.2 µm filter) and stored at 4°C up to one month.
Cardiomyocyte culture medium (for monolayer and EHT)	DMEM 10% (v/v) Horse serum 1% (v/v) Penicillin/streptomycin 10 µg/mL Human recombinant insulin 33 µg/mL Aprotinin The medium was always freshly prepared on feeding days.

3.2 Cell culture of human induced pluripotent stem cells

3.2.1 Fibroblast reprogramming to hiPSC

The PLN p.Arg14del mutation carrier was recruited with diagnosed familial DCM. Skin biopsies were taken under local anaesthesia after signature of informed consent and shipped from Amsterdam (Dr. Ingrid van Rijsingen and Prof. Dr. Yigal Pinto, AMC, Amsterdam, the Netherlands). The skin sample was washed in 1x PBS and placed in a 6-well plate in fibroblast medium. The dermal fibroblasts grew out of the explant and were collected for further passaging, freezing and reprogramming at passage 5.

The fibroblasts were transduced with reprogramming factors by lentiviral particles. Five days after transduction the cells were harvested by trypsinization and re-plated at 8×10^4 cells/10 cm² in Matrigel™-coated (growth-factor reduced, BD Biosciences) 6-well culture plates. The following day the fibroblast medium was replaced by conditioned medium (10 ng/mL bFGF) with consecutive daily medium change. HiPSC clones were picked and transferred to Matrigel™-coated 24-well plates about 4 weeks after transduction and further expanded and cultured using the standard procedure. The unrelated control hiPSC line was reprogrammed by Prof. Dr. Alessandra Moretti (Technical University of Munich, Germany) as previously described (Moretti et al. 2010). The PLN p.Arg14del fibroblast reprogramming was performed by the HEXT Core Stem Cell Facility (UKE, Hamburg, Germany) according to Takahashi et al. (2007a, b) and Ohnuki et al. (2009).

Table 2: Overview of the used reprogrammed cell lines. OSK = Oct4, SOX2, KLF4; M-c = c-MYC; p53sh = p53shRNA; DCM = dilated cardiomyopathy.

Cell line	Clone number	Reprogramming method	Reprogramming factor	Phenotype	Sex
Unrelated control	---	Lenti-/retroviral	OSK M-c	Wildtype	Female
PLN p.Arg14del	#1198	Lenti-/retroviral	OSK G +p53sh	DCM	Female
	#1201	Lenti-/retroviral	OSK G +p53sh	DCM	Female

3.2.2 Immunofluorescence staining of pluripotency markers in hiPSC

HiPSCs were rinsed briefly in 1x PBS and fixed for 15 minutes (min) with 4% paraformaldehyde at room temperature. Following this, the cell layer was washed three times with 1x PBS á 5 min and incubated in blocking solution for 1 hour at room temperature. The primary antibody (Oct-4A or TRA-1-60(S) [Cell Signaling], 1:200 in antibody dilution buffer) was applied and incubated over night at 4 °C in a humidity chamber. The following day the cells were again washed three times with 1x PBS and incubated for 1 hour at room temperature with the secondary antibody (Alexa Fluor 546 goat anti-rabbit IgG, 1:500 in antibody dilution buffer or Alexa Fluor 488 goat anti-Mouse IgM μ chain, 1:500 in antibody dilution buffer, Molecular Probes Invitrogen) and DAPI for nuclear staining. After the final three PBS washing steps the cells were mounted, analysed and stored at 4 °C in the dark. This procedure was kindly performed by the HEXT Core Stem Cell Facility (UKE, Hamburg, Germany).

3.2.3 Karyotyping

HiPSC clones were cultured in conditioned medium until 80% confluency at 37°C, 20% O₂ and transferred to the Department of Human Genetics (UKE, Hamburg, Germany) for karyotype analysis as quality control. Karyotype analysis was performed as recently published (Breckwoldt et al. 2017).

3.2.4 HiPSC culture and expansion

The cultivation of the hiPSC was done in FTDA (Frank et al. 2012). HiPSC density and morphology was checked daily. After reaching 80-100% confluency hiPSC were passaged twice a week with a 1:3 - 1:6 split ratio. For this cell culture medium, 1x PBS, EDTA solution (0.5 mM) and Accutase® were pre-warmed at 37 °C. For passaging the medium was removed and hiPSCs were washed twice with 1x PBS before adding 1 mL/10 cm² EDTA solution or Accutase® supplemented with 10 μ M Y-27632. After 5-10 min of incubation at

room temperature EDTA was removed and the hiPSCs were detached by squirting thoroughly with medium. After 10-15 min of Accutase® incubation at 37 °C the reaction was stopped by adding the same volume of medium and pipetted up and down twice. The dissociated hiPSC suspension was centrifuged at 110xg for 2-4 min and the cell pellet was re-suspended in medium. Cell culture dishes were coated with Geltrex® (1:100-1:200, diluted in DMEM, 1 mL/10 cm²) and incubated for at least 30 min at 37 °C. Before hiPSC seeding the liquid phase of Geltrex® was removed and the cells were distributed according to the determined split ratio. The hiPSC were incubated at 37 °C, 20% O₂, 90% humidity, 5% CO₂. For Accutase®-dissociated cells 10 µM Y-27632 was added to the medium for 24 hours after passaging.

Medium was changed daily with a minimum of 16 mL of pre-warmed FTDA per T75 flask and 2 mL FTDA per 6-well. The medium amount was adjusted to the increasing cell confluency (maximum 30 mL/T75-flask and 4 mL/6-well).

The hiPSC culture procedures were kindly supported by Thomas Schulze and Birgit Klampe (DEPT, UKE, Hamburg, Germany).

3.2.5 Freezing and thawing of hiPSC

After dissociation of confluent hiPSC monolayer with EDTA cells were re-suspended in 700 µL of plating medium (conditioned medium or FTDA) per one well of the 6-well plate. Directly before freezing the cell suspension was mixed 1:1 with either 2x FTDA-freezing medium (80% FTDA [v/v], 20% DMSO [v/v]) or 2x conditioned medium-freezing medium (60% FCS [v/v], 20% conditioned medium [v/v], 20% DMSO [v/v]). The hiPSCs were transferred into a cryovial and frozen down at -80°C in isopropanol container (Mr. Frosty) for the first 24 hours before being transferred to -150°C for long-term storage.

For thawing the cryovial was removed from -150 °C storage and thawed by hand for 2-3 min. The cell suspension was transferred to a 15 mL falcon tube using a 2-mL serological pipette. The empty cryovial was rinsed with 1 mL of plating medium (conditioned medium or FTDA) which was added drop-wise to the cell suspension under gentle swirling of the tube. Then, additional 5 mL of plating medium was added drop-wise. After centrifugation for 5 min at 100xg the supernatant was discarded and the cell pellet re-suspended in 2 mL of plating medium supplemented with Y-27632 and seeded into a Geltrex®-coated well of a 6-well plate.

3.2.6 Mycoplasma test and treatment

Cell culture medium supernatant (250 µL) from a 80-100% confluent cell culture plate was transferred to a sterile Eppendorf tube. 750 µL of water was added and mixed. The sample was incubated for 10 min at 100 °C and shortly centrifuged. 2 µL of the supernatant was

added to the PCR master mix (Table 3). Additionally, a positive and negative control sample was included. The PCR program was immediately started (Table 4).

The PCR products were analysed on a 1% (w/v) agarose gel. In case of positive results hiPSC lines were discarded or treated with BIOMYC antibiotics (PromoCell) by sequential treatment with BIOMYC-1 for 4 days and BIOMYC-2 for 3 days. Mycoplasma were eliminated after 2 treatment cycles.

Table 3: Mycoplasma detection PCR reaction with the Taq-DNA polymerase kit.

Substance	1x
10x Buffer	5.0 µL
Q-Solution	10.0 µL
MgCl ₂ (25mM)	4.0 µL
Primerpool (10 pM) Myco-Fw	1.0 µL
Primerpool (10 pM) Myco-Rev	1.0 µL
dNTPs	1.0 µL
Taq-DNA polymerase	0.25 µL
DNA sample	2.0 µL
Nuclease-free water	ad 50 µL

Table 4: PCR programme for mycoplasma DNA locus amplification.

Temperature	Time
95 °C	15 min
94 °C	30 sec
56 °C	30 sec
72 °C	1 min
72 °C	10 min

} 40x

Mycoplasma tests were kindly performed by June Uebeler and Thomas Schulze (DEPT, UKE, Hamburg, Germany).

3.3 CRISPR/Cas9-mediated gene editing of hiPSC

3.3.1 Validation of the PLN target sequence

a) **Amplification of the PLN target sequence**

Genomic DNA was isolated from PLN p.Arg14del #1198 hiPSC clone using the 'DNeasy® Blood & Tissue Kit' (Qiagen) according to the manufacturer's instructions. In order to validate the target gene locus primers (hPLN-1.3 kB-Fw and --Rev) were designed according to the PLN sequence provided by NCBI (NCBI Reference Sequence: NG_009082.1; Gene ID: 5350; NG_009082.1:3178-18967 Homo sapiens phospholamban [PLN], RefSeqGene [LRG_390] on chromosome 6) to perform a touchdown PCR with PrimeSTAR polymerase for hPLN sequence amplification (see Tables 5 and 6).

Table 5: PrimeSTAR PCR reaction.

Substance	1x
5x PrimeSTAR buffer	10 µL
2.5 mM dNTPs	4 µL
Primer hPLN-1.3 kB-Fw (10 µM)	0.5 µL
Primer hPLN-1.3 kB-Rev (10 µM)	0.5 µL
DMSO	1 µL
PrimeSTAR (1 kb/min) DNA polymerase	0.5 µL
Genomic DNA	25 ng
Nuclease-free water	ad 50 µL

Table 6: Touchdown PCR program.

Temperature	Time	
98 °C	10 sec	} 13x; * 0.5 °C step/cycle
63 °C *	30 sec	
72 °C	1 min 30 sec	
98 °C	10 sec	} 24x
57 °C	30 sec	
72 °C	1 min 30 sec	
72 °C	7 min	
4 °C	∞	

The quality of the PCR product with a fragment size of ~1.3 kB was analysed using an 1% (w/v) agarose gel, GeneRuler 1 kb DNA Ladder, 10 µL PCR product and 6x DNA loading

dye. The 'QIAquick® PCR purification kit' (Qiagen) was used to clean up the remaining PCR product. The DNA concentration of the 30 µL eluate was measured using NanoDrop.

b) Cloning of the PLN target sequence

The 'CloneJET PCR cloning kit' (Thermo Fisher Scientific) was used for the ligation of the 1.3 kB PLN PCR product into the pJET1.2/blunt cloning vector.

Table 7: Ligation protocol.

Substance	1x
2x Reaction buffer	10 µL
pJET1.2/Blunt cloning vector (50 ng/µL)	1 µL
T4 DNA ligase (5 U/µL)	1 µL
hPLN PCR product	50 ng
Nuclease-free water	ad 20 µL

The ligation mixture (Table 7) was incubated for 5 min at room temperature. 3 µL of ligation product was used for transformation of 40 µL TOP10 cells which were then incubated for 30 min on ice. The TOP10 cells were kindly provided by Alexandra Löser (DEPT, UKE, Hamburg, Germany). After heat shock for 45 sec at 42 °C the cells were incubated on ice for 5 min. 200 µL SOC medium was added per sample and cells were incubated for 1 hour at 37 °C under shaking at 170 rpm. Bacteria were plated on agar plates containing 0.1 mg/mL ampicillin and incubated at 37 °C over night.

Grown colonies were picked individually into 5 mL LB (lysogeny broth) medium containing 0.1 mg/mL ampicillin and incubated for 14-16 hours at 37 °C under shaking (220 rpm). 'NucleoSpin® Plasmid' kit (Macherey/Nagel) was used to isolate plasmid DNA. DNA concentration of each clone was measured with NanoDrop and sent for sequencing to Eurofins MWG Operon with the forward and reverse pJET1.2 primer.

c) Evaluation of the PLN target sequence

The sequencing result of 10 clones were aligned to the NCBI PLN wildtype sequence using the SnapGene software and checked for PLN c.40-42del mutation and single nucleotide polymorphism (SNP) occurrence.

3.3.2 Design of the CRISPR/Cas9 experiment

a) *In silico* sgRNA design

Cas enzymes are available from different bacteria and recognizing different PAM (Ran et al. 2013b). For the CRISPR/Cas-mediated gene editing of the PLN c.40-42del in hiPSCs the CRISPR/Cas9 system derived from *Streptococcus pyogenes* (Sp) was used because this

had been the best characterized system then. The protocol was established in accordance to Ran et al. (2013b).

The online CRISPR design tool provided by the Zhang lab (MIT, 2015; <http://crispr.mit.edu>) was applied for the *in silico* identification of suitable custom gRNAs for genomic sequences of interest (Ran et al. 2013b). The mutated PLN c.40-42AGAdel sequence obtained from the sequencing results was used as DNA target region, and the human genome was chosen as target genome to enable the genome wide screening for off-target matches. The software algorithm scans the target sequence for possible gRNAs preceding NGG PAM sequences. The result file provides the best 20-nt long gRNAs ranked according to their quality score with 100 being the maximum value as an indicator for target specificity and on-target activity. In addition, off-targets also have a substantial impact on the score quality. The 20 most likely off-targets for each gRNA were also provided for further analysis.

The gRNAs with the best quality scores were chosen and aligned to the target sequence. The web-based online tool of the Zhang lab stated that the most suitable gRNAs was a compromise between its score, and the proximity between the binding site and gene editing locus. The gRNA should target as close as possible to the target region to increase recombination success and probability. Also, the number of off-targets should be as low as possible especially the number of exonic off-target sequences.

b) *In silico* repair template design

The repair template was designed as single stranded oligonucleotide (ssODN) with a total length of 103 nt and according to the PLN wildtype sequence since it encodes the missing AGA codon (PLN c.40-42). The fully designed repair template was ordered in an antisense direction as a 4 nmole Ultramer® DNA Oligo with standard desalting purification from Integrated DNA Technologies (IDT). A 100 µM stock was prepared with nuclease-free water.

3.3.3 Preparation of the DNA-based CRISPR approach

To facilitate cloning of the designed 20-nt long sgRNA into the pSpCas9(BB)-2A-GFP vector (Addgene, plasmid ID: 48138; Ran et al. 2013b) overhangs were designed to enable the insertion of the sgRNA into the BbsI restricted vector as shown in small underlined letters in Figure 15A. In addition, a guanine (bold black capital letter) was added to the 5' end of the sense guide oligo in order to increase RNA polymerase III efficiency (Mali et al. 2013a).

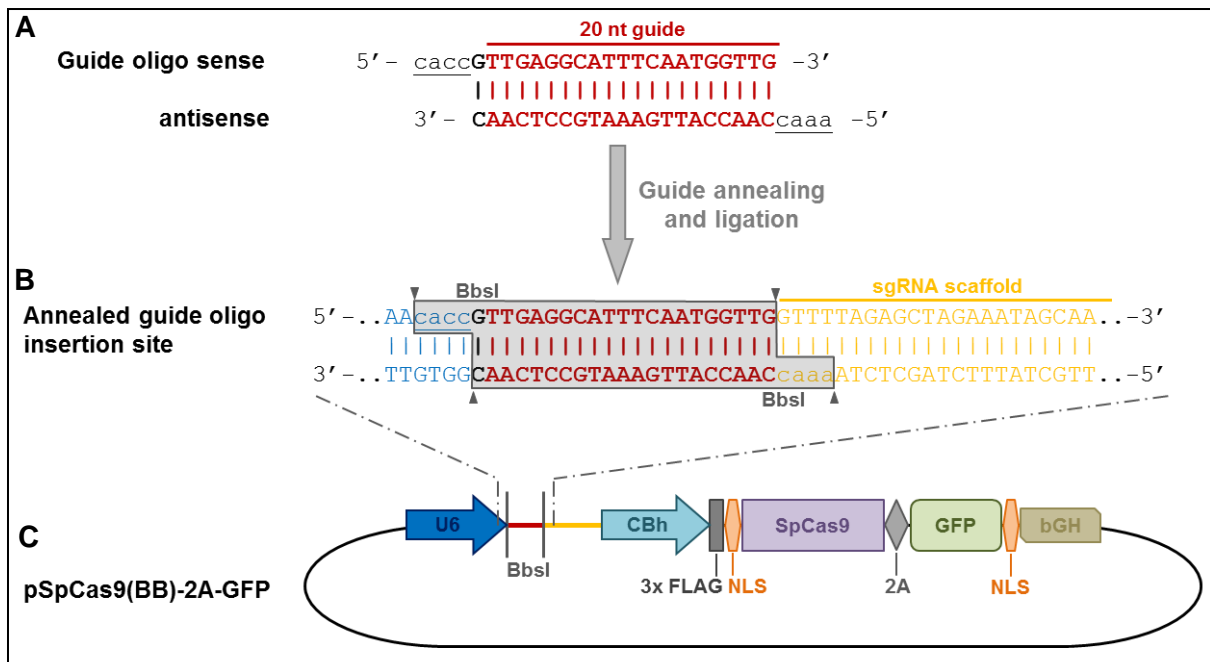


Figure 15: Cloning of the sgRNA-DNA oligo into the pSpCas9(BB)-2A-GFP vector.
A - Design of the sgRNA with addition of 5'-G (black bold) and overhangs for BbsI cloning (small underlined letters). **B** - Ligation of the annealed sense and antisense guide strands into the insertion site between U6 promoter and sgRNA scaffold after BbsI restriction digestion. **C** - Cloning site of the annealed guide oligo of the pSpCas9(BB)-2A-GFP vector (adapted from Ran et al. 2013b).

Lyophilised DNA oligomers were reconstituted in nuclease-free water setting a stock concentration of 1000 μ M. To anneal the sense and antisense DNA oligomers the annealing reaction was prepared (Table 8 and 9).

Table 8: Preparation of 10x annealing buffer.

Substance	10x
100 mM TRIS-HCl (pH 8)	1 mL of 1 M stock
500 mM NaCl	1 mL of 5 M stock
10 mM EDTA	0.2 mL of 0.5 M stock
Nuclease-free water	Ad 10 mL

Table 9: DNA oligomer annealing approach.

Substance	Volume
gRNA DNA oligo sense (200 μ M)	4 μ L
gRNA DNA oligo antisense (200 μ M)	4 μ L
10x Annealing buffer	2 μ L
Nuclease-free water	ad 20 μ L

This mixture was incubated at 95 °C in a thermo block for 5 min. The device was then turned off and the sample was remaining in the thermo block to achieve gradual cool down for another hour. The concentration of the annealed oligomers was measured by NanoDrop (target concentration: ~4500 ng/μL).

The pSpCas9(BB)-2A-GFP plasmid was linearized by restriction digest with BbsI. The digestion reaction was prepared according to Table 10 and incubated at 37 °C for 30 min.

Table 10: BbsI restriction digest approach for the linearization of pSpCas9(BB)-2A-GFP plasmid.

Substance	1x
10x Fast digest (FD)-Buffer	4 μL
BbsI restriction enzyme	2 μL
pSpCas9(BB)-2A-GFP plasmid	2.5 μg
Nuclease-free water	ad 40 μL

The linearized plasmid was detected on a 1% (w/v) agarose gel with a size of 9281 bp. The DNA was extracted and purified with the 'QIAquick® Gel Extraction Kit' (Qiagen) and the concentration was analysed with NanoDrop.

The ligation approach was calculated with the NEB (NewEngland Biolabs) ligation calculator. The ligation mix was prepared according to Table 11 and incubated for 30 min at room temperature.

Table 11: Ligation approach using the 'Rapid DNA Ligation Kit' (Thermo Fisher Scientific).

Substance	vector:insert 1:5	Religation Ctrl
pSpCas9(BB)-2A-GFP (50 ng)	1 μL	1 μL
Annealed gRNA-DNA oligo	673.4 pg	----
T4 DNA ligase	0.5 μL	0.5 μL
10x T4 DNA ligase buffer	2 μL	2 μL
Nuclease-free water	ad 20 μL	ad 20 μL

Transformation of TOP10 cells with the ligation product, picking of clones and DNA isolation was performed as already described. For the DNA isolation 3 mL of the cell suspension was used from the inoculated LB medium. The remaining suspension was stored at 4 °C. DNA of at least two clones was sent for sequencing with 'U6-Forward' primer (Ran et al. 2013b) to Eurofins MWG Operon.

Table 12: Primer annealing solution.

Substance	
T7-gRNA-Forward (10 μ M)	10 μ L
T7-gRNA-Reverse (10 μ M)	12 μ L
5x High fidelity Phusion buffer	20 μ L
10 mM dNTPs	2 μ L
Nuclease-free water	55 μ L

To amplify the annealed sgDNA product an extension PCR shown in Table 13 and Table 14 was performed with the IVT-Forward and IVT-Reverse primer (see Figure 16).

Table 13: Extension PCR of the annealed sgDNA.

Substance	1x
5x High fidelity Phusion buffer	10 μ L
10 mM dNTPs	1 μ L
Primer IVT-Forward (10 μ M)	2.5 μ L
Primer IVT-Reverse (10 μ M)	2.5 μ L
Phusion DNA polymerase	0.5 μ L
Annealed sgDNA	2 μ L
Nuclease-free water	31.5 μ L

Table 14: PCR programme of the extension PCR.

Temperature	Time
98 °C	1 min
95 °C	30 sec
64 °C	30 sec
72 °C	30 sec
72 °C	10 min
4 °C	∞

} 35x

The PCR product was analysed via 2% (w/v) agarose gel electrophoresis and purified with the 'QIAquick® PCR purification' kit. DNA concentration was determined with the NanoDrop. The sgDNA was sent for sequencing to Eurofins MWG Operon with both IVT-Forward and IVT-Reverse primer.

b) *In vitro* transcription of the sgDNA to sgRNA

The amplified sgDNA was *in vitro* transcribed to sgRNA with the 'NEB's High Scribe T7 Quick Hi Yield' kit by setting up the reaction according to Table 15. The reaction was mixed gently and incubated for 16 hours at 37 °C in a PCR cycler.

Table 15: *In vitro* transcription of the sgDNA to the sgRNA.

Substance	
NTP buffer mix	10 µL
T7 RNA polymerase mix	2 µL
sgDNA	0.1-0.3 µg
Nuclease-free water	ad 20 µL

To remove remaining template sgDNA, 30 µL nuclease-free water was added to each 20 µL reaction followed by 2 µL DNase I and incubated for 15 min at 37 °C.

c) Purification of the sgRNA

The clean-up was performed with the 'Ambio MegaClear Kit' (Ambion). Firstly, 74 µL of the sgRNA sample was gently mixed with 26 µL of 'Elution Solution' by thoroughly pipetting and 350 µL of 'Binding Solution' concentrate was added and gently mixed again. Then, 250 µL of 100% ethanol was pipetted to the sample, mixed and applied to the filter. After centrifugation for 15 sec at maximum speed the flow-through was discarded. The filter was washed twice with 500 µL 'Wash Solution'. To remove residual 'Wash Solution' an additional centrifugation step was added. 110 µL of 'Elution Solution' per sample was pre-heated to 95 °C. To eluate the sgRNA 50 µL was applied to the centre of the filter and spinned down at 15,000xg. This step was repeated with another 50 µL and the eluate was collected in the same tube and stored at -80 °C. RNA concentration was measured with NanoDrop. For checking the RNA quality 5 µL of the sgRNA sample was mixed with 5 µL of 2x RNA-denaturation buffer, incubated at 65 °C for 5 min and all was loaded on a 2% (w/v) agarose gel in a tank reserved for RNA work.

The samples were separated on a 2% (w/v) agarose gel for 120 min at 80-90 V and pictures were taken after 10 min, 20 min, 60 min and 120 min to check for possible RNA degradation and size of the product.

d) sgRNA precipitation

5 M Ammonium acetate (from 'Ambio MegaClear Kit') was added to the purified RNA (10% [v/v]) and further supplemented with 1 µg/µL glycogen stock (2.5% [v/v]). After addition of 2.5 volumes of 100% ethanol the mixture was incubated over night at -20 °C. To pellet the RNA the tube was centrifuged for 20 min at 16,100xg at 4 °C. The pellet was washed with

500 μL of ice-cold 80% ethanol under sterile conditions and centrifuged again for 5 min at 16,100 $\times g$ at 4 °C. The ethanol was aspirated carefully and the pellet was air dried for 10 min under a sterile working hood. The pellet was reconstituted in 5 μL sterile 1x PBS. To measure RNA concentration with the NanoDrop the sgRNA preparation was diluted 1:6. The sgRNA stock concentration was adjusted to 10 $\mu\text{g}/\mu\text{L}$ by addition of sterile 1x PBS.

e) *In vitro* test of the sgRNA and Cas9 nuclease functionality

Reagents were diluted to the following working concentrations: 100 ng/ μL sgRNA, 100 ng/ μL DNA template encoding 1.3 kB PLN c.40-42AGAdel target sequence (purified PCR product of locus of interest, see 3.3.1) and 0.5 $\mu\text{g}/\mu\text{L}$ Cas9 nuclease. Both, NEB- and Thermo Fisher-purchased recombinant Cas9 protein nucleases were tested to analyse biochemical functionality.

The reaction mixture according to Table 16 was prepared, gently mixed and incubated for 10 min at room temperature to enable the ribonucleoprotein complex formation. Then, 3 μL of the DNA template (100 ng/ μL) was added into each reaction tube and incubated for 1 hour at 37 °C. The whole 30 μL of the reaction mixture was loaded with 6x DNA loading dye for gel electrophoreses with a 50 mL 1.5% (w/v) agarose gel with 85 V for 1.5 hours to ensure high resolution.

Table 16: Preparation of the sgRNA and Cas9 nuclease reaction mixture for the *in vitro* test.

Substance	Thermo Fisher Cas9 nuclease		NEB Cas9 nuclease	
	+sgRNA	Negative control	+sgRNA	Negative control
NEB Cas9 buffer	3 μL	3 μL	3 μL	3 μL
Cas9 nuclease (500 ng)	1 μL	1 μL	1 μL	1 μL
sgRNA (100 ng)	1 μL	---	1 μL	---
Nuclease-free water	Ad 27 μL	Ad 27 μL	Ad 27 μL	Ad 27 μL

3.3.5 Nucleofection of hiPSC with the Amaxa 4D System

HiPSC carrying the PLN c.40-42AGAdel mutation were expanded according to section 3.2.4 in conditioned medium until 90-100% confluency. Medium change with conditioned medium supplemented with Y-27632 [10 μM] and bFGF [30ng] was done 1-2 hours before starting the experiment. Cells were washed twice with 1x PBS and dissociated with 1 mL Accutase®/6-well into single cell solution after 5 min of incubation time at 37 °C. Cell suspension was transferred into a 15 mL falcon tube and reaction was stopped by adding

conditioned medium supplemented with Y-27632 [10 μM] in a 1:1 volume ratio. The cell number was determined with Neubauer counting chamber. Per nucleofection 800,000 hiPSC were used so the appropriate cell suspension volume was transferred into a new 15 mL falcon, centrifuged for 5 min at 200xg and the supernatant was discarded. The 'P3 solution' was prepared according to the instruction of the 'Amaxa™ P3 Primary Cell 4D-Nucleofector X Kit L' (Lonza) by mixing 82 μL 'Nucleofector Solution' with 18 μL volume of 'supplement' per nucleofection approach. The cell pellet was re-suspended in 100 μL 'P3 Solution'.

For the plasmid approach 2 μg pSpCas9-sgRNA-2A-GFP and 5 μM (5 μL of a 100 μM stock) of the ssODN repair template (see 3.3.3) was added to the cell suspension, mixed and transferred to the Amaxa nucleofection cuvette (from the 'Amaxa™ P3 Primary Cell 4D-Nucleofector X Kit L').

For the protein approach the RNP complex formation was prepared first. For this 18 μg Cas9 nuclease and 4 μg sgRNA were mixed under sterile conditions and incubated at room temperature for 10 min. The RNP complex mixture was stored on ice until usage. Directly before adding the RNP complex to the cell suspension 5 μM of ssODN (5 μL of the 100 μM stock) was added and gently mixed without producing air bubbles. The 100 μL cell suspension was carefully mixed with the RNP-repair template mixture and transferred to the Amaxa nucleofection cuvette.

For both approaches the cuvette was placed into the 4D-Nucleofector™ X Unit (Lonza) and the CA-137 program was applied. The cuvette was then incubated for 5 min at 37 °C in the cell culture incubator.

Plasmid and ssODN transfected hiPSC were re-suspended with 500 μL conditioned medium supplemented with Y-27632 and transferred into the Matrigel™-coated well of a 12-well plate ($\sim 0.8 \times 10^6$ hiPSC/well). Additionally, untransfected cells were plated as a control. RNP-ssODN nucleofected hiPSC were mixed with 1 mL of conditioned medium supplemented with Y-27632 and 0.2×10^6 hiPSC were seeded per well of a 24-well plate.

1 μM SCR7 (1 mM stock in DMSO) was added to the medium for some experiments as indicated in the results part. The cells were incubated at 37 °C, 20% O₂ and 5% CO₂. The following day medium was changed with optional SCR7 and in the case of pSpCas9-sgRNA-2A-GFP nucleofection cells were checked for a GFP signal with the EVOS FL Cell Imaging System (Advanced Microscopy Group).

3.3.6 Clonal isolation by FACS, sub-cultivation and clonal expansion of nucleofected hiPSC

48 Hours after nucleofection the cells were prepared for FACS sorting or sub-cultivation. One hour before starting the dissociation the medium was changed supplemented with 10 μ M Y-27632. The fluorescence signal of the pSpCas9-sgRNA-2A-GFP transfected cells was checked and documented. The hiPSC were dissociated with Accutase® to get a single cell suspension as described in 3.3.5.

For FACS sorting the dissociated cell suspensions of untransfected control (FACS reference) and pSpCas9-sgRNA-2A-GFP nucleofected cells were transferred into a cell strainer (pore size 30 μ m) into a new falcon. The samples were then centrifuged for 5 min at 200xg and the cell pellet was re-suspended in 250 μ L 1x PBS. A 15 mL falcon was prepared to collect the GFP⁺ sorted cells in 10 mL of conditioned medium supplemented with 10 μ M Y-27632. The cells were FACS-sorted with AriaFusion (BD) under sterile conditions with a drop rate of 1-2 and a nozzle of 100 μ m. This procedure was kindly performed by the FACS Sorting Core Unit facility (UKE, Hamburg, Germany). The GFP⁺ sorted hiPSC collected in the 15 mL falcon were centrifuged for 5 min at 200xg. Seeding was performed on Matrigel™-coated 6-well dishes with densities of 1000 cells/well and 1500 cells/well in 2 mL medium per well. The SCR7 treatment was continued for the GFP⁺ FACS sorted cell clones until they were picked.

In the case of the protein approach no selection of transfected cells was possible due to the lack of a fluorescence marker. Instead, the cells were sub-cultivated. The cell number of the dissociated cells was determined with Neubauer counting chamber and trypan blue staining. The hiPSC were seeded on a Matrigel™-coated 6 well plate with a density of 3000 cells/well. From here on an optional SCR7 treatment was stopped.

During every medium change the used medium was collected and not discarded. The seeded hiPSC were fed with a double conditioned medium. This means that the collected used conditioned medium was mixed 1:1 with fresh conditioned medium, sterile filtered and supplemented with 30 ng/mL bFGF. The apoptosis inhibition was done for the following 5 days after sorting or sub-cultivation during medium change.

The low density seeding should enable a clonal growth of a single cell to a small clonal colony. To ensure this the cell clones were microscopically checked on a daily basis before medium change. 10-14 Days after FACS sorting or sub-cultivation cell clones were picked. One hour before starting the medium was replaced by conditioned medium supplemented with 10 μ M Y-27632. The plate was positioned under the EVOS FL Cell Imaging System within a sterile working hood. The colonies were picked with a 100 μ L pipette tip and transferred into a Matrigel™-coated well of a 48-well plate containing 100 μ L of conditioned

medium supplemented with Y-27632. It should be avoided to pick colonies which fused already or were about to fuse to minimize the risk of a mosaic cell population. The day after picking the cell culture medium was not removed but new medium supplemented with Y-27632 was added on top. At a density of 90-100%, cell clones were expanded. After two times washing with 1x PBS cells were dissociated with EDTA (0.5 mM) and passaged (see 3.2.4) onto a 24-well plate. After reaching 90-100% confluency, cells were expanded onto two wells via a 1:2 split. After reaching 100% confluency, the hiPSC from one well were again expanded as before and the hiPSC from the second well were frozen (10% [v/v] DMSO, 90% [v/v] FCS, heat inactivated) with isopropanol container (Mr. Frosty) for the first 24 hours and then transferred to -150 °C. This procedure was repeated to create at least two frozen aliquots of each clone. Finally, cells were harvested with 1x PBS, spinned down for 1 min at 13,400xg to freeze down a cell pellet at -80 °C for DNA isolation.

The nucleofection, FACS sorting and hiPSC culture procedures were kindly supported by Dr. Sandra Laufer HEXT Core Stem Cell Facility (UKE, Hamburg, Germany).

3.3.7 Validation of recombination efficiency and off-target activity

a) Analysis of recombination success

The genomic DNA was isolated out of the frozen cell pellet of each clone with the QIAcube HT (Qiagen) and 'QIAamp® 96 DNA QIAcube® HT kit' (Qiagen) according to the manufacturer's instructions. The PLN target sequence was amplified by PCR (see 3.3.1a) and sent for sequencing with the 'hPLN-Fw' primer for analysing the genome editing efficiency of the respective CRISPR run.

b) Amplification of the off-target sequences

The absence of off-targets was analysed in clones verified for successful recombination. The MIT website listed possible off-target locations according to their probability. The 10 most probable off-targets were investigated regardless whether they were exonic or intronic. The MIT design tool used the human GRCh37/hg19 genome which was thereby chosen for the extraction of the DNA off-target sequences from the database of the "UCSC Genome Browser" (University of California Santa Cruz; <https://genome.ucsc.edu/>). Primer pairs were designed (NCBI primer blast tool) for each of the chosen 10 off-target loci generating PCR products with sizes of 500-900 bp (see supplement, Table S4; Tables 17 and 18).

The size of the PCR product was verified by using an 1.8% (w/v) agarose gel. The PCR products were cleaned up using the 'QIAquick® PCR purification kit' (Qiagen) and sent for sequencing with their respective off-target primer (OT1-10).

The successful CRISPR/Cas9-mediated recombined hiPSC clones with no detectable off-targets were expanded on 6-well plates for freezing of additional samples. Two clones were chosen for karyotyping and for cardiomyocyte differentiation.

Table 17: AmpliTaqGold PCR-mediated amplification of suspected off-target loci. OT = off-target.

Substance	1x
10x AmpliTaqGold buffer	4 μ L
10 mM dNTPs	0.8 μ L
OT-Fw primer (10 μ M)	1 μ L
OT-Rev primer (10 μ M)	1 μ L
25 mM MgCl ₂	1 μ L
AmpliTaqGold DNA polymerase (1 kb/min)	0.4 μ L
Genomic DNA	50 ng – 150 ng
Nuclease-free water	ad 40 μ L

Table 18: Touchdown PCR programme for AmpliTaqGold PCR.

Temperature	Time	
94 °C	5 min	
94 °C	30 sec	} 11x; * 0.5 °C step/cycle
62 °C *	30 sec	
68 °C	55 sec	
94 °C	30 sec	
57 °C	30 sec	} 24x
68 °C	55 sec	
68 °C	10 min	
4 °C	∞	

3.4 Differentiation of hiPSC to cardiomyocytes

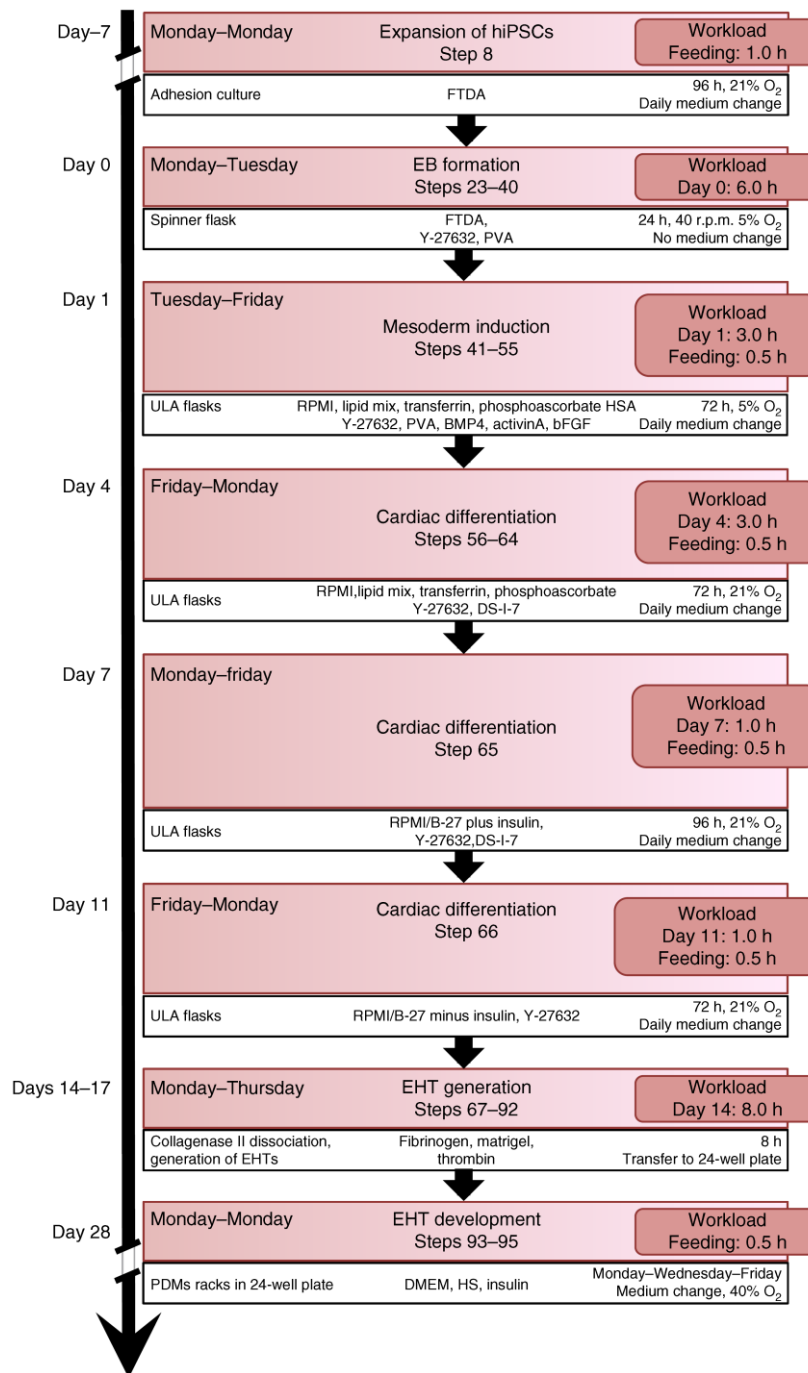


Figure 17: Embryoid body, growth factor-based three-stage protocol. The cardiac differentiation protocol shows exact time points of growth factor or small molecule addition and depletion as well as culture conditions and experimental procedure-related key aspects, e. g. usage of spinner or ultra-low attachment (ULA) flasks. Mesoderm induction was achieved by addition of BMP4, bFGF and activin A. Cardiac lineage specification was induced by DS-I-7-mediated (IWR-1 analogue) WNT inhibition. FTDA: bFGF, TGFβ1, dorsomorphin and activin A-based hiPSC culture medium; EHT: engineered heart tissue; HSA: human serum albumin; HS: horse serum; PVA: polyvinyl alcohol (Breckwoldt et al. 2017).

Efficient cardiomyocyte differentiation was achieved by the application of an optimized differentiation protocol which was recently established in our department (Breckwoldt et al. 2017, Figure 17). HiPSC pluripotency was maintained by the combination of bFGF, TGF β , activin A and dorsomorphin supplemented to the culture medium (Frank et al. 2012). EB formation was achieved by the application of stirred spinner flasks with a glass bulb impeller on a magnetic rotor. This enabled the up-scaling and a homogeneous EB formation independent of hiPSC cell density or lineage. The mesodermal pathway was induced by the growth factor cocktail of bFGF, activin A and BMP-4. To induce the cardiac lineage specification insulin was supplemented and the WNT signalling pathway was inhibited by the potent small molecule DS-I-7 or XAV-939. DS-I-7 or XAV-939 was removed after day 11 of differentiation and the on-set of beating was observed at day 8-10.

3.4.1 *Embryoid body formation in spinner flasks*

Spinner flasks were prepared by manual, careful and thorough cleaning, autoclaving and warming up in the incubator up to 37 °C before starting EB formation.

HiPSC were expanded in T80 flasks to 90-100% confluency, incubated with 10 μ M Y-27632 for one hour at 37 °C and dissociated with EDTA (1 mL/10cm², 8-10 min of incubation time). After removal of EDTA cells were detached by squirting thoroughly with 1x PBS or with the help of a cell scraper, if detachment was insufficient. After trituating the cell suspension for maximum 3 times to get single cells, it was transferred into a 50 mL flacon tube. The cell culture flask was rinsed with calcium-containing medium (RPMI, 1:5 of cell suspension volume) which was then added to the cell suspension in the 50 mL tube. After spinning down at 250xg for 5 min the cell pellet was re-suspended in EB formation medium (~10 mL, depending on cell pellet size) and the hiPSC were counted with the Neubauer counting chamber and trypan blue staining. The hiPSC were transferred to the spinner flasks with a concentration of 30x10⁶/100 mL EB formation medium. In Table 19 the medium volumes and cell ranges for each flask type are listed. The spinner flask was adjusted on the rotor with a speed of 40 rpm in the incubator so that the impeller moved smoothly and uniformly. The EB formation was incubated for 20-24 hours at 37 °C, 5% O₂, 5% CO₂ and 95% humidity.

Table 19: Overview of spinner flask types, minimal and maximal medium volumes and cell number ranges.

Spinner Flask type	Minimal medium volume [mL]	Maximal medium volume [mL]	Cell number range/flask for each flask type
Medium (0.5 L)	100	275	30-83x10 ⁶
Large (1 L)	200	550	60-165x10 ⁶

3.4.2 Mesodermal progenitor cell induction

Suspension cell culture flasks (green caps) were coated with 1 mL/10 cm² 1% (v/v) Pluronic® F-127 solution and incubated over night at 37 °C. Flasks were washed twice with 1x PBS (~2 mL/10 cm²) before usage and 40 mL mesoderm induction medium was added.

A volume of 50 mL of the EB suspension was transferred from the spinner flask to a 50 mL falcon tube for sedimentation for maximum 5 min, the remaining EB suspension volume was pipetted into the Pluronic® F 127-coated suspension cell culture flask with a maximal volume of 200 mL per T175 flask. They were placed on a pre-warmed V-shaped sedimentation rack and placed back into the incubator for EB sedimentation for 5-20 min depending on EB quality and size. During this time, the supernatant was removed from the 50 mL falcon tube. Then, 5 mL washing medium was added to transfer EBs with a wide tip 10 mL pipette to a 15 mL graduation falcon to estimate the EB volume after sedimentation. From this estimation the total EB volume was calculated. From the T175 flasks containing the sedimented EBs 90% of the EB formation medium was removed and the EBs from the falcon tube for EB volume estimation were added. If handling more than one flask, EBs from all flasks were pooled into one. The EBs were washed with pre-warmed mesoderm induction washing medium. About 90% of the washing medium was removed after EB sedimentation and mesoderm induction medium was added. The carefully re-suspended EBs were then equally distributed to the Pluronic® F 127-coated cell culture flasks using a wide tip 10 mL serological pipette with 150-250 µL EB volume in 40 mL mesoderm induction medium per flask. The EBs were incubated for three days at 37 °C, 5% O₂, 5% CO₂ and 95% humidity.

The medium was changed daily every 24 hours. For this the T175 flask was placed on a pre-warmed V-shaped sedimentation rack to sediment the EBs for maximal 5 min. Then, 50% of the medium was removed and 20 mL of mesoderm induction medium was added.

3.4.3 Cardiac specification

The cell culture flasks were placed on a V-shaped sedimentation rack for maximum 5 min sedimentation time. Up to three flasks of the same conditions were pooled together. After removal of the mesoderm induction medium, the EBs were washed with 20-30 mL warm cardiac specification washing medium and 5-10 mL of the cell suspension was transferred to a 15 mL graduation falcon and re-sedimented for again 5 min. The EB volume was estimated to calculate the total EB amount.

After supernatant removal, the EBs were re-suspended in cardiac specification medium I using a wide tip serological pipette and transferred to prepared cell culture flasks with 80-150 µL EB/T75 flask in 20 mL medium or 200-250 µL EBs/T175 flasks in 46 mL medium. Depending on the cultivation format cell culture flasks were either coated with Geltrex®

(1:200) for adherent cardiac specification or with 1% Pluronic® F 127 for cardiac EB-based (cEB) cardiac specification.

The cells were incubated in cardiac specification medium I for three days. The medium was not exchanged the following day, but then daily with 50% medium change. On day three medium was completely exchanged and replaced by cardiac specification medium II. The cells were incubated in this medium for 4 days with daily medium change (50% exchange). On day 7 of cardiac specification the cardiac specification medium II was completely removed and replaced by cardiac specification medium III. Until the day of dissociation, the cell culture medium was changed daily by removing 50% except for the first day after complete medium exchange.

3.4.4 Dissociation of hiPSC-cardiomyocytes in cEB or adherent format

Collagenase II-based dissociation buffer, calcium-free HBSS and DMEM were pre-warmed to 37 °C. For cEB-based cardiac specification the cell culture flasks were placed on the V-shaped sedimentation rack to let the cEBs sediment. The medium was aspirated as much as possible and the cEBs washed twice with 20-25 mL HBSS. Several flasks were pooled to a maximal cEB volume of 400 µL per T175 flask. In the case of monolayer cardiac differentiation the cell layer was also washed twice with 20-25 mL HBSS. After the second washing step the HBSS is completely removed, replaced by dissociation buffer with 12 mL/200 µL cEB volume or 7-8 mL/T75 and 15 mL/T175 flask for monolayer-based cardiac specification and incubated for about 3.5 hours at 37° C, 90% humidity, 5% CO₂, 20% O₂.

The dissociation progress was checked after 2 hours as quality control since dissociation is dependent on collagenase batch, cell density or cEB amount, quality and size. The flasks were tapped carefully to check for cEB dispersion into single cells or the detachment of small cell clusters. If cEBs or the cell monolayer started to disintegrate (usually after 3.5 hours) the cells were gently triturated 5-10 times and transferred to a 50 mL falcon tube. The dissociation reaction was stopped with 1:1 (v/v) pre-warmed DMEM supplemented with 6 µL/mL DNase II (type V, stock 2000 U/mL), with which the cell culture flasks were washed once and then transferred to the corresponding cell suspension. After centrifugation for 10 min at 100xg the cell pellet was carefully re-suspended in pre-warmed DMEM. The volume was adjusted according to the cell pellet size with 5 mL for small and up to 20 mL for large cell pellets. In case of DNA clumping due to dead cells the cell suspension was filtered through a 100 µm cell strainer mesh. The cell number was analysed with the Neubauer counting chamber and trypan blue staining. The volume of cell suspension used for flow cytometry and freezing was calculated and distributed.

For flow cytometric analysis two FACS tubes (unstained reference and sample) per cell line were prepared containing the appropriate volume containing 200,000 cardiomyocytes per tube. The remaining cell suspension was centrifuged for 10 min at 100xg for freezing.

3.4.5 Freezing of hiPSC-derived cardiomyocytes

The cell pellet was re-suspended in cardiomyocyte freezing medium with $2\text{-}30 \times 10^6$ cells/mL. 1 mL of the cell suspension was added per cryovial. The tubes were placed in an isopropanol container (Mr. Frosty) and frozen over night at $-80\text{ }^\circ\text{C}$. The next day the cryotubes were transferred to $-150\text{ }^\circ\text{C}$ storage freezer.

3.4.6 Flow cytometric analysis for cardiac marker positivity

The in the FACS tube collected hiPSC-CM were washed twice with 3 mL 1x PBS with centrifugation steps for 2 min at 200xg at room temperature. The cells were re-suspended in 500 μL Histofix® and fixed for 10 min at room temperature. After two washing steps with FACS-buffer the cells were permeabilized by re-suspending them in 500 μL FACS-buffer and incubating them for at least 45 min at $4\text{ }^\circ\text{C}$. To stain intracellular antigens the permeabilized cells were incubated for 30 min at $4\text{ }^\circ\text{C}$ in 100 μL FACS buffer which contained a primary or directly labelled antibody. The second sample of the same cell line was stained with the respective isotype control. The stained cells were washed twice with 2.5 mL FACS buffer. If a secondary antibody was needed, the staining procedure was repeated. For flow cytometric analysis the cells were re-suspended in 150 μL 1x PBS and analysed with the Flow Cytometer FACSCanto II (BD) and the FACSDiva software (BD) with adjusted gates according to isotype control.

3.4.7 Thawing of hiPSC-derived cardiomyocytes

The cardiomyocyte cryovial was taken from the $-150\text{ }^\circ\text{C}$ storage freezer and immersed in a water bath with $37\text{ }^\circ\text{C}$ until cell suspension was completely thawed (2-3 min). Not more than three cryovials were thawed at the same time. The tube was sprayed with 70% ethanol, placed under the sterile working bench, and the cell suspension was then transferred to a 50 mL falcon tube with a 2 mL serological pipette. The empty cryovial was rinsed with 2 mL of room temperature pre-warmed medium (RPMI 1640 or DMEM) to recover residual cells and added drop-wise over 90 sec (1 drop every 4-5 sec) to the cell suspension in the 50 mL falcon tube under gently swirling of the tube. Then, additional 7 mL of medium were slowly added, the first 1 mL drop-wise over 30-60 sec and the remaining 6 mL over 30 sec. While adding medium the tube was gently swirled. The cell suspension was gently mixed by inverting the tube for 2-3 times and then counted with trypan blue staining in the Neubauer counting chamber. Before seeding as monolayer or EHT generation the cardiomyocyte suspension was centrifuged for 10 min at 100xg at room temperature.

3.5 Engineered heart tissue model

3.5.1 EHT generation and maintenance

Agarose casting molds were prepared by adding 1.6 mL of 2% (w/v) agarose (stored at 60 °C) in each well of a 24-well plate. Teflon spacers were placed immediately into liquid agarose after pipetting 8 wells since agarose solidifies fast. Casting molds should be prepared immediately prior usage. When the agarose was solid and turned opaque after about 10 min the Teflon spacers were removed and PDMS racks placed so that the posts were directing into the casting molds.

hiPSC-derived cardiomyocytes should have a purity of at least 50-60% for EHT generation. After thawing, counting and centrifugation of hiPSC-CM the medium was removed. The hiPSC-CMs were re-suspended in the calculated amount of EHT casting medium (Table 20). The cell suspension was transferred to a red cap round bottom tube and the master mix was prepared with 10% extra volume to compensate the loss during pipetting.

Table 20: Master mixture calculated per EHT containing 1.0×10^6 cardiomyocytes.

Substance	Volume in [μ L]
EHT casting medium	86.64
2x DMEM	6.13
10% (v/v) Matrigel	11.00
0.1% (v/v) Y-27632	0.11
Fibrinogen	2.78
Thrombin	3.34
Total volume	110 μL

The master mix was triturated 10-15 times with a serological pipette until the fibrinogen was dissolved. For each EHT 100 μ L of the master mix was pipetted in one thrombin aliquot (3 μ L in 200 μ L tube), mixed and quickly pipetted into the agarose mold between the two silicone posts. For each EHT a new filter tip was used. After pipetting 8 EHTs the master mix was re-suspended with a serological pipette. EHTs were incubated for 1.5 hours at 37 °C, 40% O₂, 7% CO₂ and 98% humidity. After this, each well was covered with about 200-500 μ L of warm medium, the plate was shaken gently and incubated again for 15-20 min under the same conditions as before. PDMS racks with the attached EHTs were carefully removed from the agarose casting molds and transferred to a new plate already filled with EHT maintenance medium (1.5 mL/well). Figure 18 shows the components and procedure steps.

The EHT development was monitored. Cardiomyocyte contractions within the EHT were detectable after about day 2-5. Coherent beating EHTs deflecting the posts were usually observed after 7-9 days.

Medium change of the EHTs (1.5 mL/well) was done on Mondays, Wednesday and Fridays with always freshly prepared cardiomyocyte culture medium.

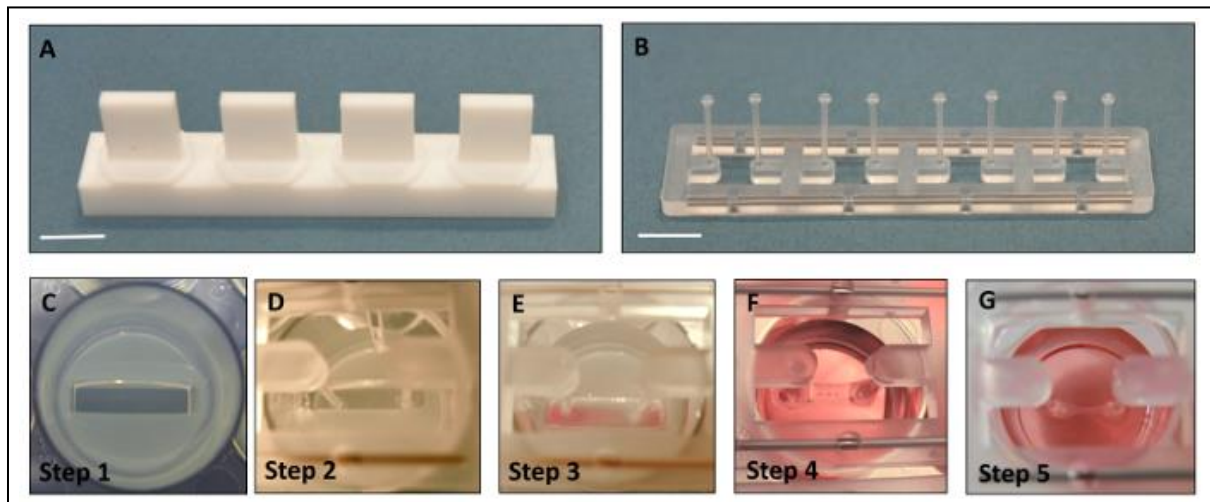


Figure 18: EHT casting and development. **A** - Teflon spacer (scale bar 1 cm); **B** - PDMS rack (scale bar 1 cm); **C** - Agarose casting mold after agarose solidification and Teflon spacer removal; **D** - Insertion of the PDMS rack with the pair of flexible posts reaching into the casting mold; **E** - Fibrin polymerization embedding the hiPSC-CM and forming around the PDMS posts; **F** - Transferred, fully polymerized EHTs from casting molds into fresh cardiomyocyte culture medium; **G** - EHT fully remodeled on day 15 after casting (Mannhardt et al. 2017).

3.5.2 Contractility measurement and electrical stimulation of EHTs

Contractility measurements of EHTs were performed by video optical recording as recently described by Mannhardt et al. (2017) and as shown in Figure 14. The EHT culture plate was placed into an incubator with a glass roof. The software analyses the contraction by automated recognition of the EHT contour at top and bottom ends (blue squares) and follows them during the course of contraction. Based on the deflection of the posts during contraction the generated force is calculated. The software represented the force-time diagram and calculated contractile parameters such as force, T1 (contraction time), T2 (relaxation time), CV (contraction velocity) and RV (relaxation velocity) as well as irregularities and beating frequency of each single EHT. T1 values were analysed at 10% ($T1_{10\%}$), 20% ($T1_{20\%}$) and 50% ($T1_{50\%}$) above baseline, T2 values at 20% above baseline ($T2_{20\%}$).

Electrical stimulation (Grass) was achieved with graphite pacing systems as previously published (Hirt et al. 2012). The pacing frequency was adapted to the measured

spontaneous average EHT frequency and set to a value 1.5 - 2.0 times higher than the spontaneous frequency. EHTs not following the pacing signal were excluded from measurement and analysis. After finishing pacing experiments, carbon electrodes were washed in a distilled water bath with daily water change over three days.

3.5.3 Monitoring of the EHT development over time

Baseline contractility of EHTs was analysed on days of medium change starting with their onset of beating. Measurement was performed at least 1.5 hours after medium change by recording each EHT for 50 sec in medium. Generated force and frequency were plotted versus days in culture. When EHTs reached their maximum forces and thereby their plateau phases the disease modelling protocol started.

3.5.4 Disease modelling protocols

Tyrode plates were prepared one day prior to the start of the experiment. They were incubated at 37 °C, 40% O₂, 7% CO₂ and 98% humidity for temperature adaptation and gas equilibration.

a) **Calcium concentration-response curve**

EHTs were incubated in 1.8 mM Ca²⁺ Tyrode's solution (2 mL/well) for at least 30 min at 37 °C, 5% CO₂, 40% O₂ and 98% humidity. Contractility was recorded for 50 sec per spontaneously beating EHT and 10 sec per paced EHT. To reduce calcium levels within the cells EHTs were washed once in 0.3 mM Ca²⁺ (isogenic controls [PLNic]) or 0.4 mM Ca²⁺ (PLN p.Arg14del) until their force was reduced to their minimal plateau phase (5-15 min). EHTs were then transferred to new 0.3 mM Ca²⁺ (PLNic) or 0.4 mM Ca²⁺ (PLN p.Arg14del) Tyrode's solution and incubated again until they reached their minimal force plateau. After the paced baseline contractility was recorded EHTs were transferred to a new 24-well plate containing the following calcium concentration. Paced EHT contractility was recorded after 15 min of incubation time. This procedure was repeated for each increasing calcium concentration step to analyse contractile parameters at calcium concentration of 0.4 - 0.5 - 0.6 - 0.7 - 0.8 - 1.0 - 1.2 - 1.4 - 1.8 - 2.4 - 3.3 - 5.0 and 10.0 mM. At the end of the experiment EHTs were incubated at 1.8 mM Ca²⁺ Tyrode's solution for washing out high calcium levels for 15 min before they were transferred back to their medium plate. The EC₅₀ values were calculated via a nonlinear regression with the 'dose-response - stimulation' equation 'log(agonist) vs. normalized response - variable slope' with the GraphPad Prism 5.0 software.

b) Average contraction peaks

Average contraction peaks were analysed from EHTs measured in 1.8 mM Ca²⁺ Tyrode's solution with electrical stimulation of 2.0 Hz. In order to plot the average contraction graphs the parameters of the video optical recording platform were reduced to a nFilter value from 10 to 1.

c) Isoprenaline and carbachol response

EHTs were incubated for 30 min in 1.8 mM Ca²⁺ Tyrode's solution for baseline contraction analysis with (2.5-3.0 Hz) and without pacing. After washing them in low calcium (0.3-0.4 mM Ca²⁺) they were incubated in [EC₅₀] calcium Tyrode's solution for at least 30 min under electrical stimulation. Baseline contractility was analysed with and without electrical stimulation. A bolus of 100 nM isoprenaline (sterile 10 µM stock in sterile water for injection) was applied and EHT contractility was recorded with and without electrical stimulation after 15-20 min. Then, carbachol stimulation (10 µM final concentration, sterile 1 mM stock in Tyrode's solution) followed for again 15-20 min before measuring the EHT's contractility with and without electrical stimulation. After finishing the experiment, the EHTs were washed three times in 1.8 mM Ca²⁺ Tyrode's solution for at least 15 min before being transferred to culture medium. The EHTs were not analysed within the following 48 hours after the experiment to ensure complete drug removal.

To compare PLNic and PLN p.Arg14del EHTs the experiments were pooled and values were normalized to 1.8 mM calcium baseline (BL). To calculate the isoprenaline (Iso) and carbachol (CCh) effects the following equations were investigated:

$$\text{Absolute Iso effect} = \left(\frac{BL(\text{Iso}[100 \text{ nM}])}{BL(\text{Calcium}[EC_{50}])} * 100 \right) - 100$$

$$\text{Absolute CCh effect} = \left(\frac{BL(\text{CCh}[10 \text{ }\mu\text{M}])}{BL(\text{Iso}[100 \text{ nM}])} * 100 \right) - 100$$

d) Long term calcium exposure

Before starting the experiments baseline EHT contractility was recorded in medium. Recording time was 50 sec per EHT without electrical stimulation. EHTs were incubated in 1.0, 1.8 or 3.0 mM Ca²⁺ Tyrode's solution for 12 hours with repeated contractility measurement every 60 min using the continuous mode of the video optical recording system. The RR-scatter (interdecile range of average beat-to-beat variation) was investigated to analyse the EHTs' beating regularity.

1.0 mM Ca²⁺

Baseline measurement was recorded at 1.8 mM Ca²⁺ Tyrode's solution after an incubation time of 30 min. Before transferring the EHTs to 1.0 mM Ca²⁺ condition, they were being washed out at 0.4 mM calcium for about 15 min.

1.8 mM Ca²⁺

EHTs were transferred to 1.8 mM Ca²⁺ Tyrode's solution and continuous mode was directly started.

3.0 mM Ca²⁺

Baseline measurement was recorded at 1.8 mM Ca²⁺ Tyrode's solution after an incubation time of 30 min. EHTs were then transferred to 3.0 mM Ca²⁺ concentration for long term experiment.

3.5.5 Immunohistochemical analysis of EHTs

EHTs were fixed directly attached to the PDMS posts with Histofix® at day 20-30 after casting. After 24 hours the EHTs were transferred to TBS/acid and stored at 4 °C. For cross-sections the EHT was removed carefully from the post and embedded in 2% (w/v) agarose in a 24-well plate. After solidification a block containing the EHT was cut out of the agarose and transferred into a 2 mL Eppendorf tube containing TBS azide. For longitudinal sections the EHTs were removed from the PDMS posts and transferred to an Eppendorf tube containing TBS azide. The following processing was kindly performed by Kristin Hartmann from the Mouse Pathology Core Facility (UKE, Hamburg, Germany). The EHTs were embedded in paraffin and 4 µm thick sections were cut. The longitudinal sections were stained for PLN (pre-treatment: 1 hour citrate buffer; 1:1000) and MLC2v (pre-treatment: 30 min citrate buffer; 1:150), the cross-sections were stained for dystrophin (pre-treatment: 2 hours EDTA; 1:200). The immunohistochemical staining including paraffin uncoating, pretreatment, incubation with primary and secondary antibody, staining and counterstaining was proceeded by the tissue stainer Ventana, BenchMark XT (Roche) with the 'Ultra View Universal DAB Detections Kit'.

3.5.6 Molecular analysis

a) RNA isolation out of EHTs

EHTs were sampled during their force of contraction plateau phase (day 20-30). The RNA was either isolated with the 'RNeasy Plus Mini Kit' (Qiagen) or with the 'TRIzol® Reagent' (Life Technologies) according to manufacturer's instructions.

EHTs were homogenized with the TissueLyser (Qiagen) for 2 min at 30 Hz in 350 µL 'RLT-Plus buffer' of the 'RNeasy Plus Mini Kit' supplemented with 2-mercaptoethanol. The extracted RNA was eluted with 30 µL nuclease-free water.

For TRIzol®-mediated RNA extraction 500 µL (for 3-4 EHTs) TRIzol®-reagent was added to the sampled tissues and homogenized with the TissueLyser (2x 1 min, 30 Hz). The extracted RNA was eluted with 30 µL nuclease-free water.

RNA concentration was measured using the Qubit 3.0 Fluorometer (Life technologies) and the 'Qubit™ RNA HS Assay Kit' (Invitrogen) according to manufactures instructions.

b) Investigation of the EHT's mRNA expression levels

RT-PCR and qPCR-mediated analysis of PLN mRNA levels

The reverse transcription PCR (RT-PCR) of RNA to cDNA was performed with the 'High Capacity cDNA Reverse Transcription Kit' (Applied Biosystems) according to the protocol in Table 21. The reaction was run for 10 min at 25 °C followed by an incubation time of 2 hours at 37 °C and a final incubation for 5 min at 85 °C.

Table 21: RT-PCR master mixture set-up.

Substance	1x
10x RT buffer	2.5 µL
10x RT Random Primer	2.5 µL
100 mM dNTP mix	1 µL
Multi Scribe Reverse transcriptase	1 µL
RNA sample	200 ng
Nuclease-free water	ad 25 µL

The qPCR was performed with SYBR-Green (Thermo Fisher Scientific) in technical duplicates (Table 22). α -Actinin 2 (*ACTN2*) as cardiac-specific housekeeping gene and glucuronidase-beta (*GUSB*) were used as reference transcripts for normalization. The target sequences were amplified within 40 cycles in an AbiPrism7900HT cyler (Applied Biosystems) according to manufacturer's instructions.

Table 22: RT-qPCR reaction set up.

Substance	1x
cDNA	2 µL
SYBR Green	5 µL
Primer mix (forward+reverse; 10 µM)	0.5 µL
Nuclease-free water	2.5 µL

NanoString-mediated analysis of mRNA levels

To analyse mRNA transcript levels the NanoString nCounter® Elements system was used according to manufacturer's instructions. 50 ng RNA was applied for hybridization with a customized NanoString Gene Expression CodeSet (see supplement, Table S10) as previously described (Prondzynski et al. 2017). The mRNA levels were normalized to a set of housekeeping genes (*ABCF1*, *CLTC*, *GAPDH*, *PGK1*, and *TUBB*) or to *ACTN2*.

c) Western blot analysis of protein levels in EHTs

Table 23: Western blot conditions of each target protein.

Target protein	SDS polyacrylamide gels percentages	Blotting condition	Blocking solution
α-Actinin 2	12-15%	PVDF or Nitrocellulose; 300 mA, 90 min or 400 mA, 50 min	5% milk in TBS-T 0.1%
hPLN total	15%	PVDF 300 mA, 90 min	5% milk in TBS-T 0.1%
hPLN-PSer16	15%	PVDF 300 mA, 90 min	5% milk in TBS-T 0.1%
p62	12%	Nitrocellulose 400 mA, 50 min	5% milk in TBS-T 0.1%
LAMP2	12%	Nitrocellulose 400 mA, 50 min	5% milk in TBS-T 0.1%
LC3-II	12%	PVDF 400 mA, 50 min	5% BSA in TBS-T 0.1%

Western blot analysis was done as previously described (Mannhardt et al. 2016). PLN^{ic} and PLN p.Arg14del EHTs were sampled after 30±1 days of cultivation. The tissues were homogenized with the TissueLyser (Qiagen, 2x 30 Hz, 30 sec). The homogenized, lysed and with 1x Laemmli supplemented samples were being heated at 95 °C for 5 min. To analyse the pentameric PLN form this step was skipped. Table 23 lists the Western Blot procedure details. SDS-PAGE was loaded with 10 µL EHT lysate and 33 µg non-failing human heart tissue (NFH). Membranes were blocked in 5% (w/v) low fat milk powder solution or 5% (w/v) BSA solution (in TBS-Tween 0.1%). Proteins were blotted wet and stained for phospholamban phospho Ser-16 (Badrilla, in TBS-Tween 0.1%), PLN total (Novus, in TBS-Tween 0.1%), α -actinin 2 (Sigma, in 1% milk in TBS-Tween 0.1%), p62 (BD Biosciences, TBS-Tween 0.1%), LAMP2 (Bio-Rad Laboratories, TBS-Tween 0.1%) and LC3-II (Cell Signalling, 5% BSA in TBS-Tween 0.1%) over night at 4 °C (Table 23, for details see supplement Table S2).

Anti-rabbit IgG peroxidase-conjugated secondary antibody (Sigma) or anti-mouse IgG peroxidase-conjugated secondary antibody (Sigma) in 5 % (w/v) low fat milk powder solution in TBS-Tween 0.1 % were incubated for one hour at room temperature.

For protein visualization 'Pierce® ECL Western Blotting Substrate' was used. Detection was performed with the Bio-Rad ChemiDoc™ Touch Imaging System (Bio-Rad Laboratories) and

densitometry analysis of the detected protein bands was investigated with the ImageLab software (Bio-Rad Laboratories). Target proteins were normalized to α -actinin 2 serving as cardiac-specific housekeeping protein.

3.6 Cardiomyocyte monolayer-based analyses

3.6.1 Cardiomyocyte plating and maintenance

A 6-well or 96-well plate was coated with 0.1% (w/v) gelatine or Geltrex® and incubated for one hour at 37 °C, 20% O₂ and 5% CO₂. Directly before plating the residual gelatine was removed from each well. hiPSC-derived cardiomyocytes were thawed and re-suspended in the appropriate volume of cardiomyocyte culture medium. The details of plating format, coating, cell numbers and medium volumes are listed in Table 24. The cardiomyocyte culture medium was changed every Monday, Wednesday and Friday.

Table 24: Plating format, coating procedure, cell number per area and medium volumes for each respective cardiomyocyte monolayer experiment.

Experiment	Plate format	Coating	Cell number	Medium volume per well
Caffeine response	6-well	0.1% gelatine	200,000/10 cm ²	2 mL
Cell area analysis	96-well	Geltrex®	10,000/0.34 cm ²	200 μ L
Confocal microscopy	96-well	Geltrex®	10,000/0.34 cm ²	200 μ L

3.6.2 Calcium transient measurements after caffeine application

PLNic and PLN p.Arg14del hiPSC-CM were seeded on gelatine-coated glass coverslips (24x24 mm, VWR) and cultivated for 7 \pm 2 days until analysis. 2.5 μ M Fura 2-AM (5 mM stock in DMSO) was dissolved in 2 mL Tyrode's solution for 2D calcium transient analysis. The cardiomyocytes were washed with 2 mL Tyrode's solution and loaded with Fura 2-AM for 15 min protected from light. The Fura 2-AM-containing buffer was replaced by 3-4 mL Tyrode's solution for a 15 min washing step and the de-esterification of Fura 2. The coverslip loaded with cells was removed from the well for analysis with the IonOptix system (IonOptix, Milton, USA). The cells were perfused with Tyrode's working solution for 2D calcium transient analysis, heated up to 37 °C and paced at 0.5 Hz. Cells were chosen according to the following criteria. They should show regular beating and should follow the pacing signal. They should also be in single cells or smaller cell clusters (3-5 cells) format and no larger aggregates. The perfusing pipette was moved to the closest vicinity of the cell. The baseline was being recorded for 1 min. Electrical stimulation was switched off and 20 mM caffeine

was applied via another perfusion channel. After 10-15 sec the perfusion was switched back to normal Tyrode's working solution and the pacer was turned on again. The recording continued for about 30 sec. A maximum of three cells per coverslip were recorded. This procedure was kindly performed by Dr. Frederik Flenner (DEPT, UKE, Hamburg, Germany).

3.6.3 Immunofluorescence analysis of 2D hiPSC-CM

The immunofluorescence staining of hiPSC-CMs was performed as previously described (Prondzynski et al. 2017). The PLNic and PLN p.Arg14del hiPSC-derived cardiomyocytes were cultured for 30 days in black 96-well plates (μ Clear/Greiner). After rinsing the cell layer once with pre-warmed 1x PBS, cells were fixed with Histofix® for 20 min at 4 °C. The fixed cells were washed twice with cold 1x PBS. They were either stored in 1x PBS at 4 °C or directly labelled with the primary antibody (anti-PLN, anti-Serca2 ATPase or anti- α -actinin). The primary antibodies were diluted in permeabilization buffer and incubated at 4 °C overnight under gentle agitation. After being washed twice with cold 1x PBS, the secondary antibody (rabbit-Alexa 546, mouse-Alexa 488) diluted in permeabilization buffer was added. At the end of the incubation time of 1-2 hours at room temperature under gentle agitation protected from light, Hoechst 33342 (350/461 nm, 1:2,500) diluted in 1x PBS was added to the well for a 20-min incubation for nuclear staining. The cardiomyocytes were washed twice with 1x PBS and were stored in this buffer protected from light. Subsequent analyses were performed by confocal microscopy with the LSM 800 Airyscan (Zeiss) and the 40x-oil objective.

3.6.4 Analysis of 2D hiPSC-CM cell area

The PLNic and PLN p.Arg14del hiPSC-CM were fixed with Histofix® for 20 min at 4 °C after 7 and 30 days in culture in black 96-well plates (μ Clear/Greiner). They were stained for α -actinin 2 and with Hoechst 33342 according to the protocol described in 3.6.3. Images of single cells were taken with the confocal microscope LSM 800 Airyscan (Zeiss, 40x-oil objective). Cell areas were investigated by usage of ImageJ Fiji makro and ROI (region of interest) manager feature. This procedure was kindly performed by Maksymilian Prondzynski (DEPT, UKE, Hamburg, Germany).

4 RESULTS

4.1 Characterization of hiPSC PLN p.Arg14del clones

4.1.1 Patient background

The female patient (born in 1981) with an identified familial PLN c.40-42delAGA mutation donated the skin biopsy at an age of ~31 in 2012. In 2007 at the age of 26 she was diagnosed with DCM with initially moderate but progressive left ventricular insufficiency and repeated episodes of ventricular arrhythmia. Initially in 2007, the ejection fraction was determined with 41% and deteriorated over time (2010: 35-40%, 2012: 30%, 2013: 29%). The diagnose was the result of an out of hospital cardiac arrest in 2007 without any symptoms of left ventricular insufficiency with consecutive ICD (implantable cardioverter-defibrillator) implantation and repeated recordings of ventricular arrhythmias in the following years under sotalol treatment.

4.1.2 Reprogramming of hiPSCs

a) **HiPSC morphology and expression of pluripotency marker**

The patients' fibroblasts were successfully reprogrammed into hiPSC. Two hiPSC clones (#1198 and #1201) showed typical morphology (Figure 20) and expressed pluripotency markers Oct4 and Tra-1-60 as exemplarily shown for the #1201 clone in Figure 19. The reprogramming and characterization was performed by the HEXT Stem Cell Core Facility (UKE, Hamburg, Germany).

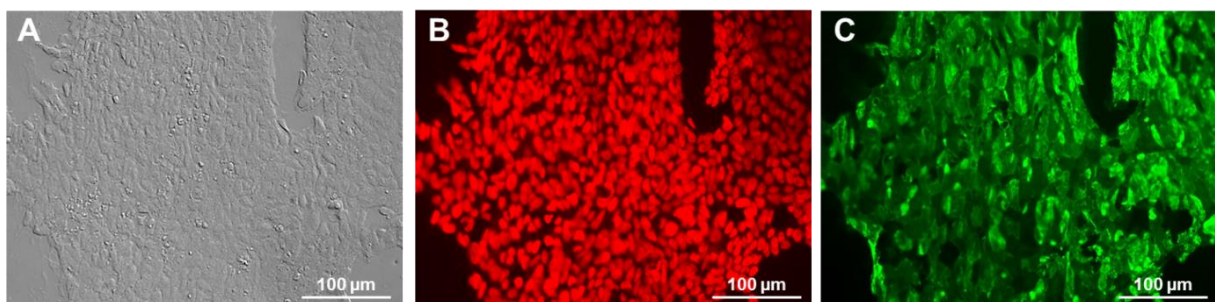


Figure 19: Representative characterization of the PLN p.Arg14del hiPSC clone #1201. A - Bright field microscopy and immunofluorescence for pluripotency markers: B - Oct4 (red) and C - Tra-1-60 (green).

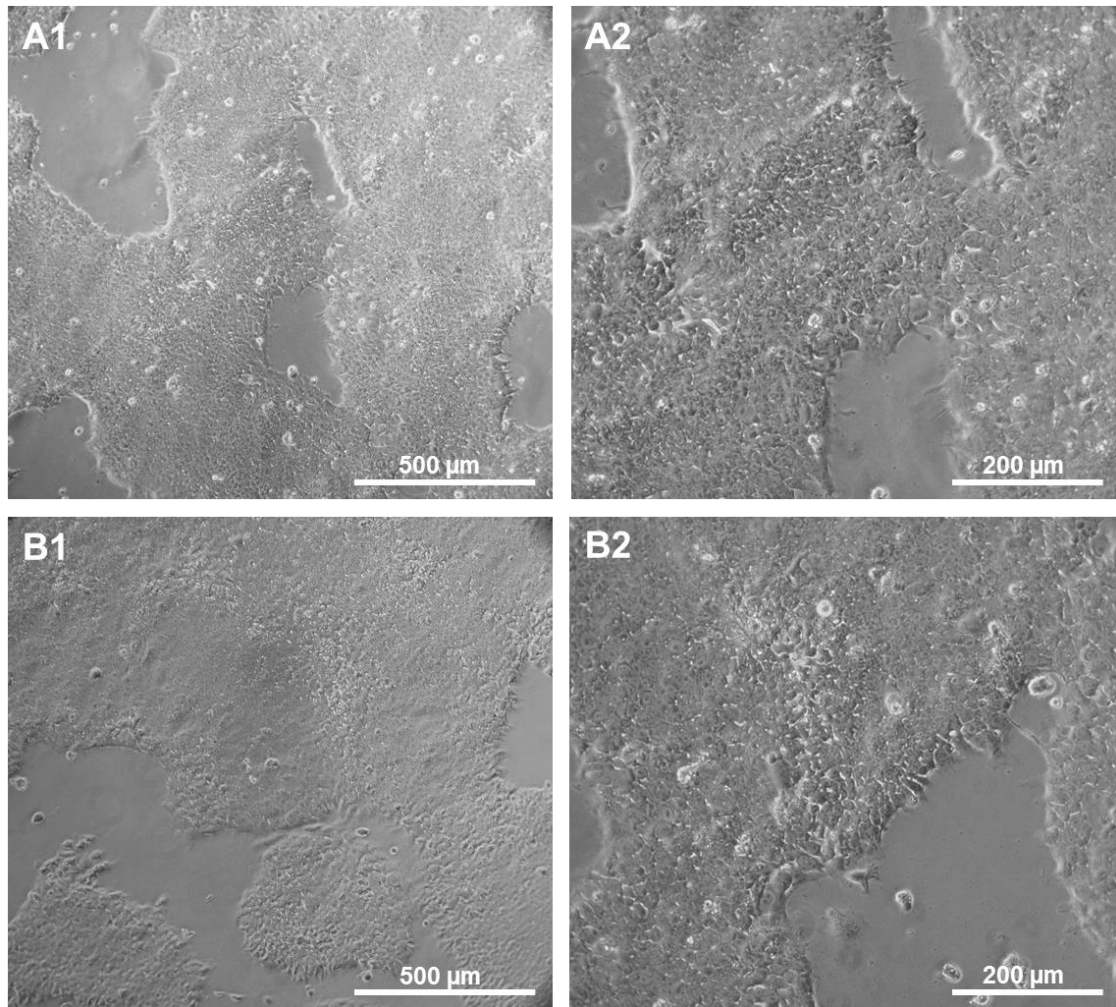


Figure 20: Morphological characterization of the selected hiPSC clones. A1, 2 – Clone #1198; B1, 2 – Clone #1201.

b) Karyotype analysis of the PLN p.Arg14del hiPSC clones

The hiPSC clones were subjected for karyotype analysis (Department for Human Genetics, UKE, Hamburg, Germany). The results for PLN p.Arg14del clone #1198 and #1201 are shown in Figure 21. 15 Metaphases were investigated with 400 bands per haploid set resolution for #1198 and with 500 bands per haploid set resolution for #1201. The karyotypes and Giemsa-banding (G-banding) structures of both cell clones showed a normal karyotype without numerical or structural chromosomal aberrations (46, XX).

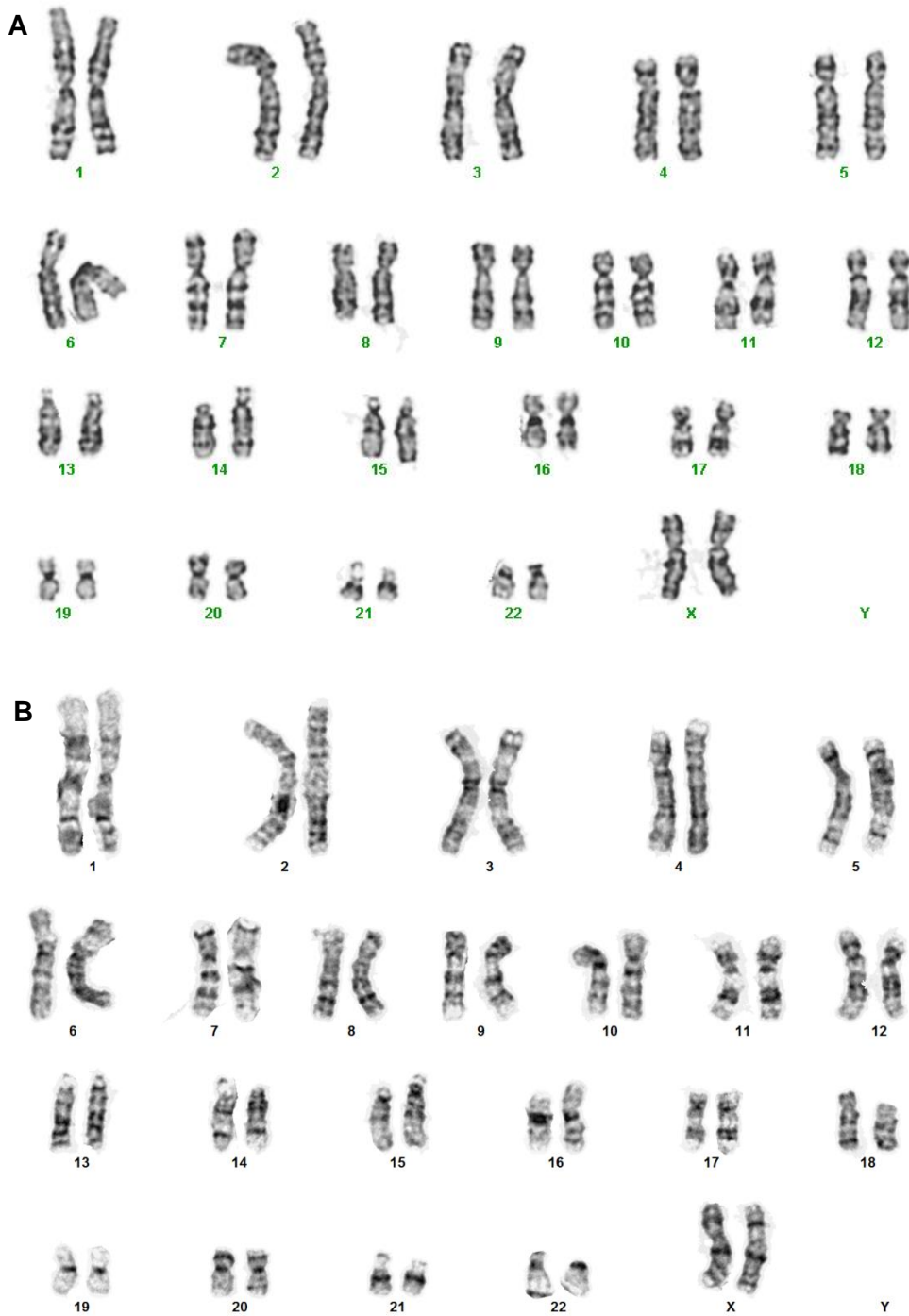


Figure 21: Karyotyping results of PLN p.Arg14del hiPSC clones. A – Clone #1198 (passage 24) and B – clone #1201 (passage 16) showed no chromosomal aberration in all analysed metaphases (46, XX).

c) PLN gene sequencing

Genomic DNA was extracted from hiPSC, and the PLN gene locus was amplified by an established PCR with 'hPLN-1.3 kB-Fw' and 'hPLN-1.3 kB-Rev' primers. The purified PCR product was sent for sequencing with 'hPLN-Fw' and the resulting sequence was analysed by aligning the sequencing results to the NCBI-derived PLN wildtype sequence (NCBI reference sequence: NG_009082.1). Figure 22 demonstrates the verification of the expected heterozygous PLN genotype of both #1198 and #1201 hiPSC clones. In both clones the electropherogram showed the wildtype sequence until PLN c.37-39AGA (PLN p.Arg13). Due to the c.40-42AGAdel (p.Arg14del) on only one allele the sequencing results of each sequenced allele overlay. This caused the double peaks and disrupted the alignment of the electropherograms.

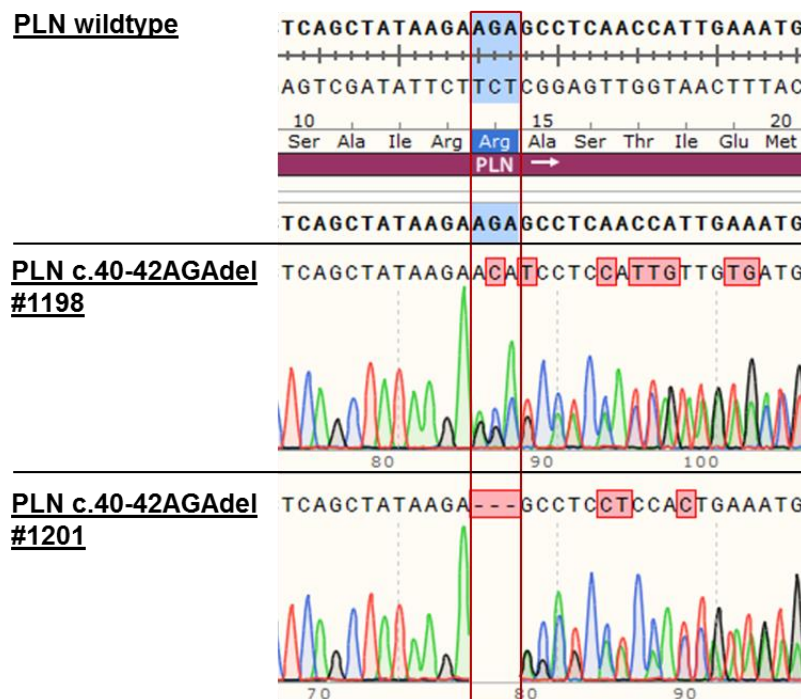


Figure 22: Representative SnapGene alignment of the PLN wildtype sequence with the hiPSC clones #1198 and #1201. The sequencing results showed the heterozygous PLN c.40-42AGAdel (~PLN p.Arg14del) mutation in both hiPSC clones.

4.2 CRISPR/Cas9-mediated genomic correction of PLN c.40-42AGAdel gene locus

4.2.1 PLN sequence validation prior to the *in silico* CRISPR experiment design

For CRISPR/Cas9-mediated genomic correction of the mutated PLN c.40-42AGAdel locus the hiPSC clone #1198 was chosen. After isolation of the hiPSC genomic DNA 25 µg were used for the PCR amplification of a ~1.3 kB PCR product (1258 bp) covering the PLN coding sequence locus. The PCR product was analysed on a 1% agarose gel and verified the correct size (Figure 23).

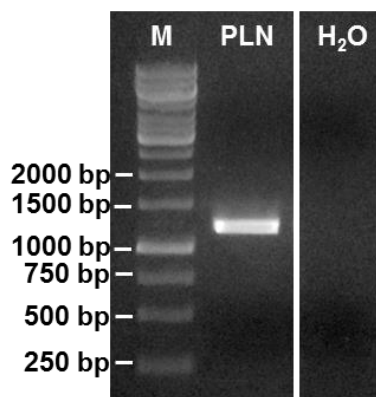


Figure 23: 1% Agarose gel electrophoreses of the PLN 1258 bp PCR product. M = Marker (GeneRuler 1 kb DNA Ladder); H₂O = quality control.

The purified PCR product with a concentration of 32.1 ng/µL was used for T4 ligation into the pJET1.2/blunt cloning vector. The vector was amplified in TOP10 bacteria. Plasmid preparation out of 10 colonies was performed and sent for sequencing with the forward and reverse pJET1.2 primer pair. This enabled the analysis of the individual alleles to screen for single nucleotide polymorphism (SNP) since the sequencing results were ambiguous due to the presence of the heterozygote c.40-42AGAdel mutation. The sequencing results are attached in the supplement in Figure S1. The alignment to the human PLN wildtype sequence derived from NCBI database revealed that 6/10 analysed clones carried the wildtype sequence and that 4/10 matched the PLN c.40-42AGAdel sequence. In the PLN coding sequence no SNPs were detected and had to be considered for the design of the following CRISPR/Cas9 *in silico* experiment.

4.2.2 *In silico* design of the gRNA and repair template

a) Design of the gRNA

The mutated PLN c.40-42AGAdel sequence was submitted to the Zhang labs' online CRISPR design tool (<http://crispr.mit.edu>). In Figure 24 the job submission result is shown providing suitable gRNA sequences ranked according to the quality score.

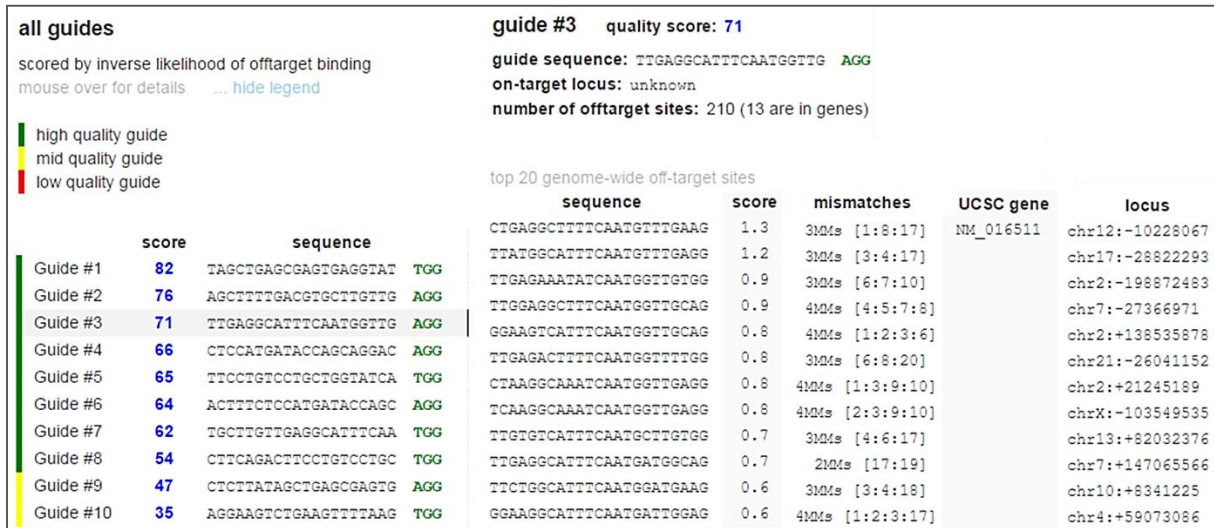


Figure 24: Job submission result of the *in silico* design using the online CRISPR design tool of the Zhang lab (MIT). The gRNAs ('guide') were ranked according to their score dependent on the on-target and off-target activity. For each guide details are given indicating its on-target locus, number of off-target sites and a ranking of the top 20 most likely genome-wide off-target locations.

Even though guide #1 and guide #2 had higher scores, guide #3 was chosen since it was closest to the mutated target locus (5 nucleotides downstream) with a low number of possible exonic off-target sites. Figure 25 depicts the exact binding location of gRNA #3 within the PLN coding sequence. In case of the mutated PLN allele, the PLN c.41-43 encoded the NGG PAM sequence and for the wildtype allele PLN c.44-46 served as the PAM sequence.

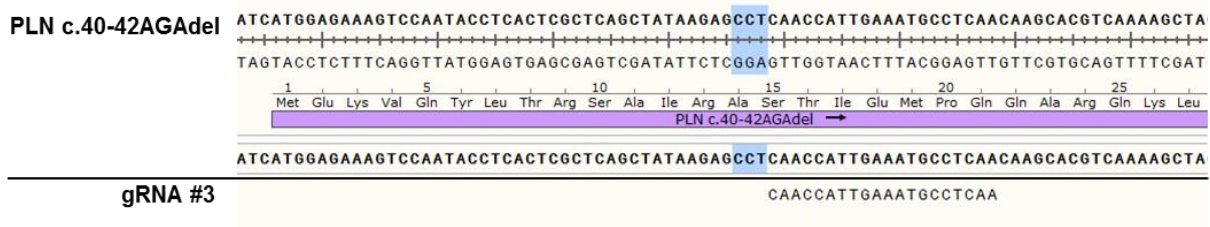


Figure 25: SnapGene alignment of the gRNA #3 sequence with the PLN c.40-42AGAdel sequence. The NGG PAM in proximity to the mutated target locus is highlighted in blue.

b) Design of the ssODN repair template

The ssODN repair template was designed with a length of 103 nt spanning the missing AGA codon (PLN c.40-42). This target locus was flanked upstream and downstream by homology arms of 50 nt each. To avoid cleavage of the repair template by the Cas9 ribonucleoprotein complex the NGG PAM motif was mutated so that the gRNAs would not recognize the ssODN. Since the PAM was located within the coding region of PLN a silent mutation was inserted to modify the NGG motif to NTG still encoding for PLN p.Ala15 (silent mutation). The repair template was designed and ordered as antisense ssODN so the repaired sequence would carry the PLN c.45C>A silent mutation then. Figure 26 illustrates the alignment of the mutated PLN sequence, the gRNA #3 and the repair template with the wildtype sequence. The inserted silent mutation within the PAM (highlighted in blue) is marked with a blue arrow.

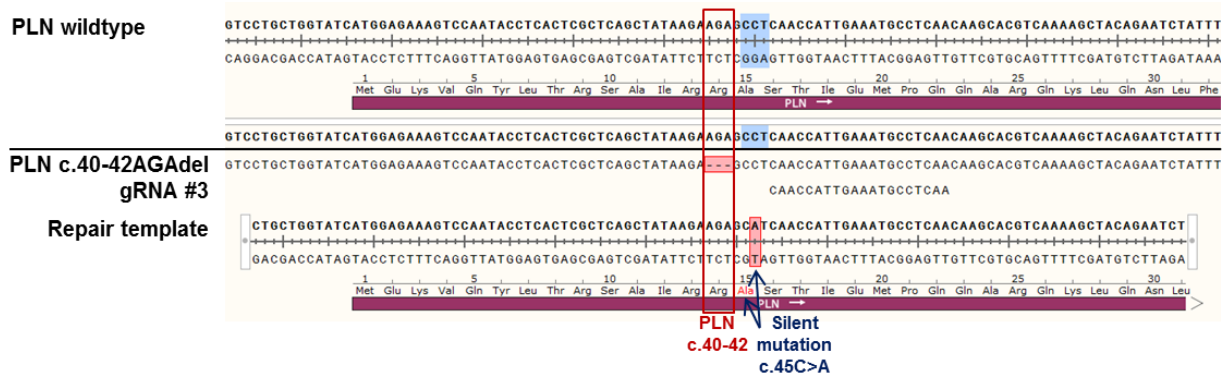


Figure 26: SnapGene alignment of the PLN c.40-42AGAdel, gRNA #3 and ssODN sequences with the wildtype PLN gene. The PAM is highlighted in light blue and the designed ssODN repair template carried the silent mutation within the PAM (PLN c.45C>A).

c) Summary of the *in silico* designed CRISPR/Cas9 experiment

Figure 27 depicts the schematic summary of the *in silico* designed and applied CRISPR/Cas9 approach.

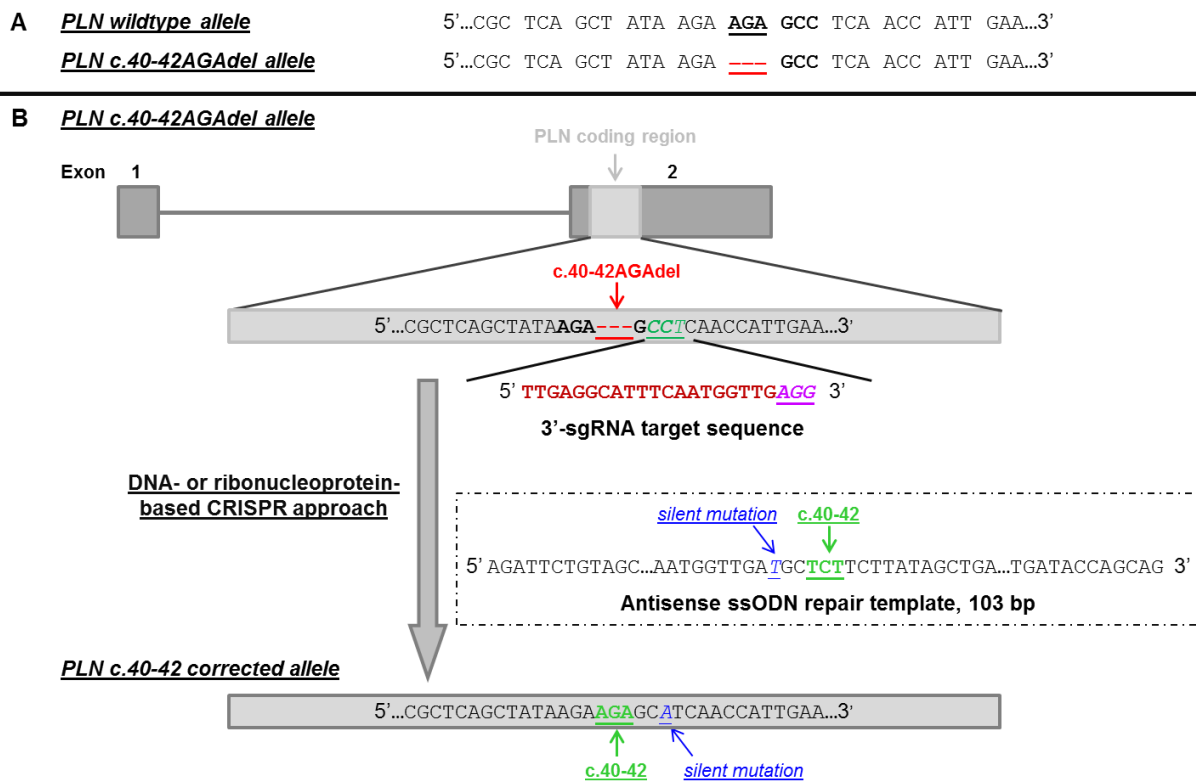


Figure 27: Schematic summary of the *in silico* design of the CRISPR/Cas9 experiment. A - Comparison of the PLN wildtype and mutated allele. B - Gene correction strategy of the PLN c.40-42AGAdel sequence to wildtype.

4.2.3 Preparation of the DNA-based approach

The pSpCas9(BB)-2A-GFP plasmid (ordered from Addgene) was linearized by BbsI restriction digestion to enable the ligation of the annealed sense and antisense gRNA #3-DNA oligomers. The vector had an expected size of 9281 bp. This was verified in an agarose gel analysis as shown in Figure 28. After gel extraction the linearized vector preparation had a concentration of 50 ng/ μ L.

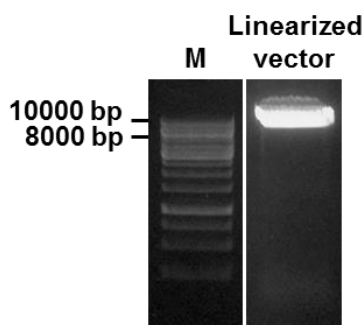


Figure 28: 1% Agarose gel electrophoresis as quality control of the linearized pSpCas9(BB)-2A-GFP vector after BbsI restriction digest. M = Marker (GeneRuler 1 kb DNA Ladder).

The annealed gRNA #3-DNA oligomers were ligated into the linearized vector. A representative vector map can be found in the supplement (Figure S2). The pSpCas9-gRNA#3-2A-GFP plasmid was transformed into TOP10 bacteria and further propagated. The isolated plasmid DNA of two clones was directly sent for sequencing with the 'U6-Forward' primer. The sequencing result confirmed the correct sequence which is depicted in Figure 29. The sequencing results for gRNA #3-DNA sequence were aligned to the designed gRNA #3-DNA and no mismatches were detected. Additionally, the sgRNA-DNA scaffold was also proven to be correct. The plasmid was further isolated out of a maxi preparation to be used as final starting product for the nucleofection of the PLN p.Arg14del hiPSC within the DNA-based CRISPR/Cas9 approach. All cloning procedures were kindly performed by Dr. Ingke Braren of the HEXT Vector Core Facility (UKE, Hamburg, Germany).

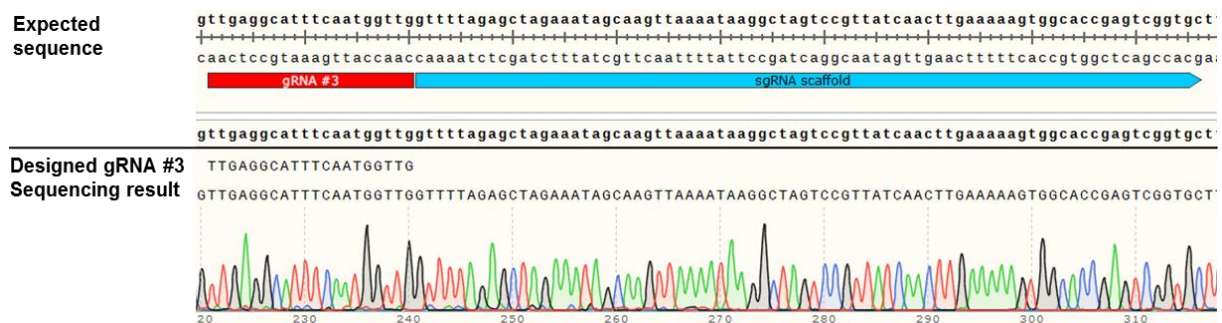


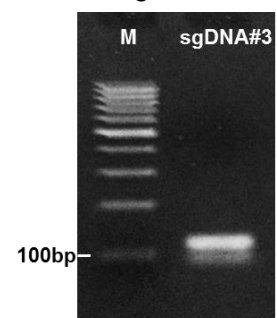
Figure 29: Representative SnapGene alignment of the sequencing result to the *in silico* designed sgRNA after the ligation of the gRNA #3 into the pSpCas9(BB)-2A-GFP vector upstream of the sgRNA scaffold. The gRNA (red) was successfully inserted upstream of the sgRNA scaffold (blue) and matched the *in silico* designed gRNA #3 sequence.

4.2.4 Preparation of the RNP-based approach

a) **Successful sgDNA synthesis**

The designed 120-bp long sgDNA template serving as template for later *in vitro* transcription is shown in Figure 29. The designed gRNA sequence was included into the T7-gRNA#3-Forward primer sequence. By primer annealing reaction and extension PCR the sgDNA was synthesized. The successful generation of the sgDNA construct was verified via agarose gel electrophoresis (Figure 30) and sent for sequencing with both, IVT-Forward and IVT-Reverse primer.

Figure 30: 2% Agarose gel electrophoresis to verify quality and size of the generated sgDNA #3 construct. M = Marker (GeneRuler 100 bp DNA Ladder).



The sgDNA appeared at the expected size of 120 bp and the correct sequence was confirmed (Figure 31). The purified sgDNA had a concentration of 44 ng/μL with a good quality (260/280 ratio: 1.82; 260/230 ratio: 2.22).



Figure 31: SnapGene alignment of the sequencing result of the generated sgDNA to the *in silico* designed sgDNA #3 construct. The T7-gRNA#3 primer pair was used for generation of the sgDNA #3 which is composed of the T7 promoter, the designed gRNA #3 DNA sequence and the sgRNA scaffold DNA sequence with a total length of 120 bp. The sequence verification was done with the IVT-primer pair.

b) *In vitro* transcription of the generated sgDNA

For sgRNA *in vitro* transcription, two sgDNA starting conditions were tested, 0.1 μg and 0.3 μg. After IVT and purification the RNA was analysed for degradation and quality in a 2% agarose gel. The analysis is shown in Figure 32 and verified the absence of RNA degradation. The RNA bands of both starting conditions, 0.1 μg and 0.3 μg sgDNA, ran at the expected size of about 100 bp and showed one strong band and no ladder of smaller bands suggesting that no degradation occurred. In the 0.3 μg condition the band appeared more bright and strong. The concentration determination matched this observation. From the 0.3 μg starting condition 1 μg sgRNA was produced, with an input of 0.1 μg sgDNA 0.4 μg sgRNA was generated. Both sgRNA preparations showed high quality scores (0.1 μg: 260/280 – 2.33, 260/230: 2.29; 0.3 μg: 260/280 – 2.37, 260/230: 2.78).

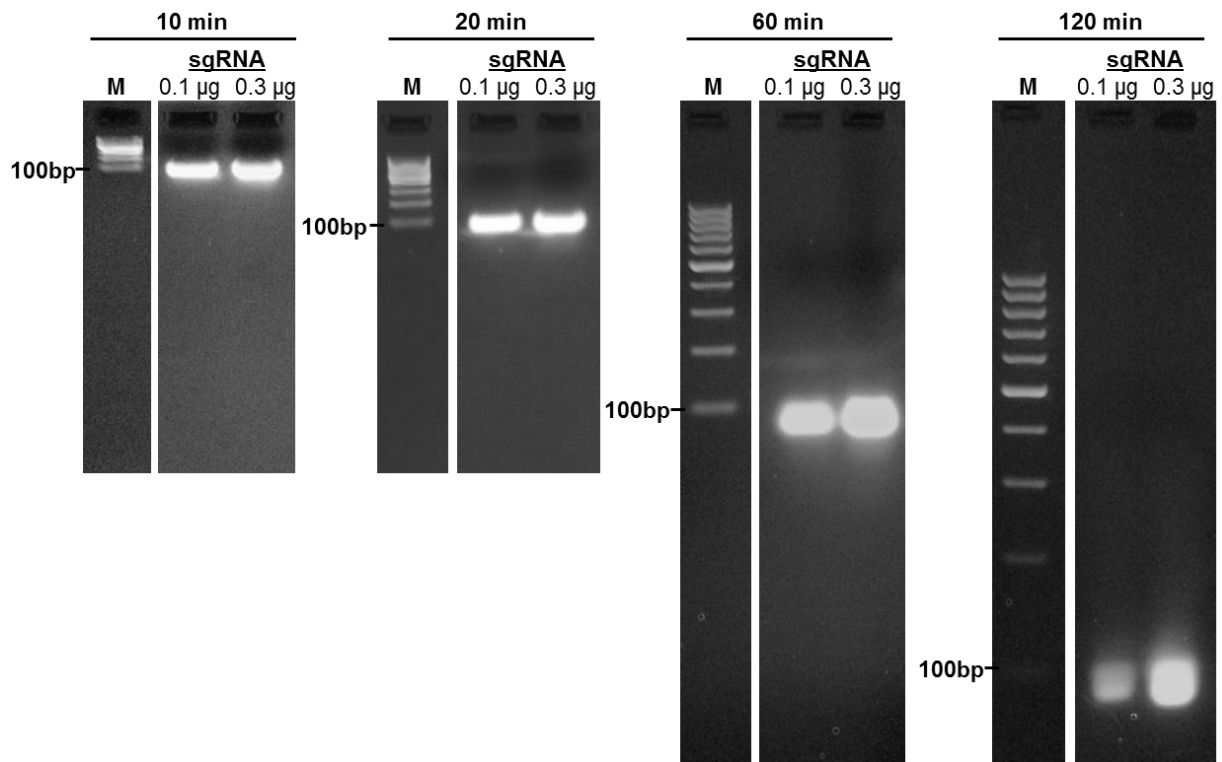


Figure 32: 2% Agarose gel analysis to check for IVT-derived sgRNA #3 and possible RNA degradation. The values 0.1 µg and 0.3 µg refer to the sgDNA starting concentration for the IVT. Pictures were taken after 10 min, 20 min, 60 min and 120 min running time at 80-90 V. M = Marker (GeneRuler 100 bp DNA Ladder).

c) *In vitro* verification of the RNP functionality

The purified *in vitro* transcribed RNA was precipitated and reconstituted at a final concentration of 10 µg/µL. In order to test the ability of the sgRNA to guide the RNP complex to the correct location and to check the functionality of the purchased Cas9 nuclease an *in vitro* digestion approach was investigated. A PCR product with 1258 bp was amplified which contained the PLN c.40-42 locus in the centre. This served as a DNA template. Since the gRNA-target sequence is located in close proximity to the PLN c.40-42 locus the Cas9 was expected to cut the PCR product into two ~600 bp long fragments. The result is shown in Figure 33. The undigested PCR product appeared at ~1300 bp. In the presence of both Thermo Fisher and New England Biolabs-purchased Cas9 nucleases an additional faint band appeared at about 600 bp. These were absent without the Cas9 guiding sgRNA #3.

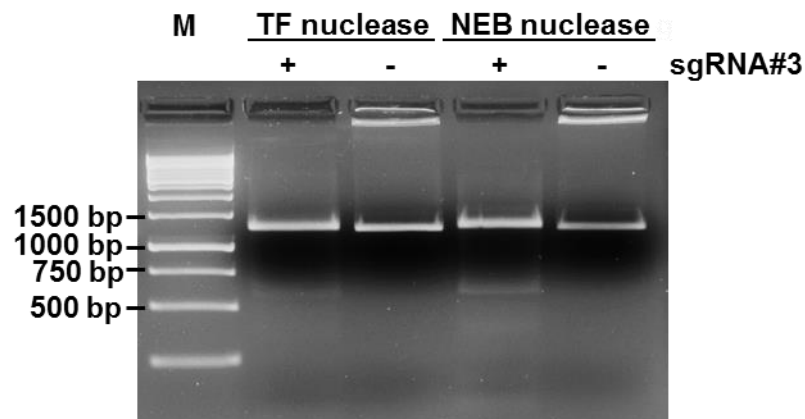


Figure 33: 1.5 % Agarose gel analysis to verify the *in vitro* Cas9 functionality and sgRNA #3 guiding ability. Thermo Fisher- (TF) and NewEngland Biolabs (NEB)-purchased nucleases were tested with (+) and without (-) sgRNA #3 supplementation. M = Marker (GeneRuler 1 kb DNA Ladder).

4.2.5 Evaluation of DNA- and RNP-based generation of PLNic

a) RNP-based approach

Since the *in vitro* test was successful, the sgRNA #3 was used in combination with the Thermo Fisher Scientific-derived Cas9 nuclease for the nucleofection of the PLN p.Arg14del #1198 hiPSC. The transfected hiPSCs were cultivated both in the presence and absence of SCR7 (1 μ M, DNA ligase IV inhibitor). Due to the lack of a selection marker no selection for nucleofected hiPSCs was performed. 48 Hours after nucleofection, the hiPSC were further sub-cultivated at low density with 3000 cells/10 cm² to enable clonal expansion. Low-density seeded cells were cultivated in the presence and absence of SCR7 for 48 hours. The growing hiPSC clones showed a normal cell and crisp clone morphology for both conditions (\pm SCR7) as exemplarily shown in Figures 34A and 34B. Figure 34C represents the picking procedure under sterile conditions with a 100 μ L pipette tip. Clones which grew too close to each other were not picked to avoid picking of mosaic cell clones.

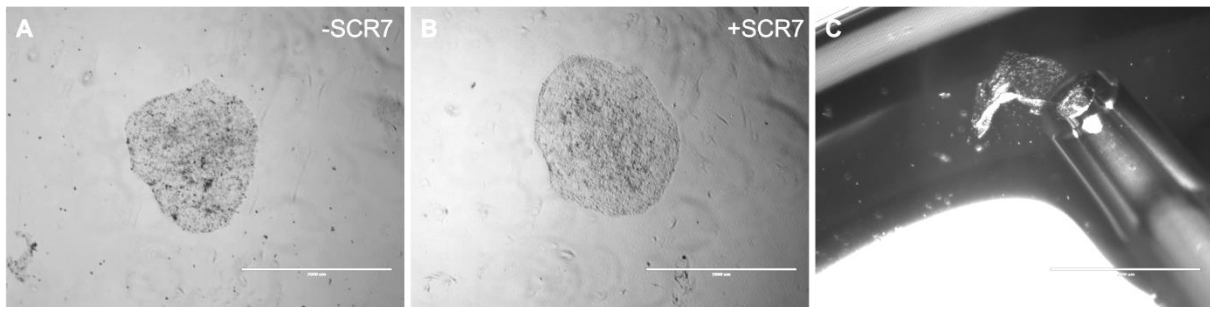


Figure 34: Clonal growth of nucleofected and low-density seeded PLN p.Arg14del hiPSC. HiPSC clones **A** - without and **B** - with addition of SCR7. **C** - Picking procedure of each single cell clone with the 100 μ L pipette tip under sterile conditions for further expansion in a 48-well plate. Scale bars: 2 mm.

For both condition 12 clones were picked 12-14 days after seeding for further clonal expansion. In total 15 clones of the -SCR7 condition and 12 clones of the +SCR7 approach were analysed for their genotype.

Sequencing results revealed the successful gene correction of 1/27 analysed clones (4% homologous recombination efficiency). This PLN isogenic control clone (PLNic #28) was derived from the -SCR7 condition and its sequencing result is depicted in Figure 35. The sequencing result was verified with a second sequencing experiment to confirm that the repair template was only recombined and inserted into the mutated allele. Two sequencing results are shown in Figure 35 for PLNic #28. In both electropherograms the heterozygous silent mutation was detected.

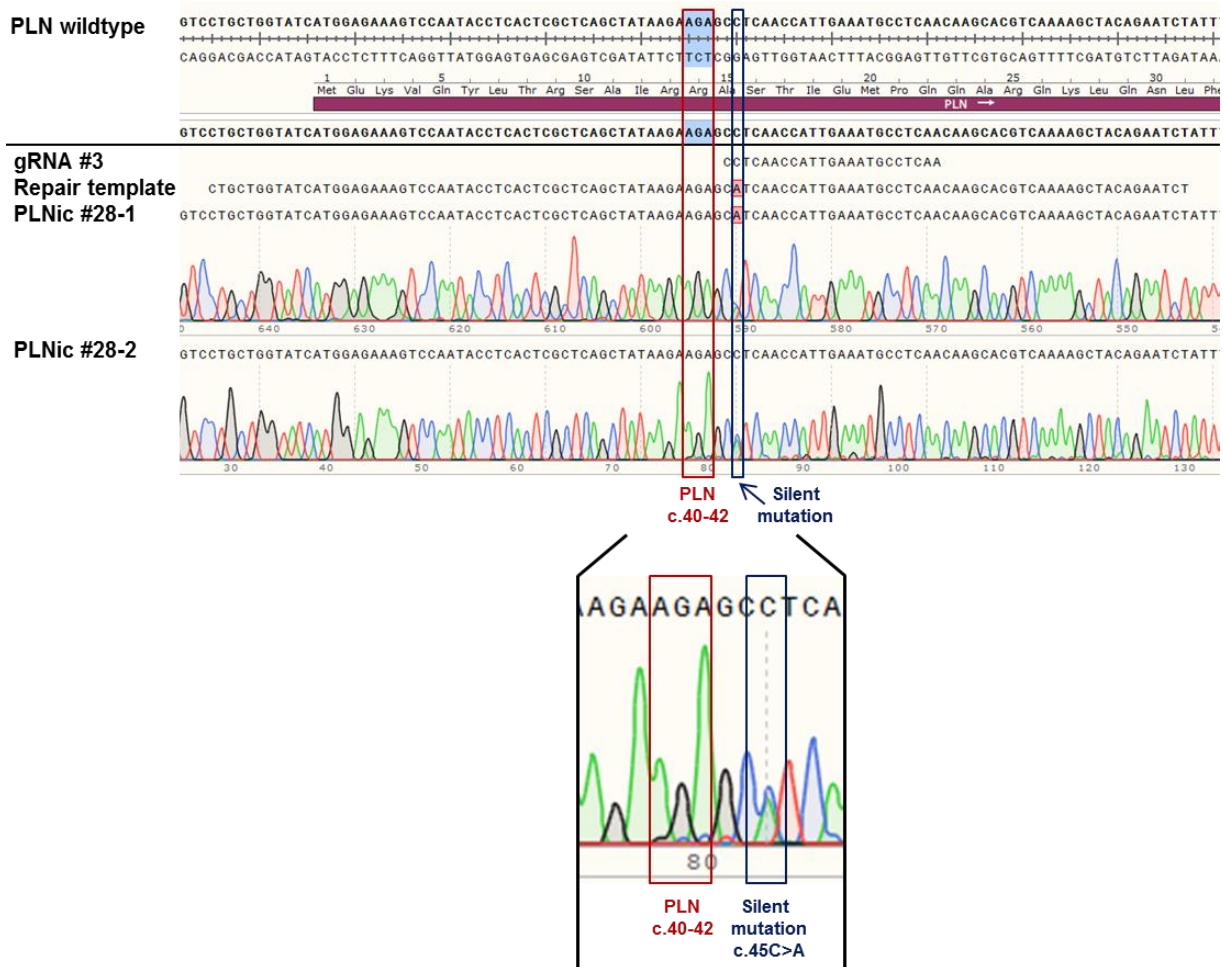


Figure 35: SnapGene alignment of the DNA sequencing result of the successfully generated isogenic control clone PLNic #28. A heterozygous insertion of the repair template was confirmed by the appearance of double peaks at PLN c.45 locus in the electropherogram as depicted in the magnified detail. In both sequencing results (PLNic #28-1, PLNic #28-2) the PLN c.45C>A silent mutation was detected.

All remaining 26 clones did not show homologous recombination. The sequencing results of two negative clones are exemplarily shown in Figure 36. The heterozygous genotype remained unchanged as shown for clone #26 (-SCR7 condition). For clone #21 (+SCR7 condition) even a truncation of the PLN coding sequence was detected in the Cas9 cutting region in close proximity to the PAM sequence. Table 25 summarizes the details and results of the RNP-based approach.

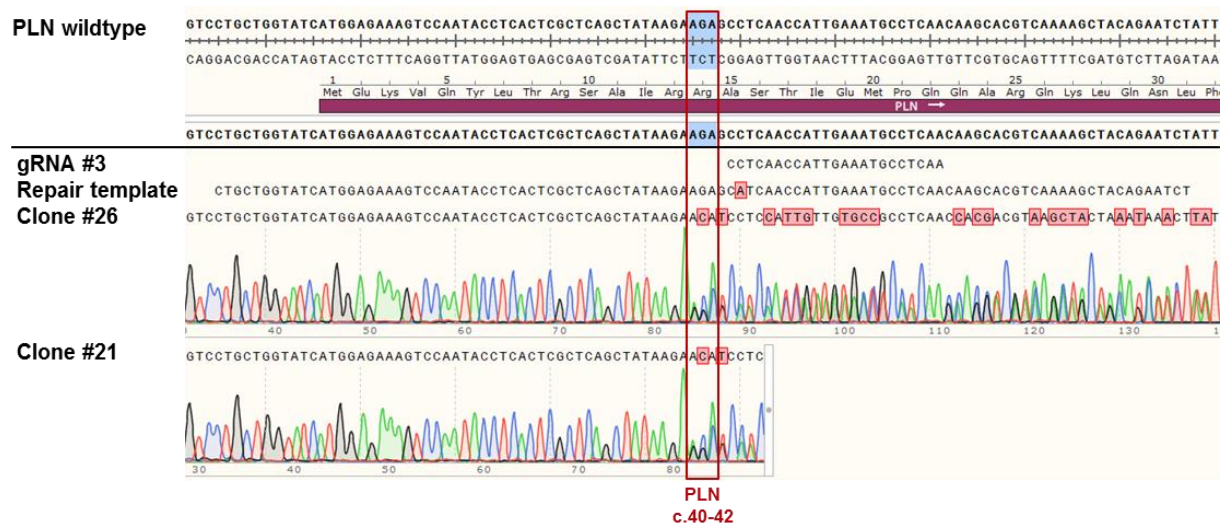


Figure 36: SnapGene alignments of the DNA sequencing results of two representative clones (#21, #26) not successfully corrected. Clone #26 was derived from the -SCR7 condition, clone #21 from the +SCR7 approach.

Table 25: Summarized overview of the RNP-based CRISPR experiment. TFE: Transfection efficiency; HRE: Homologous recombination efficiency of each experiment.

Details	TFE	Seeded cells	Picked clones	Sequencing result	HRE
RNP-approach 5 μ M ssODN; +/- SCR7	unknown	-SCR7: 3000	-SCR7: 18	-SCR7: 15 clones analysed/ 1 POSITIVE (#28)	4 %
		+SCR7: 3000	+SCR7: 12	+SCR7: 12 clones analysed/ ALL NEGATIVE	

b) DNA-based approach

In prior experiments Cas9-mediated cutting was observed without recombination of the ssODN repair template. In consequence the RNP complex was functional, but the concentration of the repair ssODN was likely too low. Therefore the ssODN concentration was increased from 0.4 μ M (Ran et al. 2013b) to 5 μ M in accordance to the RNP-based approach for the following experiments. In addition, SCR7 was added to all experiments to prevent NHEJ.

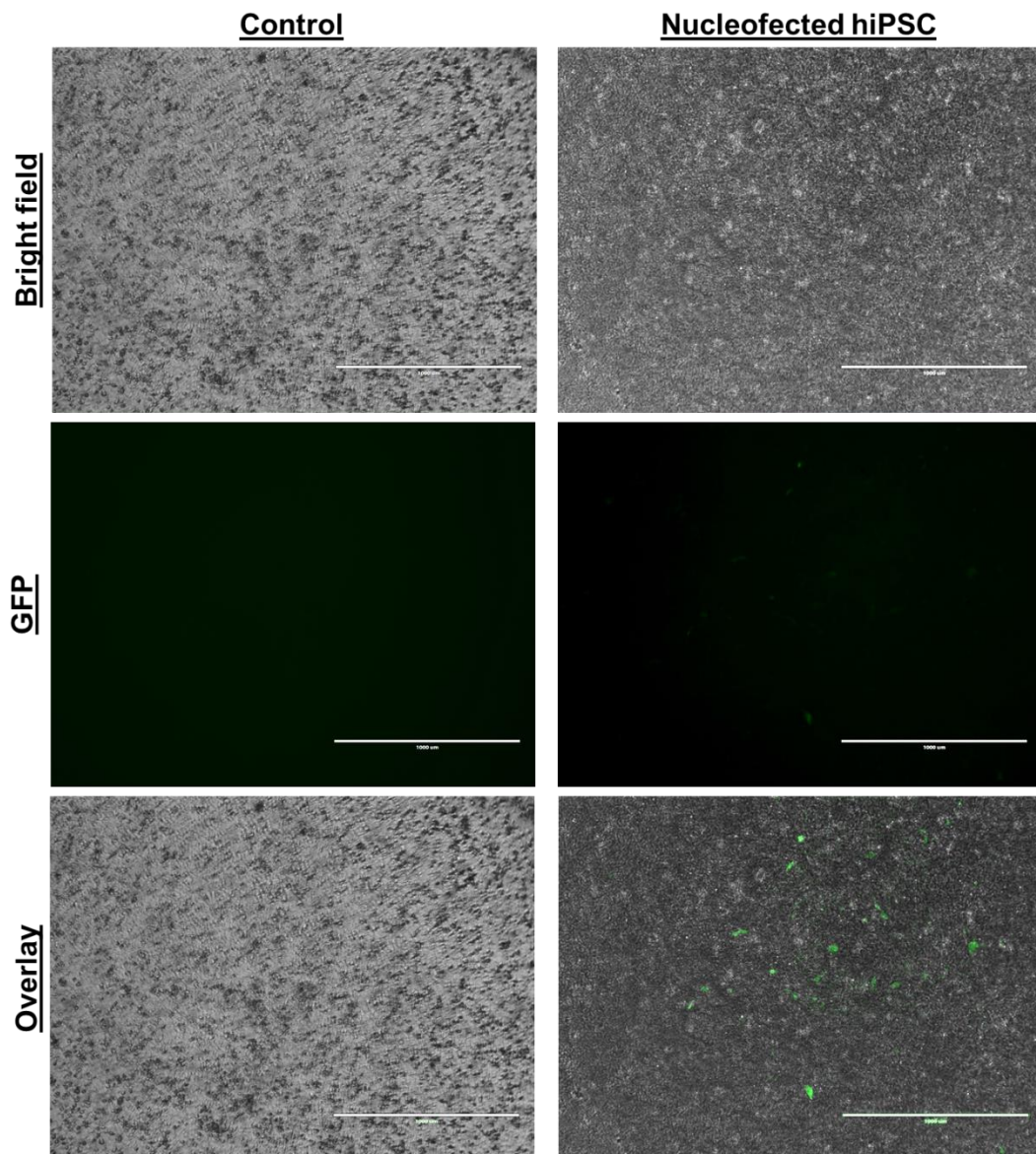


Figure 37: Microscopic analysis of pSpCas9-sgRNA#3-2A-GFP plasmid expression of confluent hiPSC monolayer to check for transfection efficiency 48 hours after nucleofection. Scale bars: 1 mm.

After 48 hours GFP-positive cells were detected in the nucleofected hiPSCs while GFP signal was absent in untransfected controls (Figure 37). Nucleofection efficiency was evaluated by analysing GFP-positive hiPSCs during FACS sorting with 6.7% (Figure 38). GFP-positive hiPSCs were sorted and plated at low density.

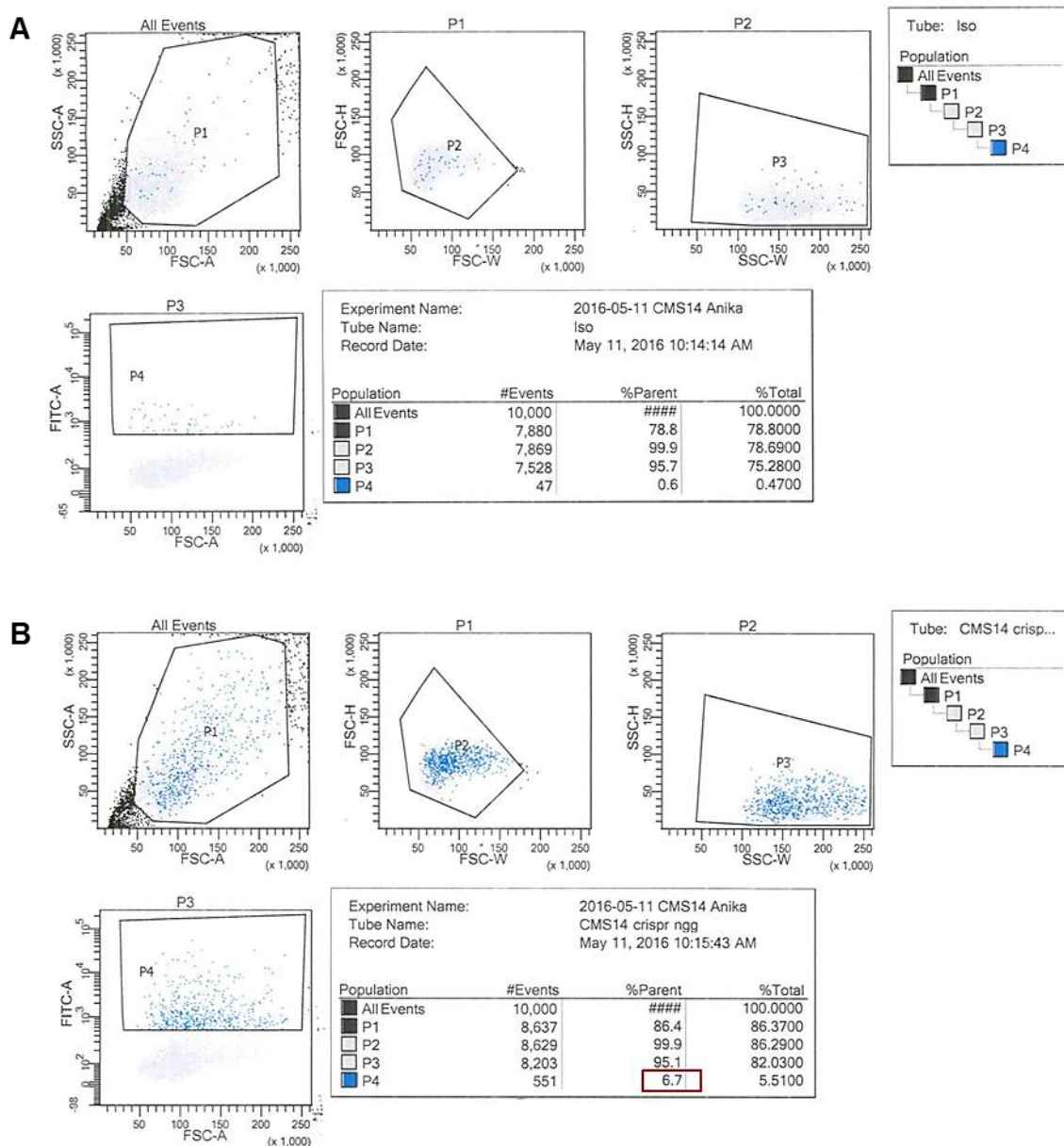


Figure 38: FACS-sorting of GFP-positive hiPSC. The results of **A** - reference and **B** - nucleofected hiPSC sorted for GFP positivity are shown. The final transfection efficiency is framed in red.

In total 62,242 hiPSCs were GFP-positive. 7,500 GFP-positive hiPSC were then further processed and seeded at low density with 1,000 cells/10 cm² and 1,500 cells/10 cm² in wells of a 6-well plate. The remaining ones were frozen down as a backup. From both cell densities in total 48 single clones were picked for further clonal expansion (Figure 39). After picking of the clones SCR7 supplementation was discontinued.

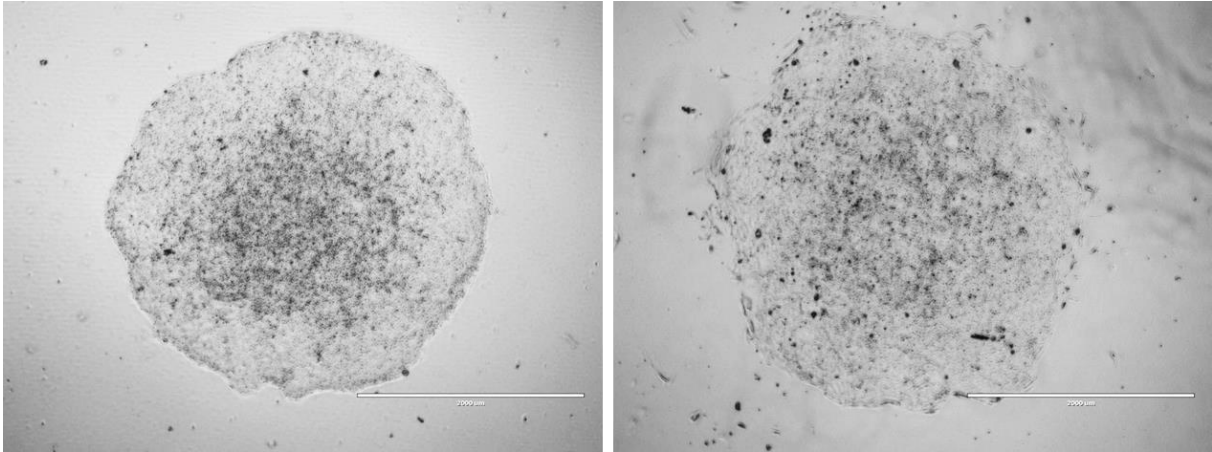


Figure 39: Representative cell clone sizes and morphologies before picking and clonal expansion. Scale bars: 2 mm.

From the 48 picked hiPSC clones, 7 clones stopped proliferating, started to differentiate or did not attach after picking. The remaining 41 clones were further clonally expanded, frozen down and finally analysed for homologous recombination.

Sequencing results revealed that three isogenic controls, PLNic #15, PLNic #24 and PLNic #45, showing homozygous wildtype genotypes, were successfully generated with a homologous recombination efficiency of 7%. The existence of a homozygous form for the silent mutation (PLN c.45C>A) is an indicator that the repair template was recombined into both alleles (Figure 40). Sequencing results of clones showing no gene correction to wildtype sequence are exemplarily depicted in Figure 41. Clone #6 showed a homozygous genotype but also a larger deletion of 20 bp from the PLN c.40 locus on. For clone #14 the PLN c.40-42AGAdel was indeed corrected, but a heterozygous genotype sequence was found within the cutting region of the Cas9.

Table 26 summarized the details of the successful DNA-based approach.

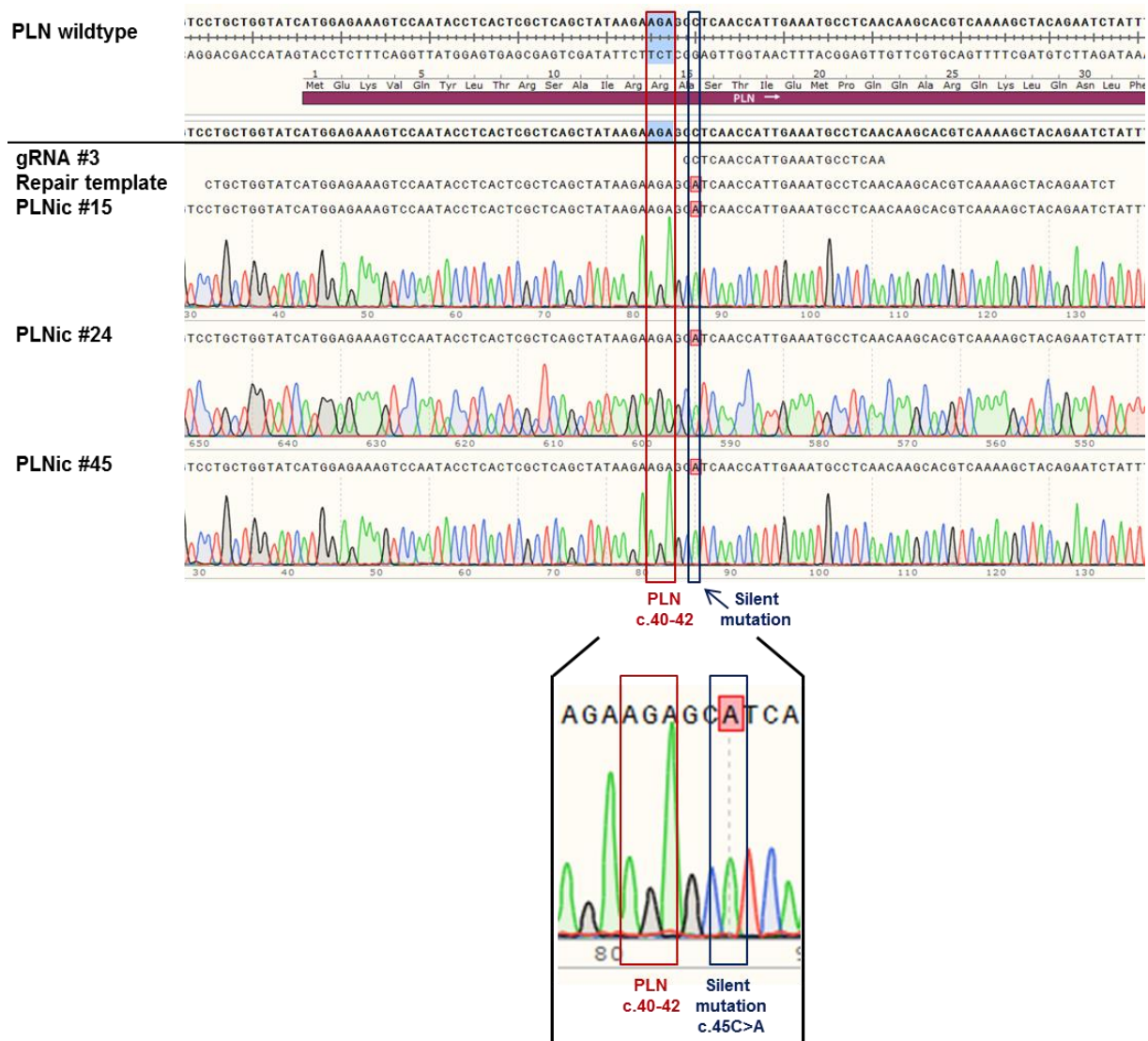


Figure 40: SnapGene alignment of the DNA sequences of the successfully generated isogenic control clones PLNc #15, PLNc #24 and PLNc #45. A homozygous insertion of the repair template was identified by checking for the PLN c.45C>A silent mutation depicted in the magnified detail of the electropherogram of PLNc #45.

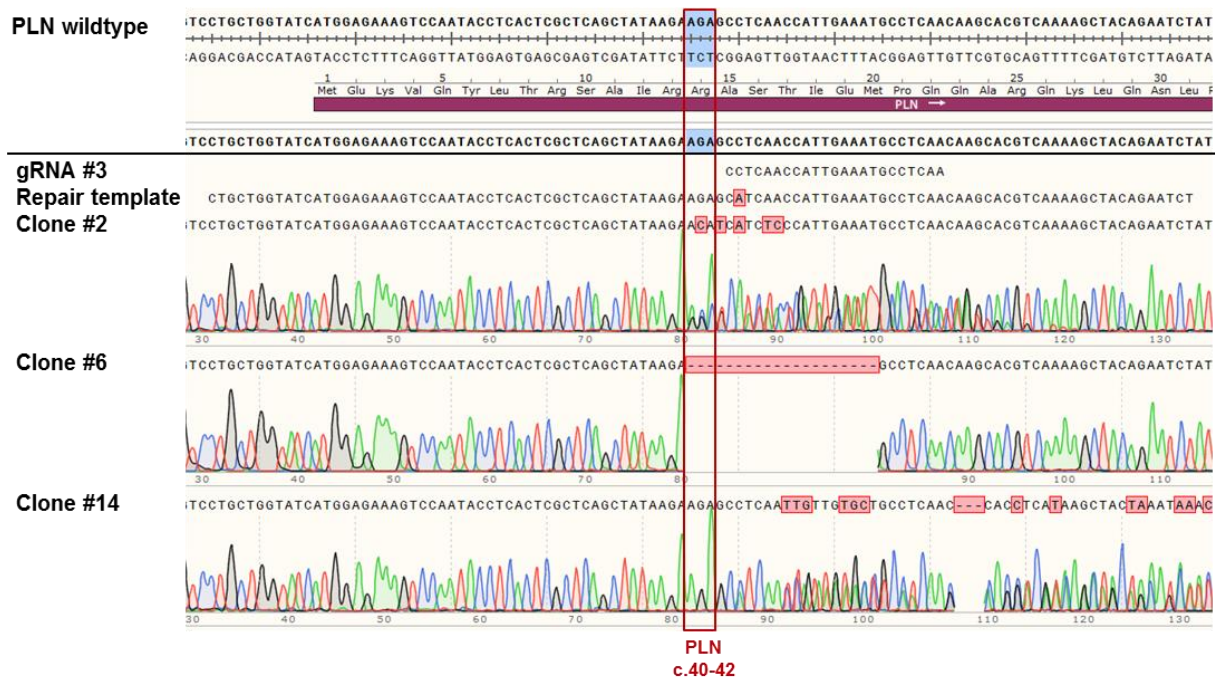


Figure 41: SnapGene alignment of the DNA sequences of three representative clones (#2, #6 and #14) not successfully corrected.

Table 26: Summarized overview of the DNA-based CRISPR experiments. TFE: Transfection efficiency; HRE: Homologous recombination efficiency of each experiment.

Details	TFE	Seeded cells	Picked clones	Sequencing result	HRE
DNA-approach II 5 µM ssODN; +SCR7	6.7 %	7500 (of 62,242 total)	48 (all)	41 clones analysed/ 3 POSITIVE (#15, #24, #45)	7 %

4.2.6 Off-target validation

All four successfully generated isogenic control clones, PLNic #28, #15, #24 and #45, were analysed for off-target activity by PCR and sequencing. Figure 42 shows the job submission result using the online CRISPR design tool of the Zhang lab (MIT, <http://crispr.mit.edu>). It displayed the top 10 most likely genome-wide off-target locations with scores ranging from 0.7 to 1.3.

guide #3 quality score: 71

guide sequence: TTGAGGCATTTCAATGGTTG AGG

on-target locus: unknown

number of offtarget sites: 210 (13 are in genes)

top 20 genome-wide off-target sites

sequence	score	mismatches	UCSC gene	locus
CTGAGGCTTTTCAATGTTTGAAG	1.3	3MMs [1:8:17]	NM_016511	chr12:-10228067
TTATGGCATTTCATGTTTGAGG	1.2	3MMs [3:4:17]		chr17:-28822293
TTGAGAAATATCAATGGTTGTGG	0.9	3MMs [6:7:10]		chr2:-198872483
TTGGAGGCTTTCAATGGTTGCAG	0.9	4MMs [4:5:7:8]		chr7:-27366971
GGAAGTCATTTCAATGGTTGCAG	0.8	4MMs [1:2:3:6]		chr2:+138535878
TTGAGACTTTTCAATGGTTTGG	0.8	3MMs [6:8:20]		chr21:-26041152
CTAAGGCCAAATCAATGGTTGAGG	0.8	4MMs [1:3:9:10]		chr2:+21245189
TCAAGGCCAAATCAATGGTTGAGG	0.8	4MMs [2:3:9:10]		chrX:-103549535
TTGTGTCATTTCAATGCTTGTGG	0.7	3MMs [4:6:17]		chr13:+82032376
TTGAGGCATTTCAATGATGGCAG	0.7	2MMs [17:19]		chr7:+147065566

Figure 42: The 10 most likely off-target loci for the gRNA #3 according to the online CRISPR design tool of the Zhang lab (MIT).

The gel analysis depicted in Figure 43 revealed clean PCR products of all 10 off-target regions representative shown for PLN^{ic} #15. All PCR products were detected at the expected sizes (see supplement Table S4 for primer sequences and expected PCR product sizes).

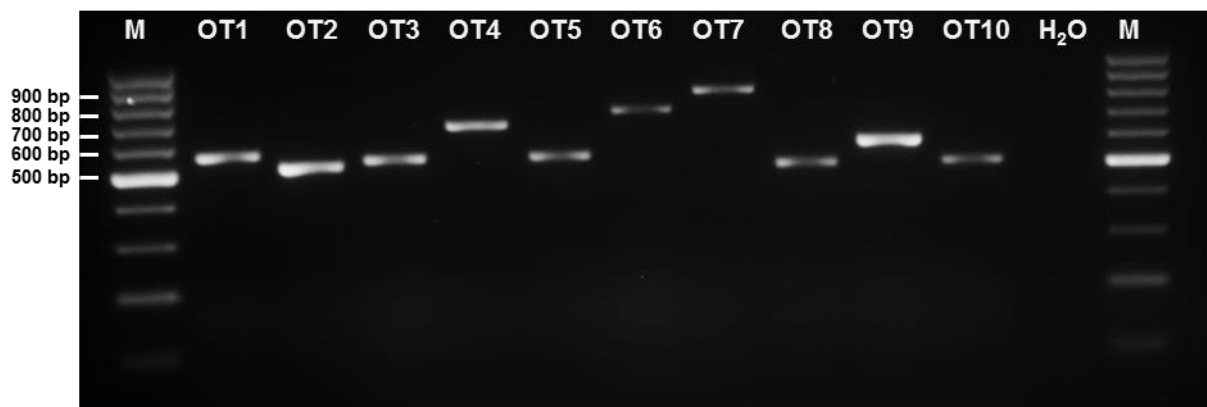


Figure 43: 1.8% Agarose gel analyses of the PCR-amplified off-target sequences (OT1-10) representative for PLN^{ic} #15. M = Marker (GeneRuler 1 kb DNA Ladder); H₂O = quality control.



Figure 44: Representative SnapGene alignment of the sequencing results of the PLNc #15, #24 and #45 clones (DNA-based approach) as well as PLNc #28 (RNP-based approach) for the validation of gRNA #3 off-targets. A - Off-target site 1 (score 1.3) and B - off-target site 2 (score 1.2).

Figure 44 represents the evaluation of the sequencing result of all four PLNc clones within the possible off-target region for off-target site 1 (score of 1.3) and 2 (score of 1.2). The investigation of the remaining 8 off-target sites was analysed similarly. No off-target-mediated gene aberrations were found within the investigated 10 most probable off-target sites.

For further analysis two PLNc clones were chosen, with one being selected from the DNA-based approach (PLNc #15) and the other one from the RNP-based approach (PLNc #28) as summarized in Figure 45. The hiPSC showed a normal morphology in culture (Figure 46).

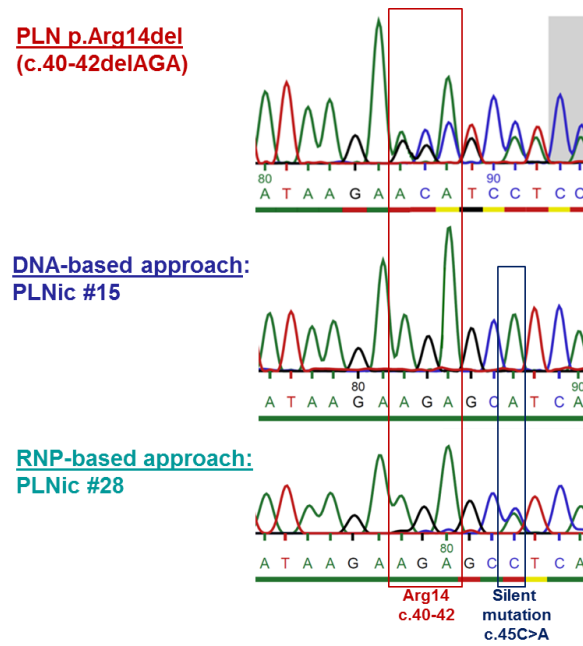


Figure 45: Sequencing results of PLN p.Arg14del hiPSC and for further experiments chosen PLN ic clones generated with DNA- or RNP-based approach, respectively.

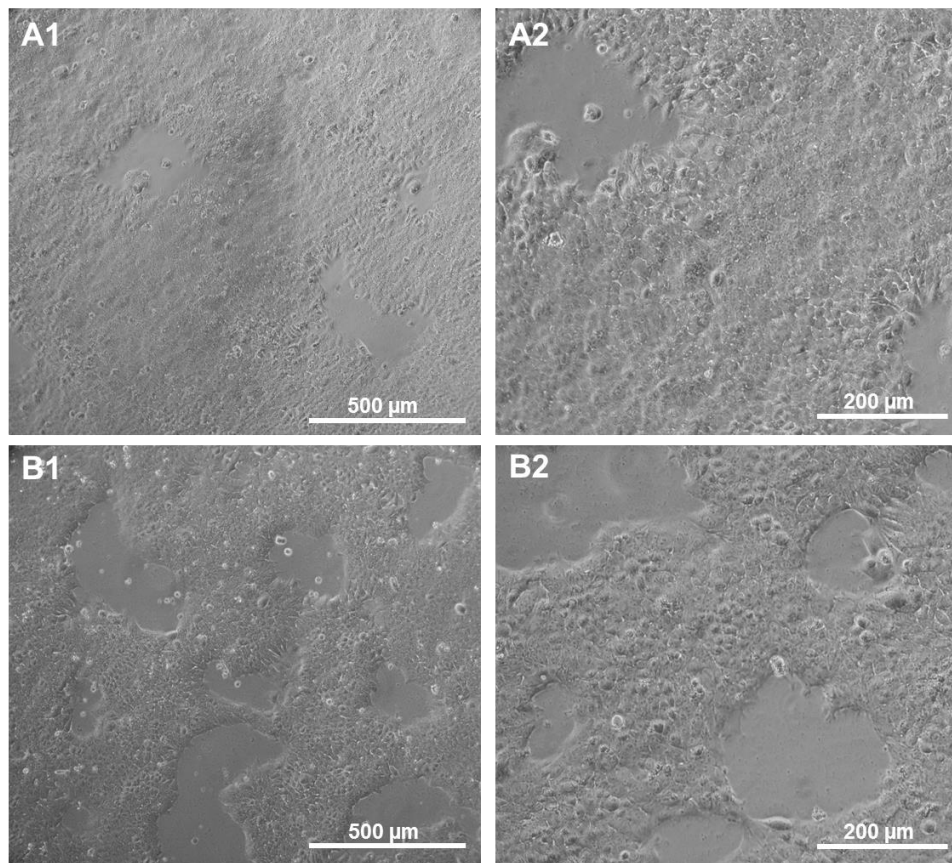


Figure 46: Morphological characterization of the selected hiPSC PLN ic clones. A1, 2 - Clone PLN #15 and B1, 2 - clone PLN #28. Scale bars as indicated 200 µm and 500 µm.

4.2.7 *Karyotype analysis of the isogenic control hiPSC clones*

The two isogenic hiPSC clones PLNic #15 (passage 51, DNA-based) and PLNic #28 (passage 48, RNP-based) were sent for karyotyping (Figure 47). For both clones 15 metaphases were analysed with a resolution of 450-500 bands per haploid set. The hiPSC showed both a normal female karyotype (46, XX) and G-banding without indicators of numerical or structural chromosomal aberrations.

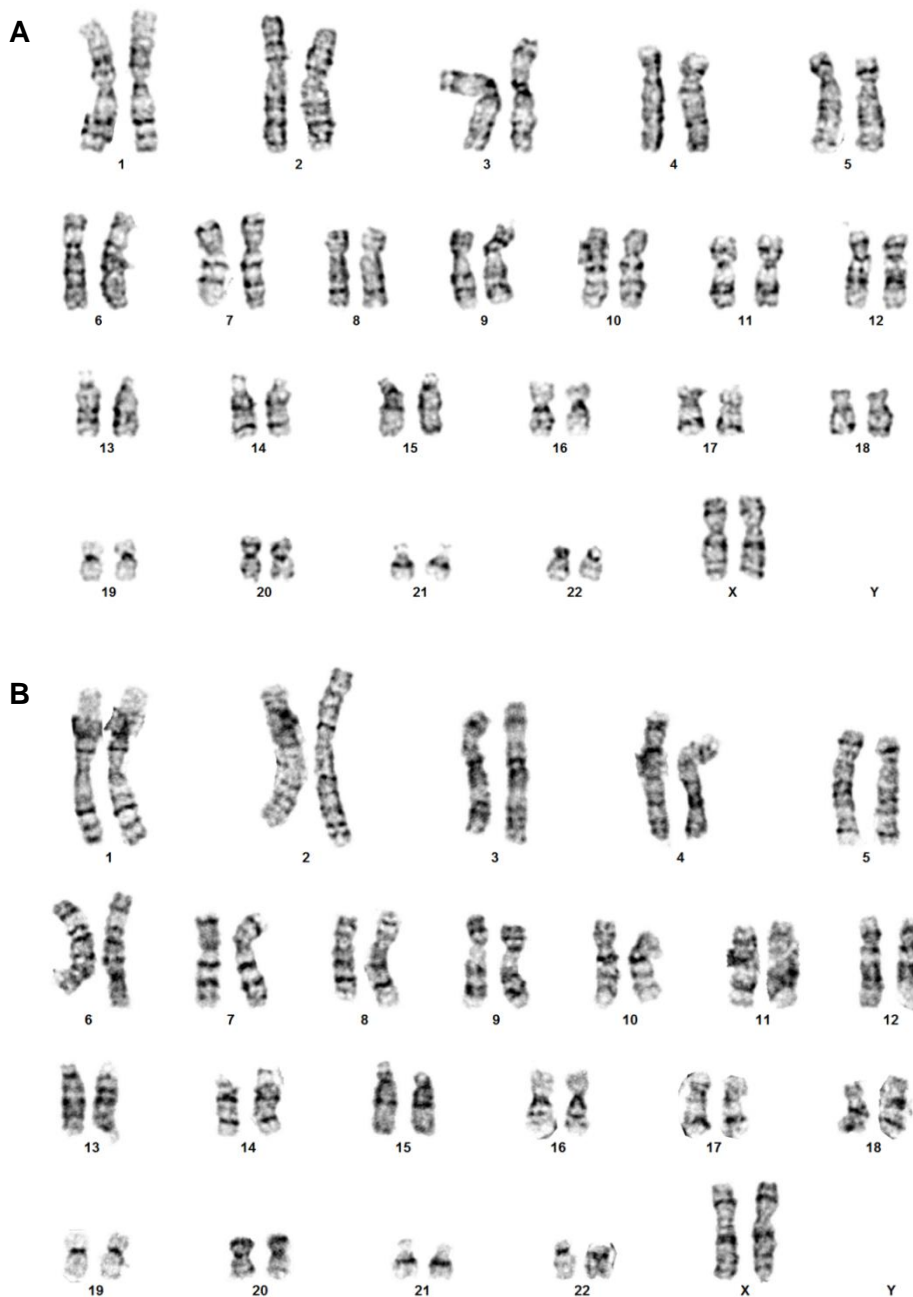


Figure 47: Karyotyping results of PLNic hiPSC clones. For **A** - PLNic #15 (passage 51) and **B** - PLNic #28 (passage 48) a normal female karyotype (46, XX) was verified.

4.3 Cardiac differentiation of PLNic and PLN p.Arg14del hiPSC

4.3.1 Successful differentiation of hiPSC into beating cardiomyocytes

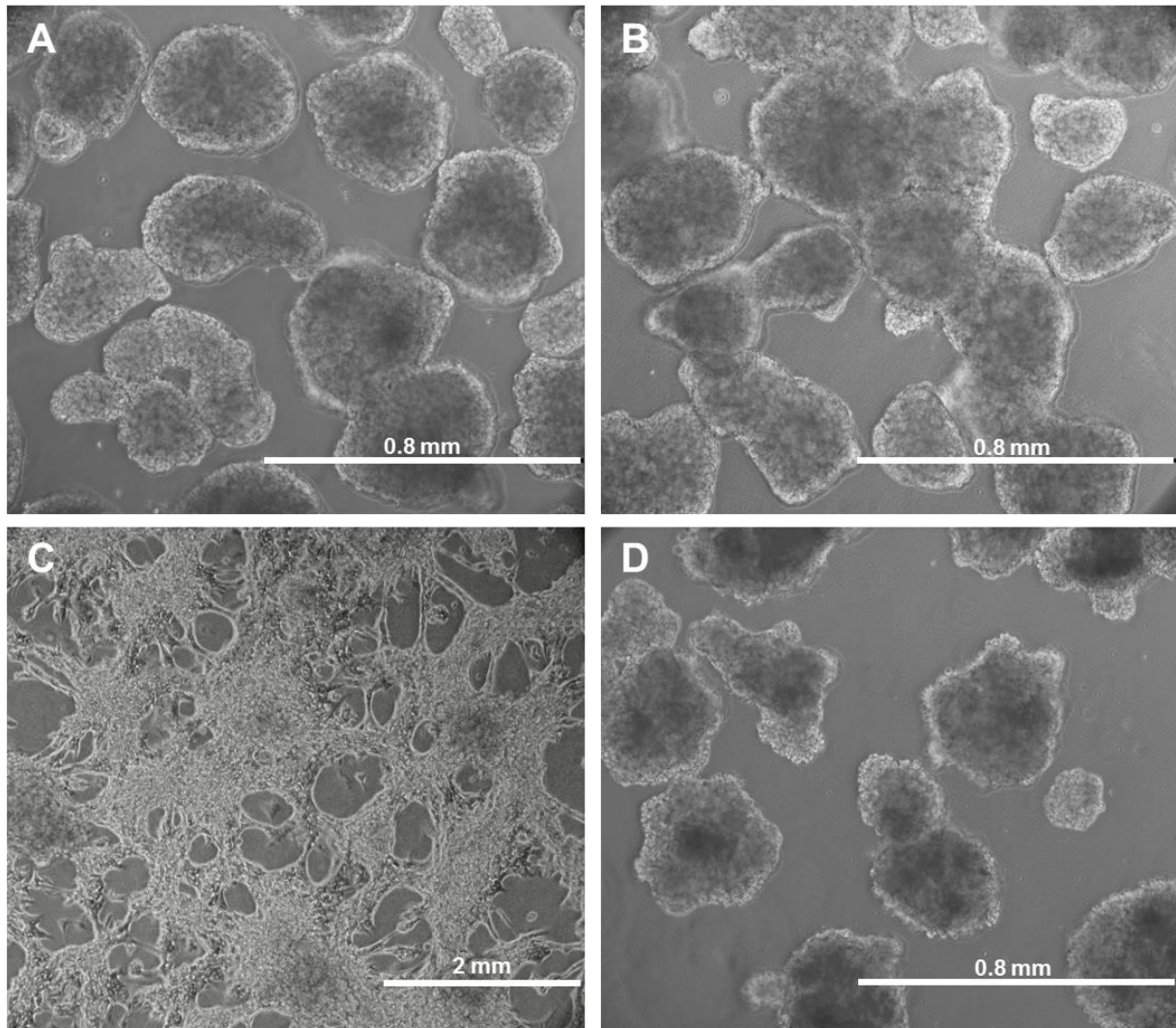


Figure 48: Spontaneously beating hiPSC-derived cardiomyocytes of the cardiac specification stage one day before dissociation. A - PLNic #15, B - PLNic #28, C - PLN p.Arg14del #1198 and D - PLN p.Arg14del #1201. A, B and D were derived from cEB-based cardiac specification protocol application while C was differentiated via monolayer-based cardiac specification. Scale bars as indicated 0.8 mm and 2 mm.

The application of the EB- and growth-factor based, three-stage differentiation protocol lead to development of beating cardiomyocytes. These were derived via both cardiac specification protocols. The PLNic #15 and #28 as well as PLN p.Arg14del #1201 clones were differentiated via the cEB-based cardiac specification while the monolayer-based one was applied for the PLN p.Arg14del #1198 clone. The cEBs showed appropriate crisp and round-shaped morphology and appeared big in size as shown in Figure 48A, B, D. Monolayer hiPSC-CM of #1198 showed a network-like structure (Figure 48C). This network of

cardiomyocytes was beating strongly throughout the entire cell layer. Original video recordings can be found on the external storage device attached to this thesis (Movie S1).

4.3.2 Cardiac differentiation with high hiPSC-cardiomyocyte yields and purities

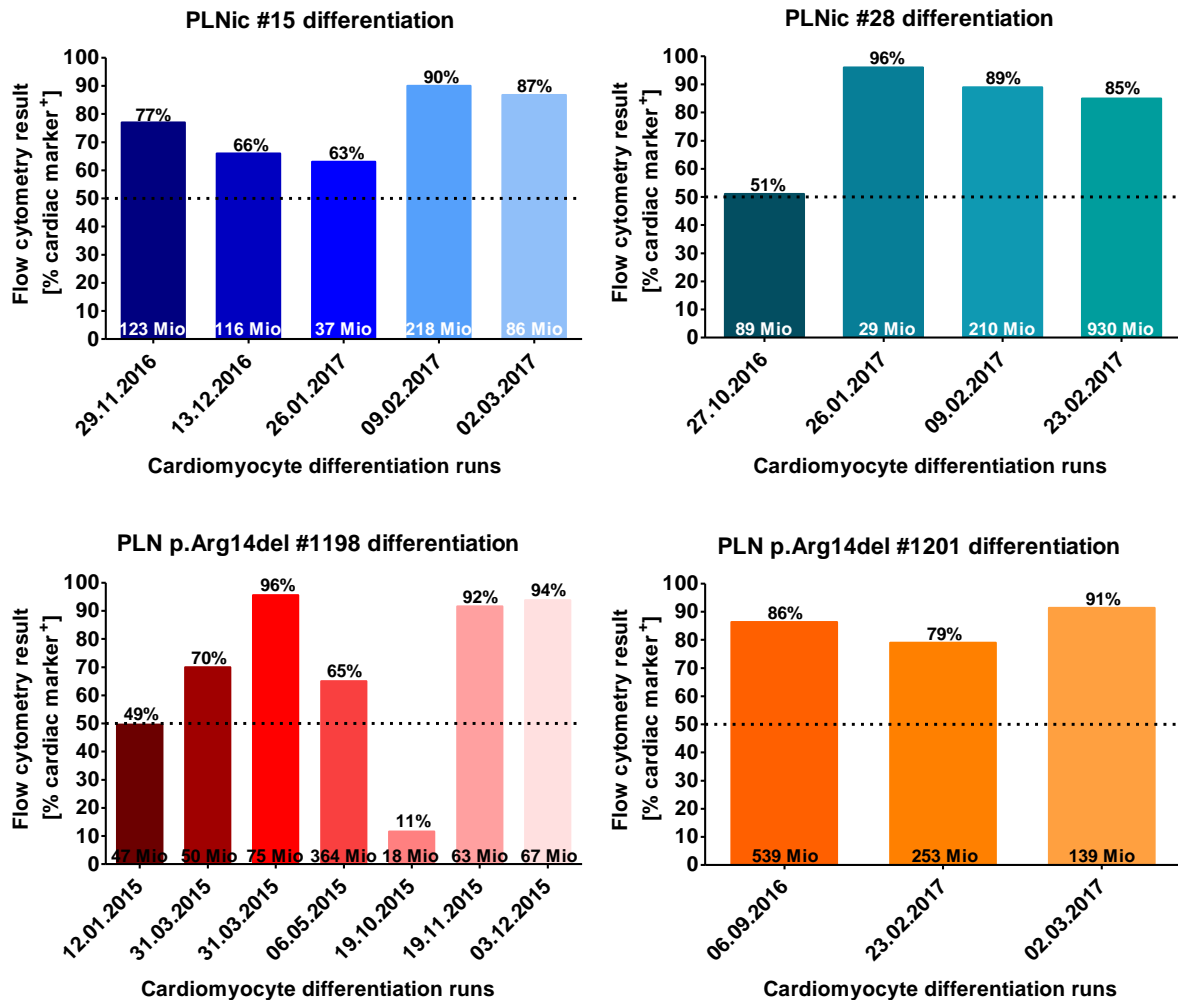


Figure 49: Cardiomyocyte differentiation results. A - PLNic #15, B - PLNic #28, C - PLN p.Arg14del#1198 and D - PLN p.Arg14del #1201. Depicted are cardiomyocyte yields and purities determined by flow cytometric analysis for cardiac marker positivity (cTNT⁺ or ACTN2⁺). The dashed line marks the 50% purity threshold. The numbers at the bottom of the columns indicate the number of differentiated cells.

The dissociated hiPSC-CM were analysed for cardiac marker positivity, either cTNT or ACTN2, by flow cytometry. Representative flow cytometry plots for each clone can be found in the supplement (Figure S3). The result of the respective differentiation runs of each cell line and clone is demonstrated in Figure 49. Differentiation runs with purities below the threshold of 50% were not considered for further investigation, e. g. EHT generation. Overall, the application of the established differentiation protocol (Breckwoldt et al. 2017) resulted in high yields of up to 930×10^6 differentiated cardiomyocytes and purities of up to 96%. The

differentiation efficiency plotted in Figure 50 was determined by calculating the ratio of input hiPSC cell number and output number of dissociated cells at the end of the differentiation procedure. Overall, the differentiation efficiency scattered mainly between 0.5 - 1.

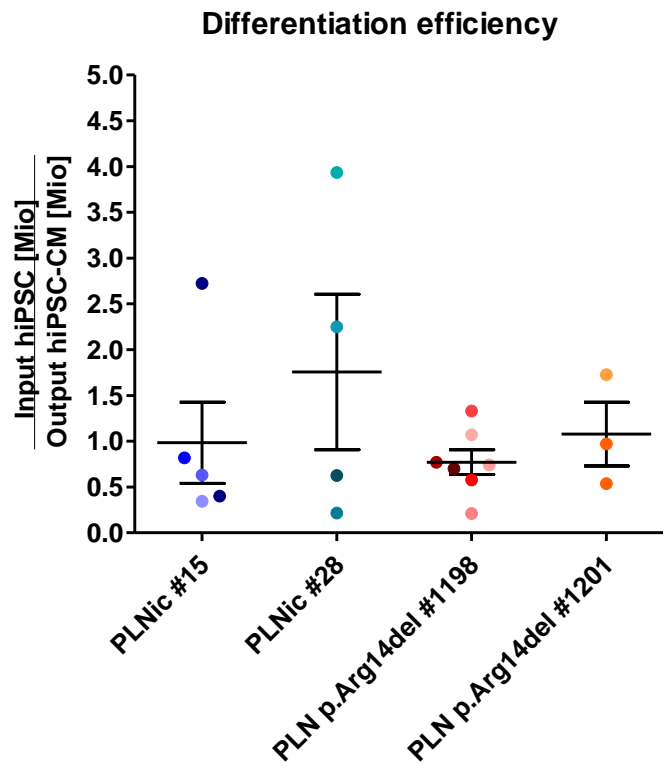


Figure 50: Differentiation efficiencies of all differentiation runs. Results of each of the hiPSC-CM clones PLNic #15 (n = 5) and #28 (n = 4) as well as PLN p.Arg14del #1198 (n = 7) and #1201 (n = 3) are shown. Depicted are mean \pm SEM.

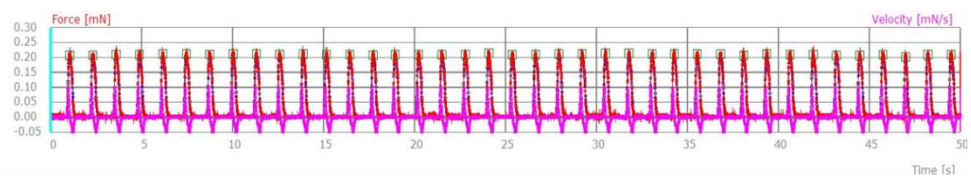
4.4 Physiological and pharmacological analysis of PLNic and PLN p.Arg14del EHTs

4.4.1 Differences in force development of spontaneously beating EHTs

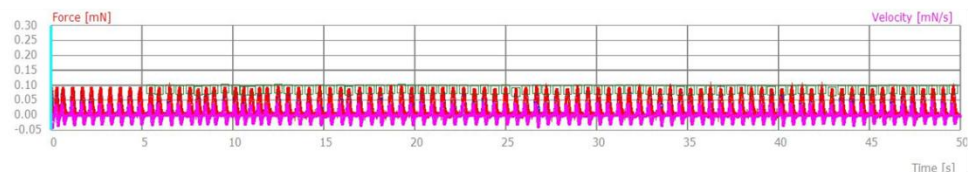
The PLNic and PLN p.Arg14del cardiomyocytes were used for EHT generation after one freeze/thaw cycle to avoid differences in pre-analytical conditions between the samples. With the video-optical recording system contractile parameters such as force, frequency, contraction and relaxation time and beating regularity of the EHTs were analysed. Since it took substantial period of time to establish the CRISPR/Cas9 system and generate the isogenic controls, PLN p.Arg14del EHTs were initially compared to unrelated controls.

In the direct comparison of force diagrams the mutated EHTs showed lower forces than unrelated controls (Figure 51). Importantly, the isogenic controls showed higher forces than the PLN p.Arg14del EHTs, indicating that the lower force in PLN p.Arg14del EHTs is an indicator for a disease-specific phenotype. Also, PLN p.Arg14del EHTs displayed irregular beating compared to both unrelated and isogenic control (15 sec of the representative force diagram in Figure 51). The original EHT video-files can be found in the supplement (Movie S2).

Unrelated control



PLN p.Arg14del #1198



PLNic #15

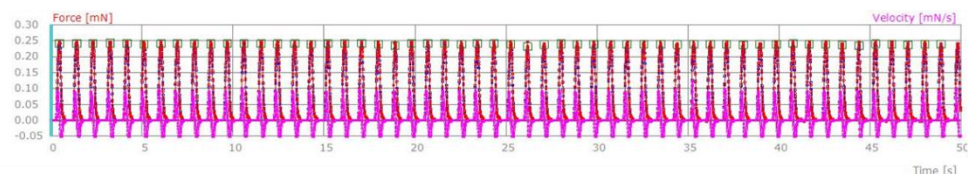


Figure 51: Representative baseline recordings of unrelated control, PLN p.Arg14del #1198 and PLNic #15 EHTs. The EHTs were analysed after reaching their force plateau (20-23 days after casting). Scale bar: 1 mm.

This difference in force was also obvious when the force development over days of EHT development was analysed (Figure 52). The isogenic controls (PLNic #15 and #28) developed higher forces from early on with similar beating frequency to

PLN p.Arg14del #1198. The force plateau phase was usually reached between the days 16-20. For this analysis the measurements of two consecutive days were analysed together, e. g. day 14 and day 15 were summarized to day 14.

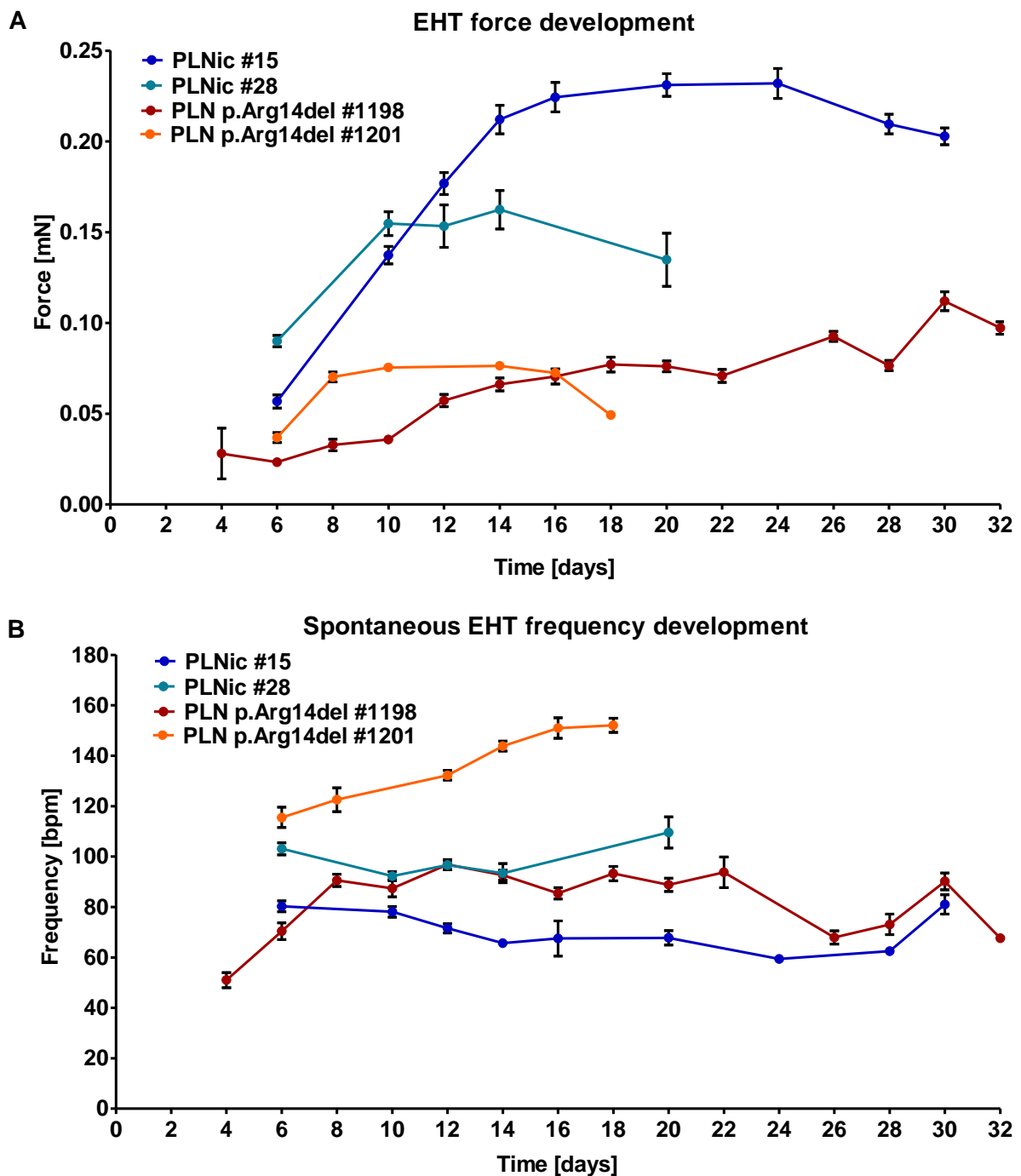


Figure 52: EHT development over time. A - EHT force and B - frequency development over time after EHT generation are shown. PLNic #15: n = 7-11/1 (77% CM); PLNic #28: n = 7-12/1 (51% CM); PLN p.Arg14del #1198: n = 32-45/3 (65-95% CM); PLN p.Arg14del #1201: n = 17-21/1 (86% CM); depicted are mean \pm SEM; n = EHT/batches; CM = cardiomyocyte purity.

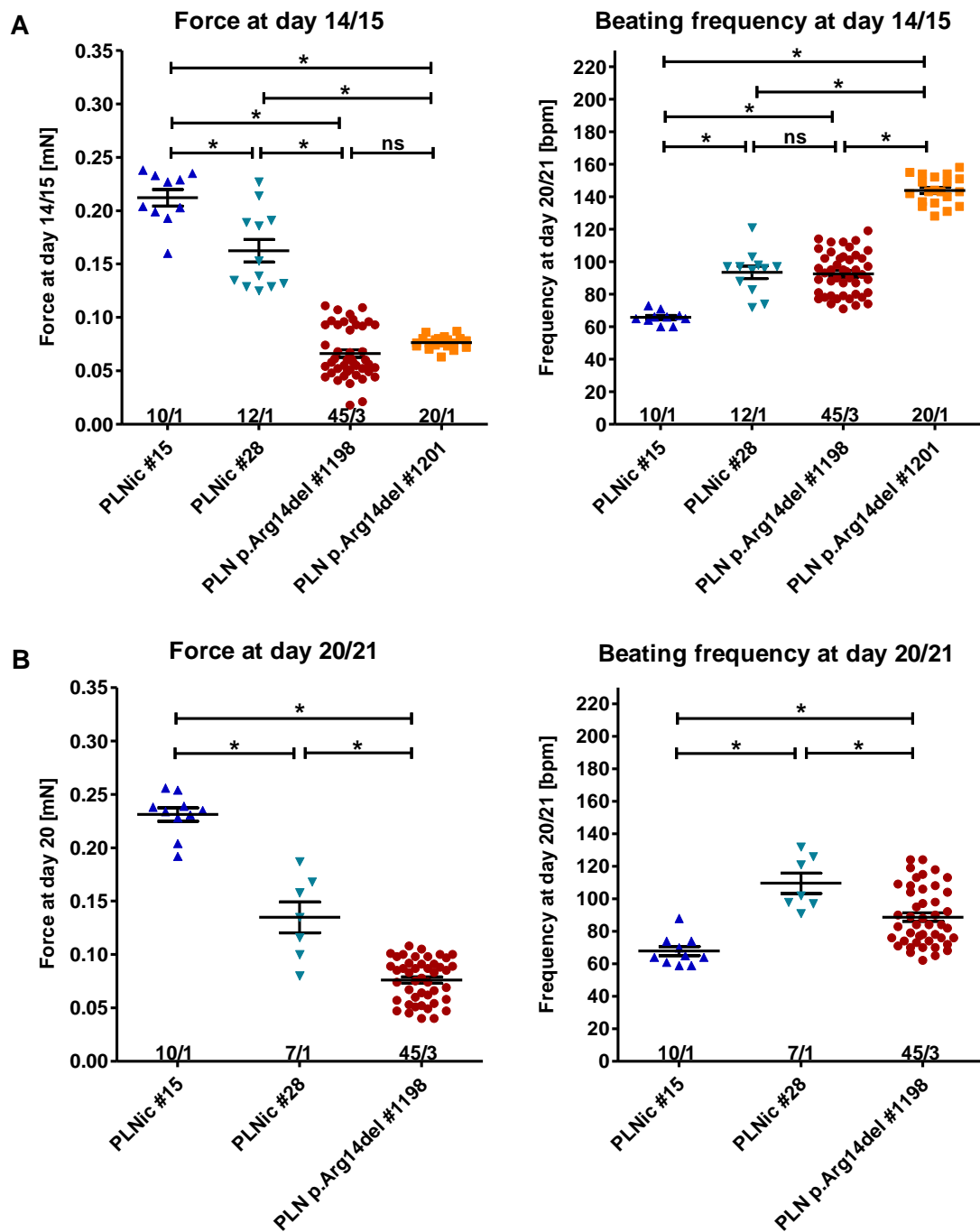


Figure 53: Comparison of EHT force and spontaneous beating frequency. Analysis was done at **A** - day 14/15 and **B** - day 20/21 of development. PLNic #15: n = 10/1 (77% CM); PLNic #28: n = 7-12/1 (51% CM); PLN p.Arg14del #1198: n = 45/3 (65-95% CM); PLN p.Arg14del #1201: n = 0-20/1 (86% CM); depicted are mean \pm SEM; n = EHT/batches; CM = cardiomyocyte purity. ns = not significant and * p<0.05, one-way ANOVA with Bonferroni post-test.

Figure 53 illustrates the force and beating frequency of EHTs in culture medium on day 14/15 and day 20/21 of development. Both PLNic clones showed significantly higher forces on

day 14/15 compared to PLN p.Arg14del #1198 and #1201. The PLNic #28 EHTs decreased in force until day 20/21. The EHTs got thinner and started to rip off the PDMS post, resulting in a decline in replicate number from 12 to 7. The PLN p.Arg14del #1201 EHTs showed a very high frequency of about 144 bpm and also ripped off the PDMS posts. For this reason the #1201 clone could not be analysed on day 20/21 anymore.

4.4.2 *Baseline characterization of paced EHTs*

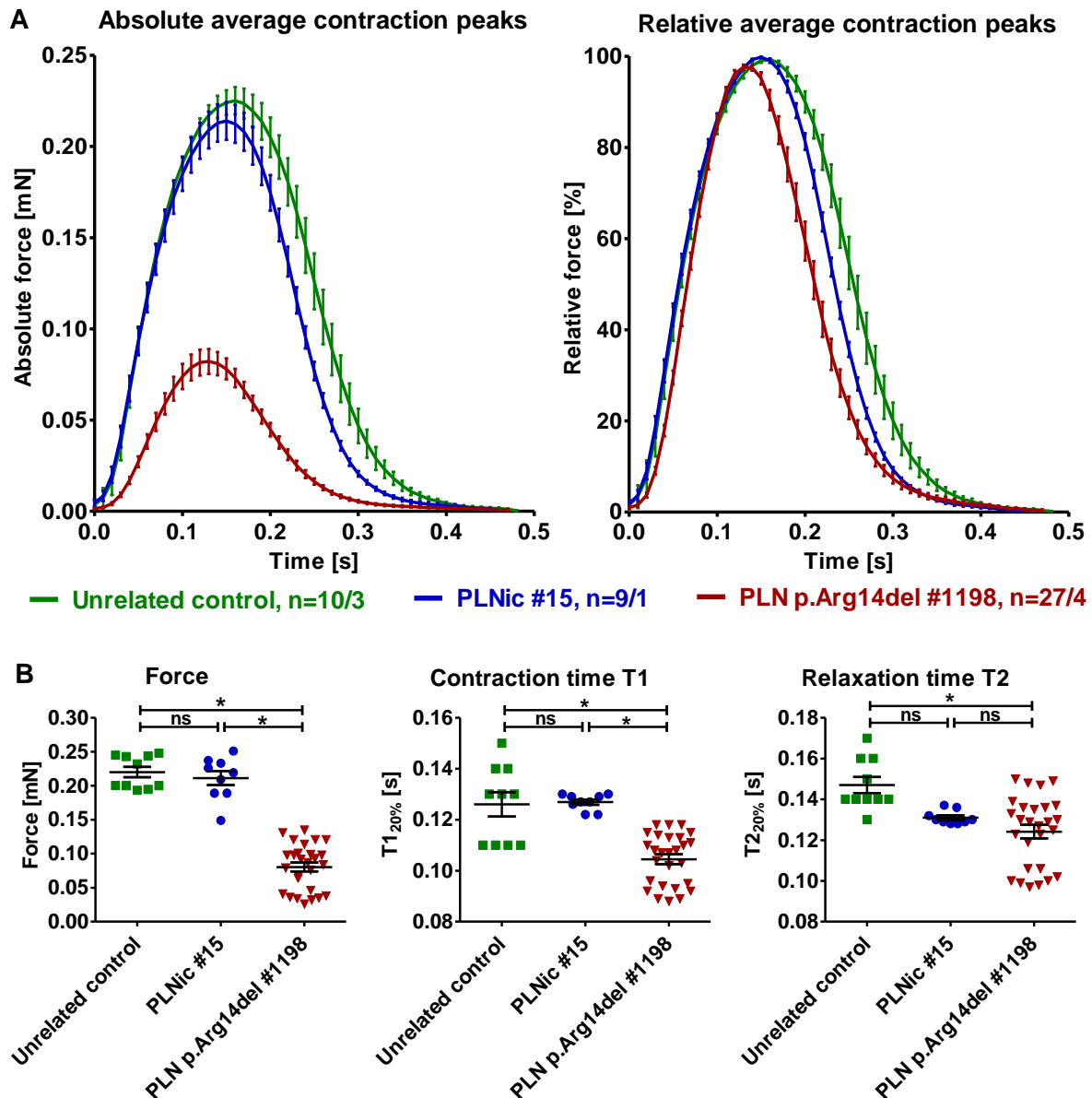


Figure 54: Analysis of the EHTs' average peaks and contractile parameters. **A** - Absolute and relative average contraction peaks of unrelated control (n = 11/1), PLNic #15 (n = 9/1) and PLN p.Arg14del EHTs (n = 27/4) at day 21±3 after casting. **B** - Quantification of force, contraction time T1 and relaxation time T2 (both at 20% above baseline). Depicted are mean±SEM; n = EHT number/batches; ns = not significant and * p<0.05, one-way ANOVA with Bonferroni post-test.

Figure 54B illustrates the quantitative analysis of average contraction peaks of paced EHTs (2 Hz) incubated in 1.8 mM Ca²⁺ Tyrode's solution on day 21±3. The analysis verified a significantly stronger force development of unrelated and isogenic controls compared to PLN p.Arg14del EHTs. Additionally, shorter contraction times and no difference in relaxation time between PLNic and unrelated control versus PLN p.Arg14del EHTs were detected. The data of the unrelated control EHTs were kindly provided by Dr. Ingra Mannhardt (DEPT, UKE, Hamburg, Germany).

In the normalized average peaks (Figure 54A) the PLN p.Arg14del EHT contraction (red line) seemed to be delayed in the earliest contraction phase, but reached their maximal force earlier than the PLNic EHTs (blue line). Also a significant difference in contraction time was detected between PLNic and unrelated control on the one hand and p.Arg14del PLN mutated EHTs on the other hand. To analyse the contraction in more detail the early contraction phase was investigated by evaluating the contraction times from 10% to 100% of peak contraction and from 50% to 100% of peak contraction according to the following equation:

$$\frac{T1_{10\%} - T1_{50\%}}{T1_{10\%}}$$

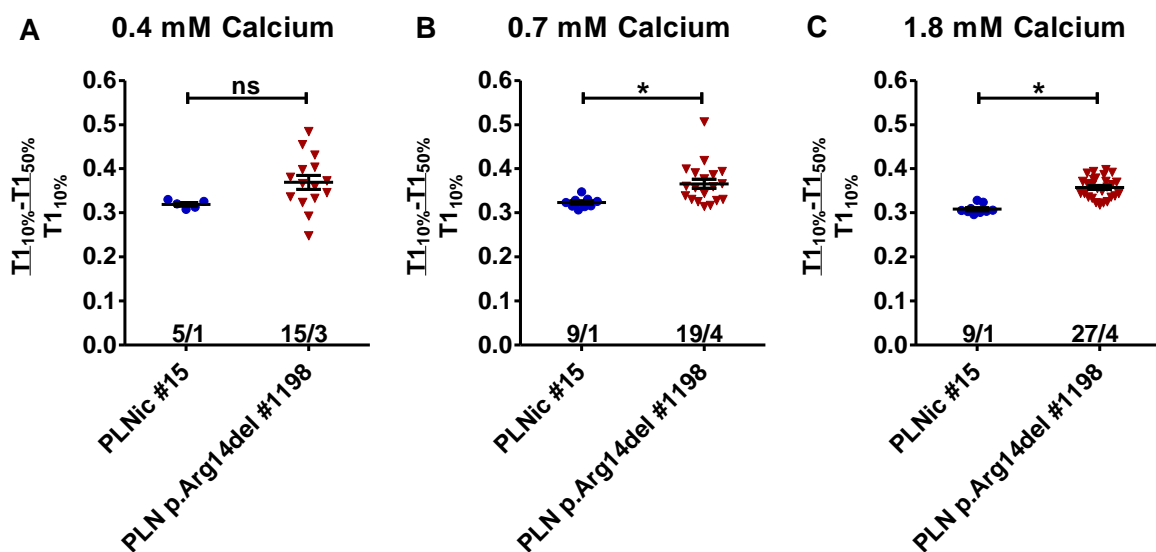


Figure 55: Comparison of the normalized early contraction phases of PLNic #15 and PLN p.Arg14del #1198 EHTs. Comparative analysis was done at different external calcium concentration in Tyrode's solution: **A** - 0.4 mM Ca²⁺ (PLNic: n = 5/1, PLN p.Arg14del: n = 15/3); **B** - 0.7 mM Ca²⁺ (PLNic: n = 9/1, PLN p.Arg14del: n = 19/4) and **C** - 1.8 mM Ca²⁺ (PLNic: n = 9/1, PLN p.Arg14del: n = 27/4). Depicted are mean±SEM; n = EHT number/batches; * p<0.05, unpaired t-test.

The result is illustrated in Figure 55 suggesting a significantly longer early contraction phase for PLN p.Arg14del EHTs. To evaluate the robustness of this equation the values were

calculated at three different calcium concentrations (0.4 mM, 0.7 mM and 1.8 mM). Since the fraction appeared to be always longer for PLN mutated EHTs this value was evaluated as stable.

4.4.3 Calcium concentration-response curve

PLNic and PLN p.Arg14del EHTs showed a positive inotropic response with increasing calcium concentrations in serum-free conditions and defined frequencies. After 15 min of incubation time under pacing at 2 Hz the force plateau was reached for each single calcium concentration. The force was then recorded and used for analysis only if the EHT followed the pacing signal. Figure 56 shows the relative force increase with increasing extracellular calcium concentrations and a strong difference between the EC_{50} values of PLNic and PLN p.Arg14del EHTs. PLNic EC_{50} is shifted to the left reaching half maximal force already at 0.32 mM Ca^{2+} , while PLN p.Arg14del EHTs EC_{50} equals 0.71 mM Ca^{2+} both with high R^2 values (PLNic: 0.94; PLN p.Arg14del: 0.97). Additionally, the Hill slopes differed strongly from each other with PLNic showing a smoother slope (Hill = 1.3) compared to the steep slope for PLN p.Arg14del EHT response curve (Hill = 2.14).

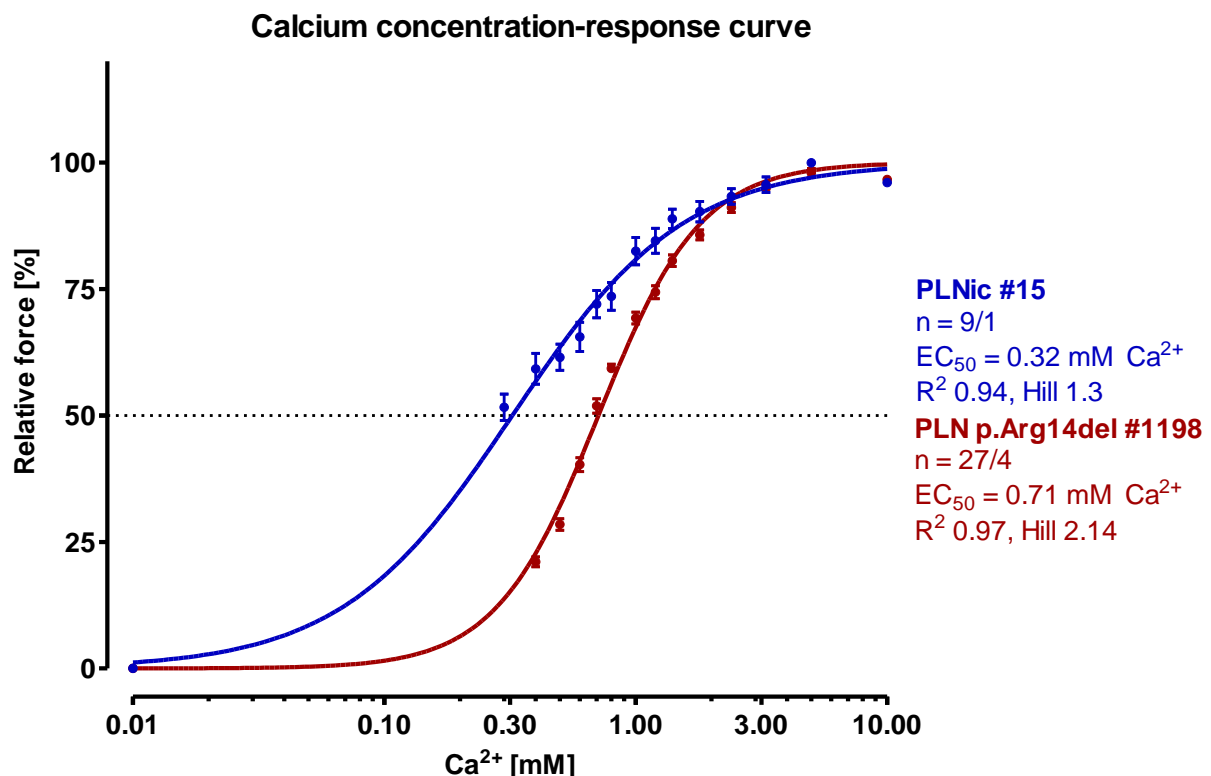


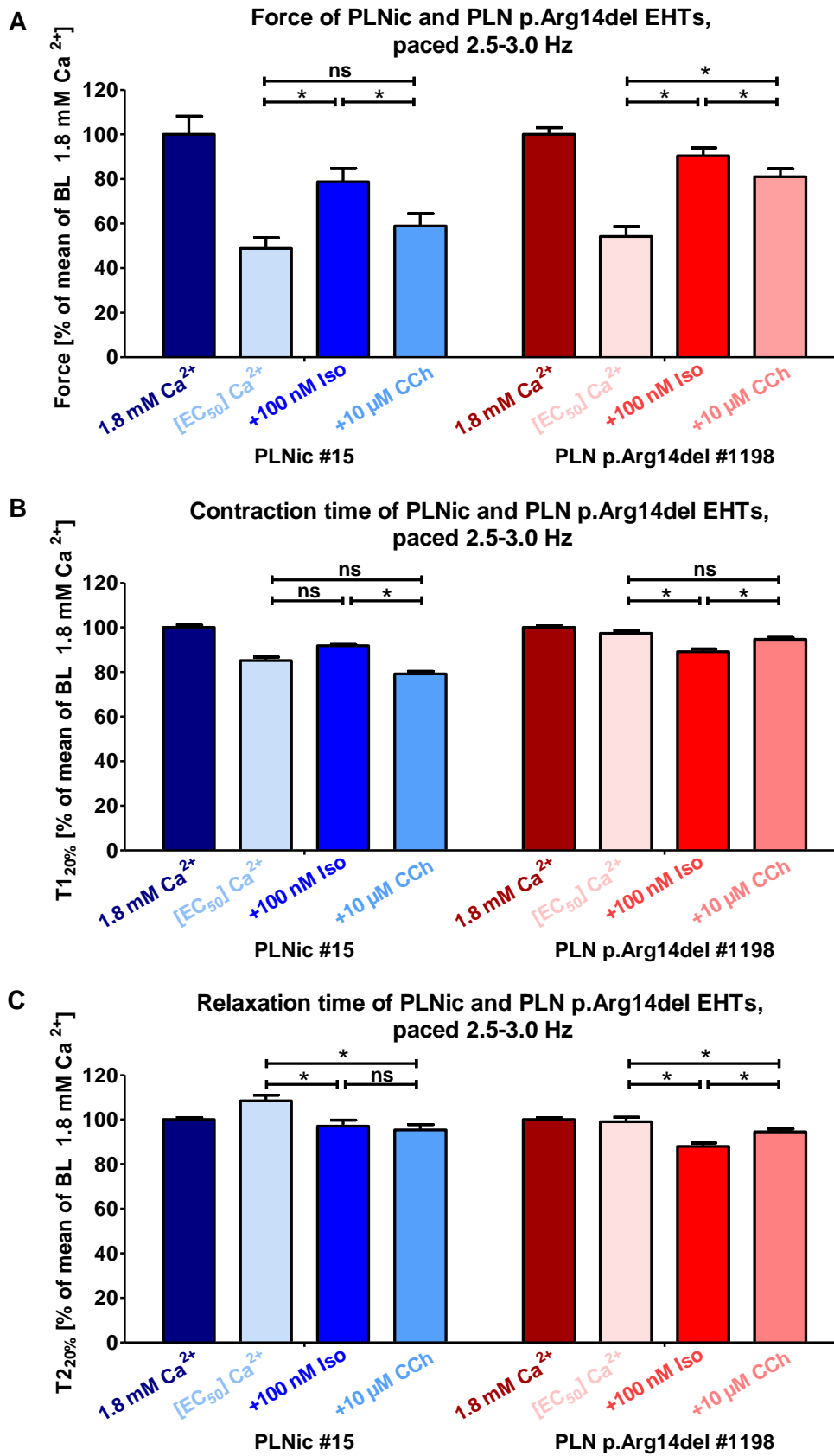
Figure 56: Calcium concentration-response curves of PLNic #15 and PLN p.Arg14del #1198 EHTs. Depicted are mean \pm SEM; n = EHT number/batches.

4.4.4 *Isoprenaline and carbachol response*

Figure 57 depicts the calculated relative force, contraction and relaxation time and spontaneous beating frequency values of EHTs exposed to 1.8 mM and $[EC_{50}]$ calcium as well as stimulated with 100 nM isoprenaline followed by 10 μ M carbachol bolus. A reduction of the extracellular calcium concentration from 1.8 mM to the EC_{50} concentration of calcium (PLNic: 0.32 mM, PLN p.Arg14del: 0.71 mM) reduced force in both lines by about 50% (Figure 57). Addition of isoprenaline (100 nM) increased the contraction force and reduced the time of relaxation to a similar extent in both lines (+61/67% force, -10/-11% relaxation time [effect to $[EC_{50}]$ Ca^{2+} baseline (BL)]; Table 27, Figure 57). The effect of isoprenaline was partially antagonized by the addition of carbachol (10 μ M). PLNic EHTs revealed a tendency to a prolonged contraction time (+8%) while PLN p.Arg14del EHTs reacted to isoprenaline with a significant reduction of contraction time by -8%. Additionally, beating frequency of PLNic EHTs in $[EC_{50}]$ calcium increased by 2.5 fold compared to 1.8 mM calcium levels. This strong increase of beating frequency under calcium concentration reduction was unusual and unexpected. In contrast to PLN p.Arg14del EHTs, isoprenaline did not further stimulate the rate in PLNic EHTs, but carbachol strongly reduced the frequency by -49.2%. In comparison, the PLN p.Arg14del EHTs showed a positive chronotropic effect with an increase of frequency by +37.2% after isoprenaline bolus compared to baseline levels which was also reversed by carbachol addition (-15.9%).

Table 27: Calculation of isoprenaline and carbachol effects. Calculated isoprenaline (Iso) effects normalized to ' $[EC_{50}]$ Ca^{2+} baseline (BL)' and calculated carbachol (CCh) effects normalized to BL at '+100 nM Iso' of PLNic #15 and PLN p.Arg14del #1198 EHTs.

Parameter	EHT line	Effect of Iso (change in % of BL at $[EC_{50}]$ Ca^{2+})	Effect of CCh (change in % of BL at +100 nM Iso)
Force	PLNic #15	+61.4%	-25.4%
	PLN p.Arg14del #1198	+66.8%	-10.3%
Contraction time	PLNic #15	+7.9%	-13.9%
	PLN p.Arg14del #1198	-8.4%	+6.1%
Relaxation time	PLNic #15	-10.4%	-1.8%
	PLN p.Arg14del #1198	-11.2%	+7.4%
Frequency (spontaneous)	PLNic #15	+0.5%	-49.2%
	PLN p.Arg14del #1198	+37.2%	-15.9%



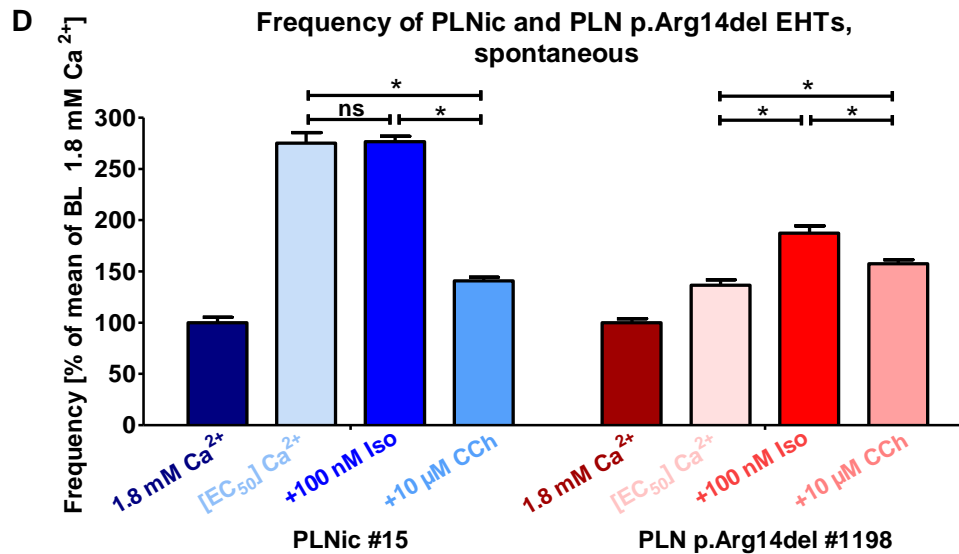


Figure 57: Isoprenaline and carbachol response. Depicted are the relative isoprenaline (Iso, 100 nM) and carbachol (CCh, 10 μM) **A** - force, **B** - contraction time, **C** - relaxation time and **D** - frequency responses of PLNic #15 (blue, n = 6/1 paced at 3.0 Hz, n = 8/1 spontaneous) and PLN p.Arg14del #1198 (red, n = 19/3 paced at 2.5 Hz, n = 17/3 spontaneous) EHTs in Tyrode's solution. n = EHT number/batches; ns = not significant and * p<0.05, two-way ANOVA, repeated measures with Bonferroni's multiple post-test; depicted are mean±SEM.

4.4.5 Long-term exposure to calcium

The observation of an irregular beating pattern (IBP) in PLN p.Arg14del EHTs (Figure 51) and the overall assumption that this mutation leads to alteration of cardiomyocyte calcium handling led to the hypothesis that the IBP can be triggered by calcium overload. To test this idea, a protocol was established in which EHTs were continuously recorded for 10-11 hours in 1.0, 1.8 and 3.0 mM Ca^{2+} in Tyrode's solution. Figure 58A shows representative force recordings in all three calcium concentrations after 4-5 hours of incubation time. The PLN p.Arg14del developed IBP at 1.8 mM and 3.0 mM calcium in contrast to PLNic EHTs. Quantitative analysis of the RR scatter (interdecile range of average beat-to-beat variation, Figure 58B) revealed significantly higher values after 4-10 hours of incubation at 3.0 mM calcium compared to 1.0 mM calcium. This time- and concentration-dependent increase of irregular beating pattern was absent in PLNic EHTs.

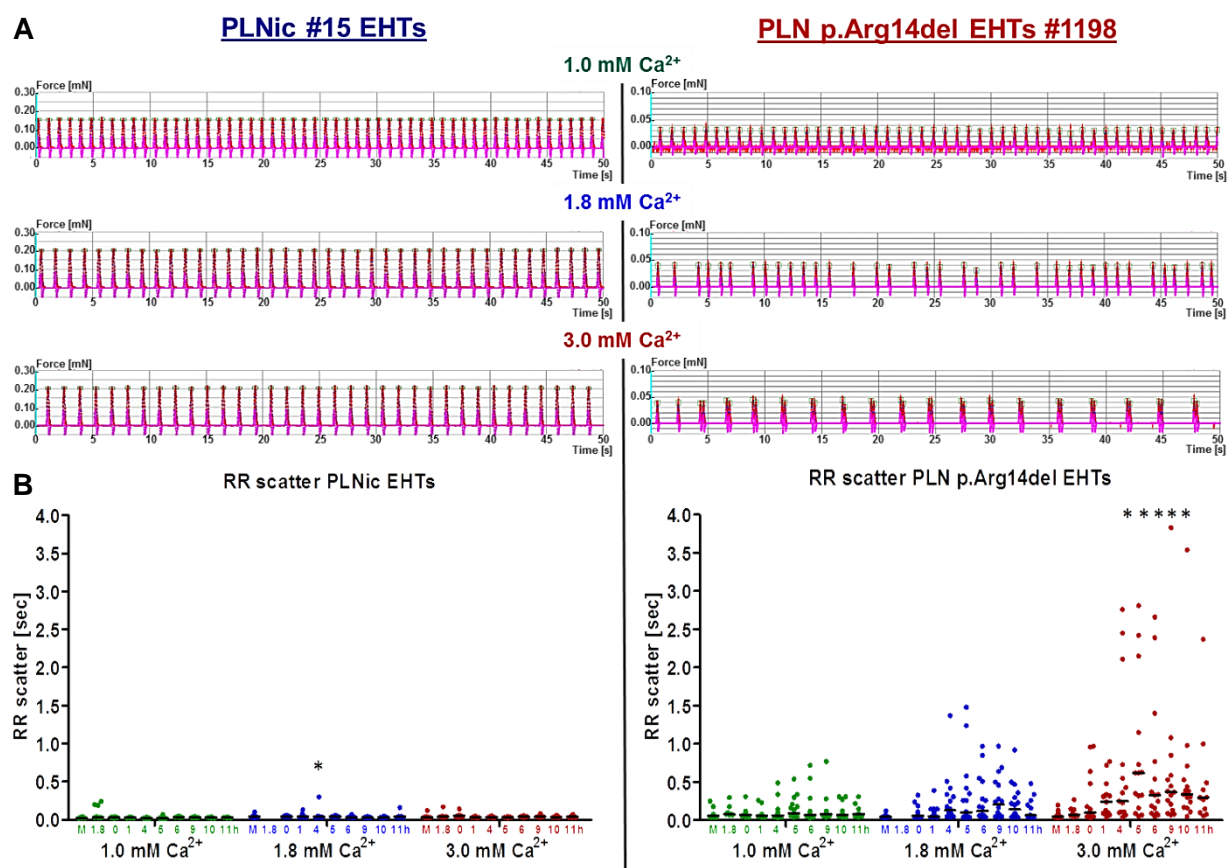


Figure 58: Long-term exposure to calcium. **A** - Original representative recordings after 4-5 hours of incubation time of PLNic #15 ($n = 8/1$) and PLN p.Arg14del #1198 EHTs ($n = 15-16/2$) in 1.0, 1.8 and 3.0 mM extracellular calcium concentrations. **B** - Scatter dot plot of RR scatter (length between 10th and 90th percentile [interdecile range] of the average beating interval length) for 50 second-recordings in 1.0, 1.8 and 3.0 mM extracellular calcium concentrations for 11 hours. * $p < 0.05$, Two-way ANOVA, not repeated measures with Bonferroni's multiple post-test vs. 1.0 mM Ca^{2+} ; depicted are mean values; n = EHT number/batches; M = Medium baseline, 1.8 = 1.8 mM Ca^{2+} baseline.

4.5 Molecular characterization of PLNic and PLN p.Arg14del EHTs

4.5.1 PLN gene expression analysis

a) NanoString analysis

PLN total mRNA levels were investigated with NanoString technology. The experiment and analysis were kindly performed by Maksymilian Prondzynski and Elisabeth Krämer (DEPT, UKE, Hamburg, Germany). Both, human heart tissue and EHT mRNA levels were evaluated. The non-failing heart (NFH) and DCM RNA preparations were kindly provided by Elisabeth Krämer (DEPT, UKE, Hamburg, Germany) and the PLN p.Arg14del RNA derived from two PLN p.Arg14del carriers were kindly given by Prof. Dr. Hendrik Milting (HDZ-NRW, Bad Oeynhausen, Germany), Prof. Dr. Yigal Pinto and Inge van der Made (AMC, Amsterdam, the Netherlands).

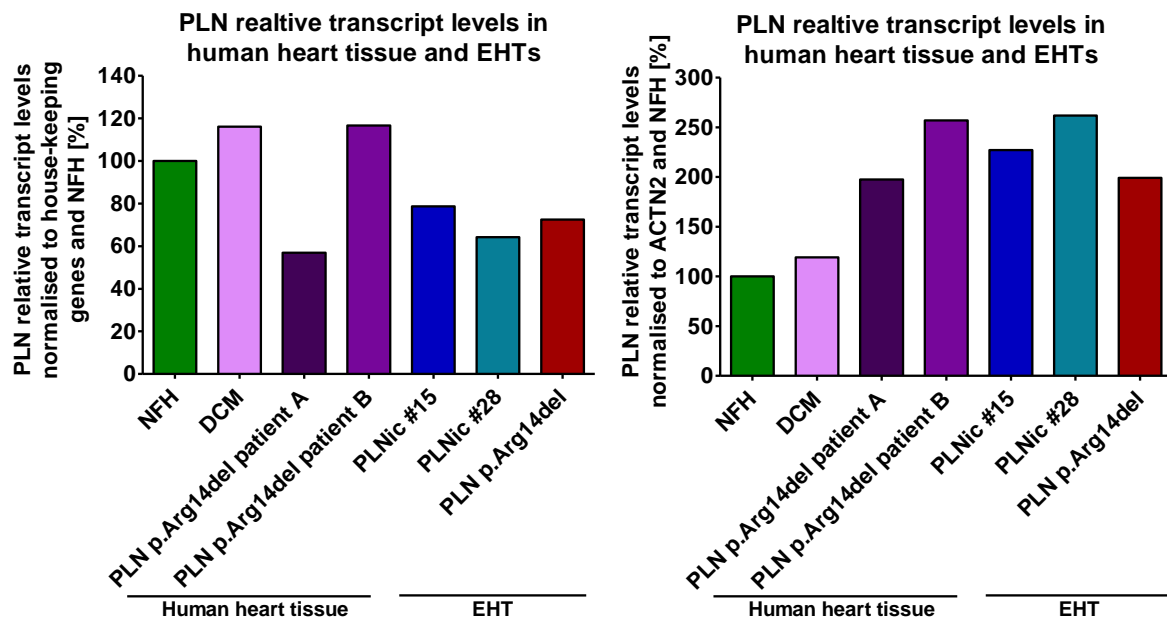


Figure 59: Total PLN relative transcript levels in human tissue and EHTs analysed with NanoString technology. Analysis of heart tissue samples from non-failing heart tissue (NFH, n = 9), DCM (n = 11), and PLN p.Arg14del patients A (n = 1) and B (n = 1) as well as EHTs from the PLNic #15 (n = 1/1, 21 days old, 77% CM), PLNic #28 (n = 1/1, 21 days old, 51% CM) and PLN p.Arg14del (n = 9/3, 28-30 days old, 65-93% CM) lines. **A** - All samples were normalized to their set of housekeeping genes (ABCF1, ACTB, CLTC, GAPDH, PGK1, TUBB) and afterwards to the NFH sample. **B** - All samples were normalized to ACTN2 and afterwards to the NFH sample. The respective RNA samples of each group were pooled together before performing the NanoString run. For human tissue: n = number of pooled heart samples; for EHTs: n = number of pooled EHTs/differentiation runs.

Figure 59 shows the PLN mRNA levels of NFH, DCM, PLN patient A and B (all left ventricular tissue samples) as well as PLNic #15, PLNic #28 and PLN p.Arg14del #1198 EHTs normalized to a non-cardiac housekeeping gene set. The NanoString analysis revealed that PLN relative transcript levels in PLNic and PLN p.Arg14del EHTs were similar and ranged between 64%-78% of NFH. Interestingly, PLN p.Arg14del patient A (56.9%) showed a by 50% reduced PLN mRNA level compared to patient B (116.6%) whose values were similar to the NFH (100%) and DCM (116.0%) samples. But after normalizing to cardiac specific ACTN2 it was apparent that NFH (100%) and DCM (119%) samples were similar and PLN mRNA levels in PLN p.Arg14del patients 2-fold higher (197% patient A; 256% patient B). In addition, the difference in PLN mRNA levels between the two PLN mutant carriers A and B decreased. The PLN mRNA levels of the EHTs were within a range of 198% to 261%. The relative transcript levels appeared now higher when normalizing to ACTN2 which is likely due to the higher cardiomyocyte purity of the small tissues.

b) RT-qPCR analysis

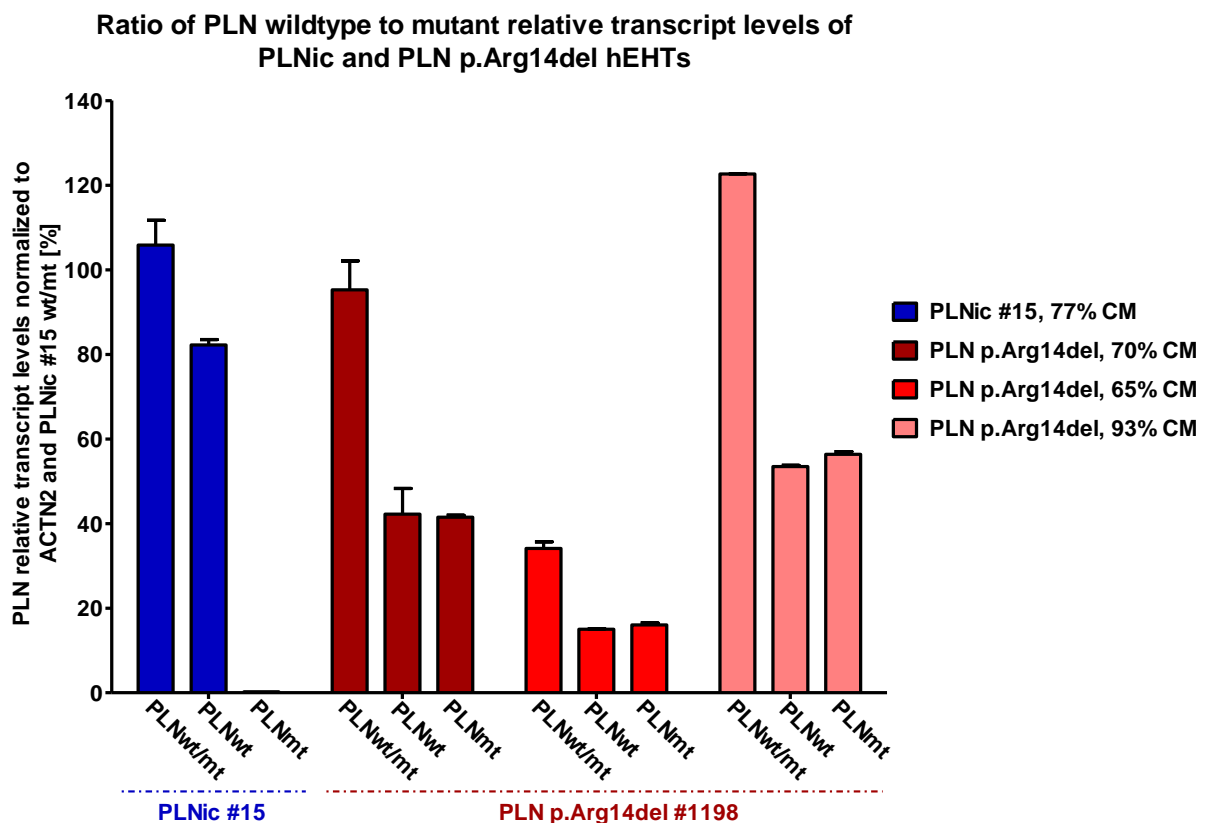


Figure 60: Ratio of PLN wildtype to mutant relative transcript levels of PLNic and PLN p.Arg14del EHTs. Relative transcript levels were analysed in PLNic #15 (n = 1/1, 21 days old, 77% CM) and PLN p.Arg14del EHTs (n = 9/3, 28-30 days old, 65-93% CM) and normalized to ACTN2 and PLNic #15 PLN total (PLNwt/mt). Depicted is mean \pm SEM of RT-qPCR duplicates; n = number of EHTs/differentiation runs; wt = wildtype, mt = mutant, CM = cardiomyocyte purity.

To evaluate allele-specific PLN mRNA expression, primers were designed to specifically detect PLN c.40-42AGAdel mRNA (PLN^{mt}) and PLN wildtype (PLN^{wt}) mRNA sequences. As a reference primers detecting both variants (PLN^{wt/mt}) were also included. Figure 60 shows the representative result for PLN^{c.40-42AGAdel} #15 (one batch) and PLN p.Arg14del #1198 EHTs (casted from three independent hiPSC-CM differentiation batches). No expression of mutated PLN mRNA was detected in the isogenic control EHTs, supporting the success of the CRISPR/Cas9-mediated gene correction. In contrast, PLN p.Arg14del EHTs revealed a 50:50 ratio of PLN wildtype:mutant mRNA concentration in all three analysed hiPSC-CM differentiation batches. The total PLN relative transcript levels differed between the three batches in accordance to the cardiomyocyte purity within the EHTs.

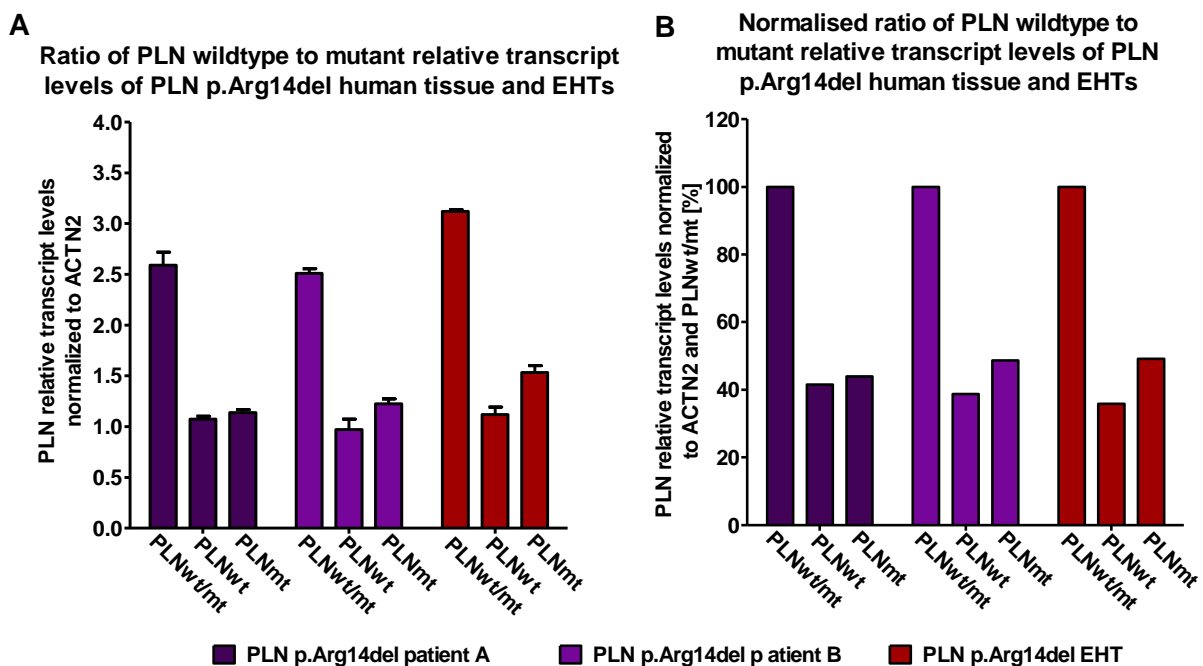


Figure 61: Ratio of PLN wildtype to mutant relative transcript levels of PLN p.Arg14del human tissue and EHTs. PLN relative transcript levels in PLN p.Arg14del patient samples A and B and PLN p.Arg14del EHT (n = 3/1 [number/batch], 30 days old, 70% cardiomyocyte purity) normalized to **A** - ACTN2 and **B** - ACTN2 and PLN^{wt/mt}. Depicted is mean±SEM of RT-qPCR duplicates in A and B; wt = wildtype, mt = PLN c.40-42AGAdel mutant.

In addition, a RT-qPCR analysis was performed to investigate the PLN mRNA ratio in the PLN p.Arg14del patients A and B in comparison to the PLN mutated EHTs shown in Figure 61. Figure 61A shows that PLN total transcript levels in patient A and B were similar. The analysis additionally revealed that PLN mutation carriers also showed a 50:50 ratio of PLN^{wt}:PLN^{mt} transcript levels to similar extends of PLN p.Arg14del EHTs (Figure 61B).

In summary, the PLN c.40-42AGAdel allele was expressed in both PLN p.Arg14del EHTs and patients and to the same extent as the PLN wildtype allele.

4.5.2 Western blot analysis of PLN protein levels and autophagy marker in PLN^{ic} and PLN p.Arg14del EHTs

a) PLN protein level investigation

For western blot analysis PLN p.Arg14del #1198 and PLN^{ic} #15 EHTs were sampled and analysed after lysate boiling (monomeric PLN form) and without boiling (pentameric PLN is not degraded). The results are demonstrated in Figure 62. They suggested that PLN expression in PLN p.Arg14del EHTs was lower than in PLN^{ic} EHTs and NFH and gave no indication for a destabilization of the pentameric form of PLN in PLN p.Arg14del EHTs.

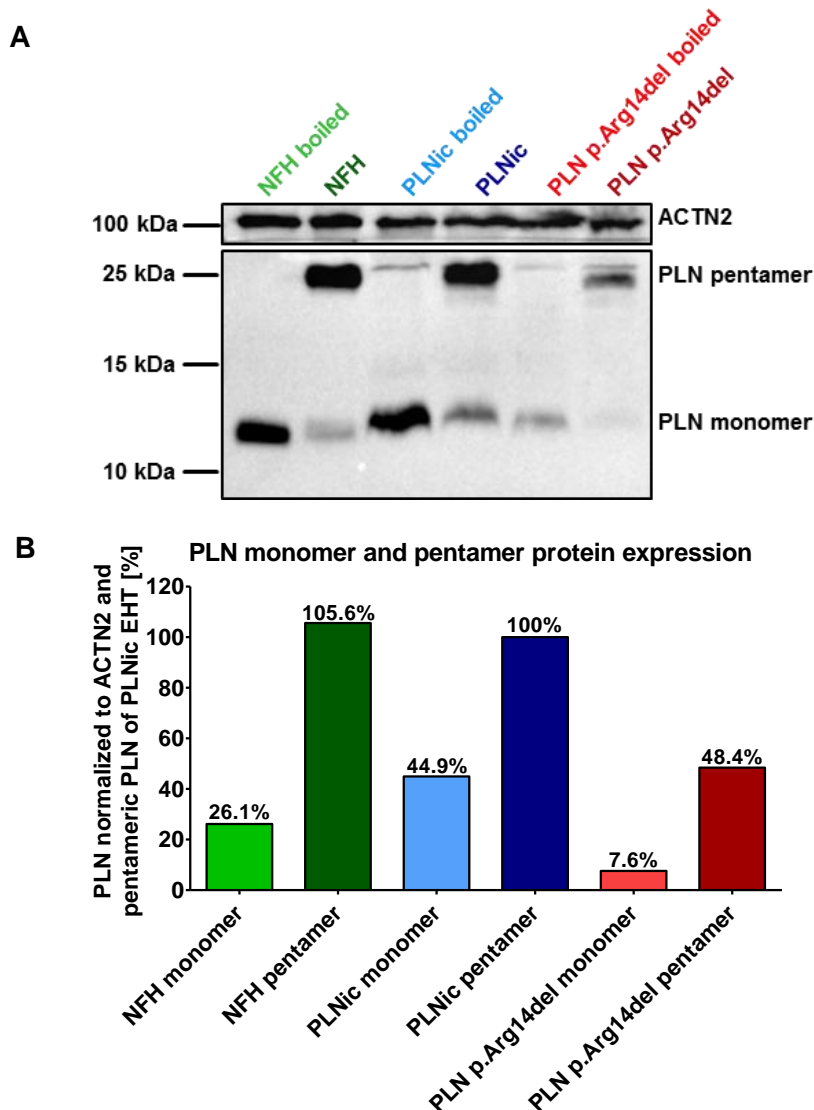
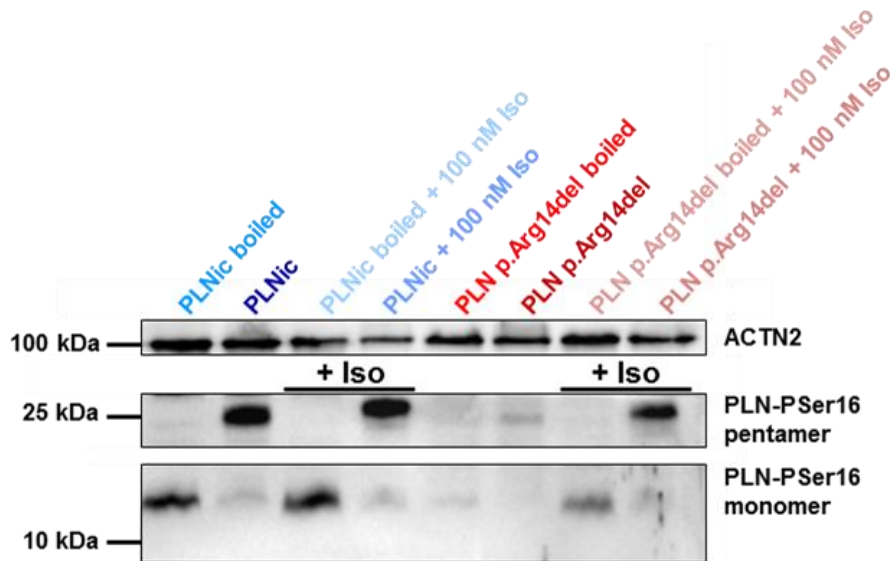


Figure 62: Western blot analysis of PLN total protein levels. Protein levels of non-failing heart (NFH, n = 1), PLN p.Arg14del #1198 (n = 3/1 [number/batch], 70% cardiomyocyte purity, 30 days old) and PLN^{ic} #15 EHTs (n = 4/1 [number/batch], 77% cardiomyocyte purity, 31 days old) were investigated. **A** - Pentameric and monomeric form of PLN under boiled and not-boiled lysate treatment, respectively, and **B** - PLN protein level quantification of pentameric and monomeric form.

A



B

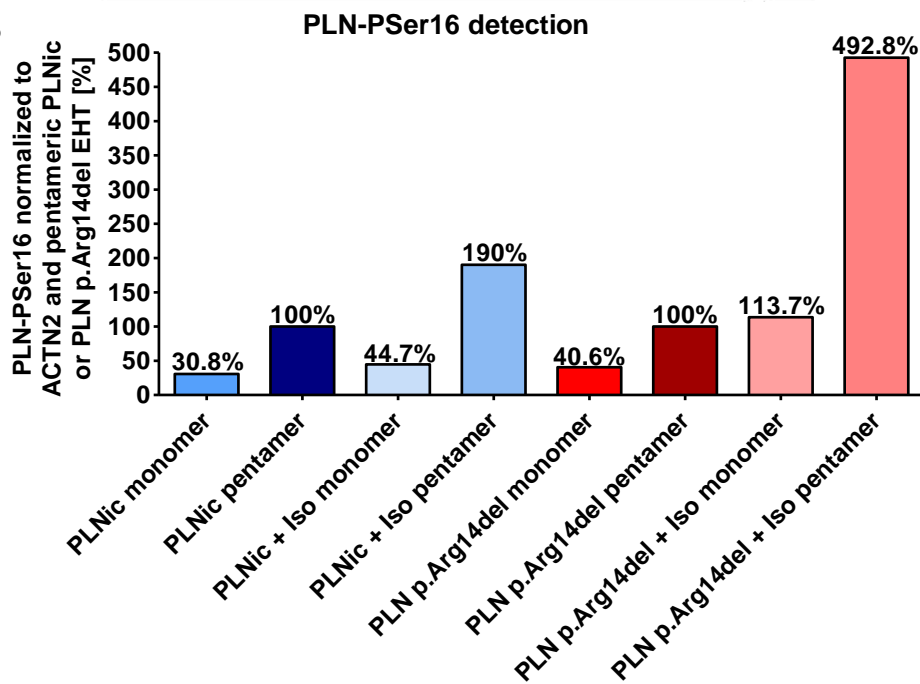


Figure 63: Western blot analysis of PLN-PSer16 protein levels. Protein levels of PLN p.Arg14del #1198 ($n = 3/1$ [number/batch], 70% cardiomyocyte purity, 30 days old) and PLNic #15 EHTs ($n = 3/1$ +Iso and $n = 4/1$ -Iso [number/batch], 77% cardiomyocyte purity, 31 days old) were investigated. **A** - Pentameric and monomeric form of PLN under boiled and not-boiled lysate treatment, respectively, and **B** - PLN-PSer16 protein level quantification of pentameric and monomeric form of PLN in the presence and absence of isoprenaline (100 nM Iso).

In a second experiment an antibody recognizing the phosphorylation of PLN-Ser16 was employed to analyse the effect of β -adrenergic stimulation by isoprenaline (100 nM, 10 min stimulation). In PLNic EHTs a much stronger signal was detected compared to PLN

p.Arg14del EHTs (Figure 63A). Upon isoprenaline stimulation a surprisingly small signal intensity increase of +90% was detected especially when comparing this to the signal intensity increase in PLN p.Arg14del EHTs. P-Ser16 signal intensity was particularly strong for PLN p.Arg14del EHTs in the presence of isoprenaline with a relative signal intensity increase of +392% of the pentameric PLN form.

b) Autophagy marker analysis

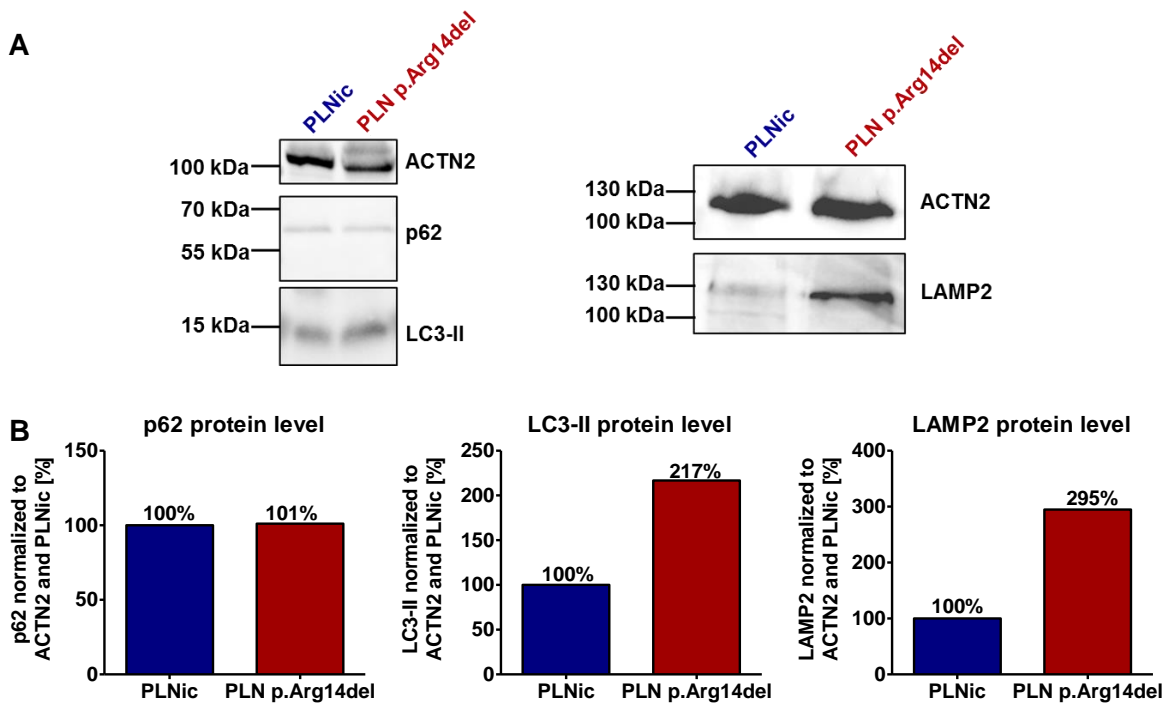


Figure 64: Western blot analysis of p62, LC3-II and LAMP2 protein levels. Protein levels of PLNic #15 (n = 4/1 [number/batch], 77% cardiomyocyte purity, 31 days old) and p.Arg14del #1198 EHTs (n = 3/1 [number/batch], 70% cardiomyocyte purity, 30 days old) were investigated. **A** - Immunoblot analysis and **B** - p62, LC3-II (autophagic marker light chain 3-II) and LAMP2 (lysosome-associated membrane protein 2) protein level quantification.

Based on the observation of te Rijdt et al. (2016) that PLN co-localized with autophagy markers the analysis of autophagy marker protein levels was investigated in this study. The analysis of p62 protein levels revealed no difference between PLN p.Arg14del and PLNic EHTs (Figure 64). On the other hand, the evaluation of the autophagy marker LC3-II (autophagic marker light chain 3-II) and LAMP2 (lysosome-associated membrane protein 2) indicated a doubling of LC3-II protein levels and tripling of LAMP2 protein levels for PLN p.Arg14del EHTs compared to isogenic controls (217% vs. 100% and 295% vs. 100%). These immunoblots were kindly performed by Antonia T. L. Zech and Birgit Klampe (UKE, DEPT, Hamburg, Germany).

4.5.3 *Histological analysis*

a) Immunohistological detection of PLN

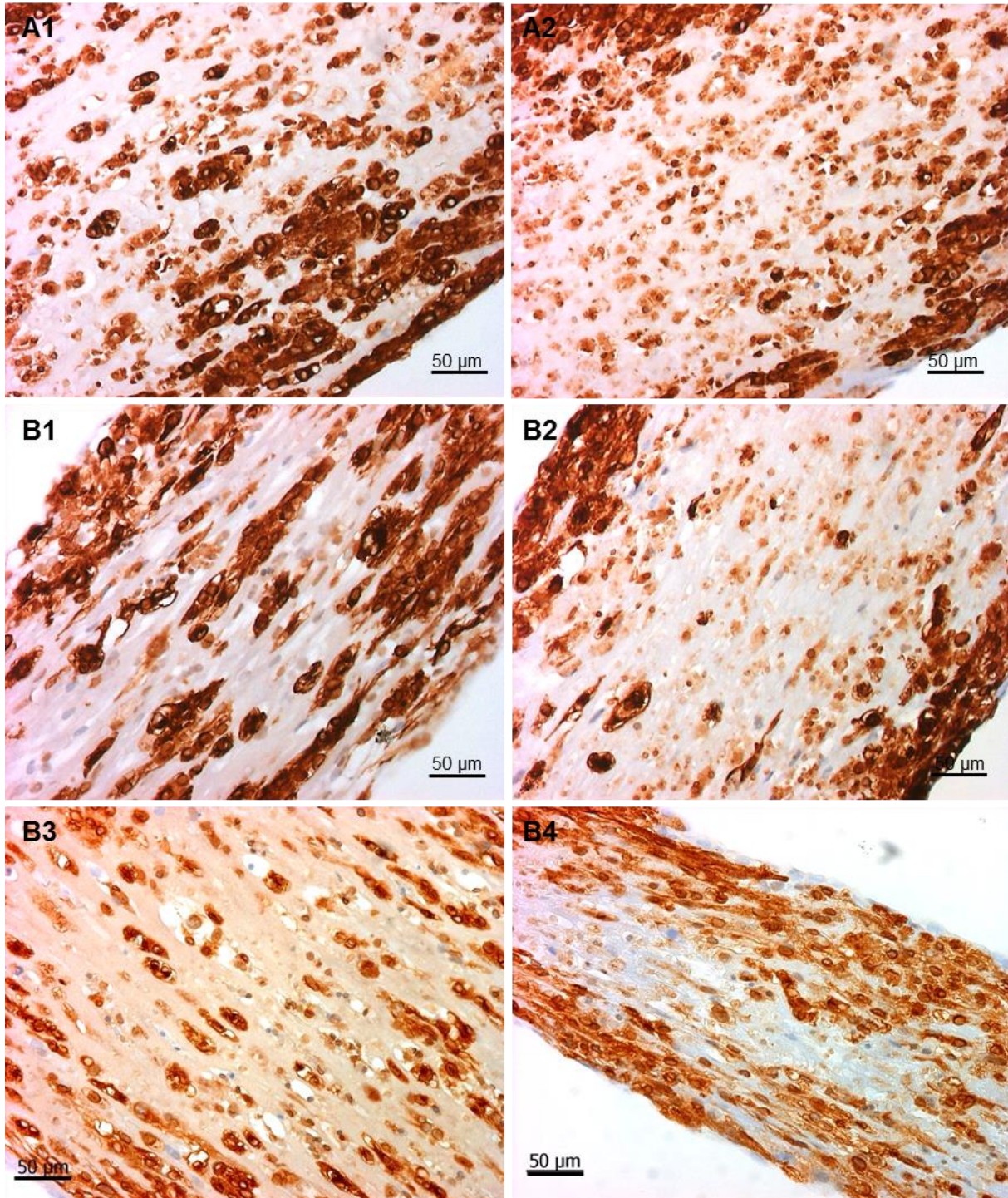


Figure 65: 20x Magnification of the immunohistological staining for hPLN in EHT longitudinal sections. A1, 2 - PLNic #28 (n = 2/1 [number/batch], 89% cardiomyocyte purity, 30 days old) and B1, 2, 3, 4 - PLN p.Arg14del #1198 (n = 4/3 [number/batch], 65-95% cardiomyocyte purity, 21-30 days old). Scale bar: 50 µm.

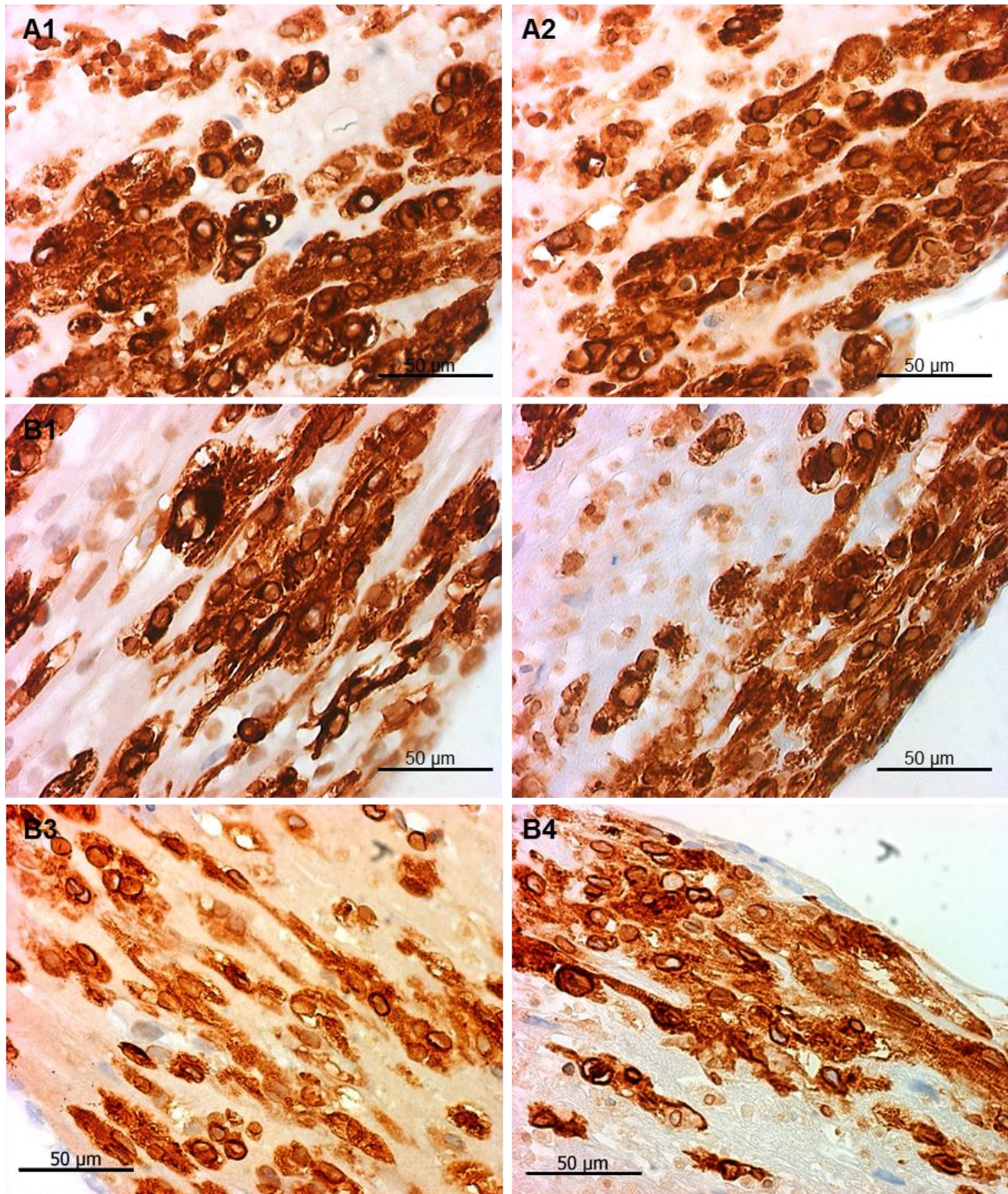


Figure 66: 40x Magnification of the immunohistological staining for hPLN in EHT longitudinal sections. A1, 2 - PLN^{Nic} #28 (n = 2/1 [number/batch], 89% cardiomyocyte purity, 30 days old) and B1, 2, 3, 4 - PLN p.Arg14del #1198 (n = 4/3 [number/batch], 65-95% cardiomyocyte purity, 21-30 days old). Scale bar: 50 μ m.

Longitudinal EHT sections of PLN^{Nic} and PLN p.Arg14del revealed no differences in PLN staining (Figures 65 and 66). A strong cellular cytosolic and perinuclear staining was detected. No aggregate formation was identified.

b) Immunohistological detection of the membrane skeleton protein dystrophin

Immunohistochemistry staining for the membrane-associated protein dystrophin revealed that in PLN p.Arg14del EHTs less distinct membrane staining could be detected compared to PLN^{ic} #28 cardiomyocytes with clearly defined dystrophin-membrane staining (Figures 67 and 68).

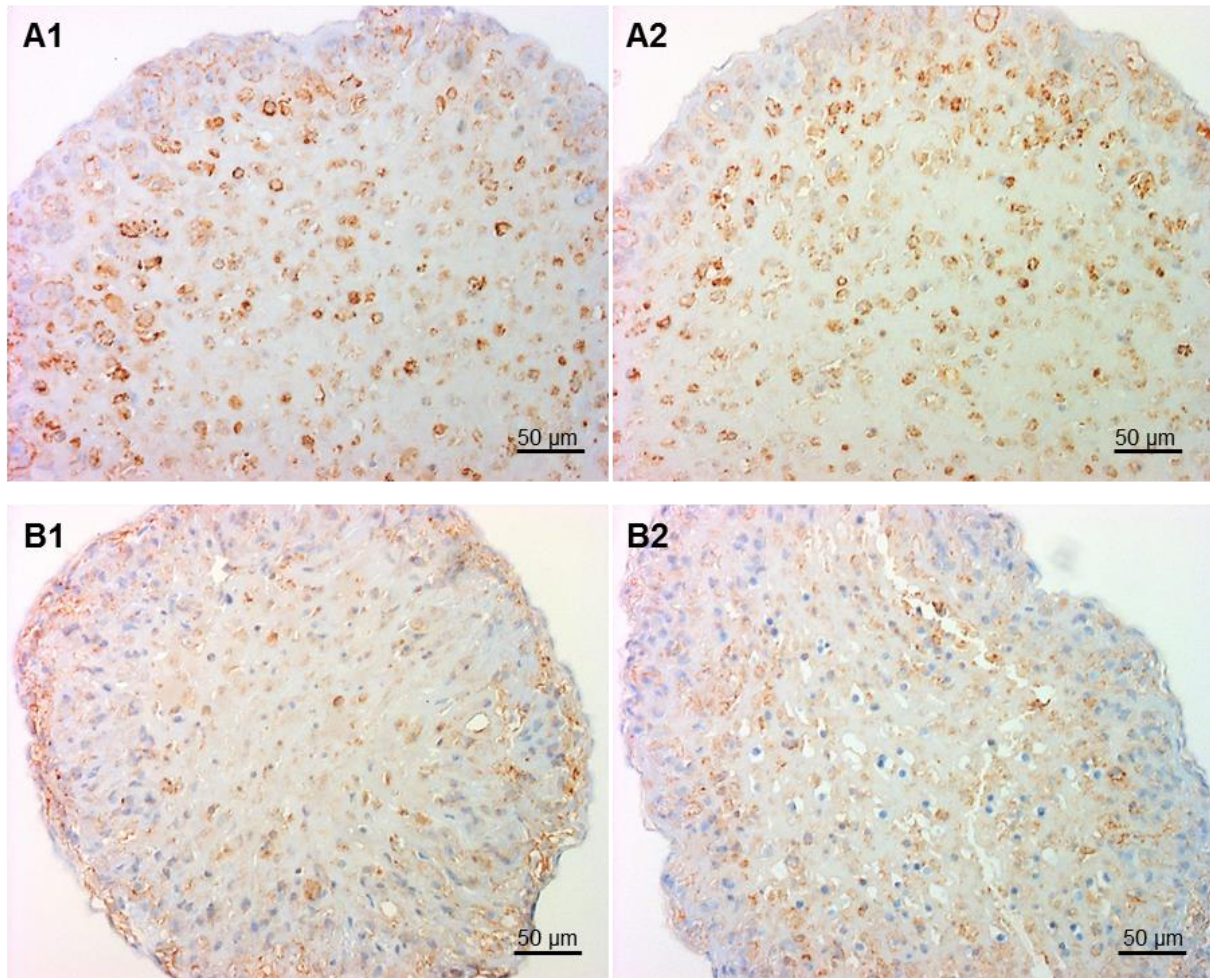


Figure 67: 20x Magnification of the immunohistological staining for dystrophin in EHT cross sections. A1, 2 - PLN^{ic} #28 (n = 2/1 [number/batch], 89% cardiomyocyte purity, 30 days old) and B1, 2 - PLN p.Arg14del #1198 (n = 2/2 [number/batch], 65-94% cardiomyocyte purity, 21-28 days old). Scale bar: 50 μm.

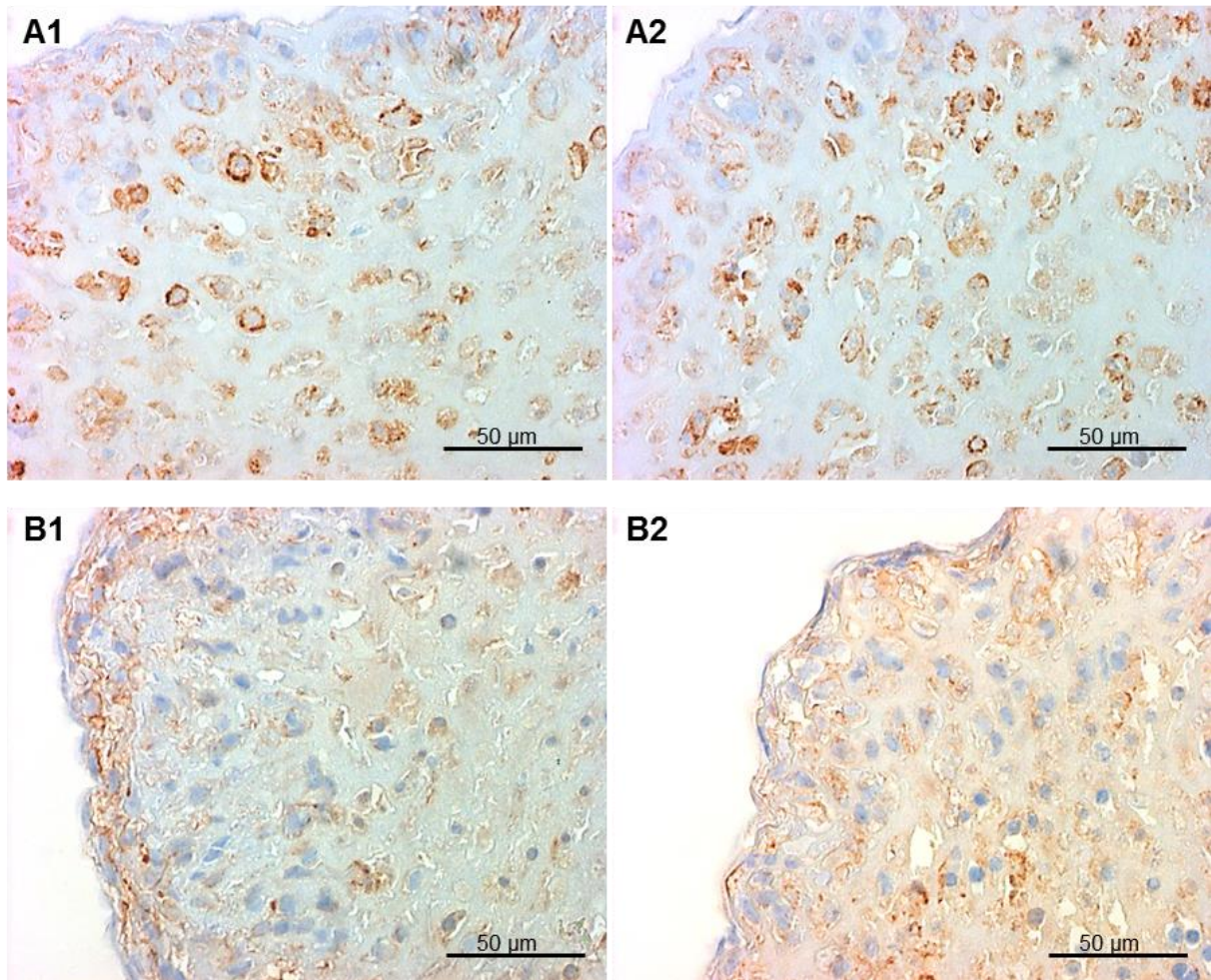


Figure 68: 40x Magnification of the immunohistological staining for dystrophin in EHT cross sections. A1, 2 - PLN^{Nic} #28 (n = 2/1 [number/batch], 89% cardiomyocyte purity, 30 days old) and B1, 2 - PLN p.Arg14del #1198 (n = 2/2 [number/batch], 65-94% cardiomyocyte purity, 21-28 days old). Scale bar: 50 μm.

4.6 HiPSC-CM characterization in 2D

4.6.1 Calcium transients and caffeine responses of PLN^{Nic} and PLN p.Arg14del cardiomyocytes in 2D format

The measurements of the hiPSC-CM and data analysis were kindly performed by Dr. Frederick Flenner (DEPT, UKE, Hamburg, Germany).

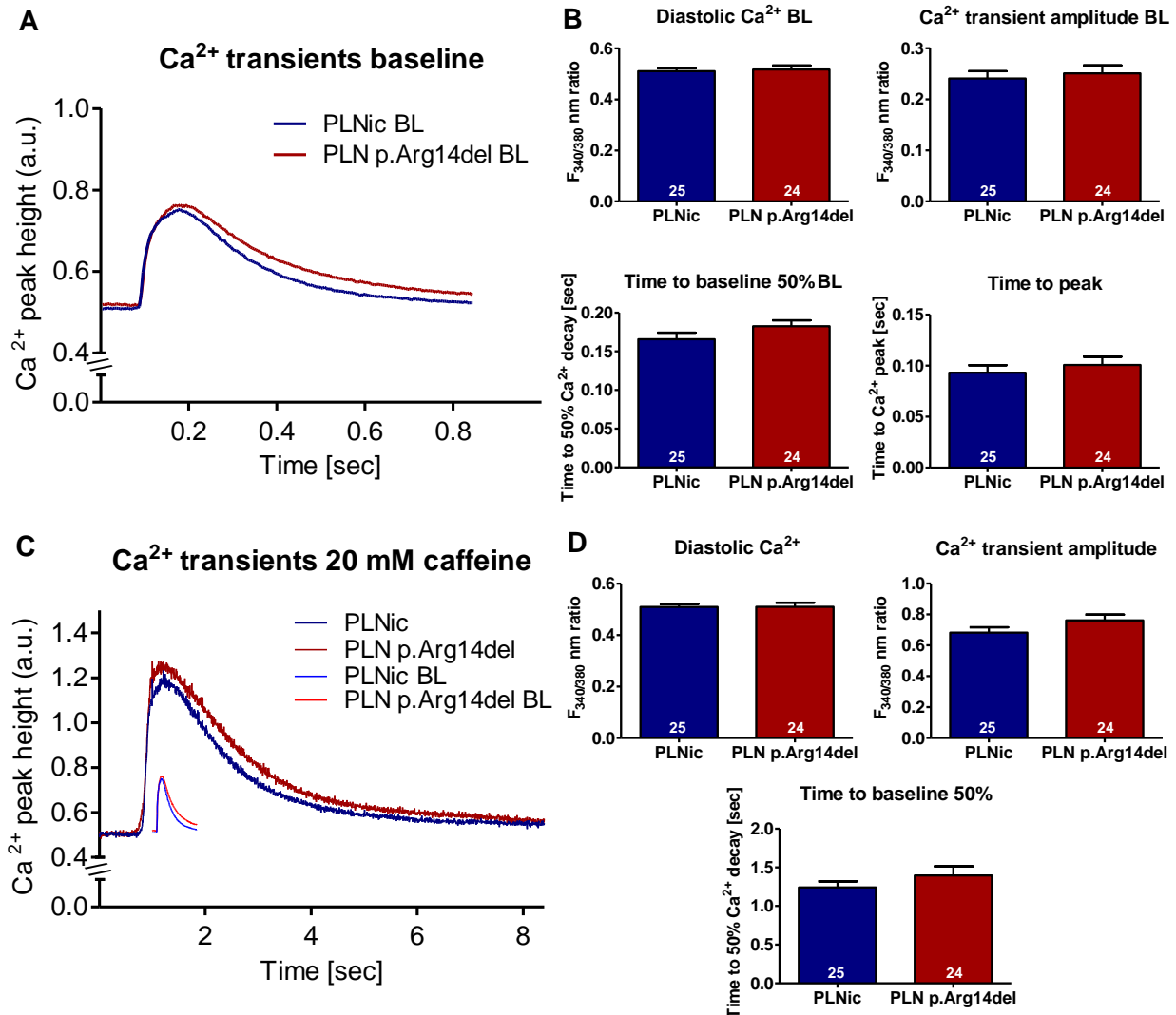


Figure 69: Calcium transient analysis in PLN p.Arg14del and PLN^{Nic} CM in 2D format.

A - Average calcium transients (n = 24-25/2, [cell number/batch]) for PLN p.Arg14del and PLN^{Nic} CM and **B** - quantification of diastolic calcium, calcium amplitude, time to calcium peak, time to calcium baseline. **C** - Average calcium transients (20 mM caffeine, n = 24-25/2 [cell number/batch]) for PLN p.Arg14del and PLN^{Nic} CM and **D** - quantification of diastolic calcium, calcium amplitude, time to calcium baseline after the caffeine puff. * p<0.05, unpaired t-test.

PLN p.Arg14del and PLNic hiPSC-CM were cultivated as 2D monolayer. The cells were seeded at a density of 10,000 cells/cm² on glass cover slips (diameter 24x24 mm) to enable single cell measurements. To avoid further cell proliferation of e. g. non-cardiomyocytes, which would hinder single cell analysis, the measurements were performed after 7±2 days after seeding. Calcium transients were analysed with IonOptix technology after loading with Fura 2-AM. After baseline calcium transients were recorded, caffeine (20 mM) was added. The caffeine-mediated calcium release from sarcoplasmic reticulum was demonstrated by the increase in transient amplitude (Figure 69C). Analysis of average calcium transients (Figure 69A, C) suggested that time to baseline (50%) was longer in PLN p.Arg14del cardiomyocytes (0.165 sec vs. 0.183 sec [Figure 69B] and 1.241 sec vs. 1.400 sec [Figure 69D]), but the quantitative analysis revealed no significant differences in calcium transients and caffeine puff between PLN p.Arg14del and PLNic hiPSCs-CM.

4.6.2 *Confocal microscopy*

Morphological analysis was performed in 2D format with immunofluorescence by applying the exact same laser intensity power for all samples. The 2D cultivated cardiomyocytes showed cytoplasmic staining pattern with perinuclear enhancement for PLN (Figures 70, 71). PLN aggregates were not identified in these samples. ACTN2-positivity had a cytoplasmic localization and in some areas this showed a sarcomeric organization (Figure 70). The ACTN2 staining appeared to show a better morphology in the PLN p.Arg14del EHTs. Due to low replicate numbers of this experiment, this should be further validated. SERCA2a staining also revealed a cytoplasmic localization, but no indication of a cross-striated pattern (Figure 71). The important difference between PLN p.Arg14del and PLNic hiPSCs-CM was not related to any specific staining pattern, but an overall weaker staining intensity for all cardiomyocyte markers in PLN p.Arg14del versus PLNic.

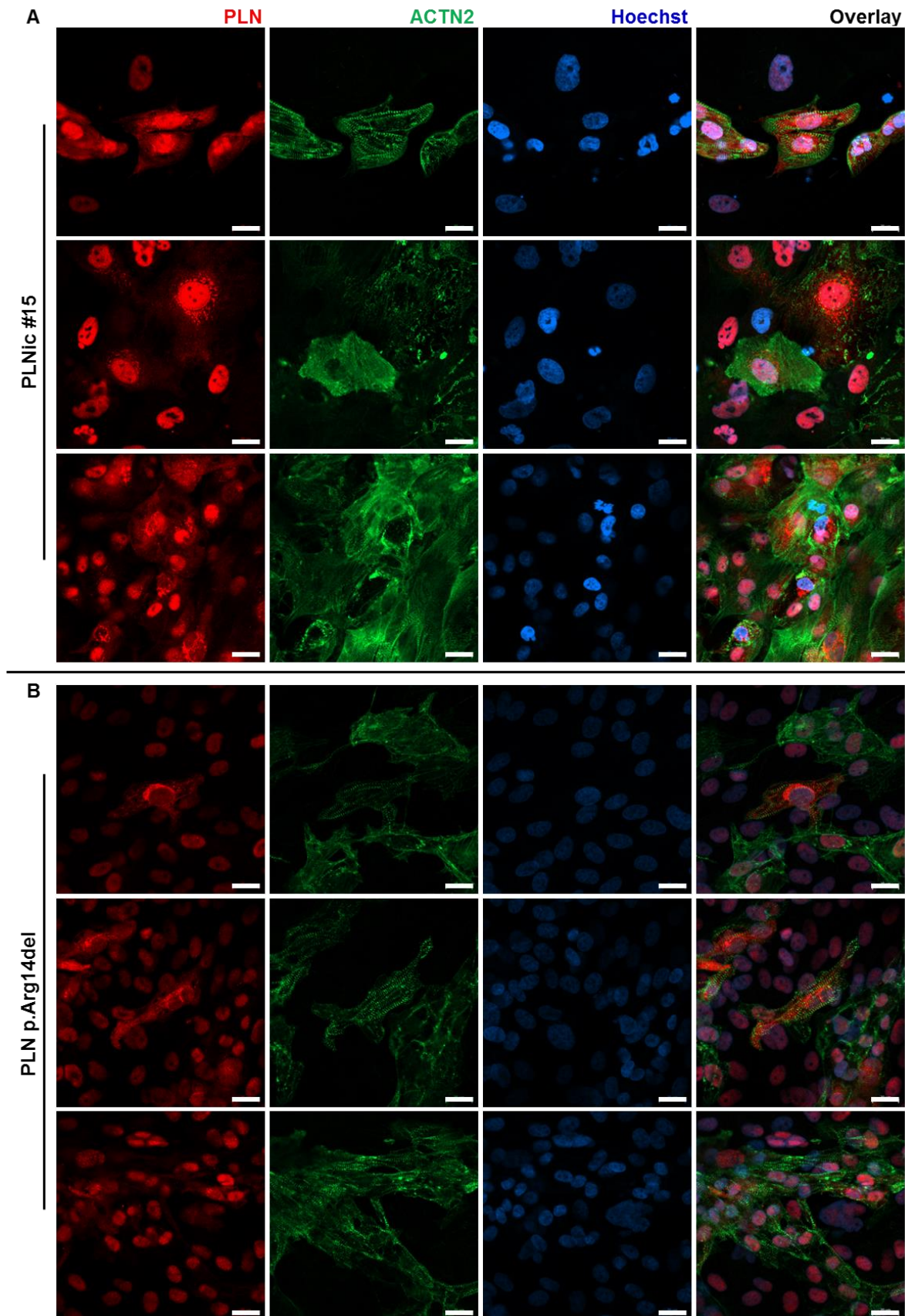


Figure 70: Immunofluorescence of PLN (red), ACTN2 (green) and Hoechst (blue) staining in 30 days old hiPSCs-CM in 2D format. A - PLN#15 (90% cardiomyocyte purity) and B - PLN p.Arg14del (91% cardiomyocyte purity). Scale bar: 20 μm.

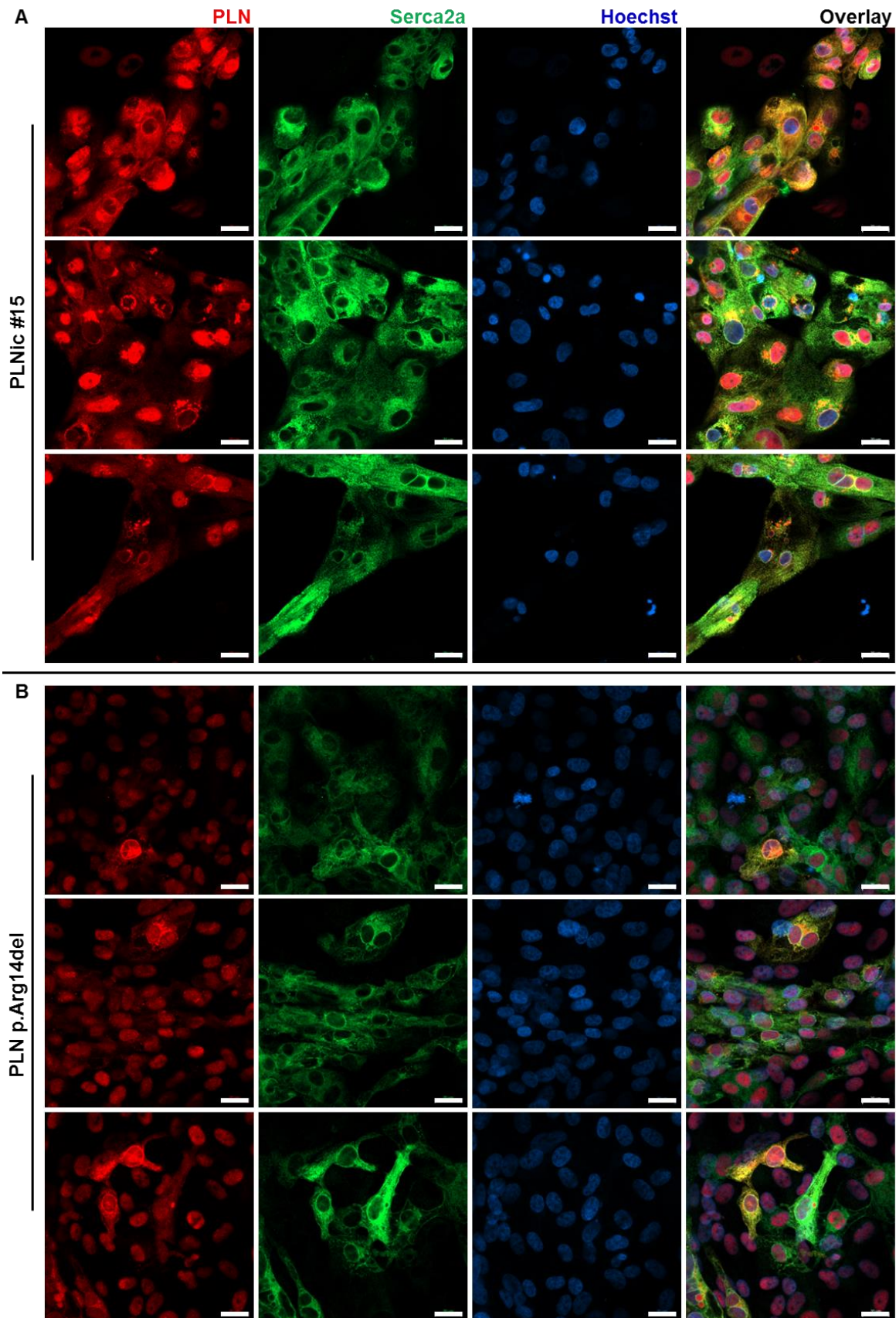


Figure 71: Immunofluorescence of PLN (red), Serca2a (green) and Hoechst (blue) staining in 30 days old hiPSC-CM in 2D format. **A** - PLN#15 (90% cardiomyocyte purity) and **B** - PLN p.Arg14del (91% cardiomyocyte purity). Scale bar: 20 μm.

4.6.3 *Cardiomyocyte cell area analysis*

Cell sizes of single cells stained for ACTN2 were investigated at day 7 and day 30 after seeding (Figure 72). After 7 days of cultivation PLNic cardiomyocytes appeared to be significantly smaller in cell area compared to PLN p.Arg14del at day 7, but increased within the following three weeks significantly while PLN p.Arg14del cells remained unchanged in size. Finally, on day 30 no significant difference could be identified between PLNic and PLN p.Arg14del cardiomyocytes with a cell area of about 1400 μm^2 . This experiment was kindly performed by Maksymilian Prondzynski (DEPT, UKE, Hamburg, Germany).

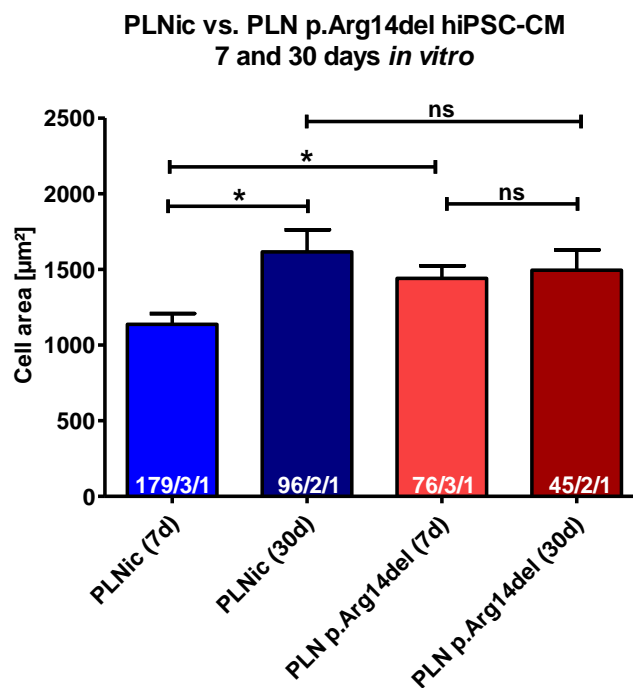


Figure 72: PLNic and PLN p.Arg14del cardiomyocyte cell area evaluation by confocal microscopy and ImageJ analysis after 7 and 30 days of cultivation. n = cell number/well number/differentiation batch number; ns = not significant and * $p < 0.05$, unpaired t-test.

5 DISCUSSION

This thesis aimed to establish an *in vitro* disease model for PLN p.Arg14del mutation in hiPSC-cardiomyocytes. Main results are 1) the establishment of isogenic control hiPSC lines from patient-specific hiPSCs by CRISPR/Cas9 genome editing technology, 2) the efficient differentiation of cardiomyocytes from disease-specific and isogenic control hiPSCs, 3) the establishment of a human cardiac *in vitro* tissue model for disease modelling with patient-specific and isogenic control hiPSC-cardiomyocytes and 4) the phenotypic analysis of hiPSC-CM in 2D and 3D format as well as the identification of a disease-specific contractility pattern consisting of low force development and susceptibility for calcium-induced irregular beating pattern.

The following chapters will discuss these main aspects in further detail.

5.1 Establishment of isogenic control hiPSC lines from patient-specific hiPSCs by CRISPR/Cas9 genome editing technology

5.1.1 CRISPR/Cas9-mediated genomic correction of PLN c.40-42AGAdel

Genetic backgrounds differ between individuals. For this reason genetically modified animal models are always compared to isogenic littermates and not to other strains of the same species. Transferring this knowledge to hiPSC disease modelling leads to the requirement to compare patient-derived hiPSC lines to an isogenic control. Since this was very difficult until recently, early hiPSC-disease modelling studies compared the phenotype against the hiPSC from a close family member (Moretti et al. 2010; Sun et al. 2012; Lan et al. 2013). The advent of advanced genome editing technologies (TALEN, ZFN, CRISPR/Cas9) allows to specifically modify target genetic loci. Among genome editing technology CRISPR/Cas9 stands out because of its simplicity and low costs. The combination of hiPSC system with the CRISPR/Cas9 technology creates a very versatile and powerful platform to study patient- and mutation-specific human diseases. The following chapters will address specific aspects of CRISPR/Cas9 technology to create a PLN p.Arg14del hiPSC disease model.

5.1.2 Application of the Cas9n approach

When the CRISPR/Cas9 technology was established in the laboratory, first experimental approaches were designed with the Cas9n approach as first choice. This nickase only performs a single stranded cut. By combining two separate sgRNAs the off-target activity was published to lead to reduced NHEJ and a preference for HDR repair mechanism (Ran et al. 2013a). Although it was published that NGG PAM sequences can be found every 8-12 bp (Cong et al. 2013; Hsu et al. 2013) this was not the case for the PLN sequence. No suitable pair of sgRNA could be designed fulfilling the criteria of both sgRNAs being in proximity to the PLN c.40-42AGAdel mutation. Instead, NAG PAM sequences were identified fitting these

requirements. This PAM sequence can also be recognized by the SpCas9 nuclease but with only one-fifth targeting efficiency (Jiang et al. 2013; Hsu et al. 2013; Zhang et al. 2014). It was never tested before whether the combination of the Cas9n and the NAG PAM targeting would lead to successful HDR mediated repair. Nevertheless, this approach was investigated with the idea to limit NHEJ events and off-target generation (data not shown). After several experimental approaches and optimizations no recombination events were detected. Therefore this approach was finally discontinued and considered to be not suitable for the PLN gene correction.

5.1.3 Comparison and evaluation of the established DNA- and RNP-based Cas9 nuclease approaches

a) **Evaluation of the *in silico* design of the gRNA and ssODN repair template**

The Cas9 nuclease wildtype approach was therefore investigated next. It was suggested that this approach is more efficient compared to the nickase-based one, but also leads to higher off-target probability since only one sgRNA is needed to induce a double strand break into the target DNA sequence (Ran et al. 2013a; Ran et al. 2013b). The design of the CRISPR experiment was based on the recommendations and instructions given in the publication of Ran et al. (2013b) in Nature Protocols. The PLN sequence validation of the hiPSC revealed that no SNPs were detected in proximity to the PLN c.40-42AGAdel which had to be taken into consideration for the gRNA and repair template design. For the gRNA design the user-friendly Zhang labs' online CRISPR design tool (<http://crispr.mit.edu>) was applied which identified gRNAs according to specificity and possible off-targets. Among different candidates, gRNA #3 was selected because of low off-target numbers especially in exonic regions and since it was in close proximity to the locus of interest with only 5 nucleotides downstream of PLN c.40-42AGAdel (Figures 24 and 25).

While the mutated sequence served as template for the design of the guide, the wildtype allele was used for the design of the ssODN (Figure 26). Homology arms of 50 nt each were chosen with the AGA codon located in the centre of the repair template. Within the NGG PAM sequence a silent mutation was inserted to avoid repair template degradation by re-editing of the recombined repaired sequence. The NGG motif was thereby mutated to a NTG (PLN c.45C>A), which does not lead to a change of the amino acid sequence (silent mutation). When analysing the sequencing result of nucleofected cells this additionally helped to identify successful recombination of the repair template into the cells genome by identifying this silent mutation in the electropherogram. An antisense orientation of the repair template was chosen. This was based on evidence demonstrated in several studies. Ran et al. (2013b) published that either way, sense or antisense direction, works the same way. It was later suggested that the antisense would lead to higher genome editing results (Miyaoaka

et al. 2016). Additionally, Richardson et al. (2016) proposed that a ssODN donor DNA creates higher HDR frequencies when it is designed to be complementary to the non-target strand and to be asymmetric meaning that the Cas9 cut site does not overlap within the centre of the annealed ssODN. The homology arms were about 40 nt in the PAM-distal site and ~90 nt on the PAM proximal side in respect to the Cas9-mediated break.

b) Preparation of the RNP- and DNA-based approaches

Two different sgRNA-Cas9-delivery approaches were investigated in this thesis. For the DNA-based approach the Cas9 was encoded on a plasmid together with the sgRNA. This plasmid was obtained from Addgene and was published in Ran et al. (2013b). It simplified the approach since the gRNA-DNA oligomer had to be simply ligated into the BbsI flanked cloning site of pSpCas9(BB)-2A-GFP plasmid.

Besides this DNA-based method, a protein-based approach was also investigated. An *in vitro* transcribed sgRNA was used to form a RNP complex with the Cas9 nuclease protein. The RNP complex is biologically active directly after nucleofection and is degraded within 72 hours. This could translate into lower off-target activity compared to the DNA-based method in which the plasmid is expressed for an extended period of time continuously reproducing Cas9 and sgRNA (Kim et al. 2014; Liang et al. 2015). It was also published that the efficiency was remarkably higher for RNP-mediated gene editing compared to the DNA-based method in hiPSC (DNA-based: 20% vs. RNP-based: 87%; Liang et al. 2015).

The preparation of the RNP-based experiment was successful. The sgRNA was *in vitro* transcribed and cleaned-up with sufficient purities and yields. Nevertheless, it was not trivial and *in vitro* transcription could also lead to low purities. In addition to low purities, RNase contaminations can limit the success of a genome correction approach. For both reasons, ordering sgRNA directly from a company would increase robustness and the probability of a successful genome editing experiment. An important advantage of the RNP approach is the possibility to test the targeting of the designed gRNA and the functionality of the purchased Cas9 nuclease *in vitro* (Figure 33). This also helped to evaluate the nuclease for batch-to-batch variabilities or batch failure before its application on the hiPSCs.

c) Application of the RNP- and DNA-based approaches

In first experiments, the ssODN concentration published by Ran et al. (2013b) was used for the DNA-based approach (0.4 μM [1 μL of a 10 μM stock]). This turned out to be not sufficient. Sequencing results of these experiments indicated that the Cas9 was indeed cutting the DNA because nucleotide deletions and insertions were detected within the Cas9 cutting region but no insertion of the repair template was identified (data not shown). This suggested that the concentration of the ssODN had to be increased. For additional

experiments, the ssODN concentration was increased to 5 μ M final concentration. This led to the successful recombination of the repair template into the target locus on both alleles for the DNA-based approach and on only the mutated allele within the RNP-based experiment, suggesting that the previous ssODN concentration was indeed too low. Therefore, it can be assumed that the adaptation of the repair template concentration is a critical step.

Due to the double stranded cut mediated by Cas9 nuclease, the NHEJ pathway can be activated in addition to HDR. This could promote indel formations and gene disruption. NHEJ is active throughout the whole cell cycle, while HDR is only available within the G2 and S phases. To shift the repair machinery towards HDR the small molecule inhibitor SCR7 was tested. SCR7 is a pharmacological inhibitor of the NHEJ mechanism. This small molecule inhibits the DNA ligase IV which is the key ligase for DNA repair via the NHEJ pathway (Chu et al. 2015; Maruyama et al. 2015). SCR7 was tested for both DNA and RNP approaches. Within the RNP-based approach, half of the preparation was incubated with the inhibitor for 48 hours after nucleofection until sub-cultivation because the Cas9 protein gets degraded over time and was not detected after 72 hours after electroporation in HEK293FT cells (Liang et al. 2015). After sub-cultivation the hiPSC colonies with SCR7 appeared to show a sharper and more distinct colony morphology compared to the cells cultured without SCR7, which appeared to grow slower. Since it was published that the RNP-approach showed higher editing efficiencies than the DNA-based one (Liang et al. 2015), only 30 clones were picked in total from the RNP approach (18 -SCR and 12 +SCR7 condition). Surprisingly, the one positive out of all 27 screened clones from the RNP-based approach was detected from the culture without SCR7 treatment (Table 25). Since no further comparable SCR7 analyses were investigated, no robust statement can be made on the question whether SCR7 is supporting homologous recombination in this RNP-based approach.

As already mentioned, deleted base pairs were detected within previous experiments of the DNA-based approach, indicating that the Cas9 cut the DNA target sequence but without successful recombination of the ssODN due to its too low concentration. This suggested that the NHEJ was the preferred mechanism. To shift this toward HDR mechanism, SCR7 was supplemented aiming to reduce indel formations. Plasmid transcription and the translation of the Cas9 protein take substantial longer for this in contrast to the RNP approach, the plasmid is continuously expressed until it is diluted during cell division or degradation. For this reason SCR7 was continuously added for the DNA approach until isolation of the hiPSC colonies. Out of 41 screened clones three showed successful recombination (Table 26). An advantage of the DNA-based approach is the possibility to control and enrich for transfected cells by FACS sorting.

d) Evaluation of the generated PLNic

The success rate to generate isogenic controls was 4% for the RNP-based approach and 7% for the DNA-based one without off-target activity within the top 10 most likely off-target locations. Interestingly, all three isogenic control clones (3/48 clones: PLNic #15, #24 and #45) derived from the DNA-based experiment showed recombination of both, wildtype and mutated, alleles, since the electropherograms of the sequencing results showed a homozygous insertion of the silent mutation (Figure 40). The PLNic #28 derived from the RNP-based approach was heterozygous for this location indicating that only the mutated allele was recombined (Figure 35). It could be assumed that this could be related to the shorter time of nuclease activity due to the degradation of the protein within less than 72 hours.

To further investigate the comparative analysis of the PLN p.Arg14del carriers to their isogenic controls, two PLNic clones were selected – one from each approach (DNA-based derived PLNic #15 and RNP-based PLNic #28). Both, PLN c.40-42AGAdel as well as hiPSC clones were evaluated for their karyotype. In the case of PLN mutated hiPSC #1198 and #1201, no abnormal karyotypes were found at a lower passage number (Figure 21). Also in the PLNic #15 and #28 hiPSC clones the karyotype was not affected despite their high passage number and the exposure to multiple stressors (Figure 47). This was surprising because the hiPSC were exposed to the nucleofection- and FACS sorting-related stress as well as high density culture at 21% oxygen and expansion until passage 50. Literature review indicates that factors promoting karyotypic abnormalities in hiPSCs are not well defined. Nevertheless, several reports are published which identify potential factors. Among these is the cultivation at atmospheric versus 5% oxygen concentration based on the hypothesis that higher ROS (reactive oxygen species) production at atmospheric oxygen drives karyotypic abnormalities. In consequence the authors suggest cultivating hiPSCs at 5% oxygen to stabilize the karyotype (Lim et al. 2011). Another publication indicated that an increased culture density correlated with increased DNA damage levels and the induction of chromosomal abnormalities in hESC (Jacobs et al. 2016). Other studies proposed that karyotypically altered pluripotent stem cells can overgrow wildtype pluripotent stem cells e. g. due to mutation-associated increased proliferation and decreased apoptosis (Spits et al. 2008; Amps et al. 2011; Lund et al. 2012; Avery et al. 2013; Nguyen et al. 2013; Nguyen et al. 2014). In hESC culture a spontaneous mutation rate of up to 35% of cells carrying abnormal chromosome counts and structural abbreviations was detected (Lim et al. 2011; Dekel-Naftali et al. 2012; Jacobs et al. 2014). Additionally, it was suggested that these abnormalities limit the differentiation potential and lead to alteration of gene-expression levels (Werbowetski-Ogilvie et al. 2009; Gopalakrishna-Pillai and Iverson 2010; Fazeli et al. 2011).

5.1.4 *Evaluation of the CRISPR/Cas9 technology in this study*

The establishment of the CRISPR/Cas9 technology for the gene correction of the heterozygous PLN c.40-42AGAdel mutation took a substantial period of time of about 1.5 years. Even though the protocol was based on the Nature Protocols publication of Ran et al. (2013b) the system needed to be further adapted for the respective gene. The suggested Cas9 nickase approach could not be applied for the gene correction in this study. Although the NAG PAM sequence was assumed to be a possible alternative Cas9 recognition motif, no successful recombination was achieved. Nevertheless, the design of a new repair template and sgRNA for the Cas9 nuclease approach was achieved much faster due to the gained knowledge and experience from other CRISPR/Cas9 experiments in our laboratories. But also this system needed further improvements. Especially the ssODN concentration appeared to be highly critical. While in other experiments a concentration of 0.4 μM was sufficient this did not apply for this study. In future investigations the ssODN concentration should be directly increased to at least 5 μM to save time and costs.

The application of the RNP-approach has several advantages and might be the preferred experimental design for further CRISPR/Cas9 studies. The cloning process of the Cas9 and sgRNA carrying plasmids would be avoided. Purchasing an already synthesized sgRNA as well as Cas9 nuclease would increase the standardization level, quality and experimental stability. In this study the RNP-based approach was only performed once and only analysed for a low number of isolated clones. Nevertheless, this approach was directly successful without additional optimization experiments. For further experiments the efficiency could be increased by adjusting Cas9 nuclease or sgRNA concentrations. Thereby a lower number of hiPSC clones would have to be picked and expanded reducing the work-, time- and cost-intensive cultivation and characterization of the isolated hiPSC clones.

5.2 Efficient differentiation of cardiomyocytes from disease-specific and isogenic control hiPSCs

The choice for an optimal human cardiac *in vitro* model would be the cultivation and analysis of primary human adult cardiomyocytes. But this is impossible due to limited availability and lack of cellular proliferation, preparation variability, poor cell viability and cardiomyocyte de-differentiation in culture (Rajamohan et al. 2013; Denning et al. 2015). Instead, heterologous expression systems were often applied. But with the overexpression of genes in other cell types but cardiomyocytes (e. g. HEK293T cells) physiological protein levels are not reached and compensatory cell-specific mechanisms cannot be evaluated since the cell's identity and integrity are neglected. With the application of animal models and non-human cardiomyocyte cultivation this issue was circumvented. But interspecies differences also substantially reduce the experimental significance. Especially mice and human cardiac physiology differ substantially from each other. Human hearts show longer action-potential duration (APD) and slower physiological beating rates (60-100 bpm vs. 600 bpm in murine hearts) as well as differences in gene expression pattern (Nerbonne and Kass 2005). Also calcium cycling mechanisms differ. In human cardiomyocytes, about 70% of the cytosolic calcium is recycled into the SR by SERCA2a, in murine cells the value is above 90% (Bers 2002). With respect to these facts the possibility to reprogram patient-derived human somatic cells to hiPSC (Takahashi and Yamanaka 2006; Takahashi et al. 2007b) and to differentiate hiPSCs into cardiomyocytes (Laflamme et al. 2007; Zhang et al. 2009) opened a new field of cardiac *in vitro* models with a big potential to improve drug screenings, disease modelling and personalized medicine.

Within this thesis, hiPSC-derived cardiomyocytes were successfully generated with an EB-formation and growth-factor-based approach (Breckwoldt et al. 2017). All hiPSC clones (PLNic #15, #28 and PLN p.Arg14del #1198, #1201) were capable of differentiating efficiently to high purity cardiomyocyte (up to 94% cTNT⁺; Figures 49 and 50). For all differentiation experiments, EBs were generated and mesoderm induction was performed in EB format. Further cardiac specification was performed in both, adherent and cEB format (Figure 48). No hiPSC-CM quality or purity difference between cEB-based and adherent cardiac specification based approach could be determined within this study.

5.3 The establishment of a human cardiac *in vitro* tissue model for disease modelling with patient-specific and isogenic control hiPSC-derived cardiomyocytes

The development of cardiac *in vitro* models has advanced substantially within the past decade after the discovery of hiPSCs. This included models in 2D monolayer as well as 3D format. 3D systems are often more complex, require higher cell numbers per data point and represent a more physiological system than 2D models. In addition, the level of cardiomyocyte maturation and the ability to measure contractile force are important differences between 2D and 3D models. HiPSC-cardiomyocytes in 2D format show poor cellular alignment and sarcomeric organisation of myofilaments. All subcellular components are poorly developed including myofilament and mitochondrial volume fraction and T-tubuli. Due to the random cellular and myofilament orientation also axial vectors of shortening during contraction are not aligned, leading to low signal-to-noise ratios of force measurements with unclear biological significance. On the other hand, 3D hydrogel systems in general and the 24-well EHT system in particular rely on the cultivation of hiPSC-CMs under load (Eschenhagen et al. 2012). This leads to the formation of force lines and in consequence to the improved cellular alignment and sarcomeric organisation of myofilament proteins (Mannhardt et al. 2016). Additionally, hiPSC-CM in the EHT model show electrophysiological maturation by an increased density of I_{Na} (Lemoine et al. 2017) and measurement of the I_{Ca} current in EHTs showed a partial maturation in comparison to monolayer hiPSC-CM (Uzun et al. 2016).

The analysis of contractile force is realised either by conventional force transducers or by video-optical systems as in case of the 24-well EHT system. The high level of automation of force analysis and the ability to perform force measurements under sterile conditions allowed a comprehensive comparison of force development under physiological and pharmacological conditions with literature values for non-failing human heart, demonstrating overall high levels of similarity between the two (Mannhardt et al. 2016). This makes the EHT model a promising versatile platform to unravel disease phenotypes. In line with this also the contractile deficiency of titin truncation variants and heterozygous PLN p.Arg14del hiPSC-CM were analysed in a human cardiac micro tissue model (Hinson et al. 2015; Stillitano et al. 2016).

5.4 **Phenotypic analysis of hiPSC-CM in 2D and 3D format**

5.4.1 Investigation of contractile parameters and pharmacological responses of hiPSC-derived PLNic and PLN p.Arg14del cardiomyocytes

The PLN p.Arg14del mutation was published as a DCM-causing founder mutation. This autosomal dominant disorder was identified in families suffering from DCM and AVRC and is causative for the most commonly inherited familial DCM form in the Netherlands (Haghighi et al. 2006; Posch et al. 2009; van der Zwaag et al. 2012; van der Heijden and Hassink 2013; van der Zwaag et al. 2013). The patient donating the fibroblast sample for this study developed DCM with typical symptoms of reduced ejection fraction, dilated ventricles and ventricular arrhythmias at mid-age. The PLN p.Arg14del mutation was inherited from her mother who was also diagnosed with DCM. Across a number of studies, a super-inhibitory function on SERCA2a activity causing a reduced calcium re-uptake rate into the SR is the most commonly hypothesised effect of PLN p.Arg14del (Haghighi et al. 2006; Ceholski et al. 2012a; Ceholski et al. 2012b). The following paragraph discusses functional results of this study with particular focus on alignment to this hypothesis.

Before the CRISPR-derived isogenic controls were successfully generated the PLN p.Arg14del EHTs were compared to unrelated control EHTs. The PLN mutated EHTs showed lower force generation (Figure 51). Additionally, irregular beating patterns (IBP) were observed for PLN p.Arg14del EHTs. With the establishment of the CRISPR/Cas9 system and successful generation of isogenic control lines the PLNic EHTs could be analysed and verified that low forces are a specific phenotype of PLN p.Arg14del EHTs (Figures 51-54). To determine the susceptibility for calcium overload-induced IBP, PLNic and PLN p.Arg14del EHTs were exposed to increasing extracellular calcium concentrations of 1.0, 1.8 and 3.0 mM calcium over a time period of 11 hours. The intention was to provoke a phenotype due to the induction of a cytosolic calcium overload. Indeed, the PLN p.Arg14del EHTs developed IBP at high calcium concentrations which remained absent in PLNic EHTs. The quantification of the RR scatter proved a significant calcium concentration- and time-dependent increase of IBP in PLN mutated EHTs. This phenotype was rescued by CRISPR/Cas9-mediated correction of the PLN p.Arg14del sequence (Figure 58). Preliminary data, which are not shown in this thesis, supported the assumption that an increase of extracellular calcium causes a cytosolic calcium overload causing the IBP. The PLN p.Arg14del EHTs were additionally stimulated with the L-type calcium channel agonist BayK-8644 at 1 mM external calcium and L-type calcium channel antagonist verapamil at 3 mM calcium (data not shown). The IBP were induced by BayK-8644 and transiently reversed by the L-type calcium channel antagonist. These pharmacological experiments should be repeated in the future with PLN p.Arg14del and PLNic EHTs to further confirm the data.

Taken together, the data support the hypothesis of disturbed calcium cycling in PLN p.Arg14del. The underlying mechanism of these IBPs could be a delayed after-depolarization (DAD) mechanism. At increased cytosolic calcium levels the calcium ions are removed by the electrogenic NCX in exchange with sodium ions, causing a transient inward current (Eisner 2014). This sodium ion influx leads to after-depolarisations probably causing the observed irregular beating pattern in the PLN p.Arg14del EHTs. Taken together, these data suggest that a disease-specific contractility pattern can be demonstrated for the PLN p.Arg14del mutation in the hiPSC-derived EHT model. Furthermore, these two main findings are compatible with a super-inhibitory function of PLN p.Arg14del, since this would result in lower SR calcium stores, higher diastolic cytoplasmic calcium and higher susceptibility for calcium overload (pro-arrhythmic trigger).

The calcium concentration-response curve analysis of the EHTs revealed a significantly lower EC_{50} value of PLNic #15 (0.32 mM) vs. PLN p.Arg14del #1198 (0.71 mM; Figure 56) and thereby a shift of the curve to the right for the mutated EHTs. Additionally, unrelated controls showed an EC_{50} of 0.6 mM calcium ($n = 8$, Hill slope 1.96; Mannhardt et al. 2016), also indicating the shift of the curve to the right of PLN p.Arg14del carriers. Calcium concentration-response curves integrate both, calcium handling mechanisms and calcium binding affinity of the myofilaments. Whether the difference in calcium sensitivity is e. g. due to a change in calcium sensitivity of the myofilaments needs to be further defined in skinned myofilament experiments in the absence of calcium handling proteins (Chung et al. 2016).

Even though average contraction peak analyses revealed a significantly shorter contraction time of the PLN p.Arg14del EHTs ($0.10 \text{ sec} \pm 0.01 \text{ sec}$, $n = 27/4$) compared to PLNic #15 ($0.13 \text{ sec} \pm 0.003 \text{ sec}$, $n = 9/1$) and unrelated controls ($0.13 \text{ sec} \pm 0.01 \text{ sec}$, $n = 10/3$; Figure 54) the earliest contraction phase was delayed in PLN p.Arg14del EHTs. Mechanistically this is not fully understood, yet. But this could probably be a first indication for the hypothesis that the myofilament adapted to the high cytosolic calcium levels suggesting that more calcium ions are needed for the induction of the contraction. Another hint for this could be the detected Hill slope value of 2.1 for the mutated EHTs while it was around 1.3 for the isogenic controls.

As a direct measurement of calcium handling in this model calcium transients were analysed under baseline and in the presence of high caffeine bolus in 2D hiPCS-CM (Figure 69). This experiment, also referred to as caffeine puff, is based on the pharmacological effect of caffeine opening ryanodine receptors. The entire sarcoplasmic calcium is released into the cytoplasm upon an applied caffeine concentration of 20 mM. The calcium transient after caffeine application is therefore a surrogate for sarcoplasmic calcium storage (O'Neill and Eisner 1990; Eisner 2014). The analysis of average calcium transients suggested a tendency

towards prolonged time to baseline (50%) in PLN p.Arg14del cardiomyocytes. This would fit to the hypothesis of a reduced calcium re-uptake into the SR due to increased SERCA2a inhibition, but the tendency was not significant. Also no significant differences were detected in diastolic calcium levels or calcium transient amplitudes neither at baseline conditions nor after the caffeine puff. These observations do not support a super-inhibitory function of PLN p.Arg14del. An incongruent picture was also reported by Karakikes et al. (2015) and Stillitano et al. (2016) who detected irregular calcium waves and lower force development of PLN p.Arg14del hiPSC-CM or human engineered cardiac tissues (hECT), respectively, but observed larger caffeine response in PLN p.Arg14del hiPSC-CM. These studies have technical shortcomings including indels in the genome of the “corrected” PLN line and low replicate numbers (see Introduction; n = 3-4, Stillitano et al. 2016). To further address this issue calcium transient analysis in hiPSC-CM in a 3D EHT format would be a next step to investigate the calcium cycling and calcium kinetics similar to Stoehr et al. (2014). Moreover, it may be that the system needs to be challenged to see differences. Direct measurements of SERCA2a mediated calcium uptake into the SR would be a next step and triggers might be important for these experiments to unmask a difference. Respective experiments are planned in collaboration with a group specialized in the evaluation of calcium handling in cardiomyocytes (Prof. Dr. Antonio Zaza, Milan, Italy).

Previous studies investigated the PKA-mediated PLN-Ser16 phosphorylation upon β -adrenergic stimulation and PLN inhibitory effects on SERCA2a (Haghighi et al. 2006; Haghighi et al. 2012; Ceholski et al. 2012b). These publications suggested reduced Ser16 phosphorylation in PLN protein, likely due to the deletion of the alkaline amino acid Arg14. This positively charged amino acid is part of the consensus sequence for PKA-mediated Ser16 phosphorylation. In consequence a removal of the positive charge due to the mutation could decrease the addition of the negative charge of the phosphate residue (Ceholski et al. 2012b). Based on this it was expected that PLN p.Arg14del EHTs would show lower responses to isoprenaline than PLNic EHTs. But unexpectedly, both EHT lines showed a positive inotropic and lusitropic effect of similar extent as well as the same antagonism by carbachol (Figure 57). This result was supported by western blot analysis (Figure 63). In fact, the isoprenaline-induced increase in PLN Ser16 phosphorylation was even higher in PLN p.Arg14del EHTs (+392%) than in PLNic EHTs (+90%). The PLN p.Arg14del EHTs seemed to be more sensitive to the β -adrenergic stimulation than the PLNic EHTs.

Overall these data directly evaluating the proposed mechanism of PLN p.Arg14del (calcium transient, western blot) are not in line with the super-inhibitor hypothesis, while secondary less specific read-outs (calcium concentration response curve, contractile phenotype) are in

concordance with the hypothesis of disease mechanism. To better characterize the model molecular and histological analysis of 2D and 3D hiPSC-CM were also investigated.

5.4.2 Investigation of possible pathological pathways based on the analysis of histological and molecular markers in PLN^{ic} and PLN p.Arg14del hiPSC-CMs

Other studies also focused on the impact of the arginine deletion on the PLN structure and function. It was assumed that the deletion of the basic amino acid arginine within the cytoplasmic domain could destabilise the membrane-associated state of PLN due to an enhanced disordered cytosolic protein domain which was assumed to orient further away from the SR membrane (Hughes and Middleton 2014; Vostrikov et al. 2015). Another study suggested an increased hydrophobic imbalance caused by the deletion of the charged amino acid which influences the inhibitory function and PLN regulation by phosphorylation reactions (Ceholski et al. 2012a). Additionally, based on heterologous expression studies in HEK293 cells and immunoblot analysis it was shown that the PLN pentamer was destabilized due to the deletion of the amino acid residue. This would shift the monomer:pentamer equilibrium towards the active monomeric PLN form and would also favour SERCA2a inhibition (Haghighi et al. 2006). This study also stated that PLN antibodies recognizing Arg14 within their target epitope were not able to detect the PLN p.Arg14del mutants. For this reason, we used a PLN total antibody that targets amino acid residues 1-11. Western blot analysis in the course of this thesis did not verify the PLN pentamer destabilization reported in the study of Haghighi et al. (2006). Thus, we found no evidence for a higher abundance of PLN monomers in PLN p.Arg14del, again arguing against super-inhibitory action of this mutated protein.

On the other hand, the total level of PLN protein (both monomer and pentamer) was 50% lower in PLN p.Arg14del EHTs than in PLN^{ic} EHTs or a human non failing heart sample (Figure 62). This was surprising since total PLN relative transcript levels of PLN^{ic} #15 and PLN p.Arg14del EHTs did not differ in NanoString and RT-qPCR analyses. Also, an allele-specific expression ratio of 50:50 between wildtype and mutated mRNA in PLN p.Arg14del EHTs (Figures 60 and 61) verified that the mutated allele is expressed at a similar concentration. Interestingly, this 50:50 ratio of wildtype and mutated mRNA was also found in PLN p.Arg14del patient samples (Figure 61).

It is unclear at present whether the reduced amount of total PLN contributes to the observed phenotype. PLN ablation was beneficial in mouse heart failure models, but this was not true for patients which was shown in the study of Haghighi et al. (2003). The homozygous PLN p.Leu39stop mutation was identified as a naturally occurring loss-of-function mutation in patients developing severe DCM and demanding heart transplantation at early age. PLN mRNA levels were diminished and no PLN protein could be detected in one explanted

patient heart. This supports on the one hand that mice models are not suitable to study especially PLN mutations and on the other hand that PLN protein reduction could contribute to the development of DCM.

Reduced PLN protein levels in the presence of normal PLN relative transcript levels argue for an instability of the mutated protein. Unfortunately, we were not able to analyse the wildtype and mutated protein specifically, yet, but it seems very likely that the total reduction was mainly or exclusively due to less mutated PLN. Similar results are known from other causes of cardiomyopathies such as HCM on the basis of mutations in cardiac myosin binding protein C (Vignier et al. 2009). A reduction of the mutated PLN levels could explain why no pentamer destabilization was found in our immunoblot experiments.

The suggested instability could be a result of an increased PLN protein degradation. In PLN p.Arg14del carriers phospholamban aggregates were identified in explanted hearts or autopsies. In immunohistochemical evaluations of the heart samples large perinuclear aggregates of PLN proteins were detected (te Rijdt et al. 2016; te Rijdt et al. 2017). Interestingly, PLN aggregates co-localized with the autophagy marker proteins p62 and LC3 exclusively in PLN p.Arg14del carriers. The aggresome formation supported the assumption of the activation of selective autophagy in PLN p.Arg14del cardiomyopathy (te Rijdt et al. 2016). Based on this data, PLNic #15 and PLN p.Arg14del EHTs were screened for the autophagy marker p62, LC3-II and LAMP2 with immunoblot analysis (Figure 64). No difference in p62 levels were detected, but LC3-II (2-fold) and LAMP2 (3-fold) protein levels were upregulated in the PLN mutated EHTs, supporting the hypothesis of an increased autophagic flux. This upregulation of autophagy marker levels could thereby explain the reduced PLN protein levels in the PLN mutated EHTs. But in contrast to the studies of te Rijdt et al. (2016, 2017), no PLN aggregate formation was observed in PLN p.Arg14del PLN-stained EHT sections (Figures 65 and 66). Questionable is whether the IHC method is suitable to detect PLN aggregates since this method includes an amplification of signal intensity based on enzymatic reactions which could cause a contortion of the result. Also no positive control was available to validate and verify aggregate abundance.

To further evaluate this immunofluorescence staining of monolayer hiPSC-CM was investigated. In former studies a polarized PLN distribution in the cytosol was detected only in PLN p.Arg14del hiPSC-CM in monolayer and three-dimensional cardiac tissue format (Karakikes et al. 2015; Stillitano et al. 2016). Neither a PLN polarization nor PLN aggregates (te Rijdt et al. 2016) were detected in the monolayer PLN p.Arg14del hiPSC-CM in this study (Figures 70 and 71). In conclusion, the important difference between PLN p.Arg14del and PLNic hiPSCs-CM was not related to any specific staining pattern but rather to an unspecific overall weaker staining intensity for all cardiomyocyte markers in PLN p.Arg14del versus

PLN^{Nic}. This observation matched the immunoblot results in which PLN p.Arg14del EHTs showed a 50% reduced PLN total signal (Figure 62). Additionally, it was striking that the PLN detection signal was not only localized within cytosol but also in the perinuclear region. The cell nuclei appeared to be PLN positive and co-localized with the nuclear staining. In accordance to this a recent study of Wu et al. (2016) identified elevated PLN levels in the nuclear envelope of cardiomyocytes probably playing a role in perinuclear/nuclear calcium handling and modulating nuclear calcium dynamics regulating i. a. gene expression. Whether the mutation would have an impact on the nuclear calcium handling would be interesting to analyse in future investigations. SERCA2a co-localized as expected with PLN and showed a cytoplasmic localization but without cross-striation (Figure 71). In addition, the cardiomyocytes showed a normal ACTN2 staining with sarcomere organisation (Figure 70).

To investigate hiPSC-CM cell sizes in the EHT cross sections of PLN^{Nic} and PLN p.Arg14del, EHTs were stained for dystrophin, a critical member of the sarcoglycan dystrophin complex. This is commonly used in our laboratory as a well-defined membrane delineation similar to the study of Hirt et al. (2012) investigating cell sizes in rat EHT cross sections. Surprisingly, dystrophin staining did not reveal a clear membrane staining in PLN p.Arg14del EHTs, while a typical pattern was observed in PLN^{Nic} (Figures 67 and 68). In a study of myocardial ischemia/reperfusion (IR) injury in isolated rat hearts, the CaMKII effect on membrane skeleton proteins such as dystrophin was investigated and their damage causing the IR injury. It was suggested that CaMKII activated calpain which consecutively induced a destructive downstream mechanism damaging membrane skeleton proteins (Kong et al. 2017). CaMKII also gets activated upon increased cytosolic calcium levels.

In line with the proposed mechanism for PLN p.Arg14del a previous study of Liu et al. (2015) analysed the PLN p.Arg25Cys mutation and also suggested a super-inhibitory function. The overexpression of the PLN p.Arg25Cys mutant in adult ventricular rat cardiomyocytes revealed a depression of contractility, systolic calcium transients and SR calcium re-uptake. The increased diastolic calcium level was assumed to activate CaMKII, which phosphorylated the RyR2 (Ser2814) and thereby provoked an elevated calcium leakage from the SR. This in turn activated the NCX, triggering aftercontractions (Liu et al. 2015; Wagner et al. 2015). Interestingly, also the clinical findings (DCM phenotype with ventricular arrhythmia) were in concordance with the reports on PLN p.Arg14del carriers.

Even though we did not find evidence for the super-inhibitory function of the PLN p.Arg14del mutant but indication for calcium cycling disturbances (IBP induction at high calcium levels) the dystrophin disorganization phenotype could be another indicator for altered calcium cycling properties. Based on the findings of Liu et al. (2015) and Kong et al. (2017) it could be hypothesized that upon increased cytosolic calcium levels due to the PLN p.Arg14del

mutation proteases such as calpain get activated via the calcium-overload induced CaMKII pathway. The calpain-mediated digestion of dystrophin would then represent a phenotype in EHTs. The destruction of membrane skeleton proteins and induction of other pathways such as apoptosis could contribute to the development and pathogenesis of DCM since dystrophin mutations and dysfunction were also associated with the DCM phenotype (Feng et al. 2002).

In summary, the suggested PLN p.Arg14del super-inhibitory function remains not uniformly supported in this study. Thereby the following question arises: How was the super-inhibitory function evaluated in former publications? The key publication of Haghighi et al. (2006) based their statement on experiments in the HEK293 cell system overexpressing PLN wildtype and PLN p.Arg14del. The pentamer destabilization was identified and microsome preparations out of these cells which were additionally transfected with Serca1 revealed the suggested super-inhibitory function of the PLN mutant which could not be fully relieved via PKA-mediated phosphorylation. In addition, this study investigated a heterozygous transgenic mouse model with cardiac specific PLN p.Arg14del overexpression. Explanted mice hearts showed similar phenotypes compared to human hearts including interstitial fibrosis, heart size increase and ventricular dilation. A SR calcium uptake assay in these mice suggested an increased EC₅₀ value for calcium (0.471 μ M, n = 1) compared to wildtype mice (0.326 \pm 0.013 μ M, n = 3) also concluding a PLN mutation-mediated super-inhibition of Serca2a. Ceholski et al. (2012b) stated that the PKA recognition motif is changed due to the Arg14 deletion and found that the mutant was not phosphorylated by PKA in proteoliposome preparations prepared with Serca1 isoform derived from rabbits and human recombinant PLN. The very first humanized study was performed by Karakikes et al. (2015) in hiPSC-derived cardiomyocytes in comparison to TALEN-generated isogenic controls. They identified calcium cycling abnormalities but the detected larger caffeine response in PLN p.Arg14del hiPSC-CM contradicts the suggested super-inhibitory PLN effect. No further direct solid evidence for the PLN super-inhibitory hypothesis was identified in human cells so far. The presented results are always discussed in conjunction with the suggested super-inhibitory PLN mutant function identified in HEK cells or microsome/proteoliposome preparations or mice models. So the applied non-human cardiac systems could be too far away from the complex situation, biology and pathophysiology of the human heart tissue. The need of a human model is thereby inevitable to analyse pathological pathways and changes in human cardiomyocytes taking the human cardiomyocyte cellular environment into account to finally nail down the role of the PLN p.Arg14del mutation.

6 FUTURE PERSPECTIVES

With the establishment of the PLN 3D EHT *in vitro* disease modelling platform within this study phenotypic and molecular differences between diseased cardiomyocytes and their isogenic control were identified suggesting a possible haploinsufficiency of the PLN p.Arg14del mutant. This model opens the possibility to monitor the early disease-defining mechanisms in a human model. This was not possible before since heart samples from patients at early time points of the disease development are not available.

Further investigations are needed to evaluate and improve the mechanistic understanding of the PLN p.Arg14del hiPSC-CM phenotype. To achieve this, experiments should be repeated for the PLNic EHTs to further confirm the stated data and additional clones of the PLNic (#28) and PLN p.Arg14del (#1201) hiPSC should be used to further verify the disease-specific phenotype.

The analysis of gene expression (Affymetrix arrays) and proteome profiles of the EHTs could help to identify patterns of difference in expression. Besides, this could be extended by overexpressing PLN wildtype and p.Arg14del constructs with an attached FLAG-tag. The FLAG-tag would be helpful to perform co-immunoprecipitation experiments to identify binding partners. Based on the study of Haghghi et al. (2012) it was found that the PLN p.Arg14del mutant delocalized to the plasma membrane interacting with the Na⁺/K⁺-ATPase when expressed homozygous in a PLN-null background mice model. It would be interesting to analyse interaction partners of the PLN p.Arg14del mutant in the hiPSC-CM as well as the localization of the mutated protein by detecting the FLAG-tagged PLN protein. This would be also useful for the detection of the PLN mutant distribution within histological analysis and immunofluorescence staining.

In addition, protocols performed in 2D should be transferred to the EHT model. Calcium transients should be analysed to see whether a lack of difference of calcium transients depends on the culture format. This technology was recently established in our laboratory and is based on lentiviral-mediated overexpression of a genetically encoded calcium sensor (GCaMP6f). Based on a higher maturity status and tissue structure calcium cycling properties and protein distribution (immunofluorescence staining) within the cell could be further clarified and significantly described.

To further address the evaluation of possible pathological molecular mechanisms the analysis of autophagy-related pathways should be in closer focus as well as evaluating the hypothesis of a possible activation of calcium-sensitive protease (e. g. calpain) due to the suggested increased cytosolic calcium level. This suggestion was based on the dystrophin staining in EHT cross section showing the tendency of disorganization. To validate this, other

membrane skeleton-associated proteins (spectrin, F-actin) should be validated concerning their localization (immunohistochemistry, immunofluorescence) and structural integrity by western blot. The suggested calpain-digestion could be further validated by applying pharmacological inhibitors of calcium-sensitive proteases and by performing immunoblot analyses.

As another proof of principle a gene-therapeutic approach should be investigated. It would be interesting to confirm that by specifically knocking down the mutated PLN mRNA the observed phenotype would be reversed similar to the CRISPR/Cas9-generated PLN^{ic} EHTs. Within the study of Karakikes et al. (2015) a miRNA-mediated PLN gene silencing was investigated to knock down endogenous PLN together with an overexpression of a codon-optimized PLN which cannot be targeted by the miRNA but an allele-specific knock-down was not proven. Besides, overexpression of wildtype PLN could also influence cardiac physiology since PLN expression levels cannot be closely regulated. In the study of Karakikes et al. (2015) endogenous PLN levels decreased probably due to a negative feedback response but still, PLN total transcript levels were strongly elevated (16-fold higher) in the hiPSC-CM in comparison to untransduced cells. However, a specific repression of the assumed dominant-negative and toxic mutant allele could alleviate the disease severity in PLN p.Arg14del carriers. PLN p.Arg14del allele-specific short hairpin (sh) RNA-mediated gene silencing would be a suitable approach, also for *in vivo* applications in the future. Suitable siRNAs should be designed to specifically recognize the mutated mRNA to induce its degradation without affecting the wildtype and healthy mRNA (Hohjoh 2013). It has to be investigated to which extent this gene silencing efficiently restores the phenotypes towards the wildtype.

7 **SUMMARY**

Phospholamban is an important transmembrane SR protein regulating the calcium homeostasis of the cardiomyocyte by modulating SERCA2a activity. Thus, it has a central role in excitation and contraction coupling. In 2006 a novel PLN mutation, the deletion of the 14th codon AGA encoding for Arg14 (PLN c.40-42AGAdel; p.Arg14del), was identified in families with an inherited form of DCM. It is an autosomal dominant disorder most common in the Netherlands. It is assumed that this mutant has a super-inhibitory function, thereby suppressing the calcium re-entry into the SR and causing impaired calcium cycling as well as increased diastolic calcium levels. Most findings are based on familial genetics, biochemical data or transgenic mice models. But as calcium cycling mechanism differ substantially between mice and human the aim was to establish a human *in vitro* model for the PLN p.Arg14del mutation with disease-specific human induced pluripotent stem cell-derived cardiomyocytes (hiPSC-CM) and CRISPR/Cas9-generated isogenic controls. Force-generating, three-dimensional engineered heart tissues (EHT) were used to define a disease-specific contractility pattern and to identify potential molecular pathological pathways.

Patient-derived skin fibroblasts with a heterozygous PLN p.Arg14del were reprogrammed to hiPSC. By CRISPR/Cas9 technology isogenic controls (PLNic) were generated by homology-directed repair using both DNA- and ribonucleoprotein-based CRISPR approaches. Seamless gene-corrected PLNic showed no off-targets and a normal karyotype. The PLN p.Arg14del and PLNic hiPSC lines were successfully differentiated into beating cardiomyocytes with an embryoid body, growth factor-based three-stage protocol. The hiPSC-CM were dissociated for the generation of EHTs which are fibrin based, spontaneously beating, force generating strip format muscle strips casted between pairs of silicone posts in a 24-well format. By video-optical recording system contractile parameters were investigated for functional analysis.

Electrically paced PLN p.Arg14del EHTs developed significantly lower peak force than isogenic control EHTs with shorter contraction time but similar relaxation time. Besides, PLN p.Arg14del-EHTs were less sensitive to extracellular calcium concentrations and showed time- and concentration-dependent arrhythmias. On the molecular basis, PLN protein levels were reduced by 50% compared to PLNic EHTs, but with similar PLN relative transcript levels between the two lines. In PLN p.Arg14del carriers a 50:50 ratio of PLN wildtype to PLN mutated mRNA level was identified. PLN p.Arg14del EHTs showed a marked increase in protein levels of autophagy markers and histological evidence for disorganization of the membrane skeleton protein dystrophin. However, calcium transient (caffeine puff) and western blot experiments do not provide evidence for the most accepted hypothesis of a

super-inhibitory PLN p.Arg14del monomer due to destabilization of the pentameric form or reduced PLN-Ser16 phosphorylation.

In summary, EHTs from PLN p.Arg14del-mutation carriers showed a robust contractile and arrhythmic phenotype which was absent in isogenic, CRISPR-corrected controls. Overall, with this model a promising human disease modelling platform for further investigations was established to unravel the pathogenesis of the PLN p.Arg14del mutation.

8 ZUSAMMENFASSUNG

Phospholamban ist ein wichtiges transmembranäres SR-Protein für die Regulation der Kalziumhomöostase in der Kardiomyozyte, indem es die SERCA2a-Aktivität moduliert. Es hat demnach eine zentrale Rolle für die Erregungs-Kontraktions-Kopplung. Im Jahre 2006 wurde eine bisher unbekannte PLN Mutation in Familien mit vererbter dilatativer Kardiomyopathieform identifiziert, bei der das 14. Kodon AGA, welches für Arg14 codiert (PLN c.40-42AGAdel; p.Arg14del), deletiert ist. Diese autosomal dominante Erkrankung kommt verstärkt in den Niederlanden vor. Es wird vermutet, dass diese Mutante eine superinhibitorische Funktion aufweist, wodurch die Kalzium-Rückaufnahme in das SR vermindert, der Kalziumzyklus in der Zelle gestört und das diastolische Kalziumlevel erhöht wird. Die meisten Ergebnisse basieren auf familiären genetischen Analysen, biochemischen Daten oder transgenen Mausmodellen. Da sich jedoch die Kalziumzykluseigenschaften grundlegend zwischen Maus und Mensch unterscheiden, war es Ziel dieser Arbeit, ein humanes *in vitro* Modell für die PLN p.Arg14del Mutation zu etablieren mit Hilfe von krankheits-spezifischen humanen induziert-pluripotenten Stammzellen (hiPSZ) sowie CRISPR/Cas9-generierten isogenen Kontrollen. Kraft-generierende, 3-dimensionale künstliche Herzgewebe (EHT) wurden verwendet, um krankheitsspezifische Kontraktilitätsmuster zu definieren sowie potentielle molekulare pathologische Wege zu identifizieren.

Die aus Patienten isolierten Hautfibroblasten mit einer heterozygoten PLN p.Arg14del Mutation wurden zu hiPSZ reprogrammiert. Mit Hilfe der CRISPR/Cas9-Technologie wurden HDR-vermittelt isogene Kontrollen (PLNic) generiert über den DNA- sowie auch den Ribonukleoprotein-basierten CRISPR-Ansatz. Die PLNic zeigten eine fehlerfreie Korrektur des PLN-Genes, keine „off-target“-Effekte sowie einen gesunden Karyotyp. Die PLN p.Arg14del und PLNic hiPS-Zelllinien wurden unter Verwendung eines Embryoidkörperchen- und Wachstumsfaktoren-basierenden dreistufigen Protokolls erfolgreich zu kontrahierenden Kardiomyozyten differenziert. Die Kardiomyozyten wurden dissoziiert, um EHTs zu produzieren. Dies sind Fibrin-basierte, spontan kontrahierende und kraftgenerierende kleine Muskelstreifen, die zwischen zwei flexiblen Silikonbeinchen im 24-Well Format hergestellt werden. Mit Hilfe eines videooptischen Aufnahmesystems wurden Kontraktilitätsparameter zur funktionellen Analyse untersucht.

Elektrisch stimulierte PLN p.Arg14del EHTs generierten signifikant geringere Kräfte und zeigten eine verkürzte Kontraktions- aber ähnliche Relaxationszeit im Vergleich zu den isogenen Kontrollen. Außerdem wiesen die PLN p.Arg14del EHTs eine geringere Sensitivität gegenüber extrazellulärer Kalziumkonzentrationen auf sowie eine zeit- und kalziumkonzentrationsabhängige Steigerung arrhythmischer Episoden. Auf molekularer

Ebene wurden um die Hälfte reduzierte PLN Proteinlevel detektiert verglichen zu PLN^{ic} EHTs. Dabei zeigten beide Zelllinien aber ähnliche relative PLN-Transkriptlevel. In PLN p.Arg14del Kardiomyozyten wurde ein 50:50 Verhältnis der PLN Wildtyp mRNA zur PLN Mutante detektiert. Darüber hinaus waren die Autophagiemarkerlevel in den PLN p.Arg14del EHTs stark erhöht. Nicht nur auf molekularer, sondern auch auf struktureller Ebene fanden sich Unterschiede. In EHT-Querschnitten erschien das Membranskelettprotein Dystrophin desorganisiert. Dennoch lieferten Kalziumtransienten (Koffein-Bolus) und Western Blot-Experimente keinen Beweis für die am stärksten akzeptierte Hypothese eines superinhibitorischen PLN p.Arg14del Monomers aufgrund einer Pentamerdestabilisierung oder reduzierten PLN-Ser16 Phosphorylierung.

Zusammenfassend zeigte sich in den PLN p.Arg14del EHTs ein robuster kontraktiler sowie arrhythmischer Phänotyp, der in den isogenen, CRISPR-korrigierten Kontrollen nicht detektiert wurde. Insgesamt wurde mit diesem Modell ein vielversprechendes humanes Krankheitsmodelsystem als Basis für weitere Untersuchungen etabliert, um die Pathogenese der PLN p.Arg14del Mutation zu enthüllen.

9 **BIBLIOGRAPHY**

- Aasen T, Raya A, Barrero MJ, et al. (2008) Efficient and rapid generation of induced pluripotent stem cells from human keratinocytes. *Nat Biotechnol* 26:1276–1284. doi: 10.1038/nbt.1503
- Amps K, Andrews PW, Anyfantis G, et al. (2011) Screening ethnically diverse human embryonic stem cells identifies a chromosome 20 minimal amplicon conferring growth advantage. *Nat Biotechnol* 29:1132–1144. doi: 10.1038/nbt.2051
- Andersson DC, Marks AR (2010) Fixing ryanodine receptor Ca leak - a novel therapeutic strategy for contractile failure in heart and skeletal muscle. *Drug Discov Today Dis Mech* 7:e151–e157. doi: 10.1016/j.ddmec.2010.09.009
- Arai M, Alpert NR, MacLennan DH, et al. (1993) Alterations in sarcoplasmic reticulum gene expression in human heart failure. A possible mechanism for alterations in systolic and diastolic properties of the failing myocardium. *Circ Res* 72:463–469. doi: 10.1161/01.RES.72.2.463
- Asahi M, Mckenna E, Kurzydowski K, et al. (2000) Physical Interactions between Phospholamban and Sarco(endo)plasmic Reticulum Ca²⁺-ATPases Are Dissociated by Elevated Ca²⁺, but Not by Phospholamban Phosphorylation, Vanadate, or Thapsigargin, and Are Enhanced by ATP. *J Biol Chem* 275:15034–15038.
- Avery S, Hirst AJ, Baker D, et al. (2013) BCL-XL mediates the strong selective advantage of a 20q11.21 amplification commonly found in human embryonic stem cell cultures. *Stem Cell Reports* 1:379–386. doi: 10.1016/j.stemcr.2013.10.005
- Bassett AR, Liu J-L (2014) CRISPR/Cas9 and Genome Editing in *Drosophila*. *J Genet Genomics* 41:7–19. doi: 10.1016/j.jgg.2013.12.004
- Bedada FB, Wheelwright M, Metzger JM (2016) Maturation status of sarcomere structure and function in human iPSC-derived cardiac myocytes. *Biochim Biophys Acta - Mol Cell Res* 1863:1829–1838. doi: 10.1016/j.bbamcr.2015.11.005
- Beqqali A, Kloots J, Ward-van Oostwaard D, et al. (2006) Genome-wide transcriptional profiling of human embryonic stem cells differentiating to cardiomyocytes. *Stem Cells* 24:1956–67. doi: 10.1634/stemcells.2006-0054
- Bers DM (2002) Cardiac excitation–contraction coupling. *Nature* 415:198–205.
- Breckwoldt K, Letuffe-Brenière D, Mannhardt I, et al. (2017) Differentiation of cardiomyocytes and generation of human engineered heart tissue. *Nat Protoc* 12:1177–1197. doi: 10.1038/nprot.2017.033
- Brillantes AMB, Ondrias K, Scott A, et al. (1994) Stabilization of calcium release channel (ryanodine receptor) function by FK506-binding protein. *Cell* 77:513–523. doi: 10.1016/0092-8674(94)90214-3
- Burridge PW, Keller G, Gold JD, Wu JC (2012) Production of de novo cardiomyocytes:

- Human pluripotent stem cell differentiation and direct reprogramming. *Cell Stem Cell* 10:16–28. doi: 10.1016/j.stem.2011.12.013
- Byrne SM, Ortiz L, Mali P, et al. (2014) Multi-kilobase homozygous targeted gene replacement in human induced pluripotent stem cells. *Nucleic Acids Res* 43:e21–e21. doi: 10.1093/nar/gku1246
- Cahill TJ, Ashrafian H, Watkins H (2013) Genetic cardiomyopathies causing heart failure. *Circ Res* 113:660–75. doi: 10.1161/CIRCRESAHA.113.300282
- Cantilina T, Sagara Y, Inesi G, Jones LR (1993) Comparative studies of cardiac and skeletal sarcoplasmic reticulum ATPases: Effect of a phospholamban antibody on enzyme activation by Ca²⁺. *J Biol Chem* 268:17018–17025.
- Cao F, Wagner RA, Wilson KD, et al. (2008) Transcriptional and functional profiling of human embryonic stem cell-derived cardiomyocytes. *PLoS One* 3:e3474, NaN-12. doi: 10.1371/journal.pone.0003474
- Carvajal-Vergara X, Sevilla A, D'Souza SL, et al. (2010) Patient-specific induced pluripotent stem-cell-derived models of LEOPARD syndrome. *Nature* 465:808–812. doi: nature09005 [pii]r10.1038/nature09005
- Ceholski DK, Trieber C a, Young HS (2012a) Hydrophobic imbalance in the cytoplasmic domain of phospholamban is a determinant for lethal dilated cardiomyopathy. *J Biol Chem* 287:16521–9. doi: 10.1074/jbc.M112.360859
- Ceholski DK, Trieber CA, Holmes CFB, Young HS (2012b) Lethal, hereditary mutants of phospholamban elude phosphorylation by protein kinase A. *J Biol Chem* 287:26596–605. doi: 10.1074/jbc.M112.382713
- Chen L, El-Sherif N, Boutjdir M (1999) Unitary current analysis of L-type Ca²⁺ channels in human fetal ventricular myocytes. *J Cardiovasc Electrophysiol* 10:692–700.
- Cho SW, Kim S, Kim J-SJM, Kim J-SJM (2013) Targeted genome engineering in human cells with the Cas9 RNA-guided endonuclease. *Nat Biotechnol* 31:230–2. doi: 10.1038/nbt.2507
- Chu VT, Weber T, Wefers B, et al. (2015) Increasing the efficiency of homology-directed repair for CRISPR-Cas9-induced precise gene editing in mammalian cells. *Nat Biotechnol* 33:543–8. doi: 10.1038/nbt.3198
- Chung JH, Biesiadecki BJ, Ziolo MT, et al. (2016) Myofilament calcium sensitivity: Role in regulation of in vivo cardiac contraction and relaxation. *Front Physiol* 7:1–9. doi: 10.3389/fphys.2016.00562
- Cong L, Ran FA, Cox D, et al. (2013) Multiplex Genome Engineering Using CRISPR/Cas Systems. *Science* (80-) 339:819–824.
- Cradick TJ, Fine EJ, Antico CJ, Bao G (2013) CRISPR/Cas9 systems targeting β -globin and CCR5 genes have substantial off-target activity. *Nucleic Acids Res* 41:9584–9592. doi:

10.1093/nar/gkt714

- Davis RP, van den Berg CW, Casini S, et al. (2011) Pluripotent stem cell models of cardiac disease and their implication for drug discovery and development. *Trends Mol Med* 17:475–484. doi: 10.1016/j.molmed.2011.05.001
- Dekel-Naftali M, Aviram-Goldring A, Litmanovitch T, et al. (2012) Screening of human pluripotent stem cells using CGH and FISH reveals low-grade mosaic aneuploidy and a recurrent amplification of chromosome 1q. *Eur J Hum Genet* 20:1248–1255. doi: 10.1038/ejhg.2012.128
- Deltcheva E, Chylinski K, Sharma CM, et al. (2011) CRISPR RNA maturation by trans-encoded small RNA and host factor RNase III. *Nature* 471:602–607. doi: 10.1038/nature09886
- Denning C, Borgdorff V, Crutchley J, et al. (2015) Cardiomyocytes from human pluripotent stem cells: From laboratory curiosity to industrial biomedical platform. *Biochim Biophys Acta - Mol Cell Res* 1863:1728–1748. doi: <http://dx.doi.org/10.1016/j.bbamcr.2015.10.014>
- Desbaillets I, Ziegler U, Groscurth P, Gassmann M (2000) Embryoid bodies: an in vitro model of mouse embryogenesis. *Exp Physiol* 85:645–651. doi: 10.1263/jbb.103.389
- Eder A, Vollert I, Hansen A, Eschenhagen T (2016) Human engineered heart tissue as a model system for drug testing. *Adv Drug Deliv Rev* 96:214–224. doi: 10.1016/j.addr.2015.05.010
- Eisner D (2014) Calcium in the heart: from physiology to disease. *Exp Physiol* 99:1273–82. doi: 10.1113/expphysiol.2013.077305
- Eschenhagen T, Eder A, Vollert I, Hansen A (2012) Physiological aspects of cardiac tissue engineering. *Am J Physiol Heart Circ Physiol* 303:H133–43. doi: 10.1152/ajpheart.00007.2012
- Eschenhagen T, Fink C, Remmers U, et al. (1997) Three-dimensional reconstitution of embryonic cardiomyocytes in a collagen matrix: a new heart muscle model system. *FASEB J* 11:683–694.
- Eschenhagen T, Forth W, Henschler D, Rummel W (2013) *Pharmakologie des kardiovaskulären Systems - das Herz. Allg. und Spez. Pharmakologie und Toxikologie* (11. Auflage). Elsevier, pp 381–435
- Eschenhagen T, Mummery C, Knollmann BC (2015) Modelling sarcomeric cardiomyopathies in the dish: From human heart samples to iPSC cardiomyocytes. *Cardiovasc Res* 105:424–438. doi: 10.1093/cvr/cvv017
- Evans MJ, Kaufman MH (1981) Establishment in culture of pluripotential cells from mouse embryos. *Nature* 292:154–156. doi: 10.1038/292154a0
- Fazeli A, Liew CG, Matin MM, et al. (2011) Altered patterns of differentiation in karyotypically

- abnormal human embryonic stem cells. *Int J Dev Biol* 55:175–180. doi: 10.1387/ijdb.103177af
- Feng J, Yan J, Buzin CH, et al. (2002) Mutations in the dystrophin gene are associated with sporadic dilated cardiomyopathy. *Mol Genet Metab* 77:119–126. doi: 10.1016/S1096-7192(02)00153-1
- Forster R, Chiba K, Schaeffer L, et al. (2014) Human intestinal tissue with adult stem cell properties derived from pluripotent stem cells. *Stem Cell Reports* 2:838–852. doi: 10.1016/j.stemcr.2014.05.001
- Frank S, Zhang M, Schöler HR, Greber B (2012) Small molecule-assisted, line-independent maintenance of human pluripotent stem cells in defined conditions. *PLoS One* 7:e41958. doi: 10.1371/journal.pone.0041958
- Freeman K, Lerman I, Kranias EG, et al. (2001) Alterations in cardiac adrenergic signaling and calcium cycling differentially affect the progression of cardiomyopathy. *J Clin Invest* 107:967–974. doi: 10.1172/JCI12083
- Fu Y, Foden JA, Khayter C, et al. (2013) High-frequency off-target mutagenesis induced by CRISPR-Cas nucleases in human cells. *Nat Biotechnol* 31:822–826. doi: 10.1038/nbt.2623
- Fusaki N, Ban H, Nishiyama A, et al. (2009) Efficient induction of transgene-free human pluripotent stem cells using a vector based on Sendai virus, an RNA virus that does not integrate into the host genome. *Proc Japan Acad Ser B* 85:348–362. doi: 10.2183/pjab.85.348
- Gabriel R, Lombardo A, Arens A, et al. (2011) An unbiased genome-wide analysis of zinc-finger nuclease specificity. *Nat Biotechnol* 29:816–823. doi: 10.1038/nbt.1948
- Garneau JE, Dupuis ME, Villion M, et al. (2010) The CRISPR/Cas bacterial immune system cleaves bacteriophage and plasmid DNA. *Nature* 468:67–71. doi: 10.1038/nature09523
- Gasiunas G, Barrangou R, Horvath P, Siksnys V (2012) Cas9-crRNA ribonucleoprotein complex mediates specific DNA cleavage for adaptive immunity in bacteria. *Proc Natl Acad Sci U S A* 109:E2579-86. doi: 10.1073/pnas.1208507109
- Geisterfer-Lowrance A a. T, Kass S, Tanigawa G, et al. (1990) A molecular basis for familial hypertrophic cardiomyopathy: A β cardiac myosin heavy chain gene missense mutation. *Cell* 62:999–1006. doi: 10.1016/0092-8674(90)90274-I
- Gopalakrishna-Pillai S, Iverson LE (2010) Astrocytes derived from trisomic human embryonic stem cells express markers of astrocytic cancer cells and premalignant stem-like progenitors. *BMC Med Genomics* 3:12. doi: 10.1186/1755-8794-3-12
- Gorski PAA, Ceholski DKK, Hajjar RJJ (2015) Altered Myocardial Calcium Cycling and Energetics in Heart Failure—A Rational Approach for Disease Treatment. *Cell Metab* 21:183–194. doi: 10.1016/j.cmet.2015.01.005

- Haase A, Olmer R, Schwanke K, et al. (2009) Generation of Induced Pluripotent Stem Cells from Human Cord Blood. *Cell Stem Cell* 5:434–441. doi: 10.1016/j.stem.2009.08.021
- Haghighi K, Kolokathis F, Gramolini AO, et al. (2006) A mutation in the human phospholamban gene, deleting arginine 14, results in lethal, hereditary cardiomyopathy. *Proc Natl Acad Sci U S A* 103:1388–1393.
- Haghighi K, Kolokathis F, Pater L, et al. (2003) Human phospholamban null results in lethal dilated cardiomyopathy revealing a critical difference between mouse and human. *J Clin Invest* 111:869–876. doi: 10.1172/JCI200317892
- Haghighi K, Pritchard T, Bossuyt J, et al. (2012) The human phospholamban Arg14-deletion mutant localizes to plasma membrane and interacts with the Na/K-ATPase. *J Mol Cell Cardiol* 52:773–82. doi: 10.1016/j.yjmcc.2011.11.012
- Haghighi K, Schmidt AG, Hoit BD, et al. (2001) Superinhibition of Sarcoplasmic Reticulum Function by Phospholamban Induces Cardiac Contractile Failure. *J Biol Chem* 276:24145–24152. doi: 10.1074/jbc.M102403200
- Hansen A, Eder A, Bönstrup M, et al. (2010) Development of a drug screening platform based on engineered heart tissue. *Circ Res* 107:35–44. doi: 10.1161/CIRCRESAHA.109.211458
- Harvey P a, Leinwand L a (2011) The cell biology of disease: cellular mechanisms of cardiomyopathy. *J Cell Biol* 194:355–65. doi: 10.1083/jcb.201101100
- Hasenfuss G, Reinecke H, Studer R, et al. (1994) Relation between myocardial function and expression of sarcoplasmic reticulum Ca(2+)-ATPase in failing and nonfailing human myocardium. *Circ Res* 75:434–442. doi: 10.1161/01.RES.75.3.434
- Hasty P, Rivera-Pérez J, Bradley A (1991) The length of homology required for gene targeting in embryonic stem cells. *Mol Cell Biol* 11:5586–5591. doi: 10.1128/MCB.11.11.5586
- van der Heijden JF, Hassink RJ (2013) The phospholamban p.Arg14del founder mutation in Dutch patients with arrhythmogenic cardiomyopathy. *Neth Heart J* 21:284–5. doi: 10.1007/s12471-013-0413-z
- Herold G (2012) *Innere Medizin: Eine vorlesungsorientierte Darstellung; unter Berücksichtigung des Gegenstandskataloges für die Ärztliche Prüfung; mit ICD 10-Schlüssel im Text und Stichwortverzeichnis.* Herold, Köln
- Hinson JT, Chopra A, Nafissi N, et al. (2015) Titin mutations in iPS cells define sarcomere insufficiency as a cause of dilated cardiomyopathy. *Science* (80-) 349:982–986. doi: 10.1126/science.aaa5458
- Hirt MN, Sörensen NA, Bartholdt LM, et al. (2012) Increased afterload induces pathological cardiac hypertrophy: a new in vitro model. *Basic Res Cardiol* 107:307. doi: 10.1007/s00395-012-0307-z

- Hockemeyer D, Jaenisch R (2016) Induced Pluripotent Stem Cells Meet Genome Editing. *Cell Stem Cell* 18:573–586. doi: 10.1016/j.stem.2016.04.013
- Hohjoh H (2013) Disease-causing allele-specific silencing by RNA interference. *Pharmaceuticals* 6:522–535. doi: 10.3390/ph6040522
- Hrvatin S, O'Donnell CW, Deng F, et al. (2014) Differentiated human stem cells resemble fetal, not adult, β cells. *Proc Natl Acad Sci U S A* 111:3038–43. doi: 10.1073/pnas.1400709111
- Hsu PD, Lander ES, Zhang F (2014) Development and applications of CRISPR-Cas9 for genome engineering. *Cell* 157:1262–1278. doi: 10.1016/j.cell.2014.05.010
- Hsu PD, Scott D a, Weinstein J a, et al. (2013) DNA targeting specificity of RNA-guided Cas9 nucleases. *Nat Biotechnol* 31:827–32. doi: 10.1038/nbt.2647
- Huang B, Wang S, Qin D, et al. (1999) Diminished Basal Phosphorylation Level of Phospholamban in the Postinfarction Remodeled Rat Ventricle Role of beta-Adrenergic Pathway, G i Protein, Phosphodiesterase, and Phosphatases. *Circ Res* 85:848–855.
- Hughes E, Middleton DA (2014) Comparison of the structure and function of phospholamban and the arginine-14 deficient mutant associated with dilated cardiomyopathy. *PLoS One* 9:e106746. doi: 10.1371/journal.pone.0106746
- Itskovitz-Eldor J, Schuldiner M, Karsenti D, et al. (2000) Differentiation of human embryonic stem cells into embryoid bodies compromising the three embryonic germ layers. *Mol Med* 6:88–95. doi: 10859025
- Itzhaki I, Maizels L, Huber I, et al. (2011) Modelling the long QT syndrome with induced pluripotent stem cells. *Nature* 471:225–229. doi: 10.1038/nature09747
- Jacobs K, Mertzaniidou A, Geens M, et al. (2014) Low-grade chromosomal mosaicism in human somatic and embryonic stem cell populations. *Nat Commun* 5:4227. doi: 10.1038/ncomms5227
- Jacobs K, Zambelli F, Mertzaniidou A, et al. (2016) Higher-Density Culture in Human Embryonic Stem Cells Results in DNA Damage and Genome Instability. *Stem Cell Reports* 6:330–341. doi: 10.1016/j.stemcr.2016.01.015
- Jiang F, Doudna JA (2017) CRISPR – Cas9 Structures and Mechanisms. *Annu Rev Biophys* 46:505–529.
- Jiang W, Bikard D, Cox D, et al. (2013) RNA-guided editing of bacterial genomes using CRISPR-Cas systems. *Nat Biotechnol* 31:233–9. doi: 10.1038/nbt.2508
- Jinek M, Chylinski K, Fonfara I, et al. (2012) A Programmable Dual-RNA-Guided DNA Endonuclease in Adaptive Bacterial Immunity. *Science* (80-) 337:816–822. doi: 10.1126/science.1225829
- Jinek M, East A, Cheng A, et al. (2013) RNA-programmed genome editing in human cells. *Elife* 2013:331–338. doi: 10.7554/eLife.00471

- Kaebisch C, Schipper D, Babczyk P, Tobiasch E (2015) The role of purinergic receptors in stem cell differentiation. *Comput Struct Biotechnol J* 13:75–84. doi: 10.1016/j.csbj.2014.11.003
- Kaji K, Norrby K, Paca A, et al. (2009) Virus-free induction of pluripotency and subsequent excision of reprogramming factors. *Nature* 458:771–775. doi: 10.1038/nature07864
- Kaneko M, Yamamoto H, Sakai H, et al. (2017) A pyridone derivative activates SERCA2a by attenuating the inhibitory effect of phospholamban. *Eur J Pharmacol* 814:1–8. doi: 10.1016/j.ejphar.2017.07.035
- Karakikes I, Stillitano F, Nonnenmacher M, et al. (2015) Correction of human phospholamban R14del mutation associated with cardiomyopathy using targeted nucleases and combination therapy. *Nat Commun* 6:6955. doi: 10.1038/ncomms7955
- Katz AM (1998) Discovery of phospholamban. A personal history. *Ann N Y Acad Sci* 853:9–19. doi: 10.1007/s13398-014-0173-7.2
- Kho C, Lee A, Hajjar RJ (2012) Altered sarcoplasmic reticulum calcium cycling--targets for heart failure therapy. *Nat Rev Cardiol* 9:717–33. doi: 10.1038/nrcardio.2012.145
- Kim D, Kim CH, Moon J II, et al. (2009) Generation of Human Induced Pluripotent Stem Cells by Direct Delivery of Reprogramming Proteins. *Cell Stem Cell* 4:472–476. doi: 10.1016/j.stem.2009.05.005
- Kim EJ, Kang KH, Ju JH (2017) CRISPR-Cas9: a promising tool for gene editing on induced pluripotent stem cells. *Korean J Intern Med* 32:42–61. doi: 10.3904/kjim.2016.198
- Kim S, Kim D, Cho SW, et al. (2014) Highly efficient RNA-guided genome editing in human cells via delivery of purified Cas9 ribonucleoproteins. *Genome Res* 24:1012–1019. doi: 10.1101/gr.171322.113
- Kimura Y, Kurzydowski K, Tada M, MacLennan DH (1997) Phospholamban Inhibitory Function Is Activated by Depolymerization. *J Biol Chem* 272:15061–15064.
- Kong L-H, Gu X-M, Wu F, et al. (2017) CaMKII inhibition mitigates ischemia/reperfusion-elicited calpain activation and the damage to membrane skeleton proteins in isolated rat hearts. *Biochem Biophys Res Commun* 1–6. doi: 10.1016/j.bbrc.2017.07.128
- Koss KL, Kranias EG (1996) Phospholamban: a prominent regulator of myocardial contractility. *Circ Res* 79:1059–63. doi: 10.1161/01.RES.79.6.1059
- Kurosawa H (2007) Methods for inducing embryoid body formation: in vitro differentiation system of embryonic stem cells. *J Biosci Bioeng* 103:389–398. doi: 10.1263/jbb.103.389
- Laflamme MA, Chen KY, Naumova A V, et al. (2007) Cardiomyocytes derived from human embryonic stem cells in pro-survival factors enhance function of infarcted rat hearts. *Nat Biotechnol* 25:1015–1024. doi: 10.1038/nbt1327
- Lan F, Lee AS, Liang P, et al. (2013) Abnormal calcium handling properties underlie familial hypertrophic cardiomyopathy pathology in patient-specific induced pluripotent stem

- cells. *Cell Stem Cell* 12:101–113. doi: 10.1016/j.stem.2012.10.010
- Lee Y, Lau Y, Cai Z, et al. (2017) Modeling Treatment Response for Lamin A/C Related Dilated Cardiomyopathy in Human Induced Pluripotent Stem Cells. *J Am Heart Assoc* 6:e005677. doi: 10.1161/JAHA.117.005677
- Lehnart SE, Mongillo M, Bellinger A, et al. (2008) Leaky Ca²⁺ release channel/ryanodine receptor 2 causes seizures and sudden cardiac death in mice. *J Clin Invest* 118:2230–2245. doi: 10.1172/JCI35346
- Lehnart SE, Terrenoire C, Reiken S, et al. (2006) Stabilization of cardiac ryanodine receptor prevents intracellular calcium leak and arrhythmias. *Proc Natl Acad Sci U S A* 103:7906–7910. doi: 10.1073/pnas.0602133103
- Lemoine MD, Mannhardt I, Breckwoldt K, et al. (2017) Human iPSC-derived cardiomyocytes cultured in 3D engineered heart tissue show physiological upstroke velocity and sodium current density. *Sci Rep* 7:1–11. doi: 10.1038/s41598-017-05600-w
- Li HL, Fujimoto N, Sasakawa N, et al. (2015) Precise correction of the dystrophin gene in duchenne muscular dystrophy patient induced pluripotent stem cells by TALEN and CRISPR-Cas9. *Stem Cell Reports* 4:143–154. doi: 10.1016/j.stemcr.2014.10.013
- Liang X, Potter J, Kumar S, et al. (2015) Rapid and highly efficient mammalian cell engineering via Cas9 protein transfection. *J Biotechnol* 208:44–53. doi: 10.1016/j.jbiotec.2015.04.024
- Lim H-J, Han J, Woo D-H, et al. (2011) Biochemical and morphological effects of hypoxic environment on human embryonic stem cells in long-term culture and differentiating embryoid bodies. *Mol Cells* 31:123–132. doi: 10.1007/s10059-011-0016-8
- Lindemann JP, Jones LR, Hathaway DR, et al. (1983) β -Adrenergic stimulation of phospholamban phosphorylation and Ca²⁺-ATPase activity in guinea pig ventricles. *J Biol Chem* 258:464–471.
- Liu G-S, Morales A, Vafiadaki E, et al. (2015) A novel human R25C-phospholamban mutation is associated with super-inhibition of calcium cycling and ventricular arrhythmia. *Cardiovasc Res* 107:164–174. doi: 10.1093/cvr/cvv127
- Loh Y-H, Agarwal S, Park I-H, et al. (2009) Generation of induced pluripotent stem cells from human blood. *Blood* 113:5476–5479. doi: 10.1182/blood-2009-02-204800
- Loh Y-H, Hartung O, Li H, et al. (2010) Reprogramming of T Cells from Human Peripheral Blood. *Cell Stem Cell* 7:15–19. doi: 10.1016/j.stem.2010.06.004
- von Lueder TG, Krum H (2015) New medical therapies for heart failure. *Nat Rev Cardiol* 12:730–740. doi: 10.1038/nrcardio.2015.137
- Lund RJ, Närvä E, Lahesmaa R (2012) Genetic and epigenetic stability of human pluripotent stem cells. *Nat Rev Genet* 13:732–744. doi: 10.1038/nrg3271
- Lundy SD, Zhu W-Z, Regnier M, Laflamme MA (2013) Structural and functional maturation of

- cardiomyocytes derived from human pluripotent stem cells. *Stem Cells Dev* 22:1991–2002. doi: 10.1089/scd.2012.0490
- Luo M, Anderson ME (2013) Mechanisms of altered Ca²⁺ handling in heart failure. *Circ Res* 113:690–708. doi: 10.1161/CIRCRESAHA.113.301651
- MacDougall LK, Jones LR, Cohen P (1991) Identification of the major protein phosphatases in mammalian cardiac muscle which dephosphorylate phospholamban. *Eur J Biochem* 196:725–734. doi: 10.1111/j.1432-1033.1991.tb15871.x
- MacLennan DH, Kranias EG (2003) Phospholamban: a crucial regulator of cardiac contractility. *Nat Rev Mol Cell Biol* 4:566–77. doi: 10.1038/nrm1151
- Mali P, Aach J, Stranges PB, et al. (2013a) CAS9 transcriptional activators for target specificity screening and paired nickases for cooperative genome engineering. *Nat Biotechnol* 31:833–8. doi: 10.1038/nbt.2675
- Mali P, Yang L, Esvelt KM, et al. (2013b) RNA-guided human genome engineering via Cas9. *Science* (80-) 339:823–826. doi: 10.1126/science.1232033
- Mannhardt I, Breckwoldt K, Letuffe-Brenière D, et al. (2016) Human Engineered Heart Tissue: Analysis of Contractile Force. *Stem Cell Reports* 7:29–42. doi: 10.1016/j.stemcr.2016.04.011
- Mannhardt I, Saleem U, Benzin A, et al. (2017) Automated Contraction Analysis of Human Engineered Heart Tissue for Cardiac Drug Safety Screening. *J Vis Exp* 2017:e55461–e55461. doi: 10.3791/55461
- Marks AR (2013) Calcium cycling proteins and heart failure : mechanisms and therapeutics. *J Clin Invest*. doi: 10.1172/JCI62834.46
- Maron BJ (2008) The 2006 American Heart Association Classification of Cardiomyopathies Is Not the Gold Standard. *Circ Hear Fail* 1:72–76. doi: 10.1161/CIRCHEARTFAILURE.108.770826
- Martin GR (1981) Isolation of a pluripotent cell line from early mouse embryos cultured in medium conditioned by teratocarcinoma stem cells. *Proc Natl Acad Sci U S A* 78:7634–7638. doi: 10.1073/pnas.78.12.7634
- Maruyama T, Dougan SK, Truttmann MC, et al. (2015) Increasing the efficiency of precise genome editing with CRISPR-Cas9 by inhibition of nonhomologous end joining. *Nat Biotechnol* 33:538–42. doi: 10.1038/nbt.3190
- Marx SO, Reiken S, Hisamatsu Y, et al. (2000) PKA Phosphorylation Dissociates FKBP12.6 from the Calcium Release Channel (Ryanodine Receptor): Defective Regulation in Failing Hearts. *Cell* 101:365–376. doi: 10.1016/S0092-8674(00)80847-8
- Mei Y, Wang Y, Chen H, et al. (2016) Recent Progress in CRISPR/Cas9 Technology. *J Genet Genomics* 43:63–75. doi: 10.1016/j.jgg.2016.01.001
- Mercadier JJ, Lompré AM, Duc P, et al. (1990) Altered sarcoplasmic reticulum Ca²⁺(+)-

- ATPase gene expression in the human ventricle during end-stage heart failure. *J Clin Invest* 85:305–9. doi: 10.1172/JCI114429
- Meyer M, Schillinger W, Pieske B, et al. (1995) Alterations of Sarcoplasmic Reticulum Proteins in Failing Human Dilated Cardiomyopathy. *Circulation* 92:778–784. doi: 10.1161/01.CIR.92.4.778
- Minamisawa S, Hoshijima M, Chu G, et al. (1999) Chronic phospholamban-sarcoplasmic reticulum calcium atpase interaction is the critical calcium cycling defect in dilated cardiomyopathy. *Cell* 99:313–322. doi: 10.1016/S0092-8674(00)81662-1
- Miyaoka Y, Berman JR, Cooper SB, et al. (2016) Systematic quantification of HDR and NHEJ reveals effects of locus, nuclease, and cell type on genome-editing. *Sci Rep* 6:23549. doi: 10.1038/srep23549
- Moretti A, Bellin M, Welling A, et al. (2010) Patient-Specific Induced Pluripotent Stem-Cell Models for Long-QT Syndrome. *N Engl J Med* 363:1397–1409. doi: 10.1056/NEJMoa0908679
- Mundiña-Weilenmann C, Vittone L, Ortale M, et al. (1996) Immunodetection of Phosphorylation Sites Gives New Insights into the Mechanisms Underlying Phospholamban Phosphorylation in the Intact Heart. *J Biol Chem* 271:33561–33567.
- Nerbonne JM, Kass RS (2005) Molecular Physiology of Cardiac Repolarization. *Physiol Rev* 85:1205–1253. doi: 10.1152/physrev.00002.2005
- Nguyen HT, Geens M, Mertzaniadou A, et al. (2014) Gain of 20q11.21 in human embryonic stem cells improves cell survival by increased expression of Bcl-xL. *Mol Hum Reprod* 20:168–177. doi: 10.1093/molehr/gat077
- Nguyen HT, Geens M, Spits C (2013) Genetic and epigenetic instability in human pluripotent stem cells. *Hum Reprod Update* 19:187–205. doi: 10.1093/humupd/dms048
- Nishimasu H, Ran FA, Hsu PD, et al. (2014) Crystal structure of Cas9 in complex with guide RNA and target DNA. *Cell* 156:935–949. doi: 10.1016/j.cell.2014.02.001
- Nunes SS, Miklas JW, Liu J, et al. (2013) Biowire: a platform for maturation of human pluripotent stem cell-derived cardiomyocytes. *Nat Methods* 10:781–7. doi: 10.1038/nmeth.2524
- O'Neill SC, Eisner DA (1990) A mechanism for the effects of caffeine on Ca²⁺ release during diastole and systole in isolated rat ventricular myocytes. *J Physiol* 430:519–536.
- Ohnuki M, Takahashi K, Yamanaka S (2009) Generation and Characterization of Human Induced Pluripotent Stem Cells. *Curr. Protoc. Stem Cell Biol.* John Wiley & Sons, Inc., Hoboken, NJ, USA, p Unit 4A.2
- Posch MG, Perrot A, Geier C, et al. (2009) Genetic deletion of arginine 14 in phospholamban causes dilated cardiomyopathy with attenuated electrocardiographic R amplitudes. *Hear Rhythm* 6:480–486. doi: 10.1016/j.hrthm.2009.01.016

- Prondzynski M, Krämer E, Laufer SD, et al. (2017) Evaluation of MYBPC3 trans-Splicing and Gene Replacement as Therapeutic Options in Human iPSC-Derived Cardiomyocytes. *Mol Ther - Nucleic Acids* 7:475–486. doi: 10.1016/j.omtn.2017.05.008
- Rajamohan D, Matsa E, Kalra S, et al. (2013) Current status of drug screening and disease modelling in human pluripotent stem cells. *BioEssays* 35:281–298. doi: 10.1002/bies.201200053
- Ran FA, Hsu PD, Lin CY, et al. (2013a) Double nicking by RNA-guided CRISPR cas9 for enhanced genome editing specificity. *Cell* 154:1380–1389. doi: 10.1016/j.cell.2013.08.021
- Ran FA, Hsu PD, Wright J, et al. (2013b) Genome engineering using the CRISPR-Cas9 system. *Nat Protoc* 8:2281–308. doi: 10.1038/nprot.2013.143
- Rebuzzini P, Zuccotti M, Redi CA, Garagna S (2016) Achilles' heel of pluripotent stem cells: genetic, genomic and epigenetic variations during prolonged culture. *Cell Mol Life Sci* 73:2453–2466. doi: 10.1007/s00018-016-2171-8
- Richardson CD, Ray GJ, DeWitt MA, et al. (2016) Enhancing homology-directed genome editing by catalytically active and inactive CRISPR-Cas9 using asymmetric donor DNA. *Nat Biotechnol*. doi: 10.1038/nbt.3481
- Richardson P, McKenna W, Bristow M, et al. (1996) Report of the 1995 World Health Organization/International Society and Federation of Cardiology Task Force on the Definition and Classification of Cardiomyopathies. *Circulation* 93:841–842. doi: 10.1161/01.CIR.93.5.841
- te Rijdt WP, van der Klooster ZJ, Hoorntje ET, et al. (2017) Phospholamban immunostaining is a highly sensitive and specific method for diagnosing phospholamban p.Arg14del cardiomyopathy. *Cardiovasc Pathol* 30:23–26. doi: 10.1016/j.carpath.2017.05.004
- te Rijdt WP, van Tintelen JP, Vink A, et al. (2016) Phospholamban p.Arg14del cardiomyopathy is characterized by phospholamban aggregates, aggresomes, and autophagic degradation. *Histopathology* 69:542–550. doi: 10.1111/his.12963
- van Rijsingen IAW, van der Zwaag P a, Groeneweg JA, et al. (2014) Outcome in Phospholamban R14del Carriers: Results of a Large Multicentre Cohort Study. *Circ Cardiovasc Genet* 7:455–465. doi: 10.1161/CIRCGENETICS.113.000374
- Robinton DA a., Daley GGQ (2012) The promise of induced pluripotent stem cells in research and therapy. *Nature* 481:295–305. doi: 10.1038/nature10761
- Sakuma T, Nishikawa A, Kume S, et al. (2014) Multiplex genome engineering in human cells using all-in-one CRISPR/Cas9 vector system. *Sci Rep* 4:5400. doi: 10.1038/srep05400
- Sande JB, Sjaastad I, Hoen IB, et al. (2002) Reduced level of serine16 phosphorylated phospholamban in the failing rat myocardium: A major contributor to reduced SERCA2 activity. *Cardiovasc Res* 53:382–391. doi: 10.1016/S0008-6363(01)00489-8

- Sato Y, Kiriazis H, Yatani A, et al. (2001) Rescue of Contractile Parameters and Myocyte Hypertrophy in Calsequestrin Overexpressing Myocardium by Phospholamban Ablation. *J Biol Chem* 276:9392–9399. doi: 10.1074/jbc.M006889200
- Schaaf S, Shibamiya A, Mewe M, et al. (2011) Human engineered heart tissue as a versatile tool in basic research and preclinical toxicology. *PLoS One* 6:e26397. doi: 10.1371/journal.pone.0026397
- Schmidt AG, Zhai J, Carr AN, et al. (2002) Structural and functional implications of the phospholamban hinge domain: Impaired SR Ca²⁺ uptake as a primary cause of heart failure. *Cardiovasc Res* 56:248–259. doi: 10.1016/S0008-6363(02)00541-2
- Schmitt J, Kamisago M, Asahi M, Li G (2003) Dilated cardiomyopathy and heart failure caused by a mutation in phospholamban. *Science* (80-) 299:1410–1413. doi: 10.1126/science.1081578
- Schwinger RH, Münch G, Bölck B, et al. (1999) Reduced Ca²⁺-Sensitivity of SERCA 2a in Failing Human Myocardium due to Reduced Serin-16 Phospholamban Phosphorylation. *J Mol Cell Cardiol* 31:479–491. doi: 10.1006/jmcc.1998.0897
- Shan J, Betzenhauser MJ, Kushnir A, et al. (2010) Role of chronic ryanodine receptor phosphorylation in heart failure and beta-adrenergic receptor blockade in mice. *J Clin Invest* 120:4375–4387. doi: 10.1172/JCI37649
- Sinnecker D, Goedel A, Dorn T, et al. (2013) Modeling long-QT syndromes with iPS cells. *J Cardiovasc Transl Res* 6:31–36. doi: 10.1007/s12265-012-9416-1
- Soldner F, Hockemeyer D, Beard C, et al. (2009) Parkinson's Disease Patient-Derived Induced Pluripotent Stem Cells Free of Viral Reprogramming Factors. *Cell* 136:964–977. doi: 10.1016/j.cell.2009.02.013
- Soldner F, Jaenisch R (2012) iPSC Disease Modeling. *Science* (80-) 338:1155–1156.
- Soldner F, Laganière J, Cheng AW, et al. (2011) Generation of isogenic pluripotent stem cells differing exclusively at two early onset parkinson point mutations. *Cell* 146:318–331. doi: 10.1016/j.cell.2011.06.019
- Song M (2017) The CRISPR/Cas9 system: their delivery, in vivo and ex vivo applications and clinical development by startups. *Biotechnol Prog* 1–38. doi: 10.1002/btpr.2484
- Spits C, Mateizel I, Geens M, et al. (2008) Recurrent chromosomal abnormalities in human embryonic stem cells. *Nat Biotechnol* 26:1361–1363. doi: 10.1038/nbt.1510
- Srivastava M, Nambiar M, Sharma S, et al. (2012) An inhibitor of nonhomologous end-joining abrogates double-strand break repair and impedes cancer progression. *Cell* 151:1474–1487. doi: 10.1016/j.cell.2012.11.054
- Stillitano F, Turnbull IC, Karakikes I, et al. (2016) Genomic correction of familial cardiomyopathy in human engineered cardiac tissues. *Eur Heart J* 37:3282–3284. doi: 10.1093/eurheartj/ehw307

- Stoehr A, Neuber C, Baldauf C, et al. (2014) Automated analysis of contractile force and Ca²⁺ transients in engineered heart tissue. *Am J Physiol Heart Circ Physiol* 306:H1353–H1363. doi: 10.1152/ajpheart.00705.2013
- Suckau L, Fechner H, Chemaly E, et al. (2009) Long-term cardiac-targeted RNA interference for the treatment of heart failure restores cardiac function and reduces pathological hypertrophy. *Circulation* 119:1241–1252. doi: 10.1161/CIRCULATIONAHA.108.783852
- Sun L, Wu J, Du F, et al. (2013) Cyclic GMP-AMP Synthase Is a Cytosolic DNA Sensor That Activates the Type I Interferon Pathway. *Science* (80-) 339:786–791. doi: 10.1126/science.1229963
- Sun N, Yazawa M, Liu J, et al. (2012) Dilated Cardiomyopathy Patient-Specific Induced Pluripotent Stem Cells as a Model for Familial Patient-Specific Induced Pluripotent Stem Cells as a Model for Familial Dilated Cardiomyopathy. *Sci Transl Med* 4:1–13. doi: 10.1126/scitranslmed.3003552
- Tada M, Kirchberger MA, Katz AM (1975) Phosphorylation of a 22,000-dalton component of the cardiac sarcoplasmic reticulum by adenosine 3':5'-monophosphate-dependent protein kinase. *J Biol Chem* 250:2640–2647.
- Takahashi K, Okita K, Nakagawa M, Yamanaka S (2007a) Induction of pluripotent stem cells from fibroblast cultures. *Nat Protoc* 2:3081–3089. doi: 10.1038/nprot.2007.418
- Takahashi K, Tanabe K, Ohnuki M, et al. (2007b) Induction of Pluripotent Stem Cells from Adult Human Fibroblasts by Defined Factors. *Cell* 131:861–872. doi: 10.1016/j.cell.2007.11.019
- Takahashi K, Yamanaka S (2006) Induction of pluripotent stem cells from mouse embryonic and adult fibroblast cultures by defined factors. *Cell* 126:663–76. doi: 10.1016/j.cell.2006.07.024
- Talosi L, Edes I, Kranias EG (1993) Intracellular mechanisms mediating reversal of beta-adrenergic stimulation in intact beating hearts. *Am J Physiol* 264:H791-7.
- ThermoFisher Scientific (2017) GeneArt Platinum Cas9 Nuclease & Lipofectamine CRISPRMAX. ThermoFisher Sci <https://www.thermofisher.com/de/de/home/life-scienc>.
- Thomson JA, Itskovitz-Eldor J, Shapiro SS, et al. (1998) Embryonic stem cell lines derived from human blastocysts. *Science* (80-) 282:1145–1147. doi: 10.1126/science.282.5391.1145
- Tulloch NL, Muskheli V, Razumova M V., et al. (2011) Growth of engineered human myocardium with mechanical loading and vascular coculture. *Circ Res* 109:47–59. doi: 10.1161/CIRCRESAHA.110.237206
- Uzun AU, Mannhardt I, Breckwoldt K, et al. (2016) Ca²⁺-Currents in Human Induced Pluripotent Stem Cell-Derived Cardiomyocytes Effects of Two Different Culture Conditions. *Front Pharmacol*. doi: 10.3389/fphar.2016.00300

- Vignier N, Schlossarek S, Fraysse B, et al. (2009) Nonsense-mediated mRNA decay and ubiquitin-proteasome system regulate cardiac myosin-binding protein c mutant levels in cardiomyopathic mice. *Circ Res* 105:239–248. doi: 10.1161/CIRCRESAHA.109.201251
- Vostrikov V V., Soller KJ, Ha KN, et al. (2015) Effects of naturally occurring arginine 14 deletion on phospholamban conformational dynamics and membrane interactions. *Biochim Biophys Acta - Biomembr* 1848:315–322. doi: 10.1016/j.bbamem.2014.09.007
- Wagner M, Weber S, El-Armouche a. (2015) Linking superinhibitory PLN mutations to CaMKII activation: a new arrhythmogenic mechanism in genetic DCM? *Cardiovasc Res* 107:5–6. doi: 10.1093/cvr/cvv163
- Warren L, Manos PD, Ahfeldt T, et al. (2010) Highly efficient reprogramming to pluripotency and directed differentiation of human cells with synthetic modified mRNA. *Cell Stem Cell* 7:618–630. doi: 10.1016/j.stem.2010.08.012
- Watanabe N, Santostefano KE, Yachnis AT, Terada N (2017) A pathologist's perspective on induced pluripotent stem cells. *Nat Publ Gr*. doi: 10.1038/labinvest.2017.81
- Wegener AD, Simmerman HKB, Lindemanns JP, Jones LR (1989) Phospholamban Phosphorylation in Intact Ventricles. *J Biol Chem* 264:1146–11474.
- Werbowetski-Ogilvie TE, Bossé M, Stewart M, et al. (2009) Characterization of human embryonic stem cells with features of neoplastic progression. *Nat Biotechnol* 27:91–97. doi: 10.1038/nbt.1516
- Wilde AAM, Behr ER (2013) Genetic testing for inherited cardiac disease. *Nat Rev Cardiol* 10:571–583. doi: 10.1038/nrcardio.2013.108
- Willems E, Spiering S, Davidovics H, et al. (2011) Small-molecule inhibitors of the Wnt pathway potently promote cardiomyocytes from human embryonic stem cell-derived mesoderm. *Circ Res* 109:360–364. doi: 10.1161/CIRCRESAHA.111.249540
- Willis MS, Patterson C (2013) Proteotoxicity and Cardiac Dysfunction — Alzheimer's Disease of the Heart? *N Engl J Med* 368:455–464. doi: 10.1056/NEJMra1106180
- Wobus AM, Wallukat G, Hescheler J (1991) Pluripotent mouse embryonic stem cells are able to differentiate into cardiomyocytes expressing chronotropic responses to adrenergic and cholinergic agents and Ca²⁺ channel blockers. *Differentiation* 48:173–182. doi: 10.1111/j.1432-0436.1991.tb00255.x
- Woltjen K, Michael IP, Mohseni P, et al. (2009) PiggyBac transposition reprograms fibroblasts to induced pluripotent stem cells. *Nature* 458:766–770. doi: 10.1038/nature07863
- Wu AZ, Xu D, Yang N, et al. (2016) Phospholamban is concentrated in the nuclear envelope of cardiomyocytes and involved in perinuclear/nuclear calcium handling. *J Mol Cell Cardiol* 100:1–8. doi: 10.1016/j.yjmcc.2016.09.008
- Wu X, Kriz AJ, Sharp PA (2014) Target specificity of the CRISPR-Cas9 system. *Quant Biol*

- 2:59–70. doi: 10.1007/s40484-014-0030-x
- Yang L, Soonpaa MH, Adler ED, et al. (2008) Human cardiovascular progenitor cells develop from a KDR+ embryonic-stem-cell-derived population. *Nature* 453:524–528. doi: 10.1038/nature06894
- Yoshihara M, Hayashizaki Y, Murakawa Y (2017) Genomic Instability of iPSCs: Challenges Towards Their Clinical Applications. *Stem Cell Rev Reports* 13:7–16. doi: 10.1007/s12015-016-9680-6
- Young HS, Ceholski DK, Trieber CA (2015) Deception in simplicity: hereditary phospholamban mutations in dilated cardiomyopathy. *Biochem Cell Biol* 93:1–7. doi: 10.1139/bcb-2014-0080
- Yu J, Hu K, Smuga-Otto K, et al. (2009) Human Induced Pluripotent Stem Cells Free of Vector and Transgene Sequences. *Science* (80-) 324:797–801.
- Yu J, Vodyanik MA, Smuga-Otto K, et al. (2007) Induced Pluripotent Stem Cell Lines Derived from Human Somatic Cells. *Science* (80-) 318:1917–1920. doi: 10.1126/science.1151526
- Yusa K, Rad R, Takeda J, Bradley A (2009) Generation of transgene-free induced pluripotent mouse stem cells by the piggyBac transposon. *Nat Methods* 6:363–369. doi: 10.1038/nmeth.1323
- Zhai J, Schmidt AG, Hoit BD, et al. (2000) Cardiac-specific overexpression of a superinhibitory pentameric phospholamban mutant enhances inhibition of cardiac function in vivo. *J Biol Chem* 275:10538–10544. doi: 10.1074/jbc.275.14.10538
- Zhang J, Wilson GF, Soerens AG, et al. (2009) Functional cardiomyocytes derived from human induced pluripotent stem cells. *Circ Res* 104:e30–e41. doi: 10.1161/CIRCRESAHA.108.192237
- Zhang X-H, Tee LY, Wang X-G, et al. (2015) Off-target Effects in CRISPR/Cas9-mediated Genome Engineering. *Mol Ther Acids* 4:e264. doi: 10.1038/mtna.2015.37
- Zhang Y, Ge X, Yang F, et al. (2014) Comparison of non-canonical PAMs for CRISPR/Cas9-mediated DNA cleavage in human cells. *Sci Rep* 4:5405. doi: 10.1038/srep05405
- Zhao W, Yuan Q, Qian J, et al. (2006) The presence of Lys27 instead of Asn27 in human phospholamban promotes sarcoplasmic reticulum Ca²⁺-ATPase superinhibition and cardiac remodeling. *Circulation* 113:995–1004. doi: 10.1161/CIRCULATIONAHA.105.583351
- Zimmermann W-H, Didié M, Wasmeier GH, et al. (2002) Cardiac grafting of engineered heart tissue in syngenic rats. *Circulation* 106:1151–1157. doi: 10.1161/01.cir.0000032876.55215.10
- Zvaritch E, Backx PH, Jirik F, et al. (2000) The transgenic expression of highly inhibitory monomeric forms of phospholamban in mouse heart impairs cardiac contractility. *J Biol*

Chem 275:14985–14991. doi: 10.1074/jbc.275.20.14985

van der Zwaag P a, van Rijsingen I a W, Asimaki A, et al. (2012) Phospholamban R14del mutation in patients diagnosed with dilated cardiomyopathy or arrhythmogenic right ventricular cardiomyopathy: evidence supporting the. *Eur J Heart Fail* 14:1199–207. doi: 10.1093/eurjhf/hfs119

van der Zwaag P a, van Rijsingen I a W, de Ruyter R, et al. (2013) Recurrent and founder mutations in the Netherlands-Phospholamban p.Arg14del mutation causes arrhythmogenic cardiomyopathy. *Neth Heart J* 21:286–93. doi: 10.1007/s12471-013-0401-3

10 SUPPLEMENT

10.1 Devices, materials and substances

10.1.1 Devices

4D-Nucleofector™ X Unit	Lonza
4D-Nucleofector™ Core Unit	Lonza
AbiPrism7900HT cycler	Applied Biosystems
Accu-jetR pro	Brand
Analytic scale Genius	Sartorius AG
AriaFusion FACS sorter	BD Biosciences
Bio-Rad ChemiDoc™ Touch Imaging System	Bio-Rad Laboratories

Centrifuges

Centrifuge 5415 R	Eppendorf
Centrifuge 5810 R	Eppendorf
Centrifuge J-6B	Beckmann
Centrifuge Rotanta/RP	Hettich
Centrifuge Universal 30 RF	Hettich
ChemiDoc™ Touch Imaging system	Bio-Rad Laboratories
Combispin FVL-2400N with vortex function	PeqLab
Contractility and calcium transient analysis system	IonOptix
FACSCanto II Flow Cytometer	BD Biosciences
Incubator shaker C25	New Brunswick Scientific

Incubators for cell culture (hiPSC, EHT)

CB 220	Binder
HERAcell 240	Thermo Fisher Scientific
HERAcell 150i	Thermo Fisher Scientific
MCO-19M	Sanyo
MCO-20AIC	Sanyo
S2020 1.8	Thermo Fisher Scientific
Kelvitron® t warming cabinet	Heraeus
Magnet plate Variomag/ Cimarec Biosystem 4 Direct	Thermo Scientific
Magnet plate Variomag/ Cimarec Biosystem Direct	Thermo Scientific
Magnet/heating plate IKA Combimag RET	Janke & Kunkel GmbH & Co KG

Microscopes

Axioskop 2 with AxioCam color camera	Zeiss
Axiovert 25 with Jenoptik ProgRes Speed XT core 5 camera	Zeiss, Jenoptik (camera)
EVOS FL Cell Imaging System	Advanced Microscopy Group
LSM 800 Airyscan	Zeiss
T1-SM Nikon Eclipse TS100	Nikon
Mini Trans-Blot Electrophoretic Transfer Cell	Bio-Rad Laboratories
Mini-Protean Tetra Cell	Bio-Rad Laboratories
nCounter SPRINT™ Profiler	NanoSring
PCR cyclers vapo.protect	Eppendorf
pH meter, digital	Mettler Toledo
Pipette 10/100/1000 µL	Eppendorf, Peqlab
Pipetus	Hirschmann
PowerPac Basic Power Supply	Bio-Rad Laboratories
QIAcube HT	Qiagen
Qubit 3.0 Fluorometer	Life technologies
S88X dual output square pulse stimulator	Grass
Scale Ohaus Precision Advanced	Ohaus
Security working hood HERAsafeR	Thermo Fisher Scientific
Spectrophotometer NanoDrop ND-1000	Thermo Fisher Scientific
<u>Sterile working benches</u>	
HeraSafe	Heraeus
Safe2020	Thermo Fisher Scientific
Mars 1200 GS	Scanlaf
Sub-cell® GT gel electrophoresis tank	Bio-Rad Laboratories
Thermal Cycler vapo.protect	Eppendorf
Thermomixer 5436	Eppendorf
TissueLyser	Qiagen
Ventana, Benchmark XT staining device for IHC	Roche
Video-optical force analysis system	EHT technologies GmbH, Hamburg, A0001
Water bath	GFL
Water bath 2590	Medax

10.1.2 Software

AxioVision Rel. 4.8.2, Zeiss

CytoVision image analysis system, Leica Biosystems

FACSDiva, BD Biosciences

GraphPad Prism 5.0

Image Lab Version 5.2.1, Bio-Rad Laboratories

ImageJ 1.46r

LSM 800 Airyscan, Zeiss

MProRes Capture Pro V. 2.8.8. (Jenoptik)

SDS 2.4.1, Applied Biosystem

SnapGene® 3.3.4

10.1.3 Materials and equipment

15 mL tubes	GreinerBio-one, 188271
24-well plates	Nunc, 144530
250 ml Vacuum Filtration "rapid"-Filtermax	TPP, 99250
500 ml Vacuum Filtration "rapid"-Filtermax	TPP, 99500
6-well cell culture plates	Nunc, 140675
Aspiration pipette 2 mL	Sarstedt, 86.1252.011
Cell culture microplate, 96 well, PS, F-bottom, μ CLEAR®, black, CELLSTAR®	Greiner Bio One, 655090
Cell culture tube, round bottom (for EHT generation)	GreinerBio One, 163160,
Cell scraper	Sarstedt, 83.1830
Cell strainer for FACS, 30 μ m	Sysmex, 04-004-2326
Cell strainer mesh, 100 μ m	Falcon, 352360
Centrifuge tubes 15 ml	Sarstedt, 62.554.502 and Greiner, 188280
Comb 10 well 0.75 mm	Bio-Rad Laboratories, 165-3354
Comb 10 well 1.0 mm	Bio-Rad Laboratories, 165-3359
Cryovial CryoPure tube 1.6 mL	Sarstedt, 72.380
EHT electrode	EHT Technologies GmbH, P0001
EHT pacing adapter/cable	EHT Technologies GmbH, P0002
EHT PDMS rack (24-well format)	EHT Technologies GmbH, C0001
EHT PTFE spacer	EHT Technologies GmbH, C0002
Falcon tube, graduated, 15 mL	Sarstedt, 62.554.502

Flow Cytometry tubes	Sarstedt, 55.1579
Glass coverslips (24x24 mm)	VWR
Isopropanol container (Mr. Frosty):	Thermo Fisher Scientific, 5100-0001
Nalgene™ Cryo 1 °C Freezing container	
Neubauer counting chamber	Karl-Hecht KG
Nitrocellulose Blotting Membrane	GE Healthcare, 10600003
Amersham™ Protan™ 0.45µm	
PDMS racks	EHT technologies GmbH, C0001
Pipette tips with filter Biosphere®	Sarstedt
PVDF Transfer Membrane, 0.45 µm	GE Healthcare, 10485289
QIAcube HT Plasticware	Qiagen, 950067
Reaction tubes Safe Lock 0.2 – 2 mL	Eppendorf
Reagent Trough (with Lid) 170 ml	Qiagen, 990556
Serological pipettes 1 mL, 2 mL, 5 mL, 10 mL, 25 mL, 50 mL; wide tip pipette 10 mL	Sarstedt
Short Plates	Bio-Rad Laboratories, 165-3308
Spacer Plates 0.75 mm	Bio-Rad Laboratories, 165-3310
Spacer Plates 1.0 mm	Bio-Rad Laboratories, 165-3311
Spinner flask, 1000 ml	Integra, 182 101
Spinner flask, 500 ml	Integra, 182 051
Sterile filter Filtropur S 0.2 µm	Sarstedt, 83.1826.001
Stirrer Variomag/ Cimarec Biosystem 4 Direct	Thermo Fisher scientific, 50088060
Stirrer Variomag/ Cimarec Biosystem Direct	Thermo Fisher scientific, 70101
T175 cell culture flask	Sarstedt, 83.1812.002
T175 suspension cell culture flask	Sarstedt, 83.3912.502
T75 cell culture flask	Sarstedt, 83.1813.002
TC dish 100, cell+	Sarstedt, 83.3902.300
Teflon spacers (dimensions: length 12 mm, width 3 mm, height 13.5 mm)	EHT technologies GmbH, C0002
Tissue Lyser Steel Beads	Qiagen
V-shaped sedimentation rack (dimensions of the two side panels of the metal bracket: 30 cm x 10 cm, angle 90°)	Custom made at UKE Hamburg
Western blot paper	Whatman, 3030917

10.1.4 Media and serum

DMEM	Biochrom, F0415
DMEM/F-12 without Glutamine	Gibco, 21331-046
Fetal Calf Serum superior (FCS)	Biochrom, S0615
Horse serum	Life technologies, 26050088
RPMI 1640	Gibco, 21875

10.1.5 Reagents, proteins and small molecules

1,4-Dithiothreitol (DTT)	Roth, 6908.2
10x DMEM	Gibco, 52100-021
1-Thioglycerol	Sigma-Aldrich, M6145
2-Mercaptoethanol	Sigma-Aldrich, M6250
2-Propanol	Merck Millipore, 107022
Accutase® Cell Dissociation Reagent	Sigma-Aldrich, A6964
Acetic acid (concentrated; glacial, 100%)	Merck, 100063
Acrylamide/Bis 40%	Bio-Rad Laboratories, 161-0146
Activin A	R&D Systems, 338-AC
Agarose	Invitrogen, 15510-027
Ammoniumpersulfate (APS)	Bio-Rad Laboratories, 161-0700
AmpliTaqGold (1kb/min)	Applied Biosystems
Aprotinin	Sigma-Aldrich, A1153
Aqua ad iniectabilia	Baxter S.A., 001428
B27 PLUS insulin	Gibco, 17504-044
Bacto™ Agar	BD, 214010
Bacto™ Tryptone	BD, 211705
Bacto™ Yeast Extract	BD, 212750
BbsI fast digest (Bpil)	Thermo Fisher Scientific, FD1014
BMP4	R&D Systems, 314-BP
CaCl ₂ x 2H ₂ O	Merck, 2382
Collagenase II	Worthington, LS004176
cOmplete® Mini, EDTA-free protease inhibitor cocktail	Roche, 11836153001
D(+)-Glucose anhydrous	Roth, X997.2
DAPI BioChemica	AppliChem, A1001
Di-sodium hydrogen phosphate dihydrate (Na ₂ HPO ₄ -2H ₂ O)	Merck, 1065800
DMSO for cell culture	Sigma-Aldrich, D4540
DMSO for molecular experiments (PCR)	Thermo Fisher Scientific, F-515

DNA loading dye, 6x	Thermo Fisher Scientific, R0611
DNase II, type V (from bovine spleen)	Sigma-Aldrich, D8764
EDTA	Roth, 8043.2
Ethanol, absolute	Chemsolute, 2246.1000
Ethidium bromide	Sigma-Aldrich, E1510
Ethylenediamine-tetraacetic acid disodium salt dihydrate (Na ₂ EDTA x 2H ₂ O)	Roth, 8043.2
FGF2 (human recombinant basic FGF)	Peprotech, #100-18B
Fibrinogen	Sigma-Aldrich, F8630
Formaldehyd	Merck Millipore, 107022
Fura-2/AM	Life technologies, F1221
Gelatine	Sigma-Aldrich, G1890
Geltrex®	Gibco, A1413302
GeneRuler 1 kb DNA Ladder	Thermo Fisher Scientific, SM0313
GeneRuler 100 bp DNA Ladder	Thermo Fisher Scientific, SM0243
Glycerol	Merck 1.04092
Glycine	Roth, 3908.2
Glycogen for mol. biol.	Roche, 10901393001
HBSS minus Ca ²⁺ /Mg ²⁺	Gibco, 14175-053
HEPES	Roth, 9105.4
Hoechst 33342, trihydrochloride trihydrate	Thermo Fisher Scientific, H3570
Human serum albumin	Biological Industries, 05-720-1B
Hydrochloric acid 1 N	Roth, K025.1
Hydrochloric acid, 37% fuming	Merck 1.00317
Insulin, human	Sigma-Aldrich, I9278
Knockout serum replacement	Gibco, 10828
L-Glutamine	Gibco, 25030-081
Lipidmix	Sigma-Aldrich, L5146
Magnesium chloride hexahydrate (MgCl ₂ x 6H ₂ O)	Sigma-Aldrich, M9272
Magnesium sulphate heptahydrate (MgSO ₄ x 7H ₂ O)	Merck, 105886
Matrigel® Basement Membrane Matrix (for EHT generation)	Corning, 354234
Matrigel® Growth Factor Reduced (GFR) Basement Membrane Matrix (for hiPSC culture)	Corning, 354230

Methanol	J. Baker, 8045
MgCl ₂	Fuka, 63063
Milk powder	Roth, T145.2
M-PER™ Mammalian Protein Extraction Reagent	Thermo Fisher Scientific, #78501
N,N,N',N'-Tetramethyl ethylenediamine (TEMED)	Bio-Rad Laboratories, 161-0801
Nitrogen, liquid (N ₂)	TMG
Non essential amino acids (NEAA)	Gibco, 11140
Nuclease-free water	Thermo Fisher Scientific, R0581
Paraformaldehyde	Merck, 104005
PBS	Gibco, 10010-049
Phosphatase inhibitor PhosSTOP	Roche, 04906837001
Phosphoascorbate (2-Phospho-L-ascorbic acid trisodium salt)	Sigma-Aldrich, 49752
Pierce® ECL Western Blotting Substrate	Thermo Fisher Scientific, 32106
Pluronic® F-127	Sigma-Aldrich, P2443
Polyvinyl alcohol	Sigma-Aldrich, P8136
Potassium chloride (KCl)	Merck, 1.04936
Potassium di-hydrogen phosphate (KH ₂ PO ₄)	Merck, 104873
Precision Plus Protein All Blue Standard	Bio-Rad Laboratories, 161-0373
Roti®-Histofix 4%	Roth, P087.3
Saponin	Sigma-Aldrich, 47036 or Merck, 558255
SDS Pellets	Roth, CN30.3
Sodium azide	Sigma-Aldrich, 71290
Sodium chloride (NaCl)	JT Baker, 7647-14-5
Sodium chloride (NaCl) solution (0.9%)	B. Braun, 3570210
Sodium di-hydrogen phosphate mono-hydrate (NaH ₂ PO ₄ x H ₂ O)	Merck, 6346
Sodium hydrogen carbonate (NaHCO ₃)	Merck, 106329
Sodium hydroxide solution 0.1 N/1 N	Roth, K020.1/K021.1
Sodium selenite	Sigma-Aldrich, S5261
TBS	Sigma-Aldrich, T6664
TGFβ1	Peprtech, 100-21
Thrombin	Sigma-Aldrich, T7513; Biopur, BP11-10-1104
Titriplex® III for analysis (ethylenedinitrilote-traacetic acid, disodium salt dihydrate)	Merck, 108418

Transferrin	Sigma-Aldrich, T8158
TRIS-hydrochloride	Roth, 9090.2
Triton X®-100	Roth, 3051.3
Trizma® base	Sigma-Aldrich, T1503
Trypan blue	Biochrom, L 6323
Trypsin-EDTA (0.05%), phenol red	Thermo Fisher Scientific, 25300054
Tween 20	Sigma-Aldrich, P1379
Urea	Merck, 818710
Y-27632 * 2 HCl	Biorbyt, orb154626

10.1.6 Small molecules and pharmacological agents

Ampicillin trihydrate	Serva, 13397.01
BIOMYC-1	PromoCell, PK-CC03-036-1B
BIOMYC-2	PromoCell, PK-CC03-037-1B
BTS (N-Benzyl-p-Toluenesulfonamide)	TCI, B3082-25G
Carbachol	Merck, 212385
Dorsomorphin	Abcam, ab120843 or Tocris, 3093
DS-I-7 (4-(cis-endo-1,3-dioxooctahydro-2H-4,7-methanoisindol-2-yl)-N-(quinolin-8-yl)-transcyclohexylcarboxamide)	Dr. Dennis Schade, Technische Universität Dortmund, Germany
Isoprenaline	Sigma-Aldrich, I6504
Mitomycin C	Serva, 29805
Penicillin/streptomycin	Gibco, 15140
SCR7	Selleckchem, S7742
XAV-939	Tocris, 3748
Y-27632	Biaffin, PKI-Y27632-010

10.1.7 Kits

Amata™ P3 Primary Cell 4D-Nucleofector X Kit L	Lonza, V4XP-3024
Ambio MegaClear Kit	Ambion, AM1903
AmpliTaq Gold® DNA Polymerase with Gold Buffer & MgCl ₂	Life Technologies, 4311806
Cas9 nuclease NLS	NewEngland BioLabs, M0641S
CloneJET PCR cloning kit	Thermo Fisher Scientific, K1232
DNeasy® Blood & Tissue Kit	Qiagen, 69504
dNTP mix, 10 mM	Thermo Fisher Scientific, R0192
GeneArt™ Platinum™ Cas9 nuclease	Thermo Fisher Scientific/Invitrogen, B25641

High Capacity cDNA Reverse Transcription Kit	Applied Biosystems, 4368813
High Scribe™ T7 Quick Hi Yield kit	New England BioLabs, E2050
Maxima SYPBR Green/ROX qPCR Master Mix	Thermo Fisher Scientific, K0222
NucleoBond® Xtra Maxi kit	Macherey-Nagel, 740414.10
NucleoSpin® Plasmid kit	Macherey-Nagel, 740588.250
Phusion Hot Start II DNA Polymerase	Thermo Fisher Scientific, F549S
PrimeSTAR® HS DNA Polymerase	Takara, R010A
QIAamp® 96 DNA QIAcube® HT kit	Qiagen, 51331
QIAquick® Gel Extraction Kit	Qiagen, 28704
QIAquick® PCR purification Kit	Qiagen, 28106
Qubit™ RNA HS Assay Kit	Invitrogen, Q32852
Rapid DNA Ligation Kit	Thermo Fisher Scientific, K1422
RNeasy® Plus Mini Kit	Qiagen, 74134
T4 DNA Ligase (5 U/μL)	Thermo Fisher Scientific, EL0014
Taq DNA Polymerase Kit (for mycoplasma test)	Qiagen, 201205
TRIzol Reagent	Life Technologies, 15596026
Ultra View Universal DAB Detections Kit	Ventana, 05269806001

10.1.8 Reagent setup, buffer and solutions

Table S1: Reagent setup, buffer and solutions.

Reagents, buffer and solutions	Ingredients
10x DMEM	134 mg/mL DMEM powder dissolved in 5 mL of sterile water for injection and filter sterilized (0.2 μm), stored at 4 °C for up to 2 months. Store DMEM powder at 4 °C. Make sure the box is properly closed as DMEM is hygroscopic.
Agar plates	15g/L Bacto™ Agar Autoclave and cast into TC dish 100
Agarose for EHT casting molds	2% (w/v) Agarose was dissolved in 300 mL 1xPBS; after autoclaving storage at 60 °C.
Aprotinin	33 mg/mL Aprotinin was dissolved in sterile water for injection; 250 μL aliquots stored at -20 °C for 1 year.

Blotting buffer (1x)	20% (v/v) 5x Blotting buffer 20% (v/v) Methanol 60% (v/v) Aqua dest.
Blotting buffer (5x)	125 mM Trizma® base 950 mM Glycine Aqua dest.
BTS solution	BTS dissolved in DMSO; 250 µL aliquots stored at -20 °C for max. 1 year.
Dissociation buffer	HBSS minus calcium/magnesium Collagenase II, 200 units/mL 1 mM HEPES 10 µM Y-27632 30 µM BTS Sterile filtered (0.2 µm)
DNase solution	100 mg DNase II, type V, dissolved in 50 mL 1xPBS; 2 mL aliquots stored at -20 °C for max. 1 year.
DS-I-7	MW: 417,5 g/mol, dissolved in DMSO at a 10 mM stock solution.
EDTA	0.5 mM EDTA in 1x PBS, filter sterilized and stored at room temperature or 4 °C.
FACS buffer	PBS 5% (v/v) FCS 0,05% (v/v) Sodium azide 0,5% (w/v) Saponin (for intracellular staining)
Fibrinogen	200 g/L Fibrinogen was dissolved in pre-warmed (37 °C) 0.9%-NaCl solution. 33 g/L Aprotinin was added to a final concentration of 100 µg/mL. 200 µL Aliquots were stored at -20 °C for short term and at -80 °C for long term.
Gelatin (0.1%)	0.1% (w/v) gelatin dissolved in water and stored at 4 °C for max. 6 months
HEPES stock solution	1 M HEPES dissolved in 1xPBS and adjusted pH to 7.4 with potassium hydroxide. Filter sterilized (0.2 µm filter) and stored at 4 °C for max. 1 year.

Laemmli buffer (1x)	0.2 g SDS 1 mg Bromphenol blue 1 g Glycerol 0.2 mL 0.5 M Tris (pH 6.8) 0.155 g DTT Aqua dest.
LB medium	10 g Bacto™ Tryptone 5 g Bacto™ Yeast Extract 10 g NaCl Ad 1 L aqua dest. pH 7.4
Permeabilization buffer for immunofluorescence	1x PBS 3% (w/v) Milk powder 0.1% (v/v) Triton X-100
Phosphoascorbate, 250 mM	1 g Phosphoascorbate 12.4 mL PBS
Pluronic F-127 solution	Pluronic F-127 dissolved in 1x PBS to a concentration of 1% (w/v), filter sterilized (0.2 µm filter) and stored at 4 °C for up to 1 year.
Polyvinyl alcohol (50x)	20 g of polyvinyl alcohol dissolved in 100 mL of aqua dest. by slow addition at ~20 °C. The temperature was increase to 80 °C under constant stirring until polyvinyl alcohol was fully dissolved. Aliquots (not sterile) can be stored at 4 °C for up to one year
RNA-denaturation buffer (2x)	7 M Urea 1 mM EDTA 6x Loading dye Nuclease-free water
SDS-PAGE electrophoresis buffer (10x)	250 mM Trizma® base 1.92 M Glycine 1% or 50% (w/v) SDS Aqua dest.

Separation gel SDS-Page	<u>Acryl concentration</u>	<u>12%</u>	<u>15%</u>
	Aqua dest.	4.3 mL	3.55 mL
	40% Acrylamide	3.0 mL	3.75 mL
	1.5 M Tris pH 8.8	2.5 mL	2.5 mL
	10% SDS	0.1 mL	0.1 mL
	10% APS	0.1 mL	0.1 mL
	TEMED	4 µL	4 µL
SOC medium	20 g Bacto™ Tryptone 5 g Bacto™ Yeast Extract 0.5 g NaCl 400 mL 1 M KCl pH 7.0, autoclave, then add 1 M MgCl ₂ (sterile) 20 mL 1M Glucose (sterile)		
Stacking gel SDS-Page	6.03 mL Aqua dest. 1.28 mL 40% Acrylamide 2.5 mL 0.5 M Tris pH 6.8 0.1 mL 10% (w/v) SDS 0.1 mL 10% (w/v) APS 0.01 mL TEMED		
TAE buffer (50x) for agarose gel electrophoresis	242 g Trizma® base 37.2 g Titriplex III (EDTA) 57.1 mL concentrated acetic acid Ad 1 L aqua dest. pH 8.5 Use 1x diluted in aqua dest.		
TBS (10x)	1 M Trizma® base or Tris-HCl 1.5 M NaCl Aqua dest.; pH 7.5 (adjust with 37% HCl)		
Thrombin	100 U/mL Thrombin dissolved in 60% (v/v) PBS and 40% (v/v) sterile water for injection; aliquots (450 µL storage, 3 µL for EHTs) stored at -20 °C for max. 1 year.		
Transferrin-selenium	100 mg Transferrin dissolved in 2 mL sodium selenite (382 µM), stored at -80 °C for max. 1 year.		

Tris 0.5 M (pH 6.8)	60.6 g Trizma® base Ad 1 L Aqua dest.
Tris 1.5 M (pH 8.8)	181.7 g Trizma® base Ad 1 L Aqua dest.
Tyrode's solution for calcium transient measurements	<p><u>IonOptix' Tyrode's stock solution:</u> 135 mM NaCl 4.7 mM KCl 0.6 mM KH₂PO₄ 0.6 mM Na₂HPO₄-2H₂O 1.2 mM MgSO₄-7H₂O 10 mM HEPES buffer (pH 7.46) 500 mL Aqua ad injectabilia</p> <p><u>IonOptix' Tyrode's working solution:</u> 20 mM Glucose 1.5 mM CaCl₂-2H₂O 500 mL IonOptix' Tyrode's stock solution</p> <p>The IonOptix' Tyrode's stock solution was prepared maximum one week in advance and stored at 4 °C. The IonOptix' Tyrode's working solution was prepared freshly.</p>
Tyrode's solution for EHT measurements	120 mM NaCl 5.4 mM KCl 1 mM MgCl ₂ x 6H ₂ O 0.1-10 mM CaCl ₂ 0.4 mM NaH ₂ PO ₄ 22.6 mM NaHCO ₃ 5 mM Glucose 0.05 mM Na ₂ EDTA 25 mM HEPES (pH 7.4, in PBS) Aqua ad injectabilia
	Calcium is added up to the needed concentration for the respective experimental step.

10.1.9 *Antibodies*a) **Primary antibodies**

Table S2: Primary antibodies used for flow cytometry/FACS, western blot (WB), immunofluorescence (IF) and immunohistochemistry (IHC) analysis.

Antibody	Details and dilution	Application	Company and order number
Anti-alpha actinin	Mouse monoclonal IgM, clone EA-53; FACS: 1:800; WB: 1:1000	FACS, WB, IF	Sigma-Aldrich, A7811
Anti-cardiac troponin T-FITC	Recombinant human IgG1; clone REA400; 1:10	FACS	Miltenyi Biotec, 130-106-687
Anti-CD107b PrecisionAb™ (LAMP2)	Purified rabbit polyclonal IgG antibody; 1:1000	WB	Bio-Rad Laboratories, VPA00316
Anti-dystrophin	Purified mouse monoclonal IgG, clone 1808; 1:200	IHC	Merck (former Millipore), MAB1645
Anti-LC3B (LC3-II)	Polyclonal rabbit; 1:1000	WB	Cell Signalling, 3863
Anti-MLC2v	Mouse monoclonal, purified IgG; 1:150	IHC	Synaptic Systems, SY 310 111
Anti-Oct4A	Rabbit monoclonal IgG; Clone C30A3, 1:200	IF	Cell Signalling, #2840
Anti-p62	Purified Mouse monoclonal IgG1, κ; Clone 3/P62; 1:2000	WB	BD Biosciences, 610832
Anti-phospholamban	Rabbit polyclonal, purified IgG; WB: 1:1000; IHC: 1:1000; IF: 1:200	WB, IHC, IF	Novus, NBP2-19807
Anti-phospholamban pSer16	Purified rabbit polyclonal antibody IgG; 1:5000	WB	Badrilla, A010-12AP
Anti-Serca2 ATPase	Mouse monoclonal IgG, clone 2A7-A1; 1:1000	IF	Thermo Fisher Scientific, MA3-919

Anti-Tra-1-60	Mouse monoclonal IgM; 1:200	IF	Cell Signalling, #4746
mIgG1 isotype control	Purified Mouse IgG1 κ ; clone MOPC-21; 1:250	FACS	BD Biosciences, 554121
PE Rat IgM, κ Isotype Control	Rat IgM clone R4-22; 1:80	FACS	BD Biosciences, 553943
REA Control (I)-FITC	Isotype control IgG1, clone REA400; 1:10	FACS	Miltenyi Biotec 130- 104-611

b) Secondary Antibodies

Table S3: Primary antibodies used for flow cytometry/FACS, western blot (WB), immunofluorescence (IF) analysis.

Antibody	Dilution	Application	Company and order number
Alexa Fluor® 488 goat anti-mouse IgG	1:800	FACS, IF	Life technologies, A11001
Alexa Fluor® 488 goat anti-mouse IgM μ chain	1:500	IF	Molecular Probes Invitrogen, A11035
Alexa Fluor® 488 goat anti-rabbit IgG	1:800	FACS, IF	Life technologies, A11034
Alexa Fluor® 546 goat anti-rabbit IgG	1:500	IF	Molecular Probes Invitrogen, A21042
Alexa Fluor® 546 rabbit anti-mouse IgG	1:800	FACS, IF	Life technologies, A11060
Anti-mouse IgG peroxidase-conjugated secondary antibody	1:5000	WB	Sigma, A3682
Anti-rabbit IgG peroxidase-conjugated secondary antibody	1:5000-1:10000	WB	Sigma, A0545

10.1.10 *Primer and oligomers*

Table S4: Primer for PCR, sequencing (Seq) and sgDNA synthesis.

Name	Sequence forward (5'-3')	Sequence reverse (5'-3')	Application
hPLN-Fw	CATATTTGGCTCCAGCTTT	-----	Seq
hPLN-1.3 kB	GGGGTCTTTATTGAGAAGT TTGG	CAGATGTGAGGAGTCA GTGGAC	PCR 1258 bp
IVT	TTAATACGACTCACTATAG	AAAAGCACCGACTCGG TGCCAC	Seq
Myco	ACTCCTACGGGAGGCAGC AGTA	TGCACCATCTGTCACTC TGTTAACCTC	PCR 703-713 bp
OT1	AGCAGGCAGCCCTATTTTC AT	AGAGAGGAGCAAGACA GACTCA	Seq, PCR 555 bp
OT10	AAGTCTGTGACAGGTTCA GGG	ATTGGCAAAGCAACT GCGAG	Seq, PCR 502 bp
OT2	GACATGGCTGATTATATTC TTGCTG	GATCCAGGCTGGCTAA GGTAG	Seq, PCR 508 bp
OT3	GGGAGCCCACTGATGTGA AG	ACAATCTCAACGTGGA ATAGGGA	Seq, PCR 530 bp
OT4	GGGTGGGCTGAGCCAATA AT	TGAGTATACATTGCTTT GGAGTACA	Seq, PCR 657 bp
OT5	AGGCACTCGCAAGCTTCTT T	CAGCAGAAGTGTACTA CAAAGACC	Seq, PCR 530 bp
OT6	CCTCATGTATCTGCAGGTG TGT	TGCCACAATGGCTAGT GTATGT	Seq, PCR 720 bp
OT7	TGTCTCACTCAACATACGT GGT	CTGAGGAAGCAGGAGA GGAGTA	Seq, PCR 815 bp
OT8	TTGTTCTGCCAGGACCCTA AG	TGAGCACCAAAAATG GGACT	Seq, PCR 501 bp
OT9	AGGGTGGGTGACTGAGTG TT	ACTTGTCATGGGAGTC GCTTT	Seq, PCR 587 bp
pJET1.2	CGACTCACTATAGGGAGA GCGGC	AAGAACATCGATTTTCC ATGGCAG	Seq

Name	Sequence forward (5'-3')	Sequence reverse (5'-3')	Application
T7 gRNA	TTAATACGACTCACTATAG GTTGAGGCATTTCAATGGT TGGTTTTAGAGCTAGAAAT AGCAAGTTAAAATAAGGCT AGTCCG	AAAAGCACCGACTCGG TGCCACTTTTTCAAGTT GATAACGGACTAGCCT TATTTAACTTGCTATTT CTAGC	sgDNA synthesis
U6- Forward	GAGGGCCTATTTCCCATG ATTCC	-----	Seq

The PCR and sequencing primer were designed with the NCBI primer blast tool (www.ncbi.nlm.nih.gov/tools/primer-blast/) and ordered from Eurofins MWG Operon.

Table S5: Primer for RT-qPCR analysis.

Primer name	NM number	Sequence forward (5'-3')	Sequence reverse (5'-3')
ACTN2	NM_001103.3 NM_001278344.1 NM_001278343.1	AAGGGGTGAAAC TGGTGTCC	AGCAGACCTTCTTT GGCAGAT
GUSB	NM_000181.3	ACGATTGCAGGGTT TCACCA	CACTCTCGTCCG TGACTGTT
PLNmt		CACTCGCTCAGCTAT AAGAGC	AGAGAAGCATCACGA TGATACAG
PLNwt	NM_002667.3	CTCGCTCAGCTATAA GAAGAGC	AGAGAAGCATCACGA TGATACAG
PLNwt/mt	NM_002667.3	CAATACCTCACTCG CTCAGC	AGAGAAGCATCACGAT GATACAG

The RT-qPCR primer were designed with the NCBI primer blast tool (www.ncbi.nlm.nih.gov/tools/primer-blast/) and ordered from Eurofins MWG Operon.

Table S6: CRISPR/Cas9 - ssODN repair template and sgRNA sequences.

Name	Sequence (5'-3')	Company
sgRNA #3	CAACCATTGAAATGCCTCAA	Eurofins MWG Operon
ssODN	CTGCTGGTATCATGGAGAAAGTCCAATACCTCACTCGCT CAGCTATAAGAAGAGCATCAACCATTGAAATGCCTCAAC AAGCACGTCAAAGCTACAGAATCT	IDT

10.2 Security information

10.2.1 Security information for the used substances

All experiments were performed in laboratories with the certified security standards S1 and S2 in consideration of the security data sheets. Chemicals, buffers and solutions were disposed according to the respective instructions and into appropriate containers. Cell suspensions and contaminated materials were autoclaved before disposal or re-usage. Surfaces which were in contact with genetically modified organisms were disinfected with 70% ethanol.

Table S7: Security information (H- and P-statements) of all used substances.

Substance	CAS number	H-statement	P-statement
1,4-Dithiothreitol (DTT)	3483-12-3	H: 302, 315, 319, 412	P: 264, 270, 273, 280, 337+313, 501
1-Thioglycerol	96-27-5	H: 302-311-315-319-335	P: 261-280-305+351+338+312
2-Mercaptoethanol	60-24-2	H: 301+331, 310, 315, 317, 318, 373, 410	P: 270, 280, 302+352, 330, 304+340, 305+351+338, 310
2-Propanol (isopropanol)	67-63-0	H: 225, 319, 336	P: 210, 261, 305+351+338
Acetic acid	64-19-7	H: 226-290-314	P: 210-280-301+330+331-305+351+338-308+310
Acrylamide/Bis solution, 29:1, 40%	79-06-1 110-26-9	H: 302, 312, 315, 319, 317, 340, 350, 361, 372	P: 260, 280, 281, 305+351+338, 405, 501
Ammonium persulfate (APS)	7727-54-0	H: 272, 302, 315, 317, 319, 334, 335	P: 221, 210, 285, 405 305+P351+P338, 501

Ampicillin trihydrate	7177-48-2	H: 317-334	P: 280-285, 302+352-304+341-333+313-342+311
Calcium chloride dihydrate (CaCl₂ x 2 H₂O)	10035-04-8	H: 319	P: 305+351+388
Carbachol	51-83-2	H: 300	P 308+310
cOmplete®, Mini, EDTA-free protease inhibitor cocktail	139-33-3 205-358-3 30827-99-7	H: 315, 319	P: 264, 280, 302+352, 332+313, 337+313, 362+364
Dorsomorphin	866405-64-3	H: 302, 312, 332	P: 301+312, 304+340, 302+352, 261, 280, 264, 270, 271, 330, 501, 363
Ethanol, absolute	64-17-5	H: 225, 319	P: 210, 240, 305+351+338, 403+233
Ethidium bromide	1239-45-8	H: 331, 341	P: 261-281-311
Ethylenediamine tetraacetic acid (EDTA)	60-00-4	H: 319	P: 305+351+338
Formaldehyde	50-00-0	H: 351-331-311-301-314-317	P: 301+310-303+361+353-305+351+338, 320-361-405-501
Hydrochloric acid	7647-01-0	H: 314-335	P: 260-301+330+331-303+361+353-305+351+338-405-501
Hydrochloric acid, 37% fuming	---	H: 290, 314, 335	P: 280, 301+330+331, 305+351+338, 308+310
Isoprenaline hydrochloride	5984-95-2	H: 315, 319, 335	P: 261, 305+351+338
Lipidmix	64-17-5	H: 225, 319	P210, 280, 305+351+338, 337+313, 403+235
Methanol	67-56-1	H: 225-331-311-301-370	P: 210-233-280-302+352

Mitomycin C	50-07-7	H: 302-351	P: 201-281, 301+310-308+313-330
N,N,N',N'-Tetramethyl ethylenediamine (TEMED)	110-18-9	H: 225, 332, 302, 314	P: 210, 233, 280, 301+330+331, 305+351+338, 308, 310
Nitrogen, liquid (N₂)	7727-37-9	H: 281	P: 282, 336+315, 403
Paraformaldehyde	30525-89-4	H: 228-302-332-351-335-315-319-317	P: 281-302+352-305+351+338-308+313-304+340
Penicillin	61-33-6	H: 317	P: 280
PhosSTOP® phosphatase inhibitor	---	H: 302	P: 264, 270, 301+312, 330, 501
Ponceau S	6226-79-5	H: 315-319-335	P: 261–305+351+338
Potassium di-hydrogen phosphate (KH₂PO₄)	7778-77-0	--	P: 260
Proteinase K	39450-01-6	H: 334	P: 304+340, 261, 342+311, 284
Roti®-Histofix 4%	50-00-0 67-56-1	H: 302, 317, 341, 350	P: 261, 280, 302+352, 308+313
Saponin	8047-15-2	H: 319, 335	P 261, 305+351+338
SCR7	14892-97-8	H: 302+400	P: 273
Sodium azide	26628-22-8	H: 300-400-410	P: 273–309-310
Sodium dodecyl sulfate (SDS)	151-21-3	H: 228, 302+332, 315, 318, 335, 412	P: 210, 261, 280, 302+352, 305+351+338, 312
Sodium hydroxide (NaOH)	1310-73-2	H: 314	P: 280–301+330+331–309–310-305+351+338
Sodium selenite	10102-18-8	H: 300+330, 315, 317, 319, 411	P: 260, 280, 301+330+331+310, 304+340+310, 403+233

Streptomycin	57-92-1	H: 302	--
Thrombin	9002-04-4	H: 315, 319, 334, 335	P: 261, 305+351+338, 342+311
Titriplex® III	6381-92-6	H: 332-373	P: 314
TRIS-Hydrochlorid (Tris-HCl)	1185-53-1	H: 315, 319, 335	P: 280, 302+352, 305+351+338
Triton X-100	9002-93-1	H: 302-318-411	P: 273-280- 305+351+338
TRIZOL reagent	108-95-2 593-84-0 1762-95-4	H: 301+311+331, 314, 335, 341, 373, 412	P: 201, 261, 261, 280, 273, 301+310, 302+352
Trypan blue	72-57-1	H: 350	P: 201-308+313
Y-27632	331752-47-7	H: 302-312-332	P: 280

10.2.2 EU-GHS Hazard (H) and Precaution (P) statements

Table S8: Hazard (H) statements according to the 8th ATP of the CLP regulation of May 19, 2016.

H statement	H phrases
H200	Unstable explosives.
H201	Explosive; mass explosion hazard.
H202	Explosive, severe projection hazard.
H203	Explosive; fire, blast or projection hazard.
H204	Fire or projection hazard.
H205	May mass explode in fire.
H220	Extremely flammable gas.
H221	Flammable gas.
H222	Extremely flammable aerosol.
H223	Flammable aerosol.
H224	Extremely flammable liquid and vapour.
H225	Highly flammable liquid and vapour.
H226	Flammable liquid and vapour.
H228	Flammable solid.
H229	Pressurised container: May burst if heated.
H230	May react explosively even in the absence of air.
H231	May react explosively even in the absence of air at elevated pressure and/or temperature.

H240	Heating may cause an explosion.
H241	Heating may cause a fire or explosion.
H242	Heating may cause a fire.
H250	Catches fire spontaneously if exposed to air.
H251	Self-heating: may catch fire.
H252	Self-heating in large quantities; may catch fire.
H260	In contact with water releases flammable gases which may ignite spontaneously
H261	In contact with water releases flammable gases.
H270	May cause or intensify fire; oxidizer.
H271	May cause fire or explosion; strong oxidizer.
H272	May intensify fire; oxidizer.
H280	Contains gas under pressure; may explode if heated.
H281	Contains refrigerated gas; may cause cryogenic burns or injury.
H290	May be corrosive to metals.
H300	Fatal if swallowed.
H300 + H310	Fatal if swallowed or in contact with skin.
H300 + H310 + H330	Fatal if swallowed, in contact with skin or if inhaled.
H300 + H330	Fatal if swallowed or if inhaled.
H301	Toxic if swallowed.
H301 + H311	Toxic if swallowed or in contact with skin.
H301 + H311 + H331	Toxic if swallowed, in contact with skin or if inhaled.
H301 + H331	Toxic if swallowed or if inhaled.
H302	Harmful if swallowed.
H302 + H312	Harmful if swallowed or in contact with skin.
H302 + H312 + H332	Harmful if swallowed, in contact with skin or if inhaled.
H302 + H332	Harmful if swallowed or if inhaled.
H304	May be fatal if swallowed and enters airways.
H310	Fatal in contact with skin.
H310 + H330	Fatal in contact with skin or if inhaled.
H311	Toxic in contact with skin.
H311 + H331	Toxic in contact with skin or if inhaled.
H312	Harmful in contact with skin.
H312 + H332	Harmful in contact with skin or if inhaled.

H314	Causes severe skin burns and eye damage.
H315	Causes skin irritation.
H317	May cause an allergic skin reaction.
H318	Causes serious eye damage.
H319	Causes serious eye irritation.
H330	Fatal if inhaled.
H331	Toxic if inhaled.
H332	Harmful if inhaled.
H334	May cause allergy or asthma symptoms or breathing difficulties if inhaled.
H335	May cause respiratory irritation.
H336	May cause drowsiness or dizziness.
H340	May cause genetic defects.
H341	Suspected of causing genetic defects.
H350	May cause cancer.
H351	Suspected of causing cancer.
H360	May damage fertility or the unborn child.
H361	Suspected of damaging fertility or the unborn child.
H362	May cause harm to breast-fed children.
H370	Causes damage to organs.
H371	May cause damage to organs.
H372	Causes damage to organs through prolonged or repeated exposure.
H373	May cause damage to organs through prolonged or repeated exposure.
H400	Very toxic to aquatic life.
H410	Very toxic to aquatic life with long lasting effects.
H411	Toxic to aquatic life with long lasting effects.
H412	Harmful to aquatic life with long lasting effects.
H413	May cause long lasting harmful effects to aquatic life.
H420	Harms public health and the environment by destroying ozone in the upper atmosphere.

Table S9: Precaution (P) statements according to the 8th ATP of the CLP regulation of May 19, 2016.

P statement	P phrase
P301+P310	IF SWALLOWED: Immediately call a POISON CENTRE/doctor/....
P301+P312	IF SWALLOWED: Call a POISON CENTRE/doctor/... if you feel unwell.
P301+P330+ P331	IF SWALLOWED: Rinse mouth. Do NOT induce vomiting.
P302+P334	IF ON SKIN: Immerse in cool water [or wrap in wet bandages].
P302+P335+ P334	IF ON SKIN: Brush off loose particles from skin. Immerse in cool water [or wrap in wet bandages].
P302+P352	IF ON SKIN: Wash with plenty of water/...
P303+P361+ P353	IF ON SKIN (or hair): Take off immediately all contaminated clothing. Rinse skin with water [or shower].
P304+P340	IF INHALED: Remove person to fresh air and keep comfortable for breathing.
P305+P351+ P338	IF IN EYES: Rinse cautiously with water for several minutes. Remove contact lenses, if present and easy to do. Continue rinsing.
P 306+P360	IF ON CLOTHING: rinse immediately contaminated clothing and skin with plenty of water before removing clothes.
P308+P311	IF exposed or concerned: Call a POISON CENTRE/doctor/...
P308+ P313	IF exposed or concerned: Get medical advice/attention.
P101	If medical advice is needed, have product container or label at hand.
P102	Keep out of reach of children.
P103	Read label before use.
P201	Obtain special instructions before use.
P202	Do not handle until all safety precautions have been read and understood.
P210	Keep away from heat, hot surfaces, sparks, open flames and other ignition sources. No smoking.
P211	Do not spray on an open flame or other ignition source.
P220	Keep away from clothing and other combustible materials.
P222	Do not allow contact with air.
P223	Do not allow contact with water.
P230	Keep wetted with...
P231	Handle and store contents under inert gas/...
P231+P232	Handle and store contents under inert gas/... Protect from moisture.
P232	Protect from moisture.

P233	Keep container tightly closed.
P234	Keep only in original packaging.
P235	Keep cool.
P240	Ground and bond container and receiving equipment.
P241	Use explosion-proof [electrical/ventilating/lighting/...] equipment.
P242	Use non-sparking tools.
P243	Take action to prevent static discharges.
P244	Keep valves and fittings free from oil and grease.
P250	Do not subject to grinding/shock/friction/...
P251	Do not pierce or burn, even after use.
P260	Do not breathe dust/fume/gas/mist/vapors/spray.
P261	Avoid breathing dust/fume/gas/mist/vapors/spray.
P262	Do not get in eyes, on skin, or on clothing.
P263	Avoid contact during pregnancy and while nursing.
P264	Wash ... thoroughly after handling.
P270	Do not eat, drink or smoke when using this product.
P271	Use only outdoors or in a well-ventilated area.
P272	Contaminated work clothing should not be allowed out of the workplace.
P273	Avoid release to the environment.
P280	Wear protective gloves/protective clothing/eye protection/face protection.
P282	Wear cold insulating gloves and either face shield or eye protection.
P283	Wear fire resistant or flame retardant clothing.
P284	[In case of inadequate ventilation] wear respiratory protection.
P301	IF SWALLOWED:
P302	IF ON SKIN:
P303	IF ON SKIN (or hair)
P304	IF INHALED:
P305	IF IN EYES:
P306	IF ON CLOTHING:
P308	IF exposed or concerned:
P310	Immediately call a POISON CENTRE/doctor/...
P311	Call a POISON CENTRE/doctor/....
P312	Call a POISON CENTRE/doctor/... if you feel unwell.
P313	Get medical advice/attention.
P314	Get medical advice/attention if you feel unwell.
P315	Get immediate medical advice/attention.

P320	Specific treatment is urgent (see ... on this label).
P321	Specific treatment (see ... on this label).
P330	Rinse mouth.
P331	Do NOT induce vomiting
P332	If skin irritation occurs:
P332+P313	If skin irritation occurs: Get medical advice/attention.
P333	If skin irritation or rash
P333+P313	If skin irritation or rash occurs: Get medical advice/attention.
P334	Immerse in cool water [or wrap in wet bandages].
P335	Brush off loose particles from skin.
P336	Thaw frosted parts with lukewarm water. Do no rub affected area.
P336+P315	Thaw frosted parts with lukewarm water. Do not rub affected area. Get immediate medical advice/attention.
P337	If eye irritation persists:
P337+P313	If eye irritation persists: Get medical advice/attention.
P338	Remove contact lenses, if present and easy to do. Continue rinsing.
P340	Remove person to fresh air and keep comfortable for breathing.
P342	If experiencing respiratory symptoms:
P342+P311	If experiencing respiratory symptoms: Call a POISON CENTRE/doctor/...
P351	Rinse cautiously with water for several minutes.
P352	Wash with plenty of water/...
P353	Rinse skin with water [or shower].
P360	Rinse immediately contaminated clothing and skin with plenty of water before removing clothes.
P361	Take off immediately all contaminated clothing.
P361+P364	Take off immediately all contaminated clothing and wash it before reuse.
P362	Take off contaminated clothing.
P362+P364	Take off contaminated clothing and wash it before reuse.
P363	Wash contaminated clothing before reuse.
P364	And wash it before reuse.
P370	In case of fire:
P370+P372+ P380+ P373	In case of fire: Explosion risk. Evacuate area. DO NOT fight fire when fire reaches explosives.
P370+P376	In case of fire: Stop leak if safe to do so.
P370+P378	In case of fire: Use ... to extinguish.

P370+P380+ P375	In case of fire: Evacuate area. Fight fire remotely due to the risk of explosion.
P370+P380+ P375 [+P378]	In case of fire: Evacuate area. Fight fire remotely due to the risk of explosion. [Use ... to extinguish]. P371+P380+P375 In case of major fire and
P371	In case of major fire and large quantities:
P372	Explosion risk.
P373	DO NOT fight fire when fire reaches explosives.
P375	Fight fire remotely due to the risk of explosion.
P376	Stop leak if safe to do so.
P377	Leaking gas fire: Do not extinguish, unless leak can be stopped safely.
P378	Use ... to extinguish.
P380	Evacuate area. P381 In case of leakage
P390	Absorb spillage to prevent material damage.
P391	Collect spillage.
P401	Store in accordance with...
P402	Store in a dry place.
P402+P404	Store in a dry place. Store in a closed container.
P403	Store in a well-ventilated place.
P403+P233	Store in a well-ventilated place. Keep container tightly closed.
P403+P235	Store in a well-ventilated place. Keep cool.
P404	Store in a closed container.
P405	Store locked up.
P406	Store in a corrosion resistant/... container with a resistant inner liner.
P407	Maintain air gap between stacks or pallets.
P410	Protect from sunlight.
P410+P403	Protect from sunlight. Store in a well-ventilated place.
P410+P412	Protect from sunlight. Do not expose to temperatures exceeding 50°C/ 122°F.
P411	Store at temperatures not exceeding ...°C/...°F.
P412	Do not expose to temperatures exceeding 50°C/ 122°F.
P413	Store bulk masses greater than ... kg/... lbs at temperatures not exceeding ...°C/...°F.
P420	Store separately.
P501	Dispose of contents/container to ...
P502	Refer to manufacturer or supplier for information on recovery or recycling.

10.3 Figures and tables

Table S10: Acronyms and names of human genes evaluated with the NanoString nCounter® Elements system.

Acronym	Name	
<i>GAPDH</i>	Glyceraldehyde-3-phosphate dehydrogenase - high heart expression = 32000 counts	Housekeeping
<i>ACTB</i>	Actin beta - high heart expression = 10000 counts	Housekeeping
<i>PGK1</i>	Phosphoglycerate kinase 1 - medium heart expression = 5000 counts	Housekeeping
<i>TUBB</i>	Tubulin beta class 1 - medium heart expression = 2000 counts	Housekeeping
<i>CLTC</i>	Clathrin heavy chain - medium heart expression = 1000 counts	Housekeeping
<i>ABCF1</i>	ATP binding cassette subfamily F member 1 - low heart expression = 400 counts	Housekeeping
<i>PLN</i>	Phospholamban	Calcium handling

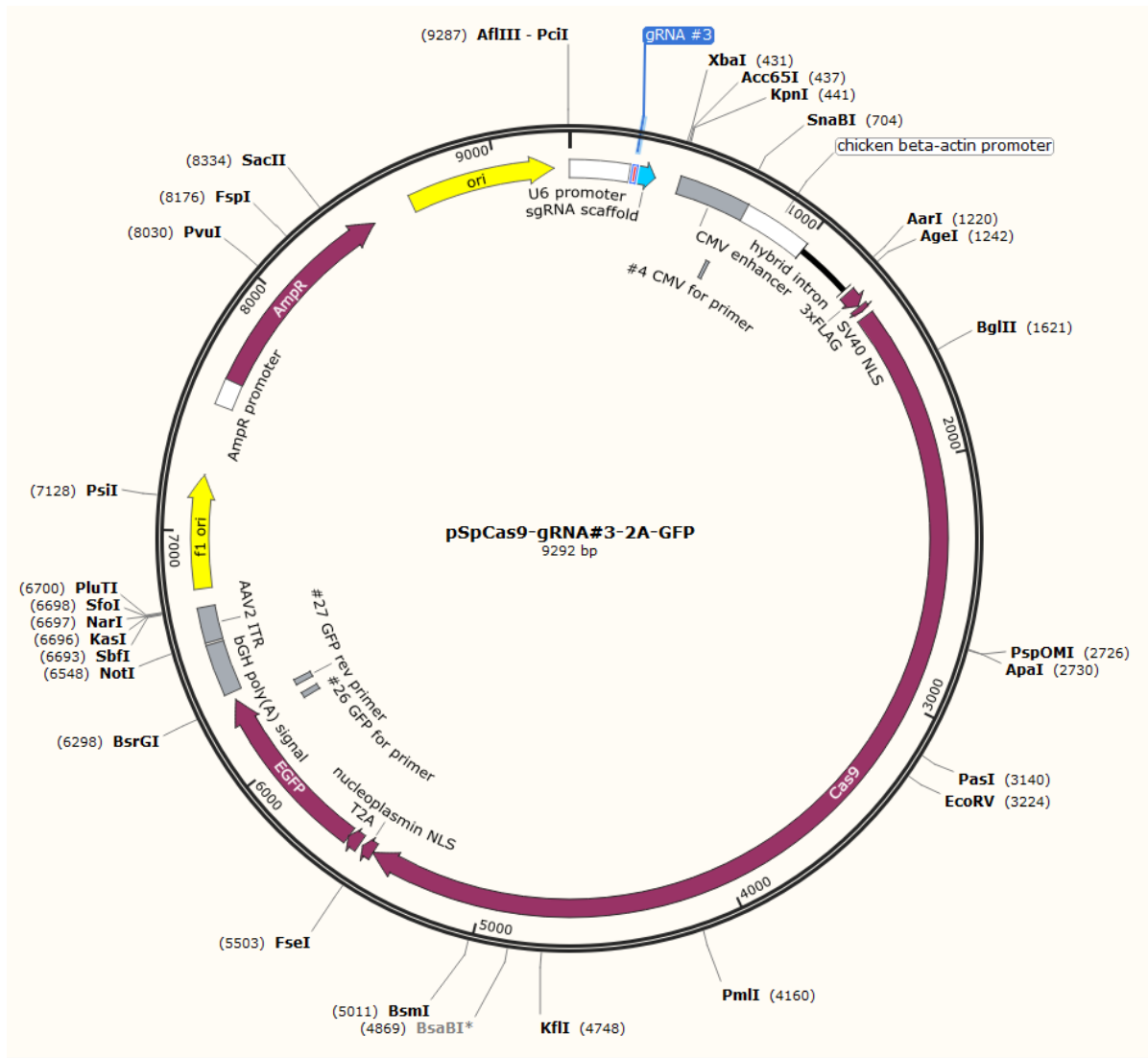
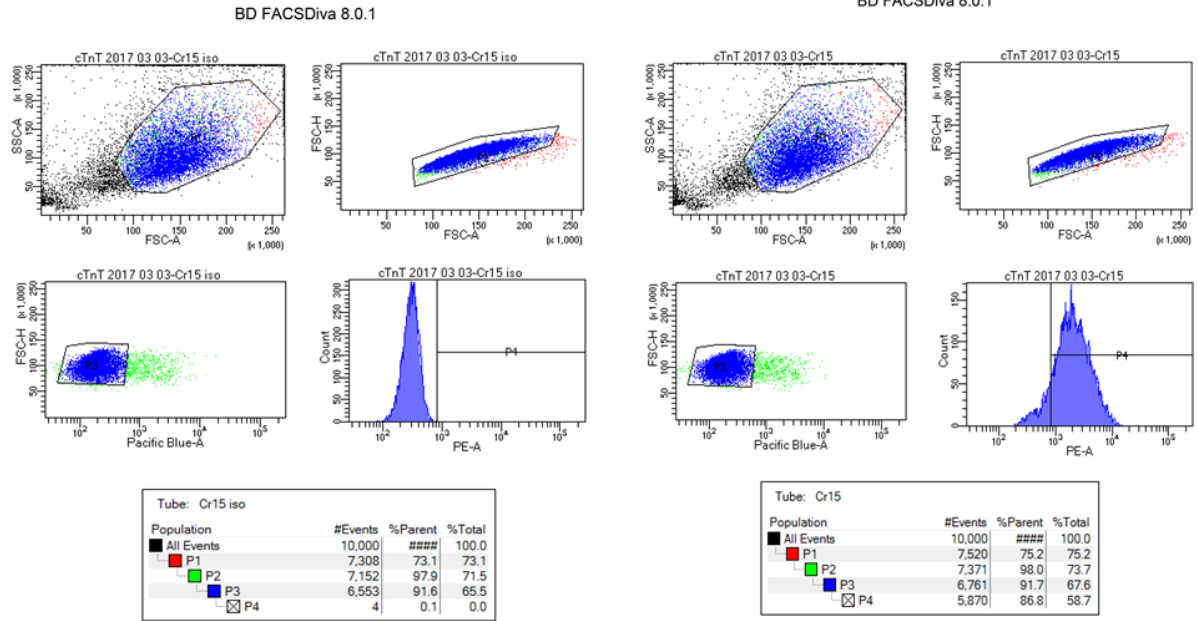


Figure S2: Vector map of the pSpCas9-gRNA#3-2A-GFP plasmid. The inserted gRNA#3 is highlighted in light blue. The plasmid was ordered from Addgene: plasmid ID 48138. This figure was created with SnapGene.

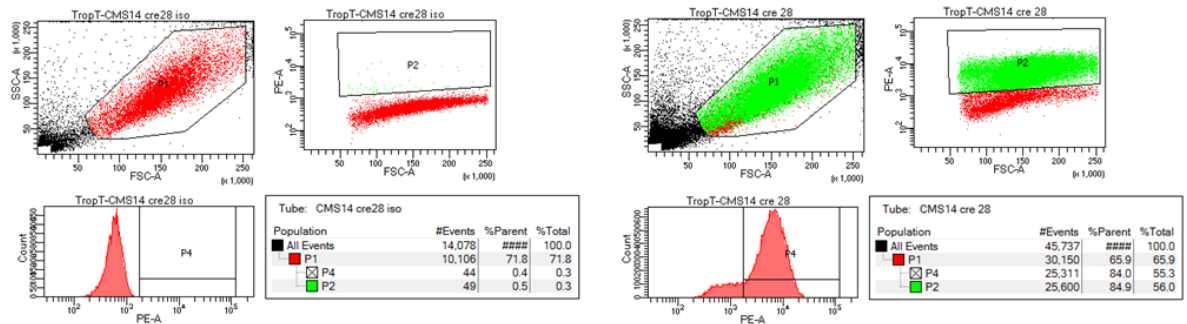
Isotype control

Sample

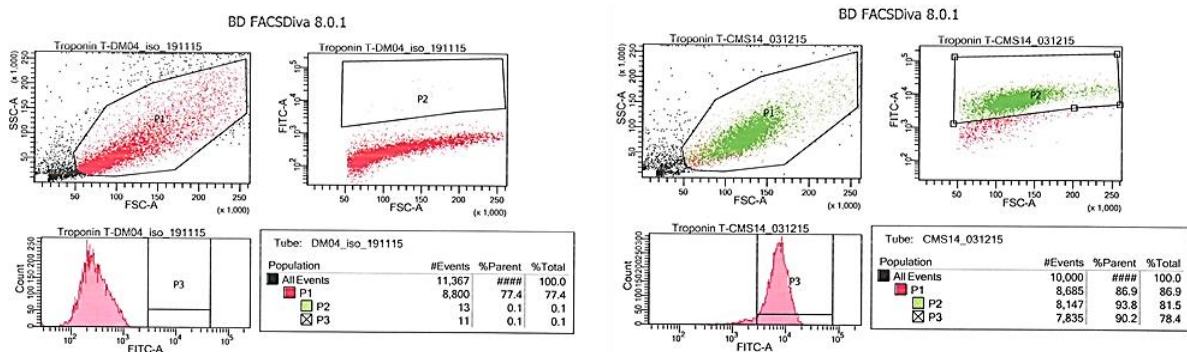
A – PLNc #15



B – PLNc #28



C – PLN p.Arg14del #1198



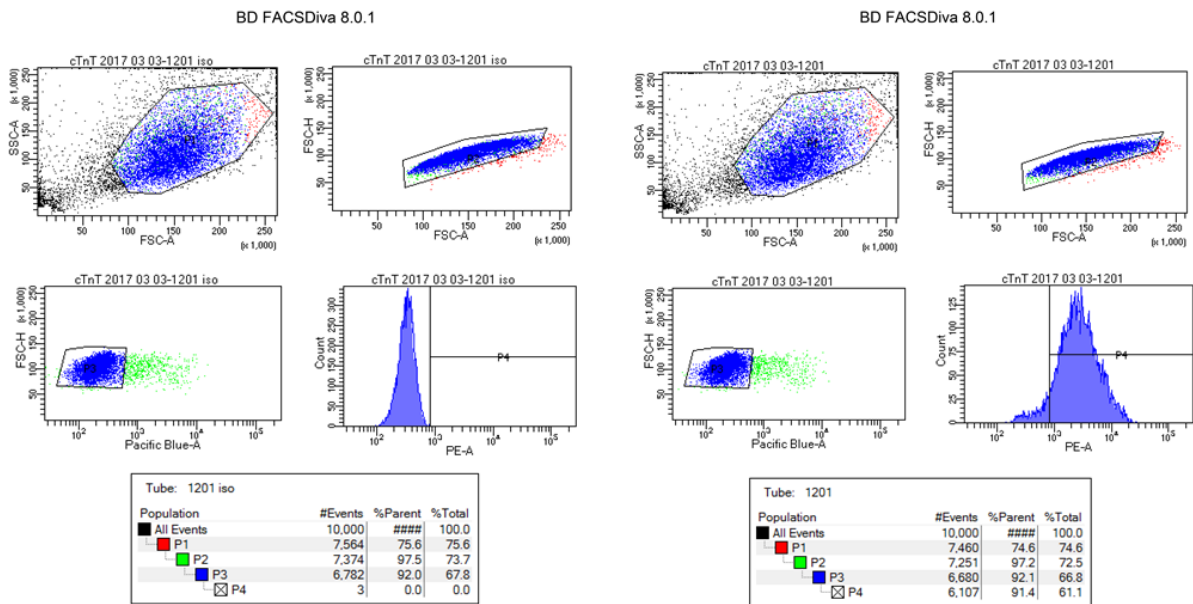
D – PLN p.Arg14del #1201

Figure S3: Representative flow cytometry plots of dissociated hiPSC-derived cardiomyocytes. A - PLNic #15, B - PLNic #28, C - PLN p.Arg14del #1198 and D - PLN p.Arg14del #1201.

10.4 Movies**Movie S1 - Cardiac differentiation.mp4**

Movie S1: Representative original video recordings of beating hiPSC-derived cardiomyocytes in their cardiac specification stage one day before dissociation. A - cEBs of PLNic #15, B - cEBs of PLNic #28, C - cardiac monolayer of PLN p.Arg14del #1198 and D - cEBs of PLN p.Arg14del#1201.

**Movie S2 - EHT.mp4**

Movie S2: Representative original video recordings of spontaneously beating 20 day old EHTs in cultivation medium. A - Unrelated control EHT, B - PLNic #15 EHT and C - PLN p.Arg14del #1198 EHT.

10.5 Financial support

This project was financially supported by the British Heart Foundation (BHF) and the DZHK (Deutsches Zentrum für Herz-Kreislauf Forschung).

10.6 Publications and congress participations

10.6.1 Publications

Schmidt SK, Ebel S, Keil E, Woite C, Ernst JF, **Benzin AE**, Rupp J, Däubener W. (2013) Regulation of IDO activity by oxygen supply: inhibitory effects on antimicrobial and immunoregulatory functions. PLoS One. 8(5):e63301.

Mannhardt I, Breckwoldt K, Letuffe-Breniere D, Schaaf S, Schulz H, Neuber C, **Benzin A**, Werner T, Eder A, Schulze T, Klampe B, Christ T, Hirt MN, Huebner N, Moretti A, Eschenhagen T, Hansen A (2016) Human Engineered Heart Tissue: Analysis of Contractile Force. Stem Cell Rep 7: 29-42

Breckwoldt K, Letuffe-Brenière D, Mannhardt I, Schulze T, Ulmer B, Werner T, **Benzin A**, Klampe B, Reinsch MC, Laufer S, Shibamiya A, Prondzynski M, Mearini G, Schade D, Fuchs S, Neuber C, Krämer E, Saleem U, Schulze ML, Rodriguez ML, Eschenhagen T, Hansen A (2017) Differentiation of cardiomyocytes and generation of human engineered heart tissue. Nat Protoc 12:1177-1197

Mannhardt I, Saleem U, **Benzin A**, Schulze T, Klampe B, Eschenhagen T, Hansen A (2017) Automated Contraction Analysis of Human Engineered Heart Tissue for Cardiac Drug Safety Screening. J Vis Exp 2017:e55461–e55461

Müller-Fielitz H, Stahr M, Bernau M, Richter M, Abele S, Krajka V, **Benzin A**, Wenzel J, Kalies K, Mittag J, Heuer H, Offermanns S, Schwaninger M (2017) Tanycytes control the hormonal output of the hypothalamic-pituitary-thyroid axis. Nat Commun. 8:1-13

10.6.2 Congress and meeting participations

Anika Eike Benzin: Disease modeling of phospholamban mutations in iPSC-derived cardiomyocytes, NCCR Meeting Lübeck, Germany, 30th November 2015

Anika Eike Knaust: CRISPR/Cas9-derived isogenic hiPSC controls reveal a mutation-specific contractile and arrhythmic phenotype of hiPSC-cardiomyocytes from PLN-R14del carriers, 34th Annual Meeting of the European Section of the ISHR, Hamburg, Germany, 24th-27th July 2017

Benzin A, Vollert I, Klampe B, Letuffe-Brenière D, Laufer S, Shibamiya A, van Rijnsingen I, Pinto Y, Harding S, Eschenhagen T, Hansen A: Disease modelling of phospholamban mutations in human iPSC-derived cardiomyocytes, Joint BSCR and BSGCT Conference: Cell therapy for cardiovascular disease in the 21st century, Glasgow, June 11th-12th, 2015

Benzin A, Vollert I, Klampe B, Letuffe-Brenière D, Laufer S, Shibamiya A, van Rijnsingen I, Pinto Y, Harding S, Eschenhagen T, Hansen A: Disease modelling of phospholamban mutations in human iPSC-derived cardiomyocytes, Cardiac Regeneration and Vascular Biology Conference, San Servolo, Venice, Italy, 17th-19th June 2015

Benzin A, Vollert I, Klampe B, Letuffe-Brenière D, Laufer S, Shibamiya A, van Rijnsingen I, Pinto Y, Harding S, Eschenhagen T, Hansen A: Disease modelling of phospholamban mutations in human iPSC-derived cardiomyocytes, NCCR Retreat, Tremsbüttel, Germany, 29th-30th January 2016

Benzin A, Mannhardt I, Klampe B, Letuffe-Brenière D, Laufer S, Shibamiya A, van Rijnsingen I, Pinto Y, Harding S, Eschenhagen T, Hansen A: Disease modelling of phospholamban mutations in human iPSC-derived cardiomyocytes, Stem cells in drug discovery conference, Cambridge, UK, 5th-6th April 2016

Benzin A, Mannhardt I, Klampe B, Letuffe-Brenière D, Laufer S, Shibamiya A, Braren I, van Rijnsingen I, Pinto Y, Hajjar R, Harding S, Eschenhagen T, Hansen A: Disease modelling of phospholamban mutations in human iPSC-derived cardiomyocytes, Joint BHF Regenerative Medicine Centre's Event 2016, Cambridge, United Kingdom, 23rd June 2016

Knaust AE, Prondzynski M, Klampe B, Saleem U, Zech ATL, Flenner F, Mannhardt I, Laufer S, Shibamiya A, Braren I, van Rijnsingen I, Pinto Y, Harding S, Eschenhagen T, Hansen A: CRISPR/Cas9-derived isogenic hiPSC controls reveal a mutation-specific contractile and arrhythmic phenotype of hiPSC-cardiomyocytes from PLN-R14del carriers, 34th Annual Meeting of the European Section of the ISHR, Hamburg, Germany, 24th-27th July 2017; Poster Prize Award

11 ACKNOWLEDGEMENTS

After four years of interesting, exciting and intense research it is finally completed – my PhD thesis. This chapter is dedicated to all the people who helped, supported and encouraged me within this intense journey at the beginning of my scientific career.

First of all, I want to thank Prof. Dr. Thomas Eschenhagen for giving me the opportunity to do my PhD thesis at his department and especially for his great support, supervision, encouragement and advice. I really appreciate that he gave me the trust and great possibility to be part of the British Heart Foundation-based collaboration with the BHF centres in the UK.

In reference to this I also want to express my special appreciation to Prof. Dr. Arne Hansen. I am really thankful for his great support, guidance and advice in any case of theoretical and practical issues and that his door was always open for me.

I want to thank Prof. Dr. Elke Oetjen for being the second referee of this thesis and for her interest in my scientific work.

Parts of this project were a huge group effort, so many thanks to the CRISPR and the EHT group as well as hiPSC-CM differentiation team. Together with the great CRISPR group we were able to successfully establish this technology at our department. Without the help of the differentiation team it would not have been possible to differentiate the sufficient amount of cardiomyocytes in time for this project. Also, the disease modelling protocols were successfully established thanks to the support of the EHT group. Therefore I want to thank all the people involved - Prof. Dr. Arne Hansen, Prof. Dr. Lucie Carrier, Dr. Ingra Mannhardt, Dr. Bärbel Ulmer, Dr. Christiane Neuber, Dr. Pierre Bobin, Dr. Kaja Breckwoldt, Dr. Marita Roudrigez, Dr. Marina Reinsch, Dr. Giulia Mearini, Dr. Sandra Laufer, Dr. Ingke Braren, Dr. David Letuffe-Breniere, Alexandra Löser, Mirja Schulze, Umber Saleem, Maksymilian Prondzynski, Antonia T. L. Zech, Tessa Werner, Marta Lemme, Thomas Schulze, Birgit Klampe and Elisabeth Krämer.

I want to highlight my thanks to Dr. Ingra Mannhardt, Dr. Frederik Flenner, Maksymilian Prondzynski and Antonia T. L. Zech for providing data and for the experimental cooperation for this thesis. I thank Thomas Schulze and Birgit Klampe for their great stem cell work and I am also thankful for Birgit Klampe's great technical assistance not only concerning western blot experiments but also for always having a helping hand especially for large scale EHT generation projects.

A very important thank you is dedicated to Alexandra Löser who always encouraged me not only as a colleague but also as a friend. With her great advice she supported me during

experimental issues, a few gaps in knowledge or with her proof-reading of this thesis but she also always had a friendly ear for any other issue. Also, I want to thank Mirja Schulze, Umber Saleem, Antonia T. L. Zech and Maksymilian Prondzynski for the great PhD-to-PhD student encouragement and backup while spending numerous hours together studying, discussing and working on EHT-, differentiation- and CRISPR-related experiments.

I really appreciate the support from the HEXT Core facilities of the UKE. The HEXT Core Stem Cell Facility including Dr. Sandra Laufer and Dr. Aya Shibamiya supported the CRISPR experiments, hiPSC culture as well as characterization and performed the reprogramming of the patient skin fibroblasts. The UKE FACS Core Sorting unit and Dr. Ingke Braren from the HEXT Core Vector Facility supported the CRISPR experiments. The immunohistological EHT staining was performed by Kristin Hartmann of the UKE Mouse Pathology Facility.

I want to acknowledge the British Heart Foundation for the generous financial support of this study. I am thankful to all the people of the BHF centres, especially Prof. Dr. Sian Harding, Thomas Owen (Faculty of Medicine, National Heart & Lung Institute, Imperial College of London, UK), Prof. Dr. Chris Denning's laboratory including Diogo Mosqueira Alves Moreira Da Silva (Centre for Biomolecular Sciences, University of Nottingham, UK) for the great collaboration and for having an interesting, highly informative and great time in the UK.

Also many thanks to Prof. Dr. Yigal Pinto, Dr. Ingrid van Rijsingen, Inge van der Made (AMC, Amsterdam, the Netherlands) and Prof. Dr. Hendrik Milting (HDZ-NRW, Bad Oeynhausen, Germany) for providing the PLN p.Arg14del fibroblast and RNA samples.

Last but not least I want to thank the whole Department of Experimental Pharmacology and Toxicology for a great working atmosphere, the numerous helping hands at any time and great scientific exchange.

In the end, I especially want to appreciate my family and friends. My journey would not have been possible without their support and encouragement. I am really thankful not only for the financial but especially the emotional support of my parents. They always pick up the phone at any time of the day or night and gave the best words of advice. Without them I would not be where I am, how I am and who I am. Many thanks for always being there for me. I want to thank my grandfather for his great interest in my personal and also work-related news. I really enjoyed our time together as well as his frequent questionnaires about my scientific work progress and discussions about science. And finally, I want to really appreciate the love and support of my husband. He always backed me up in any situation and at any time. I am really thankful for his patience, encouragement and presence in my life as well as for being a huge part of my journey.

12 DECLARATION OF ACADEMIC HONESTY - EIDESSTATTLICHE ERKLÄRUNG

Hereby, I declare that this thesis entitled

“Disease modelling of a phospholamban p.Arg14del mutation in hiPSC-derived cardiomyocytes“

and carried out at the Department of Experimental Pharmacology and Toxicology, UKE Hamburg under the direction of Prof. Dr. med. Thomas Eschenhagen, the guidance of Prof. Dr. med. Arne Hansen and the supervision of Prof. Dr. med. Elke Oetjen for the Department of Chemistry, was completed independently by myself. Further, I did not use any other sources or aids other than those indicated. The submitted written form of the thesis complies with the electronic version. Moreover, this thesis was not handed in in any other form for another examination procedure.

Hamburg, 21st December 2017


Anika Eike Knaust

Hiermit versichere ich an Eides statt, dass die vorliegende Dissertation mit dem Titel

„Disease modelling of a phospholamban p.Arg14del mutation in hiPSC-derived cardiomyocytes“,

durchgeführt am Institut für Experimentelle Pharmakologie und Toxikologie des Universitätsklinikums Hamburg-Eppendorf unter der Leitung von Herrn Prof. Dr. med. Thomas Eschenhagen, der Anleitung von Herrn Prof. Dr. med. Arne Hansen und der Betreuung durch Frau Prof. Dr. med. Elke Oetjen für den Fachbereich Chemie, selbst verfasst wurde und keine anderen als die angegebenen Hilfsmittel benutzt worden sind. Die eingereichte schriftliche Fassung entspricht der elektronischen Version. Ich versichere, dass diese Dissertation nicht in einem früheren Promotionsverfahren eingereicht wurde.

Hamburg, den 21. Dezember 2017


Anika Eike Knaust